R. Hu

NRL Report 6930
(Second Edition of NRL Report 5868)

A Guide to Basic Pulse-Radar Maximum-Range Calculation

Part 1 - Equations, Definitions, and Aids to Calculation

L. V. BLAKE

Radar Geophysics Branch
Radar Division

December 23, 1969

NAVAL RESEARCH LABORATORY
Washington, D.C.

CONTENTS

Preface		iii
Abstract		iv
Problem Status		iv
Authorization		iv
1.	INTRODUCTION	1
	Conventions	1
	Range Prediction Philosophy	2
	Historical Notes	2
2.	RANGE EQUATIONS	4
	Radar Transmission Equation	4
	Maximum Range Equation	4
	Pulse Radar Equation	6
	Probabilistic Notation	7
	Range Equation for Automatic Detection	8
	Bistatic Radar Equation	9
	Equations in Practical Units	9
3.	DEFINITION AND EVALUATION OF RANGE FACTORS	10
	Transmitter Power and Pulse Length	11
	Antenna Gain	12
	Antenna Beamwidth	12
	Target Cross Section	13
	Wavelength (Frequency)	14
	Bandwidth and Matching Factors	14
4.	MINIMUM DETECTABLE SIGNAL-TO-NOISE RATIO	17
	Integration of Signals	18
	Evaluation of Probabilities	18
	Required Signal-to-Noise Ratio	20
	Detector Laws	29
	Curves for Visual Detection	42
	Other Detection Methods	44
5.	SYSTEM NOISE TEMPERATURE	46
	Antenna Noise Temperature	48
	Transmission-Line Noise Temperature	50
	Receiver Noise Temperature	50

6. PATTERN-PROPAGATION FACTOR 51

Flat-Earth Reflection 53
Rough-Surface Reflection Coefficient 57
Spherical-Earth Reflection 58
The Intermediate Region 63
Refraction and Coverage Diagrams 64

7. LOSS FACTORS 70

Antenna Pattern Loss 70
Atmospheric Absorption Loss 72
Collapsing Loss 82
Miscellaneous Losses 83
Integration Loss and Operator Loss 84
System Degradation Loss 84

8. JAMMING AND CLUTTER 85

Jamming 85
Range Equations for Noise Jamming 85
Clutter 86
Targets in Clutter 87

9. BLIP-SCAN RATIO AND CUMULATIVE PROBABILITY 88

Range Dependence of the Blip/Scan Ratio 89
Cumulative Probability and Operator Factor 90

10. ACCURACY OF RADAR RANGE PREDICTIONS 91

11. A SYSTEMATIC PROCEDURE FOR RANGE PREDICTION 93

12. ACKNOWLEDGMENTS 93

REFERENCES 99

APPENDIX 103

INDEX 147

PREFACE

The first edition of this report was published in 1962 as NRL Report 5868. (In turn, Report 5868 was preceded by NRL Memorandum Report 1106, dated 1960, and it in turn was preceded by a number of informal documents.) It was reprinted in 1963 with a few minor corrections and revisions. Part 2 was begun at that time, but it was never finished because of the pressure of other work. Part 1 has now been rewritten to incorporate new material and bring it up to date. Much of the new material is the result of applying the digital computer and machine plotting to radar detection problems.

This revision of Part 1 has taken precedence over completion of Part 2, and some of the material originally intended for Part 2 has now been incorporated into Part 1. Work on Part 2 continues.*

The principal revisions in the second edition of Part 1 are: addition of signal-to-noise-ratio curves for various probabilities of detection and for fluctuating as well as steady signals, discussion of the problem of curved-earth reflection-interference, extension of the antenna-noise-temperature curve to 100 GHz, change of the reference point for system-noise-temperature computation to the antenna output terminals (to conform to the new IEEE standard definition of antenna noise temperature), discussion of detection of targets in clutter, and updating of the material on reflection from a rough sea (citing experimental and theoretical material not previously included, although it had been previously published). Numerous minor revisions have been made which are intended to clarify discussions without changing their technical content.

*As this report goes to press, Part 2 has been completed and has been assigned NRL Report No. 7010.

ABSTRACT

This report extensively revises NRL Report 5868 of the same title and introduces updated material on many of the topics and extended treatment of others. The basic equation for pulse-radar maximum-range calculation is presented in a form convenient for numerical computation. Charts, graphs, tables, and auxiliary equations are presented for evaluation of the various factors in the range equation. Included are graphs for the required signal-to-noise ratio as a function of probability of detection, false-alarm probability, and number of pulses integrated, for both nonfluctuating and fluctuating (Swerling Cases 1 and 3) echoes. Also treated are the effects of receiver bandwidth, antenna and receiver noise, sea-reflection interference, refraction and absorption by the atmosphere, and various system losses. Standard definitions of range-equation quantities are given. The effects of jamming and clutter echoes are treated briefly, as are also cumulative probability of detection and accuracy of radar range prediction. A systematic procedure for range calculation, employing a work sheet, is presented.

PROBLEM STATUS

This is an interim report on the problem; work is continuing.

AUTHORIZATION

NRL Problem R02-55.101
Project RF 05-151-402-4011

Manuscript submitted May 8, 1969.

A GUIDE TO BASIC PULSE-RADAR MAXIMUM-RANGE CALCULATION

PART 1 — EQUATIONS, DEFINITIONS, AND AIDS TO CALCULATION

1. INTRODUCTION

This report presents the basic information required for calculating the maximum range of a conventional pulse radar. It is presented without detailed explanation or proofs, but references to sources of some of the information are given. Part 2 will contain more detailed information on some subjects that are less basic than those treated here in Part 1 and will contain derivations of some of the results presented here.

Although the basic physics governing the prediction of radar range has been well known since the earliest days of radar, the problems of evaluating some of the factors in the radar range equation are still not completely solved for all circumstances. Some of these problems pertain to the vagaries of electromagnetic wave propagation in the earth's atmosphere, and others are related to the statistical or probabilistic nature of the radar signal detection process, arising partly from the nature of the noise from various sources which competes with signals. There are also problems of definition of terms.

In this report these and other problems will be considered, and a method of predicting radar range in certain standard situations will be given. Insofar as possible, information will be given on how to extend this method to nonstandard situations.

The report applies primarily to conventional pulse radars in the 100 MHz to 100 GHz frequency range, especially those located at or near the earth's surface. However, much of the material is applicable to radars of other types. The word "basic" in the title refers to the emphasis on calculation for the simplest type of situation. Through most of this report it is assumed that the detection is based on discrimination between a signal and the ever-present receiver noise, without complications such as clutter echoes, jamming, or interference by other signals. Normal environmental conditions are assumed (no precipitation and no abnormal refraction). The target is assumed to be a point target (small in size compared to the radar's resolution cell) and to be moving at a speed that does not result in appreciable movement during an integration period. Near the end of this report elementary theory will be given for detection of targets in clutter and in the presence of jamming. Further details will be discussed in Part 2.

Conventions

The maximum detection range of a radar depends partly on conditions of the environment — geophysical factors; these are not controllable by the radar designer and are subject to unpredictable variation. Examples are atmospheric refraction and absorption of radio waves, noise radiation by extraterrestrial sources such as the sun and the galaxy, and reflection from the earth's surface, which varies in its reflective properties from place to place and, expecially in the case of the ocean, from time to time. Consequently a prediction of radar maximum range cannot be guaranteed to be accurate in the exact sense. Even if the geophysical factors were invariant and exactly known, prediction of maximum range would still not be exact because of the statistical nature of the detection process for signals embedded in a background of electrical noise.

The signal-in-noise problem is amenable to a well-established statistical analysis, which leads to the concepts of probability of detection and probability of false alarm. But the statistics of variation of the geophysical phenomena are not sufficiently well established to allow a statistical treatment, at least not with the degree of refinement possible for the signal-in-noise problem. Therefore, to make radar maximum range calculations at all, it is necessary to adopt *conventions* for the effects of the relevant geophysical phenomena.

A convention, in simplest terms, is a generally accepted assumption for the value of some variable factor. An example is the value 6370 km for the radius of the earth. This is a convention because the earth is not a perfect sphere; its approximate surface curvature has different radii at different latitudes. The 6370-km value is not even a statistically mean value. Rather, it is a round number that lies somewhere between the maximum and minimum values observed and that is not unreasonable as a typical value. Thus conventions are physically realistic and convenient but statistically imprecise. They contain an element of arbitrariness. Nevertheless, they have great value from two points of view. First, they permit calculations to be made which are physically realistic even though imprecise. Second, for two or more different systems they permit precise comparison.

Ideally, conventions should be promulgated by some recognized standards organization, preferably one that is internationally recognized. Unfortunately this has been done for only a few of the conventions needed in radar performance calculation. Other conventions have no formal status but are widely accepted by the engineering profession. Where such conventions are known to exist, they are followed in this report. Where they do not, but where they are needed, arbitrary conventions are adopted. Wherever possible the range of variation likely to be encountered in nature is indicated.

Range Prediction Philosophy

Since environmental conditions are variable and to some extent unpredictable, a range prediction based on a conventional assumption will not always be accurately confirmed by individual experimental results. This conclusion is further indicated by the basically statistical character of the signal-detection process, which means that a range prediction is not likely to be verified exactly by the result of a single experiment even if all the quantities in the range equation are known exactly, including those determined by the environment. Finally, there is practically some indeterminacy associated with all of the range equation factors, even those measurable in the laboratory. Therefore, range prediction is not an exact science.

Nevertheless, calculations to predict radar range are useful. However inexact they may be on an absolute basis, they permit meaningful comparisons of the relative performance of competing designs, and they indicate the relative improvement that will result from a design improvement. They are therefore a powerful tool for the system designer. Moreover, despite the inexactness of predictions, the error can be made small enough so that the calculated range is a reasonable indication of performance to be expected under average environmental conditions. The predicted range is a figure of merit for a radar system, though not necessarily a complete one, since other factors such as target-position measurement accuracy, data rate, reliability, serviceability, size, weight, and cost may also be important.

Historical Notes

Possibly the first comprehensive treatise on radar maximum-range prediction was that of Norton and Omberg (1), issued as a U.S. Army Signal Corps report in 1943 and

published as a paper in the Proceedings of the IRE in 1947. It presented a fairly detailed range equation and contained information on evaluating some of the more problematical factors, such as multipath interference and minimum-detectable signal, within the limitations of the then-available knowledge. The signal-detection process was assumed to be based on visual observation of a cathode-ray-tube display. The antenna was assumed to searchlight the target. Statistical aspects of signal detection were not considered.

D. O. North, in a classic report published with a military security classification in 1943 (2), outlined the basic theory of a statistical treatment of signal detection. This report was later republished in the Proceedings of the IEEE, but not until 1963. He introduced the concepts that are now called *probability of detection* and *false-alarm probability*, and he clearly delineated the role of integration in detection of pulse signals. This report also introduced the concept of the *matched filter*, a contribution for which it had achieved some recognition prior to 1963, but its contribution to signal-detection theory was virtually unrecognized by radar engineers generally until the report was republished 20 years later.

In a famous report first published in 1948 (3) and also republished in IRE Transactions on Information Theory in 1960, J. I. Marcum extensively developed the statistical theory of detection, with the aid of machine computation, employing the basic concepts of North's report, which he referenced. He computed probabilities of detection as a function of a range parameter related to signal-to-noise ratio for various numbers of pulses integrated and for various values of a false-alarm parameter which he designated *false-alarm number*. He employed this type of computation to study the effects of various amounts and kinds of integration, different detector (rectifier) laws, losses incurred by collapsing one spatial coordinate on the radar display, and various other effects. His results are presented as curves for probability of detection as a function of the ratio of the actual range to that at which the signal-to-noise ratio is unity on the assumption that the received signal power is inversely proportional to the fourth power of the range. Since this proportionality holds only for a target in free space, application of Marcum's results is sometimes complicated by this mode of presentation.

Marcum considered only steady signals (target cross section not varying during the period of observation), and most of his results assume the use of a square-law detector. Robertson (4) has published exceptionally detailed and useful steady-signal results applicable to the linear-rectifier detector, which is the type of detector almost universally used. The square-law-detector results are also useful, however, because they differ but little from the linear-detector results. Swerling (5) extended Marcum's work to include the case of fluctuating signals. His report was also republished in IRE Transactions on Information Theory, in 1960. Fehlner (6) has recomputed Marcum and Swerling's results and presented them in the more useful form of curves with signal-to-noise power ratios as the abscissas. The fluctuating signal problem has been further treated by Kaplan (7), Schwartz (8), Heidbreder and Mitchell (9), Bates (10), and others.

Hall (11) published in 1956 a comprehensive paper on radar range prediction in which the concepts of probability of detection, false-alarm probability, and the relative effects of predetection and postdetection integration were considered, and the effects of scanning the antenna beam. The range equation was formulated in terms of an ideal (matched filter) utilization of the available received signal power, with loss factors to account for departures from the ideal. This paper constituted a survey and updating of the subject.

A paper further updating the subject was published by Blake (12) in 1961. It applied recent advances in system-noise-temperature calculation, atmospheric absorption, plotting of coverage diagrams for a realistic refractive-index model, and multipath interference calculation. It was based on the material of NRL Memorandum Report 1106, issued in 1960. NRL Report 5868 (13) presented the same material in greater detail.

Contributions to the subject of range prediction have also been made by many others, far too numerous to name. Only the major contributions can be recognized in this brief history. Special mention should be made, however, of the many contributions made by two volumes of the Radiation Laboratory Series, volume 13 edited by Kerr (14) and volume 24 edited by Lawson and Uhlenbeck (15). Much use is made in this report of results originally published in those volumes.

2. RANGE EQUATIONS

Radar Transmission Equation

The basic transmission equation for radar is given here in the form derived by Kerr (14):

$$\frac{P_r}{P_t} = \frac{G_t G_r \sigma \lambda^2 F_t^2 F_r^2}{(4\pi)^3 R^4} . \tag{1}$$

The symbols are defined as follows:

P_r - received signal power (at antenna terminals),

P_t - transmitted signal power (at antenna terminals),

G_t - transmitting antenna power gain,

G_r - receiving antenna power gain,

σ - radar target cross section,

λ - wavelength,

F_t - pattern-propagation factor for the transmitting-antenna-to-target path,

F_r - pattern-propagation factor for target-to-receiving-antenna path,

R - radar-to-target distance (range).

(Actually this equation is not quite identical to Kerr's; he assumed that the same antenna is used for transmission and reception, so that $G_T G_r$ becomes G^2 and $F_t^2 F_r^2$ becomes F^4.) The only factors in the equation that may require explanation are the pattern-propagation factors F_t and F_r. Factor F_t is defined as the ratio of the field strength E at the target position to the field strength E_0 which would exist at the same distance from the radar in free space and in the antenna-beam maximum-gain direction. F_r is analogously defined. These factors account for the possibility that the target is not in the beam maxima (G_t and G_r are the gains in the maxima) and for any propagation effects that would not occur in free space, such as absorption, diffraction and shadowing, certain types of refraction effects, and multipath interference, to mention the most common ones. Detailed definitions of these and other range-equation factors will be given in Sections 3 through 7.

Maximum Range Equation

Equation (1) is not a range equation as it stands, although it can be rewritten in the form

$$R = \left[\frac{P_t G_t G_r \sigma \lambda^2 F_t^2 F_r^2}{(4\pi)^3 P_r} \right]^{1/4} , \tag{2}$$

which says that R is the range at which the received echo power will be P_r if the transmitted power is P_t, the target size is σ, and so forth. It becomes a maximum-range equation by the simple expedient of attaching subscripts to P_r and R, so that they become $P_{r(\min)}$ and $R_{(\max)}$. That is, when the value of P_r in Eq. (2) is the minimum detectable value, then the corresponding range is the maximum range of the radar. However this is a rudimentary and unsophisticated maximum-range equation. In fact the very term "maximum range" has no clear meaning without certain qualifying words or phrases, although it is a useful expression for conversational purposes.

A first step toward a more useful equation is replacement of $P_{r(\min)}$ by a more readily evaluated expression. This expression is obtained by first defining the signal-to-noise power ratio:

$$S/N = \frac{P_r}{P_n} , \tag{3}$$

where P_n is the power level of the noise in the receiving system, which determines the minimum value of P_r that can be detected. This noise power, in turn, can be expressed in terms of a receiving system noise temperature T_s:

$$P_n = kT_sB_n , \tag{4}$$

where k is Boltzmann's constant (1.38×10^{-23} watt-second per degree Kelvin) and B_n is the noise bandwidth (hertz) of the receiver predetection filter. (These quantities will be defined more completely in Sections 3 and 5.) Therefore

$$P_r = (S/N)\, kT_sB_n . \tag{5}$$

This expression may now be substituted for P_r in Eq. (2). It is advantageous to do so, because, as will be shown, $(S/N)_{\min}$ (or other quantities related to it) can be directly evaluated more readily than can $P_{r(\min)}$, and so also can T_s and B_n.

Sometimes the range equation is written in terms of a system noise factor (noise figure) F_s instead of a system noise temperature. The relationship between them is $F_s = T_s/T_0$, where $T_0 = 290^\circ$K is the standard reference temperature established by the IEEE for noise-factor definition (16). This system noise factor is not, however, an IEEE-defined quantity, although it was introduced by D. O. North (17) in 1942. The term "system noise temperature," though widely used, is also not found in IEEE standard definitions (16), but the concept is there defined as a quantity called the "operating noise temperature (of a system)."

The system noise factor (called by North the operating noise factor) is different in concept from the more familiar noise factor of a two-port transducer F_n. The relationship between the latter factor and transducer input noise temperature T_e is $F_n = (T_e/T_0) + 1$. If the terminals of a receiver whose noise factor is F_n are connected directly to the antenna terminals, or if the transmission line is lossless, the relationship between the system and receiver noise factors is (as was shown by North) $F_s = (T_a/T_0) + F_n - 1$, where T_a is the antenna noise temperature discussed in Section 5. The two noise factors are then equal if $T_a = T_0$. The minimum possible value of F_n is 1 (perfect receiver), but that of F_s is zero (noise-free receiver and noise-free antenna and environment).

Another slight modification that is convenient is to define P_t as the transmitter power output rather than (as in Eq. (1)) the power at the terminals of the transmitting antenna. With this changed definition, P_t must be replaced by P_t/L_t, where L_t is a loss factor defined as the ratio of the transmitter power output to that actually delivered to the antenna ($L_t \geqq 1$). It will later prove convenient to introduce additional loss factors; all of them are basically required to compensate for redefinition of certain quantities as compared with the definitions that apply for Eq. (1). These loss factors are multiplicative; that is, if there are three loss factors L_1, L_2, and L_3, they can be represented by a single loss factor $L = L_1L_2L_3$. This generalized loss factor is placed in the denominator of the range equation.

The resulting maximum range equation is

$$R_{max} = \left[\frac{P_t G_t G_r \sigma \lambda^2 F_t^2 F_r^2}{(4\pi)^3 (S/N)_{min} k T_s B_n L}\right]^{1/4} . \tag{6}$$

Pulse Radar Equation

Equation (6) does not specify the nature of the transmitted and received signals — they may be CW, amplitude or frequency modulated, or pulsed. Because of the special importance of pulse radar, it is justifiable to modify the equation in certain ways that are advantageous for this special case. The modified equation is then restricted to pulse radars.

If the radar pulse is of duration (length) τ, it is demonstrable that the detectable signal power will have its minimum value when the receiver bandwidth has a particular value $B_{n(opt)}$ of the order of the reciprocal of the pulse length (2,15,18). That is, in general

$$B_{n(opt)} = \alpha/\tau , \tag{7}$$

where α is of the order of 1. Following Omberg and Norton (1), a visibility factor is defined by

$$V = \frac{P_r \tau}{k T_s} = \frac{E_r}{N_0} , \tag{8}$$

which is the ratio of the received pulse energy E_r to the noise power per unit bandwidth (spectral density), N_0. From Eqs. (5) and (8) it is readily apparent that the product $(S/N)B_n$ in Eq. (6) can be replaced by the quotient V/τ, provided that now V is understood to mean V_{min}. Next, it is convenient to define V_0 as the value of V_{min} corresponding to $B_n = B_{n(opt)}$. Obviously as B_n is varied, V_{min} will have its smallest value when $B_n = B_{n(opt)}$. In general,

$$V_{min} = V_0 C_B , \tag{9}$$

where $C_B \geqq 1$ is a bandwidth correction factor. Making these various substitutions yields the range equation for pulse radar:

$$R_{max} = \left[\frac{P_t \tau G_t G_r \sigma \lambda^2 F_t^2 F_r^2}{(4\pi)^3 k T_s V_0 C_B L}\right]^{1/4} \tag{10}$$

Evaluation of the factors α and C_B will be discussed in Section 3. (Note that α does not appear explicitly in the range equation; its only effect is in determination of C_B.)

Among the virtues of this form of the range equation is its demonstration of the significance of the transmitted pulse energy $P_t \tau$ as the determining factor in radar range performance, rather than the pulse power P_t by itself. This conclusion was emphasized by Omberg and Norton (1) by writing E_t in place of $P_t \tau$ in their range equation.

North (2) reached the same conclusion in his analysis and noted the fundamental importance of the ratio $P_r \tau / kT_s = E_r / N_0$ (here called V_0 as it was by Norton and Omberg). Lawson and Uhlenbeck (15) have also used this ratio as a logical parameter for presenting the results of their minimum-detectable-signal studies (designating it S_{min}).

The pulse energy is the significant quantity for single-pulse detection, and also when pulses are integrated if the integration is done for a fixed number of pulses. If integration is done for a fixed length of time, however, then the transmitted average power is the determining factor; it is the pulse energy multiplied by the pulse repetition frequency.

North also showed that the signal-to-noise power ratio at the output of the predetection filter (e.g., IF amplifier) has its maximum possible value when the filter characteristic is matched to the pulse waveform (matched filter) and that this value is equal to E_r / N_0. In some of the literature it is stated that the matched-filter output signal-to-noise ratio is $2E_r / N_0$, but this result is based on definition of signal power as that not only at the maximum of the pulse waveform but also at the peak of an RF cycle. North's definition, based on the power averaged over an RF cycle, is appropriate for the case of a pulsed carrier signal in a background of band-limited thermal noise and is the one ordinarily used by radar engineers. In particular it is the definition used in computing the signal-detectability curves of Figs. 4 through 7.

This concept of the significance of the pulse energy also provides a simple answer to the question of what pulse length to use in the radar equation if the radar employs pulse compression, in which a coded pulse waveform of relatively long duration is transmitted, and is compressed to a short pulse on reception. In fact, either the long transmitted pulse length or the short compressed pulse length can be used, provided that an appropriate value is used for P_t so that the product $P_t \tau$ is equal to the transmitted pulse energy.

Probabilistic Notation

It has been mentioned (Section 1) that the radar signal detection process is basically probabilistic or statistical in nature. This fact results from the nature of the noise voltage that is always present in the receiver circuits. This voltage is randomly varying or fluctuating, and when it is intermixed with a pulse signal, it becomes impossible to tell with certainty whether a momentary increase of the receiver output is due to a signal or a chance noise fluctuation. However, it is possible to define probabilities for these two possibilities and to discuss the detection process in terms of them, in a quantitative manner. Thus the probability that the signal, when present, will be detected is called the *probability of detection* P_d, and the probability that a noise fluctuation will be mistaken for a signal is called the *false alarm probability* P_{fa}.

The notations R_{max} and $P_{r\,(min)}$ can then be replaced by more precise notation, using subscripts to denote the applicable values of P_d and P_{fa}. However, the P_{fa} subscript is ordinarily suppressed, though implied. Thus R_{50} denotes the range for 0.5 (50%) probability of detection and some separately specified false-alarm probability.

If the target cross section σ fluctuates, as often happens with moving targets, and if σ in the range equation is defined as the average value, then if the visibility factor is given a particular value such as $V_{0(90)}$ determined on a steady-signal basis, the range that will be calculated from Eq. (10) will *not* be, in general, R_{90}. In other words, $V_{0(90)}$ for a steady target is not the same as $V_{0(90)}$ for a fluctuating target. As mentioned in the historical notes (Section 1), this problem has been analyzed by Swerling (5) and others (6-10), and curves have been calculated that allow determining the appropriate value of V_0 for the fluctuating-signal case.

Sometimes the fluctuating target cross section is defined in terms of a percentile value; e.g., σ_{90} denotes the value of σ that is exceeded 90% of the time. It fortuitously happens (13) that if the cross section fluctuates and σ_{50} is used in Eq. (10), then the steady-signal value of $V_{0(50)}$ will result approximately in R_{50}. However, this is a special case, and the procedure cannot be applied for other probabilities of detection. Thus in general when the target cross section fluctuates, σ in the radar range equation is defined as the average value, and V_0 is then assigned the value appropriate to fluctuating signals.

Range Equation for Automatic Detection

Detection is said to be automatic if the decision concerning presence or absence of a received signal is made by a purely physical device without direct human intervention. Such a device, described by North (2), establishes a threshold voltage level (for example, by means of a biased diode). If the processed (e.g., integrated) receiver output exceeds the threshold (as evidenced by diode current flow), some mechanism is actuated to indicate this fact in an unequivocal fashion — by lighting a light, ringing a bell, or more generally by setting a bit equal to 1 in a binary data channel wherein a zero corresponds to no-signal. (Various additional consequences may then of course automatically ensue.) The analysis of radar detection then becomes a problem in statistical decision theory, and this analysis has been extensively pursued in terms of the probability of detection (probability that the voltage will exceed the threshold when a specified nonzero signal-to-noise ratio exists) and of the probability of false alarm (probability that the voltage will exceed the threshold when in fact no signal is present).

For the ordinary radar situation the signal-to-noise ratio that must be used for this analysis is that which exists at the input terminals of the detector,* corresponding to the output of the predetection filter. In the derivation (14) of Eq. (1), P_r refers to the received signal power at the antenna. Consequently (S/N) in Eq. (6) and V_0 in Eq. (10) are also referred to the antenna terminals. These facts must be reconciled if the equation is to be used for an automatic-detection radar.

The relationship of the signal-to-noise ratio in one part of a cascade system to that in another is a subject that requires careful definition of terms if confusion is to be avoided. A distinction must be made between the ratio of the signal power at a point to the actual noise power at that point and the ratio of the signal power to the equivalent noise. The latter concept will always be meant here. Equivalent noise at a point means,

*A note on meanings of the words "detector" and "detection" is desirable here. In radio usage, a detector has come to mean either a frequency converter (e.g., superheterodyne first detector) or a demodulator (often the second detector of a superheterodyne receiver, which is usually a linear rectifier). This second meaning is intended here. An automatic detector, however, means a decision-making device, as described above — a device that replaces, for example, the human observer of a cathode-ray-tube display. In the following discussion the meaning should be evident from the context. Where confusion might otherwise result, the term detection-decision device may be used to denote an automatic detector.

in effect, the output noise power of the predetection filter divided by the power gain between that point and the output.

With this definition, if the filter is of such a nature that it does not change the signal waveform, the signal-to-noise ratio will not change from point to point in the cascade. In general, however, the filter does change the signal waveform, and therefore the signal-to-noise ratio is different at the input and output of the receiving system.

Fortunately, however, as has been discussed following Eq. (10), if a matched filter is used, the output signal-to-noise power ratio will be equal to the quantity V_0 in the range equation. Therefore, Eq. (10) can be used for an automatic-detection radar if V_0 is understood to be the value that applies when a matched filter is used and C_B is a correction factor that takes into account not only the bandwidth of the filter but its complete transfer characteristic in relation to the pulse waveform. This matter will be discussed further in Section 4.

Bistatic Radar Equation

The foregoing equations assume that the transmitting and receiving antennas are at the same location (monostatic radar). A bistatic radar is one for which the two antennas are widely separated, so that the distance from the transmitting antenna to the target is not necessarily the same as the distance from the target to the receiving antenna. Moreover, since the signal reflected from the target to the receiving antenna is not directly backscattered as it is for monostatic radar, the target cross section is not usually the same (for a given target viewed in a given aspect by the transmitting antenna). Thus a *bistatic radar cross section* σ_b is defined. The symbol σ in the preceding equations implies the monostatic cross section. The range equation for a bistatic radar is obtained from the foregoing monostatic equations by simply replacing σ by σ_b, and by replacing R by $\sqrt{R_t R_r}$, where R_t is the distance from the transmitting antenna to the target and R_r is the distance from the target to the receiving antenna.

Equations in Practical Units

The equations that have been given are valid when a consistent system of units is used, such as the rationalized mks system. In many applications, however, it is convenient or necessary to employ "mixed" units, such as nautical miles for range, square meters for target cross section, kilowatts for transmitter power, microseconds for pulse length, etc. Moreover, it is usually more convenient to express the wavelength λ in terms of the equivalent frequency in megahertz. It is also desirable to combine all the numerical factors and the various unit-conversion factors into a single numerical constant. For a particular system of mixed units the following equations are obtained from Eqs. (6) and (10):

$$R_{max} = 726.8 \left[\frac{P_{t\,(kW)} G_t G_r \sigma \; F_t^2 F_r^2}{f_{MHz}^2 T_s (S/N)_{min} B_{kHz} L} \right]^{1/4}, \tag{11}$$

$$R_{max} = 129.2 \left[\frac{P_{t\,(kW)} \tau_{\mu sec} G_t G_r \sigma \; F_t^2 F_r^2}{f_{MHz}^2 T_s V_0 C_B L} \right]^{1/4} \tag{12}$$

The subscript notation R_{max} is now meant to imply the range corresponding to specified detection and false alarm probabilities. For these equations the range is given in

international nautical miles. (One international nautical mile is exactly 1852 meters.) The target cross section is in square meters, transmitter power in kilowatts, pulse length in microseconds, frequency in megahertz, system noise temperature in degrees Kelvin, and bandwidth in kilohertz. (All other quantities are dimensionless.)

If the range is desired in units other than nautical miles, in place of the numerical factors 726.8 and 129.2 the following factors should be used:

Range Units	Factor, Eq. (11)	Factor, Eq. (12)
Statute miles	836.4	148.7
Kilometers	1346	239.3
Thousands of yards	1472	261.7
Thousands of feet	4416	785.0

A decibel-logarithmic form of the range equation is often useful. The equation of this type corresponding to Eq. (12) is

$$R_{max} = \text{antilog}\left\{2.111 + \frac{1}{40}\left[10 \log P_{t\,(kW)} + 10 \log \tau_{\mu sec} + G_{t\,(dB)} + G_{r\,(dB)} + 10 \log \sigma - 20 \log f_{MHz} - 10 \log T_{s\,(°K)} - V_{0\,(dB)} - C_{B\,(dB)} - L_{dB} + 20 \log F_t + 20 \log F_r\right]\right\} \text{ naut mi}, \quad (13)$$

where all logarithms are to the base 10. Equation (11) can be converted to this form by substituting the numerical factor 2.861 for 2.111, deleting the terms $10 \log \tau$, $V_{0\,(dB)}$ and $C_{B(dB)}$, and inserting in their place the terms $(S/N)_{dB}$ and $10 \log B_{kHz}$. To obtain the range in other units of distance with these equations, use the following numerical factors in place of 2.861 (for the logarithmic form of Eq. (11) or in place of 2.111 in Eq. (13)):

Range Units	Log Form of Eq. (11)	Eq. (13)
Statute miles	2.922	2.172
Kilometers	3.129	2.379
Thousands of yards	3.168	2.418
Thousands of feet	3.645	2.895

3. DEFINITION AND EVALUATION OF RANGE FACTORS

There is an element of arbitrariness in the definitions of most of the factors of the radar range equation, and for some of them more than one definition is in common use. Since the definitions in these cases are arbitrary, one definition is in principle as good as another. However, once a definition has been chosen for one factor, the freedom of choice no longer exists for one or more of the others. They are interdependent, and mutual compatibility is essential. A set of definitions will be given here that are believed to be mutually compatible. Also, information needed for evaluating these factors will be given insofar as is practicable. Certain range-equation factors that present special problems will be considered at greater length in subsequent sections of the report.

Transmitter Power and Pulse Length

The radar transmission equation, from which all of the subsequent range equations are derived, is an equation for the ratio P_t/P_r. Consequently, the most basic requirement on the definition of P_t is that it agree with the definition of P_r. For a CW radar, the power (averaged over an RF cycle) is constant, and there is no definition problem. For a pulse radar, both P_t and P_r are usually defined as the pulse power, which is the average power during the pulse. More precisely

$$P_t = \frac{1}{\tau} \int_{-T/2}^{T/2} W(t)\, dt \ , \tag{14}$$

where $W(t)$ is the instantaneous power. The definition of $W(t)$, however, excludes spikes, tails, and any other transients that are not useful for radar detection. T is the pulse period (= 1/prf, where prf is the pulse repetition frequency in pulses per second). Because of the exclusion of nonuseful portions of the waveform (as it exists at the transmitter output terminals), P_t as thus defined may be called the effective pulse power.

In the transmission equation (Eq. (1)) P_t and P_r are the transmitted and received powers at the antenna terminals. If P_t is instead defined at the transmitter output terminals, any loss between these terminals and the antenna must be expressed as a loss factor L_t, and the quotient P_t/L_t substituted for P_t, as has been mentioned in Section 2. This definition of P_t will henceforth be used, because in system specifications it is the power output of the transmitter that is usually quoted.

The pulse power P_t and the pulse length τ must be defined so that their product is the pulse energy. Any definition of τ will produce this result if the same definition is used in the range equation and in Eq. (14). The customary definition, and the one recommended here, is the time duration between the half-power points of the power envelope of the RF pulse (0.707-voltage points). For some purposes, such as analyzing the range resolution or accuracy, arbitrary definition of the pulse length is not permissible. But the half-power definition is convenient and acceptable for use in the range equation.

Pulse power is often measured by measuring the average power (for example, by a calorimetric method) and dividing this figure by the duty factor, which is the product of the pulse length and the pulse repetition frequency (prf). The definition of pulse length must of course be the same in this procedure as it is in the range equation.

The range equation can be written, as was mentioned in Section 2, with the product $P_t\tau$ replaced by the pulse energy E_t. The more detailed notation is used here because, for ordinary pulse radars, P_t and τ are usually given explicitly and E_t is not. However, the use of E_t in the equation has the advantage of avoiding the problems of defining P_t and τ and is especially useful when complicated waveforms (e.g., pulse bursts) are transmitted.

The equation can also be written with the transmitted average power (which for simple pulse radars is the product of pulse power, pulse length, and pulse repetition frequency) in the numerator, if coherent integration for a fixed integration time is assumed. In the average-power formulation, the integration time (assumed to be long compared to the interpulse period) also appears in the numerator, and the value of V_0 used is that which would apply if detection were based on observation of a single pulse, or signal sample. The average-power formulation is especially useful for CW or pulse-doppler radars.

Antenna Gain

The gains G_t and G_r are defined as the power gains of the antennas in the maximum gain direction. The maximum power gain of an antenna is equal to its directivity (maximum directive gain) multiplied by its radiation efficiency (19). The directivity is defined (20) in terms of the electric-field-intensity pattern $E(\theta,\phi)$ by the expression

$$D = \frac{4\pi E_{\max}^2}{\int_0^{2\pi}\int_0^{\pi} E^2(\theta,\phi)\,\sin\theta\,d\theta d\phi}, \tag{15}$$

where θ and ϕ are the angles of a spherical coordinate system whose origin is at the antenna and $E_{\max}$ is the value of E in the maximum-gain direction.

The radiation efficiency, defined in terms of the transmitting antenna, is the ratio of the power delivered by the transmitter at the antenna terminals to the total power actually radiated (including minor-lobe radiation). In terms of the receiving antenna it is the ratio of the total signal power extracted from the incident field by the antenna with a matched load impedance to the signal power actually delivered to such a load. The reciprocal of the radiation efficiency is the antenna loss factor L_a, which plays a part in the calculation of antenna noise temperature (Section 5).

Measured antenna gains are usually power gains, while gains calculated from pattern measurements or theory are directive gains. If the antenna gain figures supplied for use in the range equations are directive gains, they must be converted to power gains by dividing them by the appropriate loss factors. For many simple antennas the ohmic losses are negligible, and the power gain and the directive gain are virtually equal. However, this is by no means a safe assumption in the absence of specific knowledge.

If separate transmitting and receiving antennas are used, and if their maximum gains occur in different directions, or if appreciable angular motion of the target occurs between the instants of transmission and reception, appropriate correction is made by means of the pattern factors f_t and f_r contained in the pattern-propagation factor F to be discussed in Section 6.

Antenna Beamwidth

The beamwidth of the antenna does not appear explicitly in the range equations, but it does affect the range calculation through its effect on the number of pulses integrated when the antenna scans. The conventional definition is the angular width of the beam between the half-power points of the pattern. "Pattern" is used here in the usual sense, for one-way transmission — not the "two-way" pattern that would be measured by plotting the echo signal received from a stationary target (constant cross section) by a radar using the same antenna for transmitting and receiving as the antenna scans past the target.

If a radar target, as viewed from the radar antenna, has an angular dimension that is appreciable compared to the beamwidth, the target cross section σ becomes a function of the beamwidth (see Section 8). For computing σ in this case, a special definition of beamwidth is needed, in principle (14, p. 483). For practical work, however, negligible error results from using the half-power beamwidth in this application.

Target Cross Section

The definition of radar target cross section that applies for use in the foregoing radar range equations is given by Kerr (14), and the reader is referred to that source for a detailed discussion of the subject. Here mention will be made of a few aspects of the definition that are of particular significance to the range prediction problem. Targets may be classified as point targets and distributed targets. A point target is one for which the maximum lateral separation of significant scattering elements is small compared to the length of the arc intercepted by the antenna beam (which at distance R from the antenna is R times the beamwidth in radians), and for which the maximum radial separation of scattering elements is small compared to the range extent of the pulse (which is $c\tau/2$ where c is the speed of wave propagation in free space, 3×10^5 km/sec, and τ is the pulse duration in seconds). Most of the targets for which range prediction is ordinarily of interest are point targets, such as aircraft at appreciable distances from the radar. However, range predictions for distributed targets are sometimes wanted; for example the moon is a distributed target if the radar beamwidth is comparable to or less than 0.5 degree or if the pulse length is less than about 11.6 milliseconds. A rainstorm is another example of a distributed target. Often, distributed targets are of interest because echoes from them tend to mask the echoes from the point targets whose detection is desired. In this context, distributed-target echoes are called clutter echoes. (See Section 8.) (Echoes from rain may be regarded as clutter when they interfere with aircraft or other point-target detection, but they are themselves the signals of prime interest for weather radar.)

The radar range equation is derived initially for a point target, and when it or the subsequent equations derived from it are used to predict the range for distributed targets, complications arise. In many cases, however, the point-target equation can be used by using a suitable effective value of σ (Section 8).

The cross section of any irregular-shaped target is a function of the aspect angle from which it is viewed by the radar and of the polarization of the radar electromagnetic field. Therefore, to be wholly meaningful a radar range prediction for a specific target, such as an aircraft, must stipulate the target aspect angle assumed and the polarizations employed. Ordinarily, the nose aspect of an aircraft (approaching target) is of principal interest. Tabulations of radar cross section measurements of aircraft sometimes give nose, tail, and broadside values. If the values are obtained from dynamic (moving-target) measurements, they are then usually time averages of fluctuating values; otherwise they are static values for a particular aspect.

Because of the wide variation of cross section values of real targets, the range performance of a radar system is often stated for a particular target-cross-section assumption. A favorite value for many applications is 1 square meter. This represents the approximate cross section of a small aircraft, nose aspect (although the cross sections for different "small" aircraft may range from less than 0.1 square meter to more than 10 square meters). Radars are often performance tested by using a metallic sphere, sometimes carried aloft by a free balloon, as the target, because the cross section can be accurately calculated and does not vary with the aspect angle or the polarization.

A special definition problem arises when the target is large enough to be nonuniformly illuminated by the radar. A ship, for example, may be tall enough so that the pattern-propagation factor F has different values from the water line to the top of the mast. Solutions to this problem are discussed by Kerr (14).

Since the instantaneous cross section of a target is a function of the aspect angle, targets that are in motion involving random changes of aspect will have cross sections that fluctuate randomly with time, as was mentioned in Section 2. This fluctuation must

be taken into account in the calculation of probability of detection. As was mentioned in Section 2, when σ fluctuates the value to be used in the range equation is ordinarily the time average, because the signal-detectability curves for fluctuating signals (to be presented as Figs. 6 and 7) will be based on that definition. For some purposes, however, the percentile values are useful, as discussed in Sections 2 and 9.

Wavelength (Frequency)

There is ordinarily no problem in definition or evaluation (measurement) of the frequency to be used in the radar range equation. However, some radars may use very large bandwidth or may change frequency on a pulse-to-pulse basis, so that a question can exist as to the value to be used for predicting range. The presence of λ (or f) in the range equations makes it clear that the range can be frequency dependent, but the exact nature of the frequency dependence is not always obvious, because other factors in the range equation are sometimes implicitly frequency dependent. Therefore an analysis of how the range depends on frequency can be quite complicated, and the answer depends on what factors are regarded as frequency dependent and which ones are held constant as the frequency is changed. (For example, most antennas have gain that is strongly frequency dependent, but some types are virtually frequency independent over a fairly wide frequency band.)

Bandwidth and Matching Factors

The frequency response width (bandwidth) of the receiver selective circuits appears explicitly in Eqs. (4) through (7), but it is an implicit factor in the other range equations as well, through the factor C_B. From Eq. (4) it is clear that B_n directly affects the noise level in the receiver output. In general it also affects the signal but not necessarily in the same manner that the noise is affected, since the signal spectrum is not usually uniform. It turns out that there is a value of B_n that optimizes the output signal-to-noise ratio, as indicated by Eq. (7), and this optimum bandwidth is of the order of $1/\tau$. This statement can be applied to pulse compression radars as well as to simple pulses if τ is taken as the compressed value.

Since the range equation given as Eq. (6) and those subsequently derived from it incorporate the assumption of Eq. (4), either explicitly or implicitly, the definition of B_n must conform to this assumption. It has been mentioned (Section 2) that a particular definition known as the noise bandwidth is appropriate in the radar range equation. This definition, due to North (17), is

$$B_n = \frac{1}{G_0} \int_0^\infty G(f)\, df \,, \tag{16}$$

where G_0 is the gain at the nominal radar frequency, and $G(f)$ in principle describes the frequency response of the receiver predetection circuits (overall gain from antenna to detector). In practice it is usually equivalent to the receiver IF filter response. With this definition of B_n the noise power at the detector will be $kT_sB_nG_0$. The definition specifies $G(f)$ as the response characteristic of the predetection circuits only, because it is demonstrable that the video (postdetection) bandwidth should be equal to at least half the predetection bandwidth for best results and that if it is of this width or wider, its exact width has little or no effect on signal detectability.

It is common practice, however, to measure predetection receiver bandwidth as the value between half-power points of the frequency response curve. Fortunately this value

is usually very close to the true noise bandwidth, though the exact relationship to the two bandwidths depends on the shape of the frequency response characteristic (15, p. 177).

The bandwidth correction factor C_B in Eqs. (10), (12), and (13) accounts for the fact that if B_n is not the optimum value, a larger value of V is required, whereas V_0 is defined as the optimum-bandwidth value. Therefore $C_B \geq 1$. Haeff (18), from data obtained in signal-detection experiments during World War II at the Naval Research Laboratory, devised the empirical expression

$$C_B = \frac{B\tau}{4\alpha}\left(1 + \frac{\alpha}{B\tau}\right), \tag{17}$$

where B is the bandwidth, τ is the pulse length, and α is the product of τ and $B_{opt} = 1/\tau$, that is, $\alpha = 1$. However, on the basis of experiments at the MIT Radiation Laboratory, conducted somewhat later, it was concluded (15) that $\alpha \cong 1.2$ for detection of signals by visual observation of cathode-ray-tube displays. This value has subsequently been widely used for determining B_{opt} in radar design, and for computing C_B in radar range prediction (11,12). However, North, in a private communication to the author in 1963, suggested that the $\alpha = 1.2$ figure may be based on a misinterpretation of the Radiation Laboratory data. He points out that an analysis of the minimum detectable signal power as a function of the product $B\tau$, employing the theory of his 1943 report (2), results in an unsymmetrical curve if the observer's "mental range gate" is assumed adjusted to an optimum value for each $B\tau$ value. The asymmetry is in such a direction that the experimental data, if plotted with a forced symmetry, would seem to have its minimum at too high a value. Consequently it is possible that the value of α for human observation of visual displays is much closer to 1 than reported by Lawson and Uhlenbeck. Fortunately, for the usual range of values of $B\tau$ the exact value of α does not make much difference. Figures 1 and 2 are plots of Haeff's equation and of the Radiation Laboratory experimental results.

The interpretation of C_B as a factor that accounts only for nonoptimum *width* of the predetection filter is permissible for simple pulse shapes and approximate results, but in principle it must also account for the complete amplitude-phase characteristic of the filter, that is, for its departure from a matched-filter characteristic. The matched-filter condition as stated by North (2) is that the receiver transfer characteristic must be the complex conjugate of the spectrum of the echo at the receiving antenna terminals.

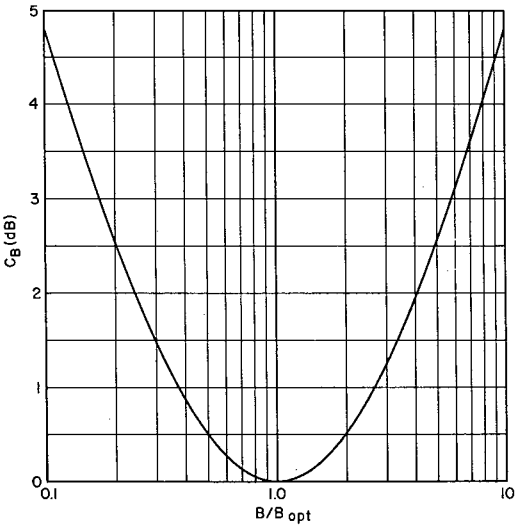

Fig. 1 - Bandwidth correction factor C_B plotted as a function of the ratio of bandwidth B to optimum bandwidth B_{opt} using Haeff's (20) empirical formula (Eq. (17)). (Note: This figure also appears in a larger size in an appendix at the end of the report.)

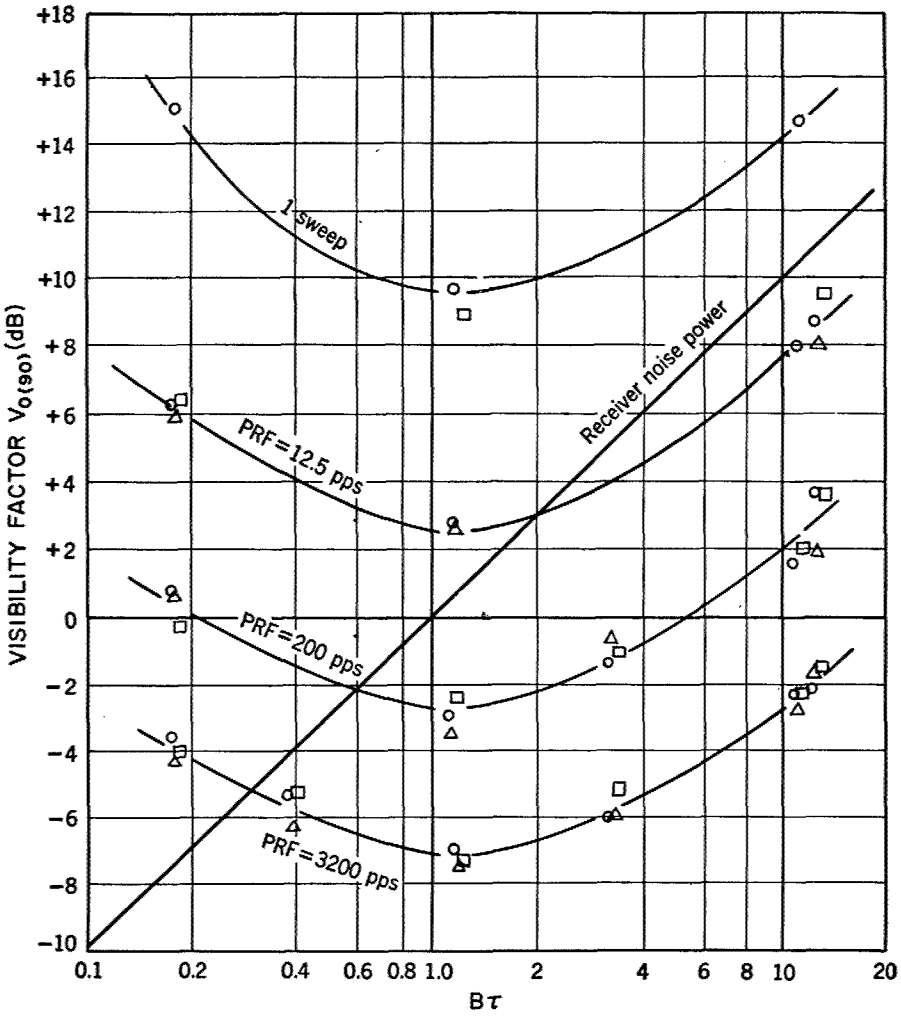

Fig. 2 - Experimental results showing the effect of bandwidth (parameter $B\tau$) on signal detectability (visibility factor V_0) with the pulse repetition frequency (PRF) as a parameter. The experiments were performed during World War II at the MIT Radiation Laboratory, and the figure is from Ref. 15, Fig. 8.7.

Calculated values of C_B based on this concept are shown for some representative response characteristics and pulse waveforms in Fig. 3. The values are found from these curves by the formula

$$C_B = \text{antilog}\left[\frac{1}{10}(y-3)\right], \tag{18a}$$

where y is the decibel ordinate value. Therefore,

$$C_{B\,(\text{dB})} = y - 3 . \tag{18b}$$

One of the passband shapes plotted is gaussian, with an assumed gaussian pulse shape, which represents a matched-filter condition ($C_B = 1$). For this combination $\alpha = 0.44$, but

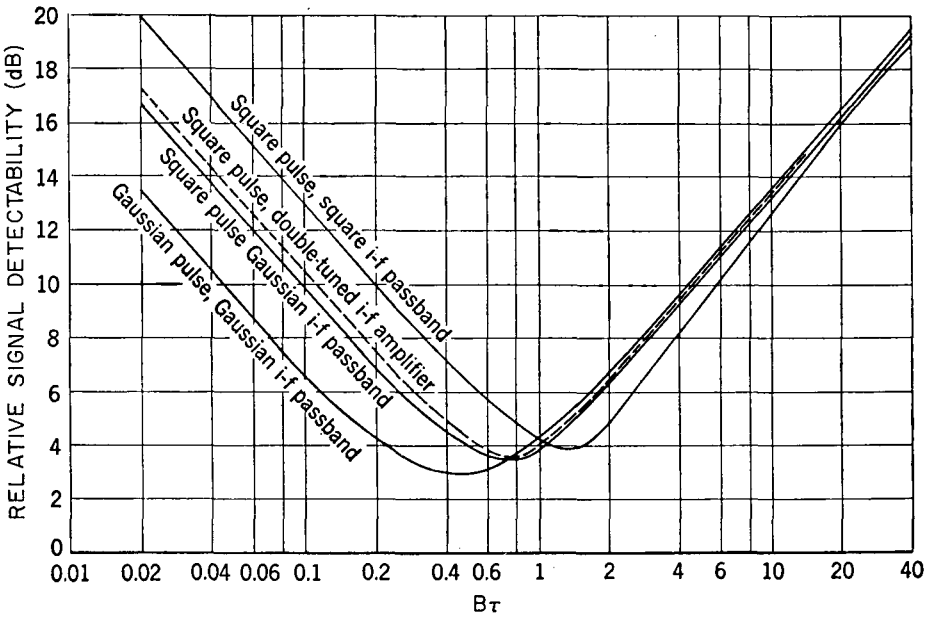

Fig. 3 - Effect of the bandwidth ($B\tau$) on the relative signal detectability, calculated for various pulse-shape and filter-shape combinations (from Ref. 15, Fig. 8.11)

this result is based on the half-power definition of bandwidth. For a rectangular pulse and optimum-width transitionally-coupled-circuit passband, $\alpha = 0.7$, also on a half-power basis. For this case, $C_B = 1.12$, indicating that the mismatch loss is not great (0.5 dB).

The pulse radar equations of this report and the definitions and evaluation procedures that are given here interpret the echo pulse spectrum, in the light of the foregoing matched-filter definition, as that of a single pulse. The spectrum of a train of periodically repeated pulses has, of course, a line structure. A delay-line integrator can be regarded as a filter having spectral lines that match those of the pulse train, and in this sense the effect of integration can be analyzed from the matched-filter (frequency domain) point of view. Here, however, it is regarded from a time-domain point of view (principle of superposition). That is, B_n is evaluated without including the effective line structure of an integrator in the definition of $G(f)$ (Eq. (16)). Instead the benefits of integration are expressed by regarding the detectable signal-to-noise ratio (S/N, V_0) to be a (monotonic decreasing) function of the number of pulses integrated (as will be discussed in the next section). The outcome is the same for either procedure, but this approach is more convenient when the integration is actually performed by time-domain methods.

4. MINIMUM DETECTABLE SIGNAL-TO-NOISE RATIO

In the preceding section, factors in the range equations were defined, and some information on how to evaluate them in typical cases was given. However, several very important factors were not covered, because they are of sufficient importance to warrant more extensive treatment in separate sections. In this section and in Sections 5 through 7 these additional factors will be discussed.

The quantities $P_{r\,(\min)}$, $(S/N)_{\min}$, and $V_{\min}$ are all related, as indicated in the development of Eqs. (3) through (9). Determination of the appropriate numbers to use for

these quantities in their respective range equations is a basic problem of radar range prediction. As will be seen, one of the problems is to define "detectable."

Integration of Signals

The calculation of signal detectability must take into account the effect of integration, if this process is employed. With this process, detection is based on the combined effect of a group of pulses rather than on observation of individual pulses. Pulse radar systems commonly employ some form of integration, although some do not.

Integration improves the signal-to-noise ratio, because signals combine additively, while the result of added noise samples has a fluctuation that is not the direct sum of the added fluctuations. The sum of M signal voltages each of unit amplitude is M, while M added noise samples, each having unit "standard deviation" before the addition, will have a standard deviation (fluctuation of voltage) equal to $\sqrt{M}$. Therefore, the signal-to-noise *voltage* ratio improvement is $M/\sqrt{M} = \sqrt{M}$. Consequently, the signal-to-noise *power* ratio improvement is M.

Integration can in principle be done either before or after detection (demodulation). In the former case the full M-fold improvement is realized, in principle. If the integration is done after detection (video or postdetection integration) the improvement is in general something less than M-fold.

Integration is a specific form of the more general process of crosscorrelation. It can be accomplished by using a storage device, such as a delay line, so that the signals received at a particular instant can be added to signals received earlier. Video (postdetection) integration is the rule; predetection integration is attempted only when the need justifies the complexity and cost of the required circuitry.

Integration occurs if the phosphor of a cathode-ray-tube display has sufficient persistence. It has also been found (15) that integration occurs in the eye-brain system of human observers. (This is of course postdetection integration.) MIT Radiation Laboratory experiments during World War II have indicated that an experienced observer has an effective integration time of up to several seconds, although the average human being may not do this well.

Evaluation of Probabilities

If a threshold device is employed to make a decision as to the presence or absence of a signal in a background of noise, then as already mentioned its performance can be described in terms of two probabilities: the probability of detection P_d and the false-alarm probability P_{fa}. The device is characterized by a threshold value of receiver output voltage v_t (equivalent to Marcum's (3) bias level), which, if exceeded, results in the decision report that a signal is present. If the threshold voltage is not exceeded at a particular instant, the detector reports "no signal." The report that a signal is present can be in the form of any physical indication whatever. In modern systems the usual indication is the setting of a one in a binary data channel in which a zero corresponds to "no signal." The term detectable signal is thus given a precise meaning.

There is always a definite probability that the threshold voltage will be exceeded when in fact no signal is present, because the statistics of the random noise voltage are such that there is a usually small but nonzero probability that it can attain a value equal to the saturation level of the receiver. (In the mathematical theory of gaussian noise, there is a nonzero probability that it can attain any finite value, however large.) The

probability that v_t is exceeded when no signal is present is the false-alarm probability. It is calculated from the equation

$$P_{fa} = \int_{v_t}^{\infty} p_n(v)\, dv \ , \tag{19}$$

where $p_n(v)$ is the probability density function of the noise. The probability of detection is given by the same expression with the probability density function that of the signal-and-noise combination (usually called signal plus noise, but the addition indicated by the word plus is not necessarily linear):

$$P_d = \int_{v_t}^{\infty} p_{sn}(v)\, dv \ . \tag{20}$$

The function p_{sn} depends on the signal-to-noise ratio as well as on the signal and noise statistics, and both p_n and p_{sn} are functions of the rectification law of the receiver detector and of any postdetection processing or circuit nonlinearities.

But primarily the probability of detection is a function of the signal-to-noise ratio. By assigning different values to the signal-to-noise ratio and applying Eq. (20) the variation of P_d with (S/N) (or V_0) can be determined. As would logically be assumed, it is a monotonic increasing function of (S/N), for a given value of v_t. Similarly, the variation of P_{fa} as a function of v_t can be found from Eq. (19); it is a monotonic decreasing function.

The method of applying these concepts to the prediction of radar range consists of four steps: (1) decide on a value of false alarm probability that is acceptable; (2) for this value of P_{fa} find the required value of threshold voltage v_t through Eq. (19); (3) decide on a desired value of P_d (in different circumstances, values ranging from below 0.5 up to as high as 0.99 may be selected); and (4) for this value of P_d and the value of v_t found in step 2, find the required signal-to-noise ratio through Eq. (20). This is the value of V_0 that must be used in the range equation (Eq. (10)).

This procedure is greatly facilitated by curves that relate P_d to V_0 with P_{fa} as a parameter. Many such curves have been published, and some representative ones are given in this report. The principal difficulty in computing them is determination of the probability density functions p_n and p_{sn}. North (2) gives the exact functions that apply for single-pulse detection with a linear rectifier as detector and approximations that apply when many pulses are integrated. The density functions appropriate to other situations, such as square-law detection, and fluctuation of signals, are given by various authors (3-10).

The decision as to the acceptable level of false alarm probability is usually made in terms of a concept called false alarm time, which will here be defined as the average time between false alarms. Other definitions of false alarm time are possible; Marcum (3) defines it as the time for which the probability of at least one false alarm is 0.5. However, the average time between false alarms seems a more useful concept. With it, for example, one can compute the average number of false alarms that will occur per hour, day, year, etc. With this definition the false alarm time is given by

$$t_{fa} = \frac{M\tau}{P_{fa}} \ , \tag{21}$$

where M is the number of pulses integrated and τ is the pulse duration. This formula assumes that the integrator output is sampled at time intervals equal to τ. If range gates are employed and M pulses are integrated, if the on time of the gate t_g is equal to or greater than the pulse length τ, and if there is some fraction of the time δ when no gates are open (dead time), then the formula is

$$t_{fa} = \frac{M t_g}{P_{fa}(1-\delta)} . \tag{22}$$

These false-alarm-time formulas assume that the receiver predetection noise bandwidth B_n is equal to or greater than the reciprocal of the pulse length and that the postdetection (video) bandwidth is equal to or greater than $B_n/2$ (as it usually will be). These assumptions, usually met, amount to assuming that values of the noise voltage separated by the pulse duration are statistically independent; this independence occurs for times separated by $1/B_n$, sometimes called the Nyquist interval. Since ordinarily $B_n \approx 1/\tau$ and $t_g \approx \tau$, $1/B_n$ is sometimes used in place of τ or t_g in the false-alarm-time equations.

Marcum's false-alarm number n' is related to the false-alarm probability by the equation:

$$1 - (1-P_{fa})^{n'} = 0.5 . \tag{23a}$$

For the usual large values of n' that are of interest, a highly accurate approximate solution of this equation for P_{fa} is

$$P_{fa} \approx -\frac{\log_e 0.5}{n'} = \frac{0.6931}{n'} . \tag{23b}$$

Required Signal-to-Noise Ratio

The signal-to-noise ratio required for detection by a threshold device when there is integration is found, using Eqs. (19) and (20), by calculating p_n and p_{sn} for the integrator output rather than for the receiver output before integration. Such calculations are quite complicated, but they have been carried out for many cases of interest (2-13). A representative set of curves is presented in Figs. 4 and 5. They are calculated for a steady (nonfluctuating) signal, a linear-rectifier detector, a fixed-threshold decision device, and complete postdetection integration of M pulses. These curves can be used with Eq. (10) and subsequent equations derived from it. The method of calculation will be described in Part 2. Calculations for this case have also been made by Robertson (4), using a different computational method and a different range of the false-alarm parameter. Where the ranges overlap, the results shown in Figs. 4 and 5 are in complete agreement with Robertson's results. These linear-detector results are given here, rather than those for a square-law detector as published by Marcum (3) and others, because, as discussed in the following pages, the linear-rectifier detector is the one usually employed in radar receivers. (It also happens, as will be discussed, that the results for the two detector laws differ only slightly.)

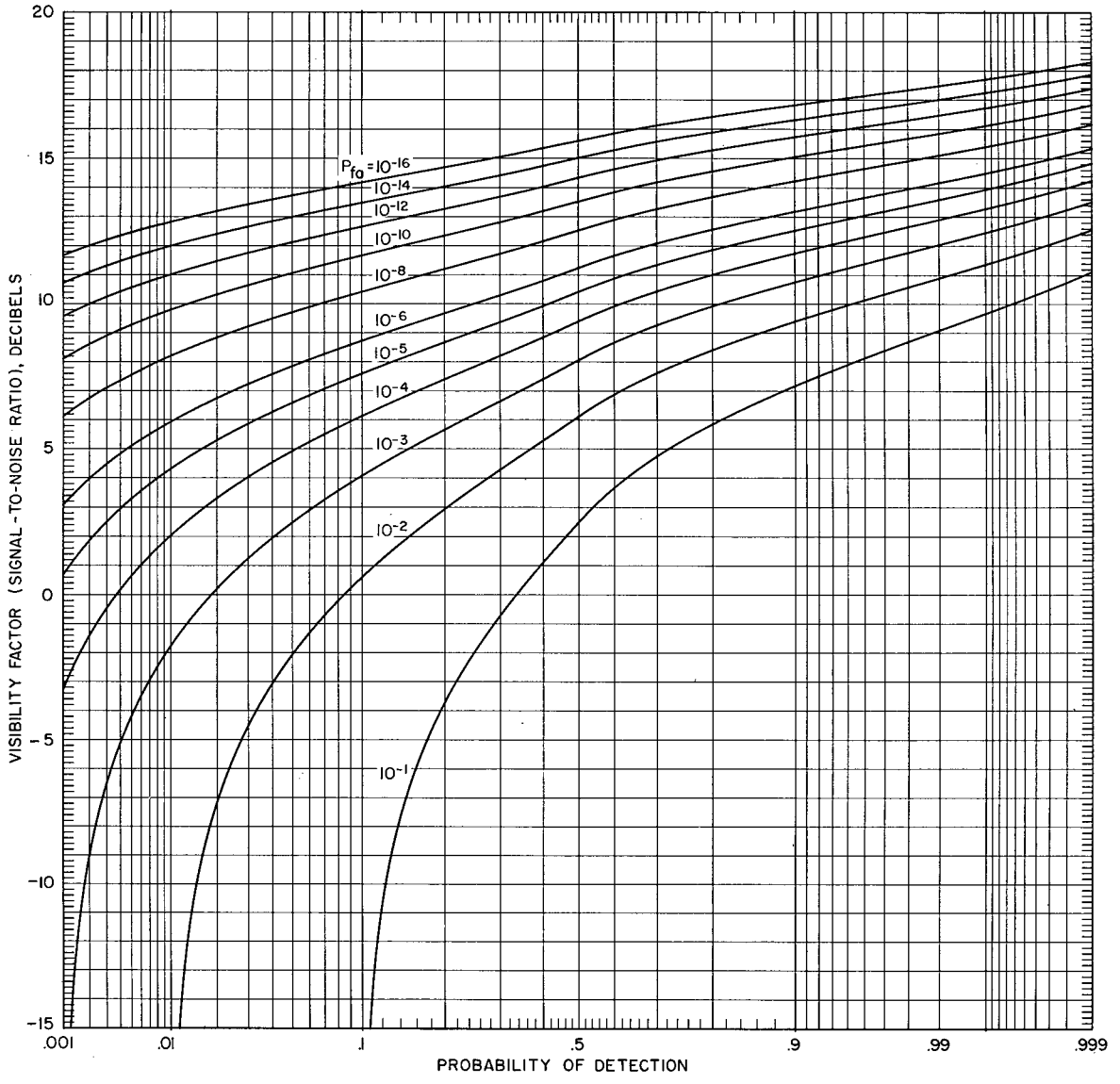

Fig. 4 - Required signal-to-noise ratio (visibility factor) at the input terminals of a linear-rectifier detector as a function of probability of detection for a single pulse, with the false-alarm probability (P_{fa}) as a parameter, calculated for a nonfluctuating signal. (Note: This figure also appears in an appendix at the end of the report.)

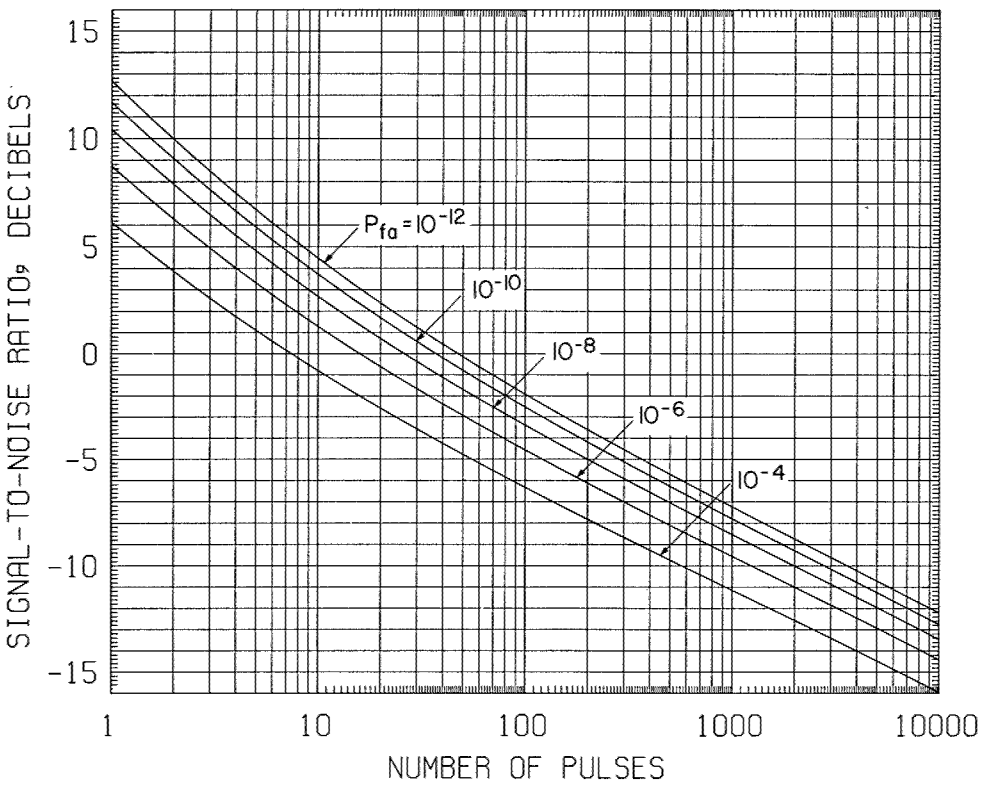

Fig. 5a - Required signal-to-noise ratio (visibility factor) for a linear detector as a function of number of pulses integrated, for 0.1 probability of detection, calculated for a nonfluctuating signal for five values of false-alarm probability (P_{fa}). (Note: This figure also appears in a larger size in an appendix at the end of the report.)

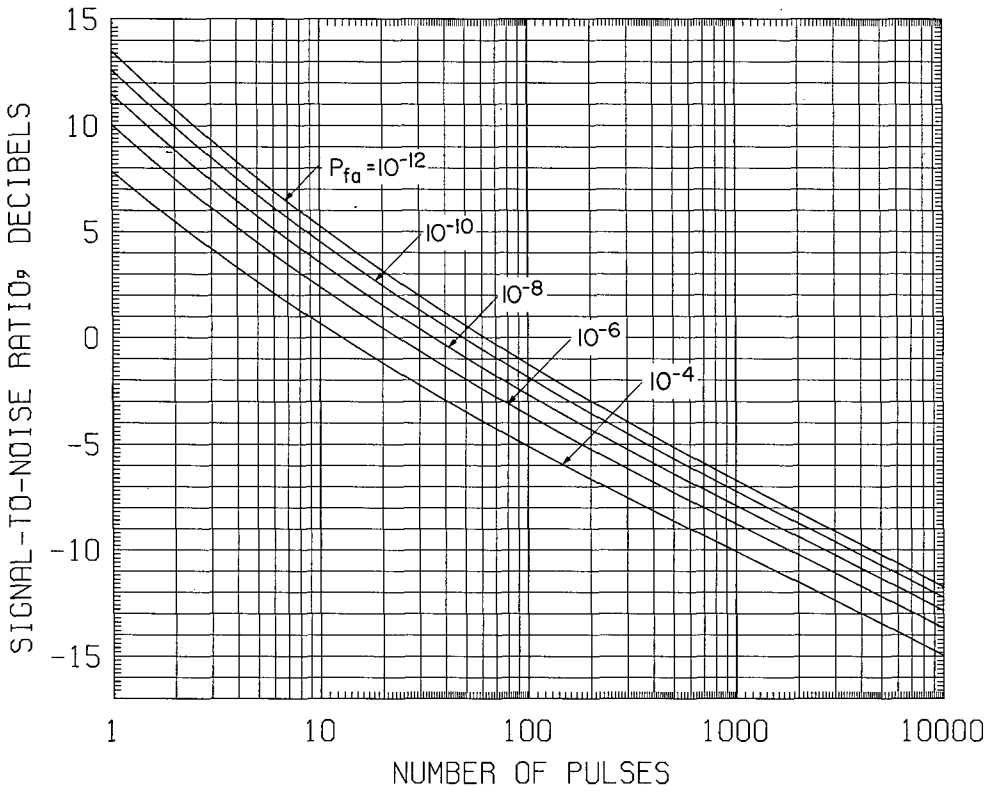

Fig. 5b - Required signal-to-noise ratio (visibility factor) for a linear detector as a function of number of pulses integrated, for 0.25 probability of detection, calculated for a nonfluctuating signal for five values of false-alarm probability (P_{fa}). (Note: This figure also appears in a larger size in an appendix at the end of the report.)

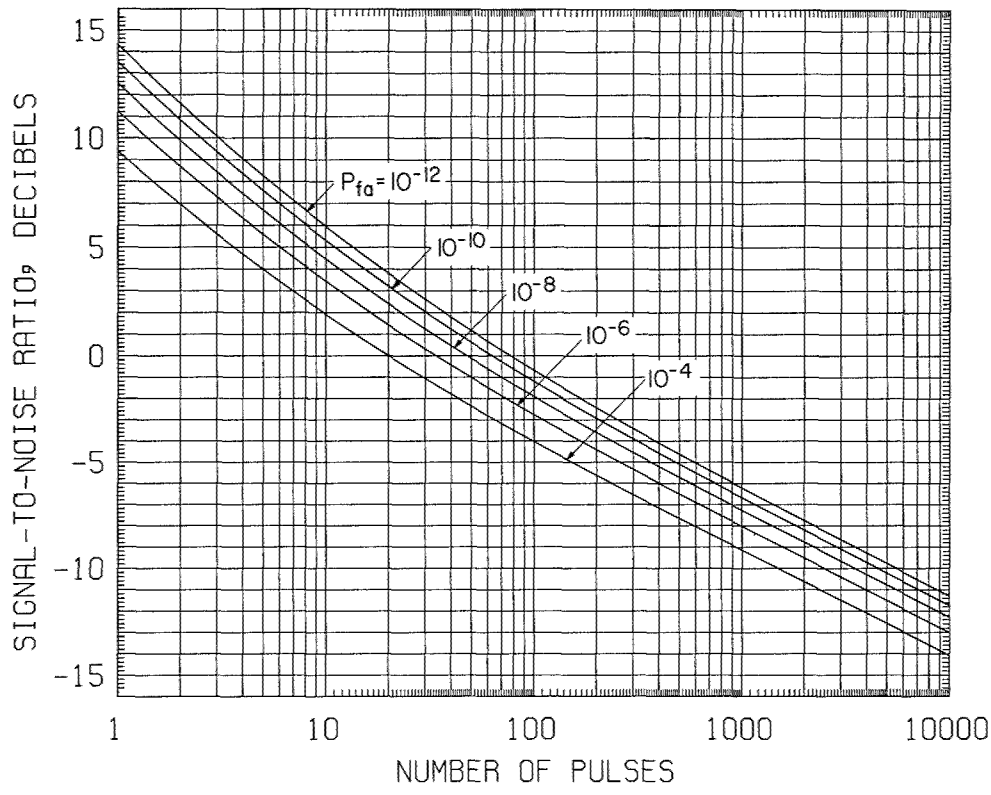

Fig. 5c - Required signal-to-noise ratio (visibility factor) for a linear detector as a function of number of pulses integrated, for 0.5 probability of detection, calculated for a nonfluctuating signal for five values of false-alarm probability (P_{fa}). (Note: This figure also appears in a larger size in an appendix at the end of the report.)

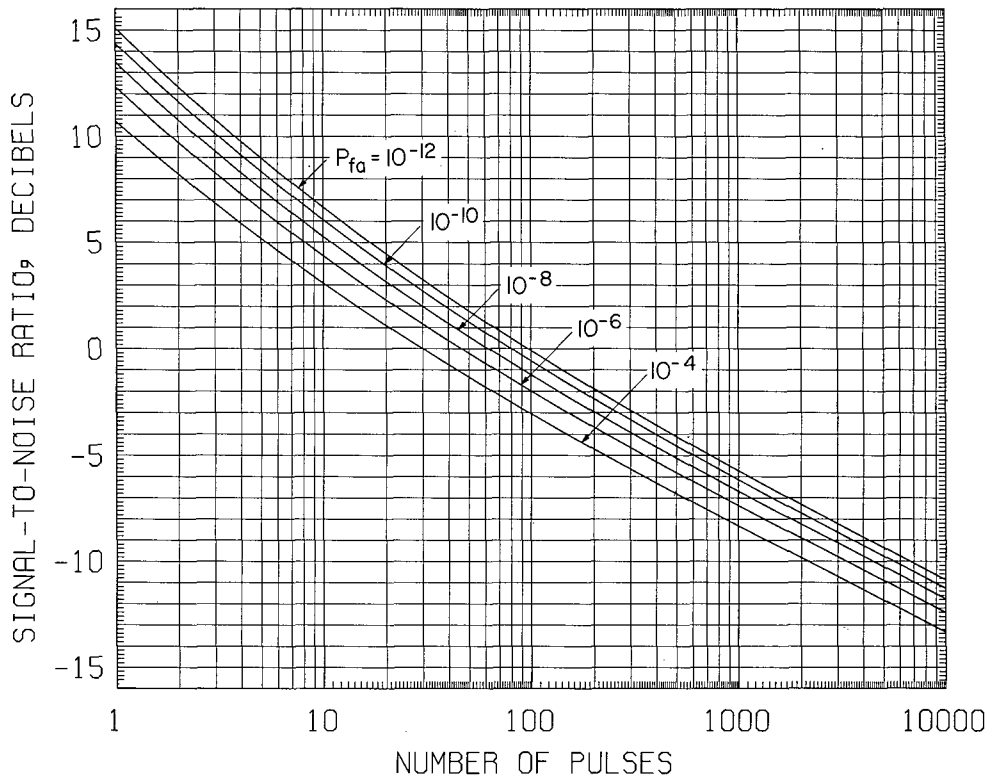

Fig. 5d - Required signal-to-noise ratio (visibility factor) for a linear detector as a function of number of pulses integrated, for 0.75 probability of detection, calculated for a nonfluctuating signal for five values of false-alarm probability (P_{fa}). (Note: This figure also appears in a larger size in an appendix at the end of the report.)

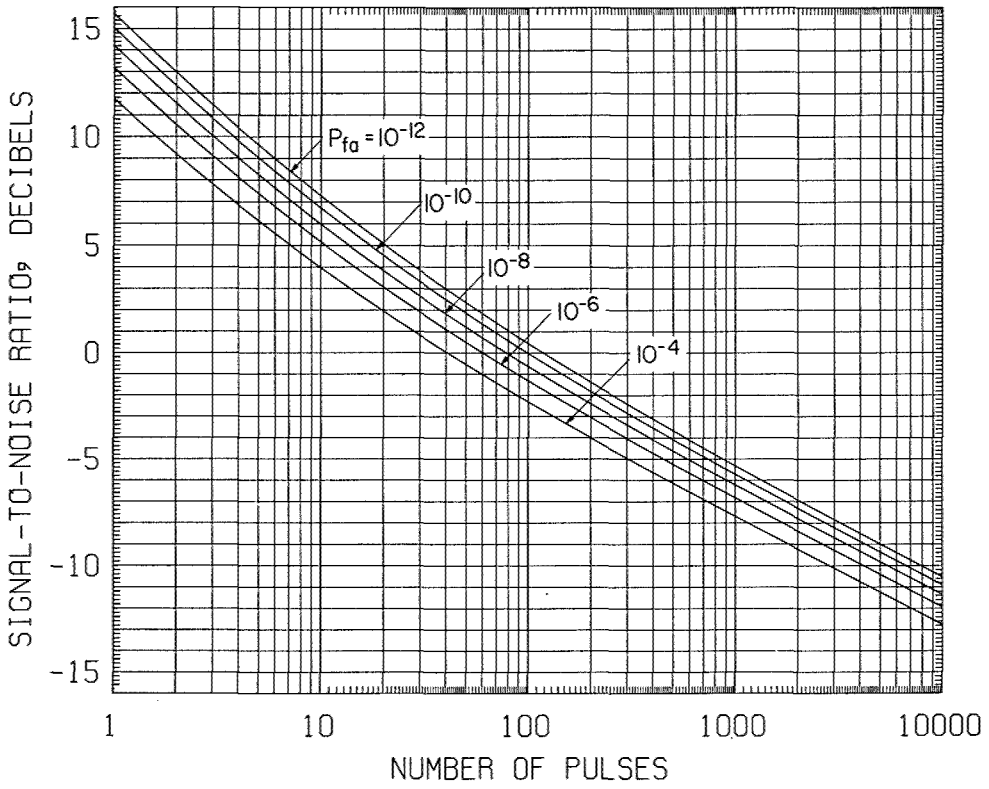

Fig. 5e - Required signal-to-noise ratio (visibility factor) for a linear detector as a function of number of pulses integrated, for 0.90 probability of detection, calculated for a nonfluctuating signal for five values of false-alarm probability (P_{fa}). (Note: This figure also appears in a larger size in an appendix at the end of the report.)

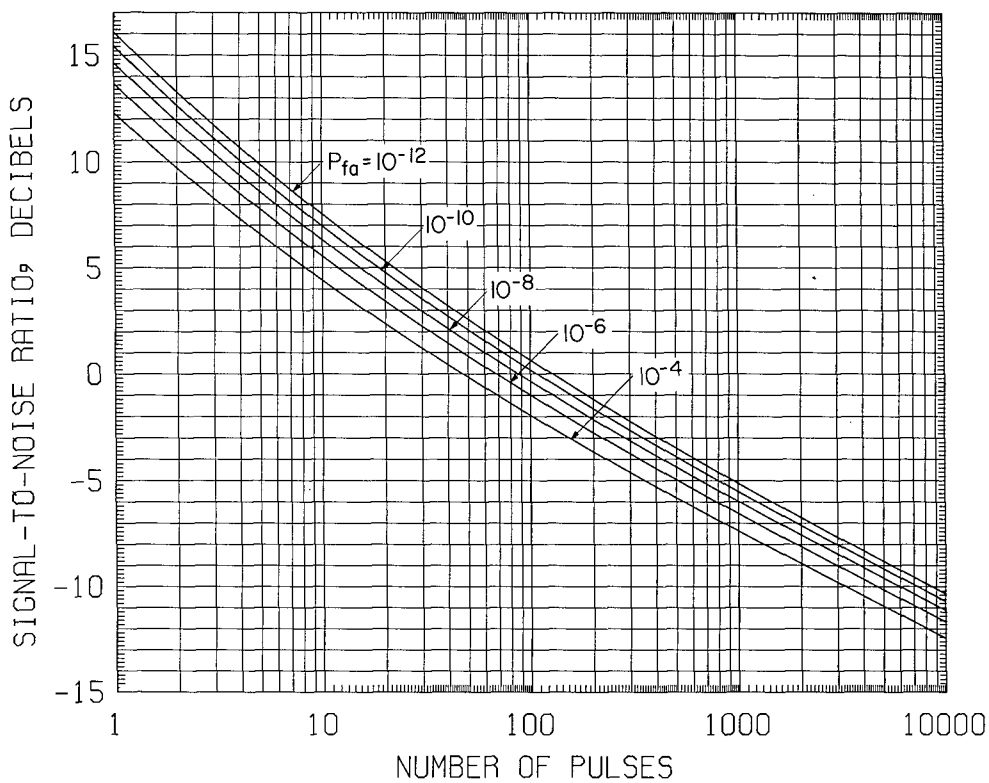

Fig. 5f - Required signal-to-noise ratio (visibility factor) for a linear detector as a function of number of pulses integrated, for 0.95 probability of detection, calculated for a nonfluctuating signal for five values of false-alarm probability (P_{fa}). (Note: This figure also appears in a larger size in an appendix at the end of the report.)

Curves for the fluctuating-target case are given by Swerling (5), Fehlner (6), Heidbreder and Mitchell (9), and others. In general the effect of fluctuation is to require higher signal-to-noise ratios for high probability of detection and lower values for low probability of detection than those required with nonfluctuating signals. Swerling has considered four cases, which differ in the assumed rate of fluctuation and the assumed statistical distribution of the cross section. The two assumed rates are (a) a relatively slow fluctuation, such that the values of σ for successive scans of the radar beam past the target are statistically independent but remain virtually constant from one pulse to the next, and (b) a relatively fast fluctuation, such that the values of σ are independent from pulse to pulse within one beamwidth of the scan (i.e., during the integration time). The first of the two assumed distributions for the received signal voltage is of the Rayleigh form, which means that the target cross section σ has a probability density function given by

$$p(\sigma) = \frac{1}{\bar{\sigma}} e^{-\sigma/\bar{\sigma}} , \tag{24}$$

where $\bar{\sigma}$ is the average cross section. (This is a negative-exponential density function, but a target having this distribution is called a Rayleigh target.) The second assumed cross-section density function is

$$p(\sigma) = \frac{4\sigma}{\bar{\sigma}^2} e^{-2\sigma/\bar{\sigma}} . \tag{25}$$

The first distribution is observed when the target consists of many independent scattering elements, of which no single one nor just a few predominate. Many aircraft have approximately this characteristic at microwave frequencies, and large complicated targets are usually of this nature. (This result is predicted by the Central Limit Theorem of probability theory.) The second distribution corresponds to that of a target having one main scattering element that predominates, together with many smaller independent scattering elements. In summary, the cases considered by Swerling are:

Case 1. Eq. (24), slow fluctuation,

Case 2. Eq. (24), fast fluctuation,

Case 3. Eq. (25), slow fluctuation,

Case 4. Eq. (25), fast fluctuation.

The distribution of Eq. (25) is sometimes assumed for a small, rigid, streamlined aircraft at the lower radar frequencies (e.g., below 1 GHz). More recently it has been concluded that many targets of the non-Rayleigh type are better represented by the so-called log-normal distribution, and analyses have been made for this case (9).

Swerling's Case 1 is the one most often assumed when range prediction is to be made for a nonspecific fluctuating target, and results for this case are presented in Fig. 6. Corresponding curves for Swerling Case 3 are given in Fig. 7. Cases 2 and 4 are of lesser interest, because they are less frequently encountered, and because for more than about 10 pulses integrated the results are very nearly the same as those for the steady-signal case. Figures 6 and 7 are based on the work of Marcum (3) and Swerling (5) as revised by Fehlner (6).* The original results of Marcum and Swerling were presented in

*Figures 6 and 7 were machine plotted by the author from data obtained using a computer program due to L. F. Fehlner, R. G. Roll, and G. T. Trotter of the Johns Hopkins University Applied Physics Laboratory. The program was modified by Stanley Gontarek to run on the NRL CDC-3800 computer. It was further modified by the author to accept false-alarm probability rather than Marcum's false-alarm number as an input parameter and to plot curves for specified values of probability.

terms of the range-ratio R/R_0, where R_0 is the free-space range when the signal-to-noise ratio (visibility factor) is unity, with the assumption that the free-space propagation law applies, although it often does not (Section 6). They were also presented in terms of Marcum's false-alarm number, rather than the false-alarm probability (Eq. (23)). Figures 6 and 7 are in terms of the signal-to-noise ratio and false-alarm probability. They are for a square-law detector rather than a linear detector; but as previously stated the results for the two detector types differ only slightly (less than 0.2 dB).

For predetection integration the appropriate values of required signal-to-noise ratio (V_0) can be found from Figs. 4 through 7 by reading the value of $V_{0(\mathrm{dB})}$ for $M = 1$ and subtracting from it $10 \log M$. That is $V_0(M) = V_0(1)/M$.

Detector Laws

The curves of Figs. 4 and 5 are for a so-called linear detector. This means that it has the rectification characteristic

$$\begin{aligned} I_o &= \alpha V_i , \quad V_i \geq 0 , \\ I_o &= 0 , \qquad V_i < 0 , \end{aligned} \tag{26}$$

where I_o is the instantaneous output current, V_i is the instantaneous input voltage, and α is a positive constant. Typical diodes of either the vacuum-tube or solid-state variety approximate this law if V_i is larger than some very small value. Such a diode is ordinarily used as the second detector of a superheterodyne radar receiver. Also, appreciable RF and IF gain usually precedes the second detector, so that the voltage applied to it is usually large enough to insure this linear operation. It is important to note that a large *signal-to-noise ratio* is not stipulated, only a large *detector input voltage* (relative to the value at which the transition from square-law to linear input-voltage/output-current relationship occurs). Therefore, the second detector of a superheterodyne radar receiver is usually operating as a linear detector even for very small signal-to-noise ratios, or even in the complete absence of a signal, because the noise voltage alone is sufficient to insure operation in the linear region.

Many calculations of signal-to-noise ratio required for detection have been made assuming that a full-wave square-law detector is used, for which

$$I_o = \alpha V_i^2 . \tag{27}$$

Such a detector is almost unheard of in actual radar receivers. There are probably three reasons for its use as a detector law in theoretical analyses: (a) the square-law detector is slightly superior to the linear detector for many-pulse integration (it results in a smaller signal-to-noise ratio required for detection), (b) the mathematical analysis is much more difficult for the linear than for the square-law detector, and (c) it has been shown (2,3,15) that the difference in performance of the square-law and linear detectors is miniscule (about 0.2 dB at most). The square-law detector is actually slightly inferior to the linear detector for integration of only a few pulses. For single-pulse detection the two detectors perform equally well.

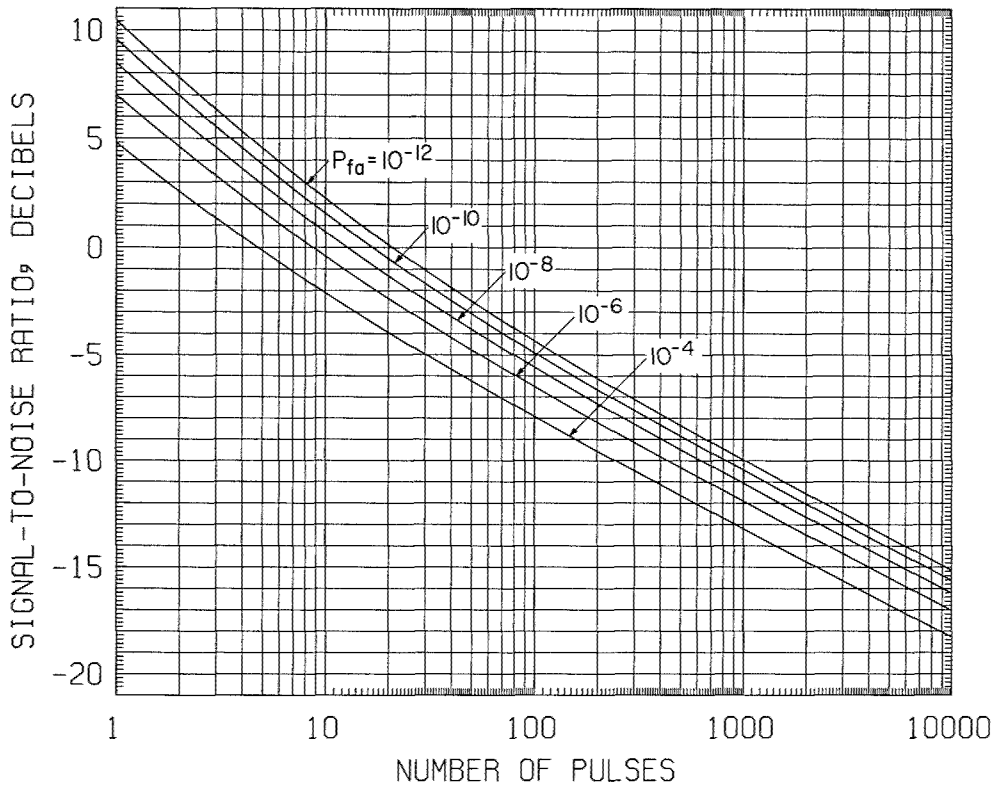

Fig. 6a - Required signal-to-noise ratio (visibility factor) for a square-law detector as a function of number of pulses integrated, for 0.1 probability of detection, calculated for Swerling Case 1 fluctuation for five values of false-alarm probability. (Note: This figure also appears in a larger size in an appendix at the end of the report.)

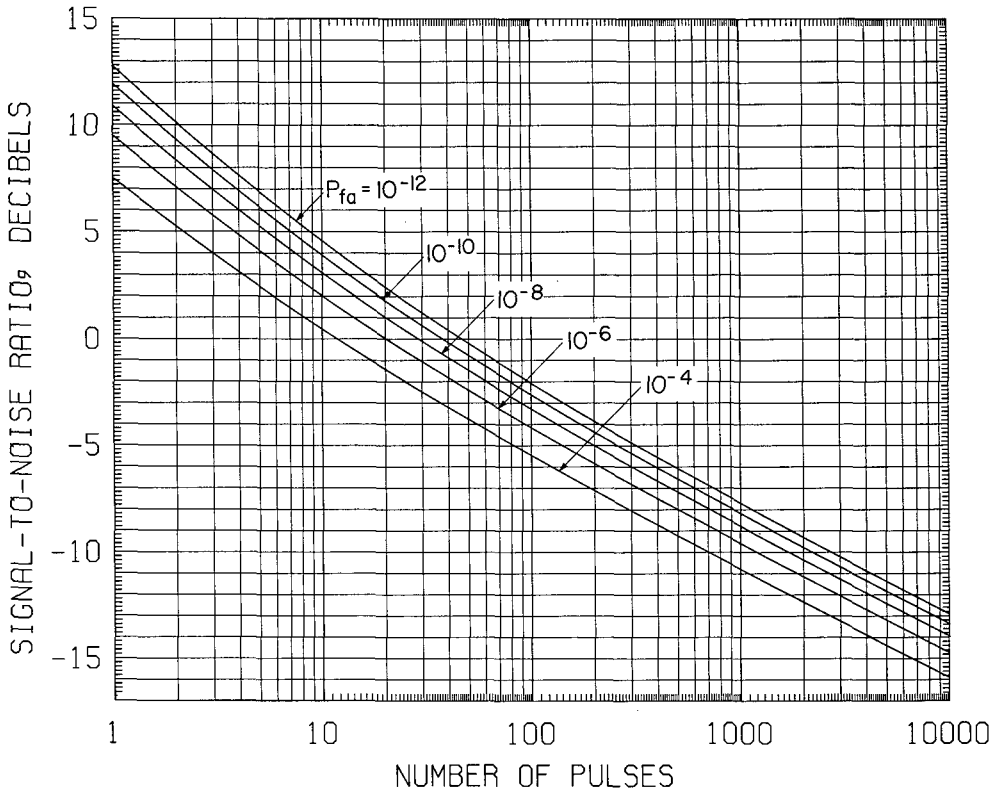

Fig. 6b - Required signal-to-noise ratio (visibility factor) for a square-law detector as a function of number of pulses integrated, for 0.25 probability of detection, calculated for Swerling Case 1 fluctuation for five values of false-alarm probability. (Note: This figure also appears in a larger size in an appendix at the end of the report.)

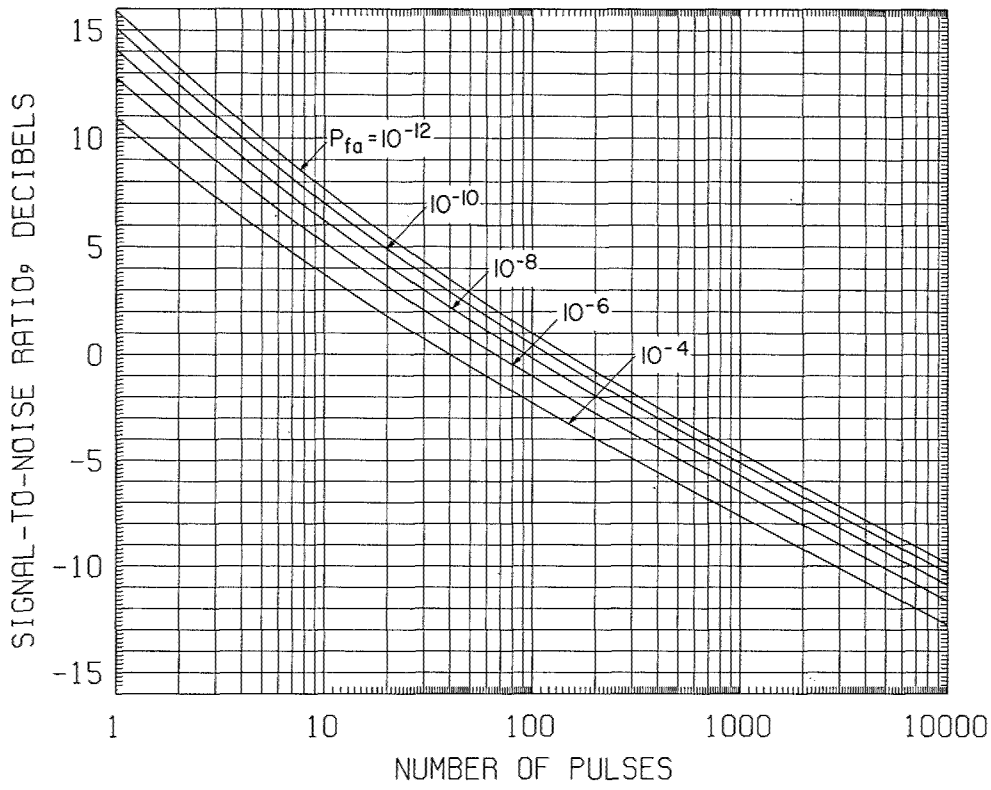

Fig. 6c - Required signal-to-noise ratio (visibility factor) for a square-law detector as a function of number of pulses integrated, for 0.50 probability of detection, calculated for Swerling Case 1 fluctuation for five values of false-alarm probability. (Note: This figure also appears in a larger size in an appendix at the end of the report.)

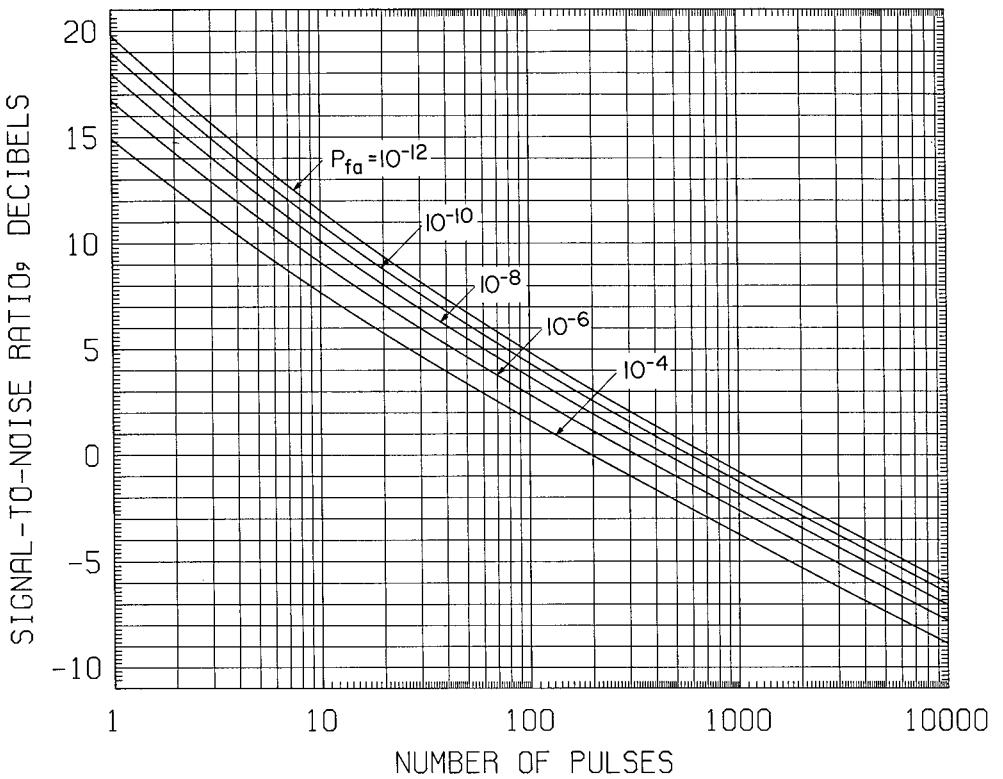

Fig. 6d - Required signal-to-noise ratio (visibility factor) for a square-law detector as a function of number of pulses integrated, for 0.75 probability of detection, calculated for Swerling Case 1 fluctuation for five values of false-alarm probability. (Note: This figure also appears in a larger size in an appendix at the end of the report.)

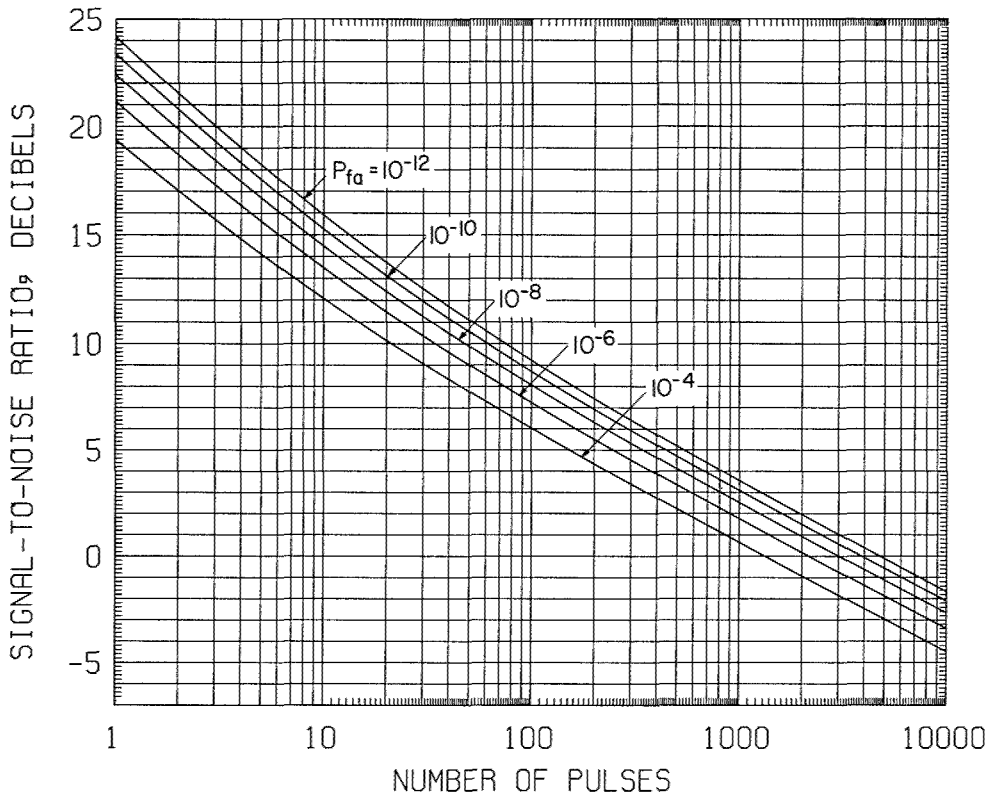

Fig. 6e - Required signal-to-noise ratio (visibility factor) for a square-law detector as a function of number of pulses integrated, for 0.90 probability of detection, calculated for Swerling Case 1 fluctuation for five values of false-alarm probability. (Note: This figure also appears in a larger size in an appendix at the end of the report.)

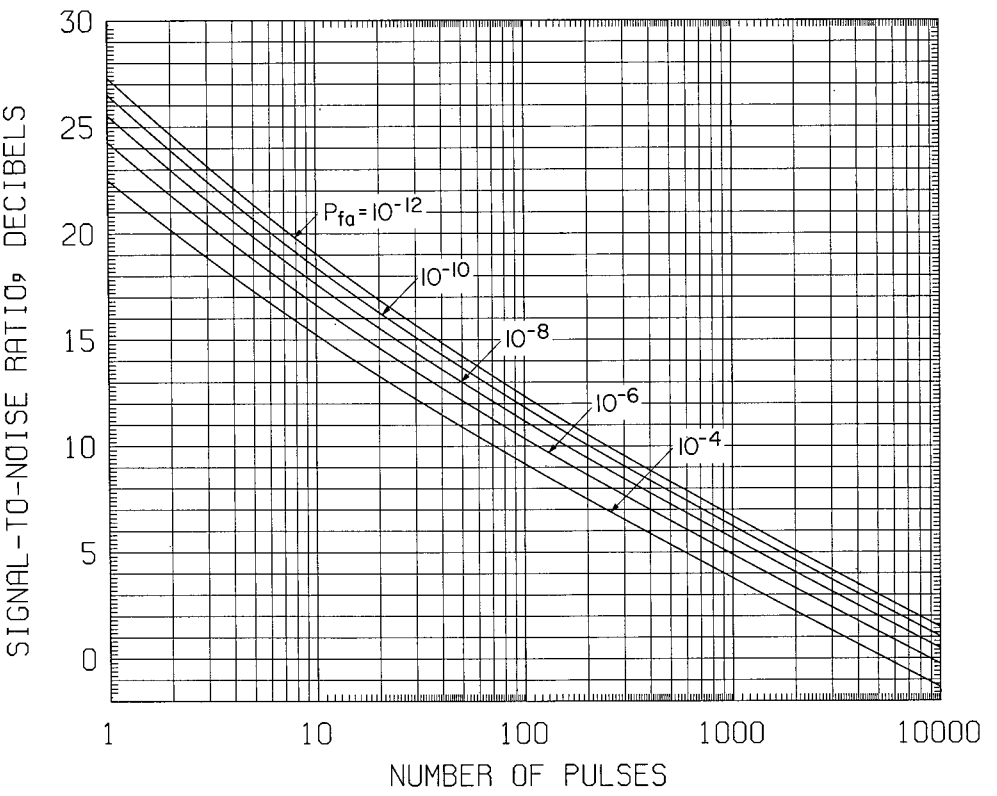

Fig. 6f - Required signal-to-noise ratio (visibility factor) for a square-law detector as a function of number of pulses integrated, for 0.95 probability of detection, calculated for Swerling Case 1 fluctuation for five values of false-alarm probability. (Note: This figure also appears in a larger size in an appendix at the end of the report.)

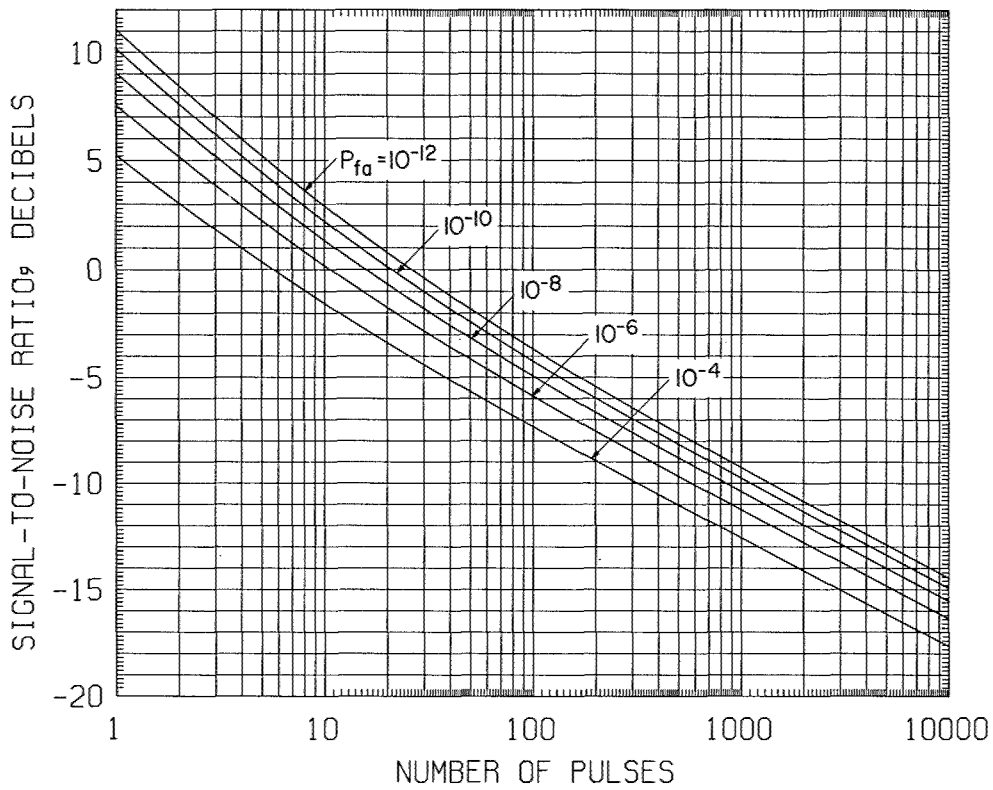

Fig. 7a - Required signal-to-noise ratio (visibility factor) for a square-law detector as a function of number of pulses integrated, for 0.10 probability of detection, calculated for Swerling Case 3 fluctuation for five values of false-alarm probability. (Note: This figure also appears in a larger size in an appendix at the end of the report.)

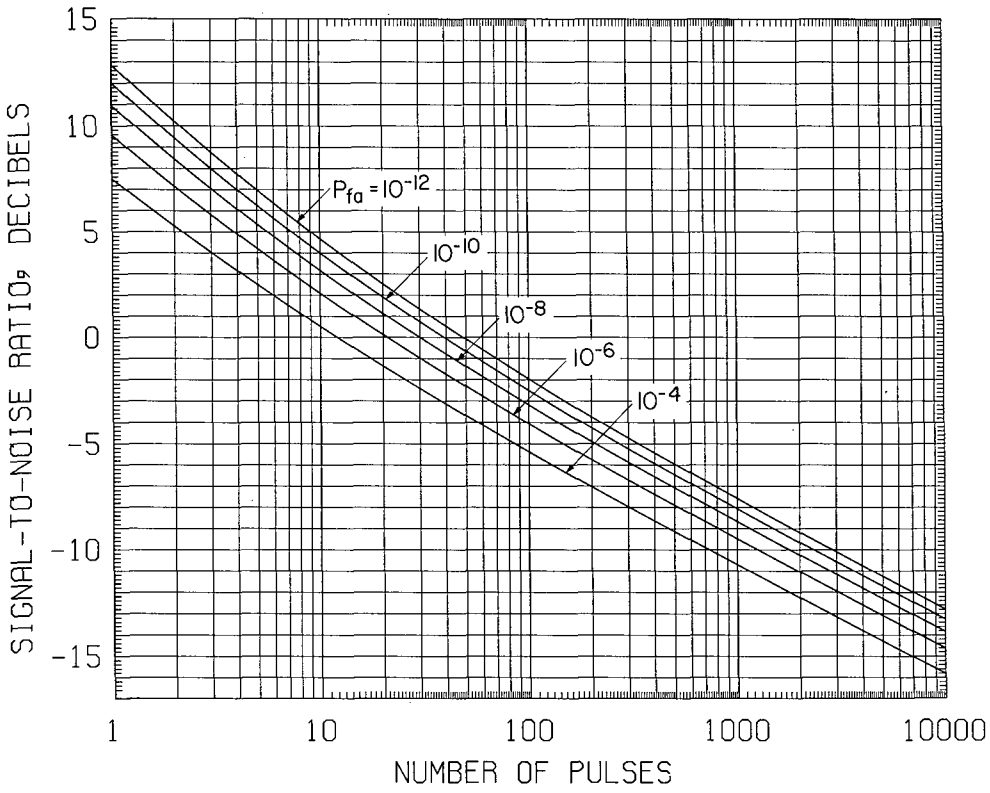

Fig. 7b - Required signal-to-noise ratio (visibility factor) for a square-law detector as a function of number of pulses integrated, for 0.25 probability of detection, calculated for Swerling Case 3 fluctuation for five values of false-alarm probability. (Note: This figure also appears in a larger size in an appendix at the end of the report.)

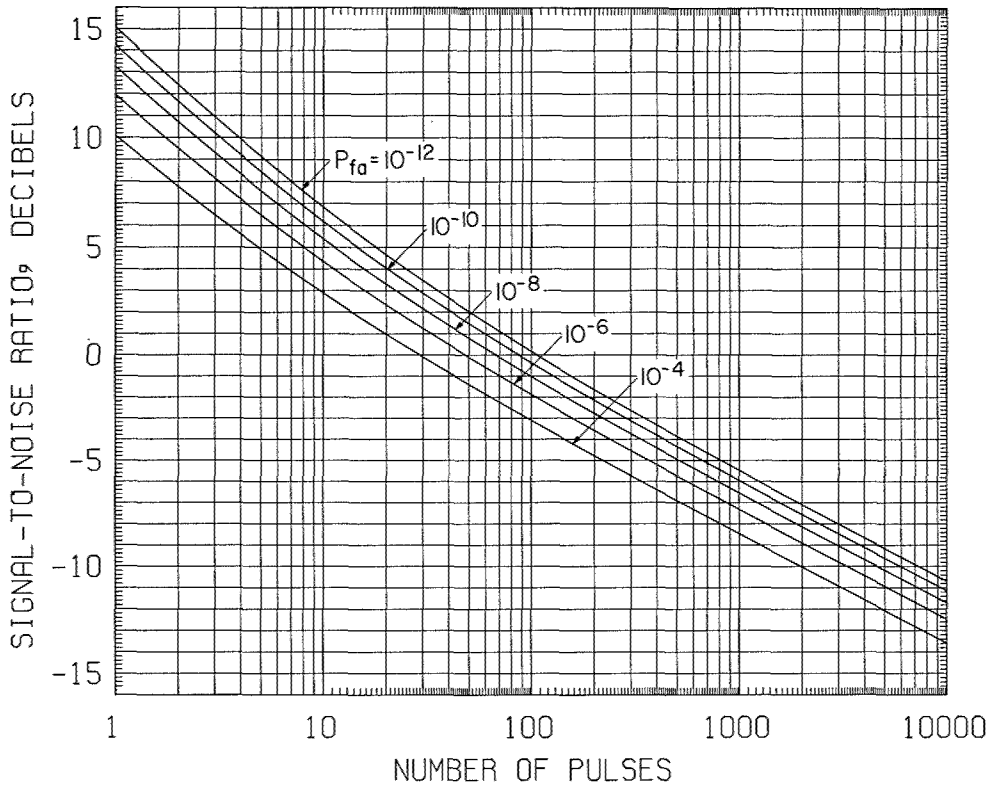

Fig. 7c - Required signal-to-noise ratio (visibility factor) for a square-law detector as a function of number of pulses integrated, for 0.50 probability of detection, calculated for Swerling Case 3 fluctuation for five values of false-alarm probability. (Note: This figure also appears in a larger size in an appendix at the end of the report.)

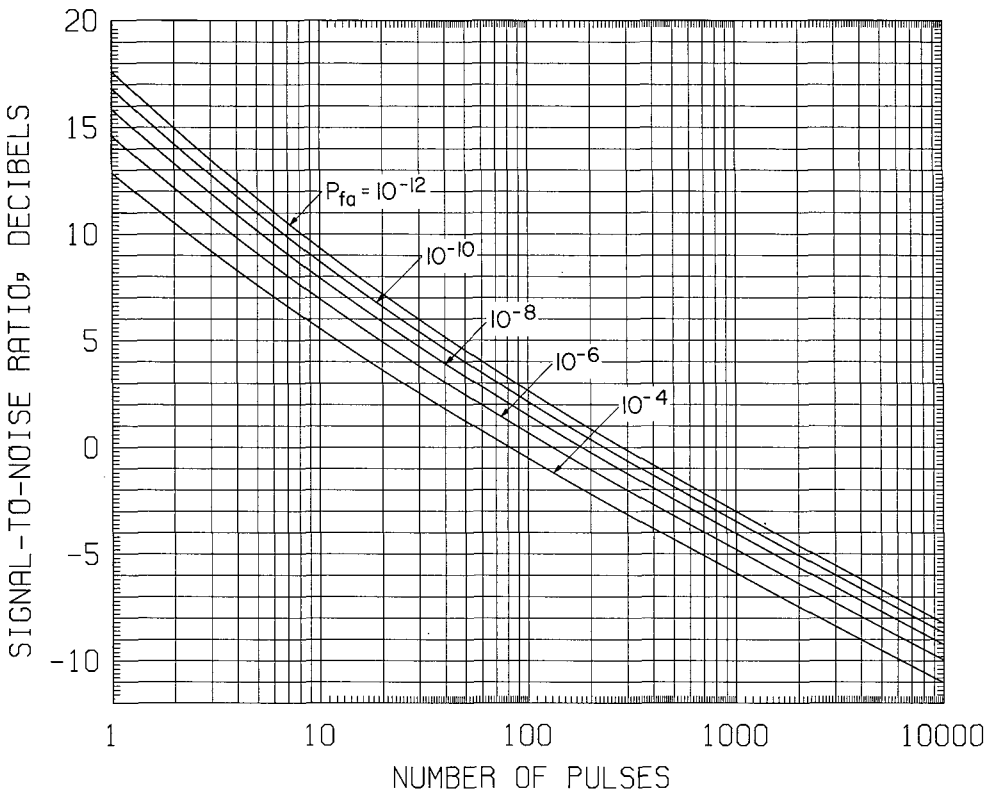

Fig. 7d - Required signal-to-noise ratio (visibility factor) for a square-law detector as a function of number of pulses integrated, for 0.75 probability of detection, calculated for Swerling Case 3 fluctuation for five values of false-alarm probability. (Note: This figure also appears in a larger size in an appendix at the end of the report.)

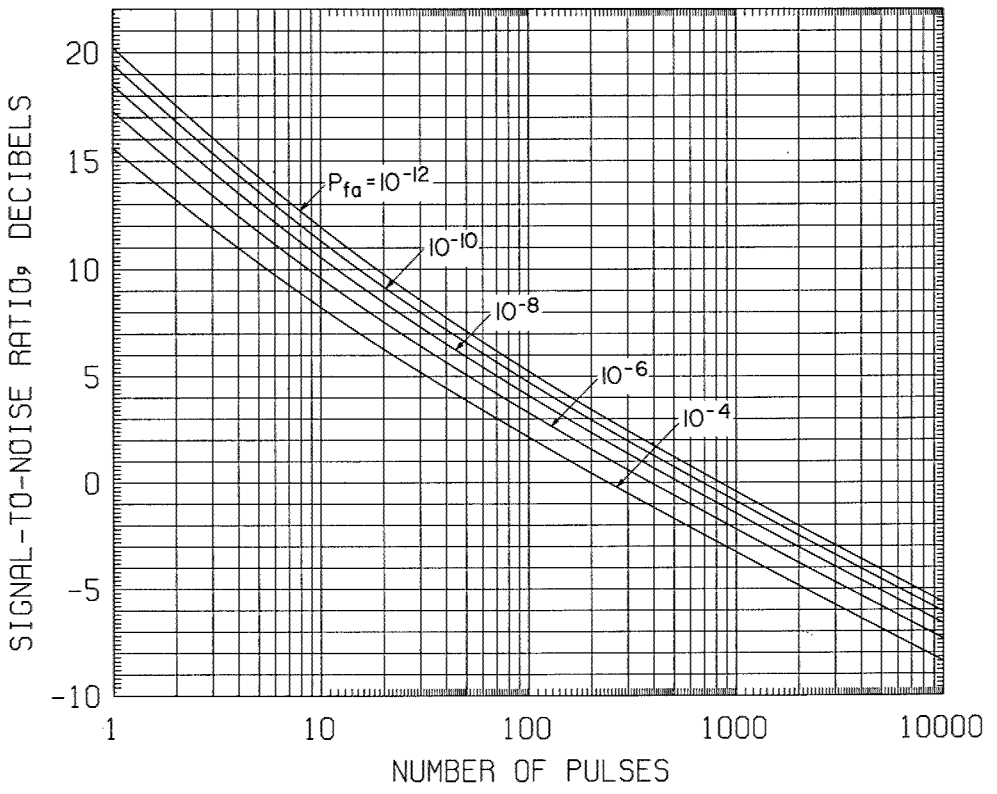

Fig. 7e - Required signal-to-noise ratio (visibility factor) for a square-law detector as a function of number of pulses integrated, for 0.90 probability of detection, calculated for Swerling Case 3 fluctuation for five values of false-alarm probability. (Note: This figure also appears in a larger size in an appendix at the end of the report.)

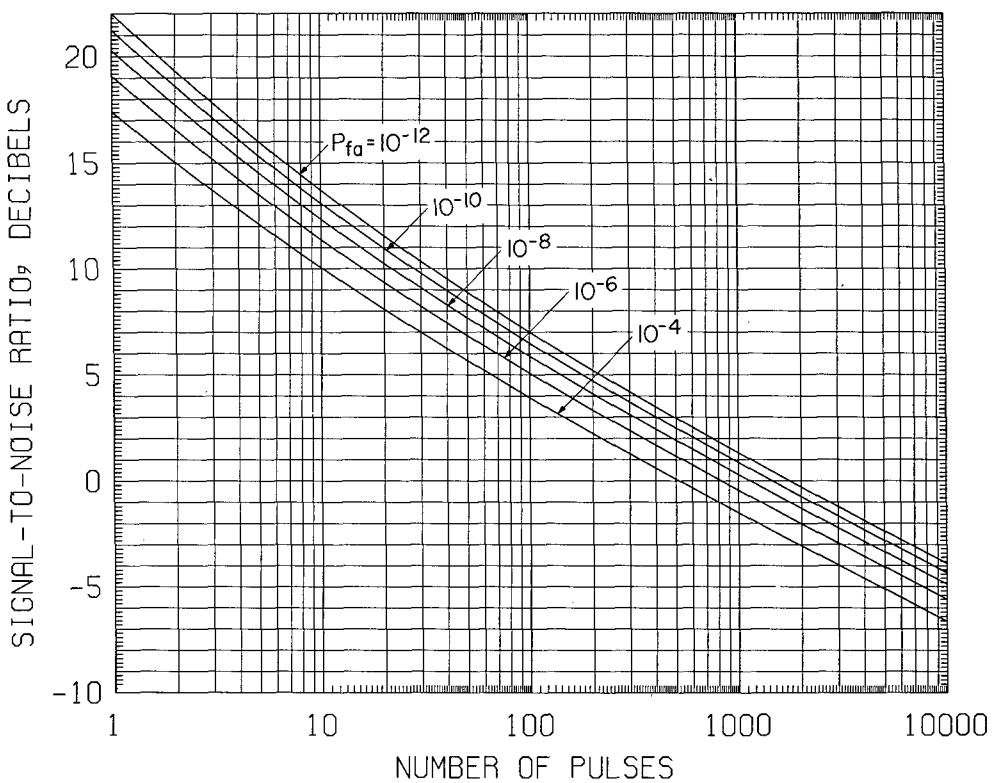

Fig. 7f - Required signal-to-noise ratio (visibility factor) for a square-law detector as a function of number of pulses integrated, for 0.95 probability of detection, calculated for Swerling Case 3 fluctuation for five values of false-alarm probability. (Note: This figure also appears in a larger size in an appendix at the end of the report.)

A diode linear detector will, it is true, be approximately a square-law half-wave rectifier for very small input voltages; that is, its characteristic will be

$$I_o = \alpha V_i^2 , \quad V_i \geq 0 ,$$
$$I_o = 0 , \quad V_i < 0 . \tag{28}$$

However, as noted, diodes are seldom operated on this part of their characteristic in actual receivers; but the existence of it has led some to think that the linear detector becomes a square-law detector for small *signal-to-noise ratios*, which is not true. It is also to be noted that Eq. (28) is not exactly the same as Eq. (27), which is the one usually assumed in detection analyses, but they both represent the same relationship between input and output waveforms.

The complexity of this matter is further compounded by the fact that, because of the statistics of the signal-and-noise superposition, in a *linear rectifier* there is a square-law relationship between the signal input voltage and the signal-plus-noise output voltage for small signal-to-noise ratios. This relationship becomes linear for large signal-to-noise ratios, as shown by Bennett (21), North (2), and Rice (22). But this effect is the result of the statistics and the linear rectification, and not of a square-law voltage-current characteristic. It is the cause of the so-called noise suppression effect for small signal-to-noise ratios. It does not mean that a linear detector becomes a square-law detector for small signal-to-noise ratios.

Curves for Visual Detection

The curves of Figs. 4 through 7 apply when detection-decision is based on an automatic threshold device as described. It is reasonable to suppose, however, that a human observer makes decisions in an analogous manner. That is, the equivalent of a threshold voltage (which would be a luminosity level for the PPI-scope display, and a pip-height level for the A-scope display) exists somewhere in his eye-brain system. This threshold, resulting in a particular false-alarm probability, is probably related to the observer's experience and personality — his innate cautiousness or daring. The probability of detection probably depends not only on the signal-to-noise ratio in relation to the threshold, but also on the observer's visual-mental acuity, alertness or fatigue, and experience. Consequently, curves calculated for an automatic threshold decision device cannot be assumed to apply directly to the performance of a human observer of a cathode-ray-tube display. At the same time, such an assumption does not give grossly erroneous results and is justifiable when experimental human-observer data either are not available or are of questionable accuracy.

Curves that do apply for human observers can be obtained only through carefully conducted experiments under laboratory conditions designed to produce statistically valid results (conditions which may or may not apply in operational situations); that is, the experiments must be repeated many times with different observers so that a good measure of average or typical performance is obtained. Such experiments were conducted at the MIT Radiation Laboratory during World War II, as reported by Lawson and Uhlenbeck (15), and by Haeff (20) at the Naval Research Laboratory at about the same time.

Some of the Radiation Laboratory results can be translated into curves of the type of Figs. 4 through 7. The result for the A-scope display is given by Fig. 8, in which the abscissa axis is the radar pulse repetition frequency (prf) rather than the number of pulses integrated. The connection between the two quantities is obtained by assuming

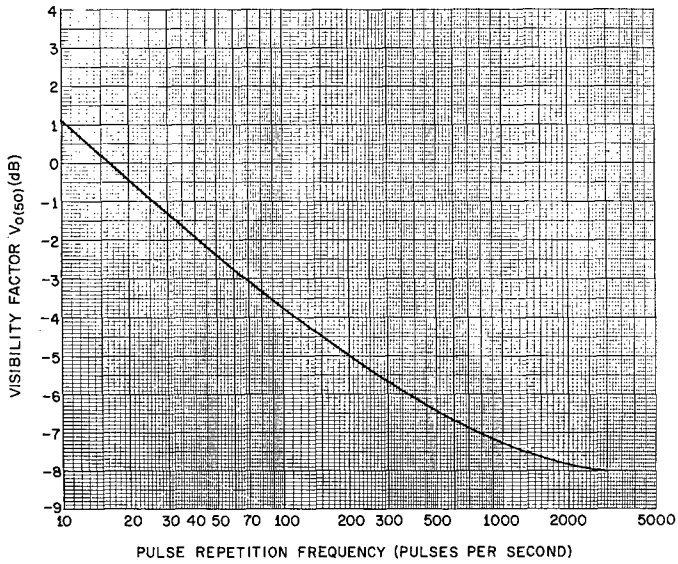

Fig. 8 - Visibility factor as a function of pulse repetition frequency for A-scope visual detection of signals by a human observer (from Ref. 15, Fig. 8.23) replotted to apply for 0.5 probability of detection (in accordance with Fig. 8.2 of Ref. 15), based on World War II experiments conducted at the MIT Radiation Laboratory. (Note: This figure also appears in a larger size in an appendix at the end of the report.)

that the human observer has a characteristic integration (memory) time t_i of the order of seconds. His "number of pulses integrated" M is then given by

$$M = t_i \overline{\text{prf}} \ , \tag{29}$$

where $\overline{\text{prf}}$ is the pulse repetition frequency. However, t_i is not an exactly known quantity; it has been variously estimated at from 1 to 10 seconds. A fairly conservative assumption is probably about 2 seconds.

Figure 8 applies for approximately $P_d = 0.5$, a value that is sometimes accepted as a conventional value for calculating a range performance figure. (One of the merits of this assumption is that the variation of required signal-to-noise ratio as a function of P_d is steeper in the $P_d = 0.5$ region than it is at much higher or much lower values; hence the range performance at $P_d = 0.5$ is a more definitive measure than that at much higher or lower values.) The probability of detection was measured in the Radiation Laboratory experiments. However, false-alarm probability was not measured. Consequently all that can be said about the false-alarm probability for Fig. 8 is that it may be assumed to be a value that is representative of typical human-observer performance.

The curve is seen to be flattening at the right-hand end, where the visibility factor is much less than unity ($<$-6 dB). This effect is attributed to the human observer's inability to detect luminous contrast ratios less than some critical small value (15). When the signal-to-noise ratio is very small, detection cannot be accomplished on a pip-height basis on the A-scope; a luminosity increase must be looked for on the A-scope as well as on the PPI and similar displays. When the fractional increase becomes less than this critical value, as it must at very small signal-to-noise ratios, integration of additional

pulses (e.g., by increasing the prf) can produce no further integration gain (reduction of the visibility factor required for detection).

The ordinate axis of Fig. 8 is labeled $V_{0(50)}$, signifying that it is the optimum-bandwidth value of V_0 for $P_d = 0.5$ (50%). Figure 9 is a similar curve for a PPI scope. Here the abscissa axis is number of pulses integrated, because the PPI is used with azimuth-scanning radars for which a definite number of pulses occurs each time the antenna beam traverses a target. This number is given for low-elevation-angle targets by

$$M = \frac{\theta_h \cdot \overline{\text{prf}}}{\omega} = \frac{\theta_h \cdot \overline{\text{prf}}}{6 \cdot \text{rpm}} , \tag{30}$$

where θ_h is the beamwidth of the antenna in the horizontal plane (azimuth beamwidth in degrees), $\overline{\text{prf}}$ is the pulse repetition frequency in pulses per second, ω is the angular scanning speed in degrees per second, and $\overline{\text{rpm}}$ is the antenna rotation rate in revolutions per minute (typically ranging from about 1 to 30).

This formula would be correct if the antenna beam pattern, in a polar-coordinate plot, were perfectly wedge-shaped with uniform gain within the wedge and zero gain elsewhere. Since the beam is not so shaped, the use of M thus calculated in conjunction with Figs. 5 through 9 causes some error in the range prediction, which can be corrected by including an antenna pattern loss factor L_p in the overall system loss factor L (to be discussed in Section 7).

The curve for the PPI, Fig. 9, is also for $P_d = 0.5$ and some unspecified false-alarm probability. The original data points are shown. Since there was no point at $M = 1$, the curve has been extrapolated to that value by applying knowledge gained from the automatic-detector performance calculations as to the change in slope of the curve in the region $V_0 > 1$ (0 dB). Note that this curve also begins to flatten in the low-visibility-factor region, where the luminous contrast is low. (The automatic detector does not suffer from this effect, because the integration is on a voltage-addition basis rather than luminosity addition. Therefore the "contrast" can be increased to any desired value after integration simply by providing voltage amplification in the region of the threshold level.)

Other Detection Methods

The discussion and results that have been presented have assumed perfect postdetection (video) integration of M pulses prior to detection by an automatic threshold device. The noise statistics have been implicitly assumed to be those of ordinary receiver noise (equivalent to thermal noise), of quasi-uniform spectral density and (before detection) of gaussian probability density. A great many other detection procedures and signal-noise statistics are possible. To attempt to give detection-probability curves for all of them would be hopeless. For all of them, however, there is some kind of a definite relationship between the detection probability, the false-alarm probability, and the required signal-to-noise ratio (defined as an average value for fluctuating signals). Consequently, in principle, curves of the type of Figs. 4 through 7 can be derived and applied to the prediction of radar range, through Eq. (10) or one of its derivatives.

Much work has been done on signal-detection problems from the information-theory and statistical-decision-theory points of view (23-26). The signal detection theory developed from the point of view of ordinary pulse radar can be extended to apply to CW and pulse doppler radar (27).

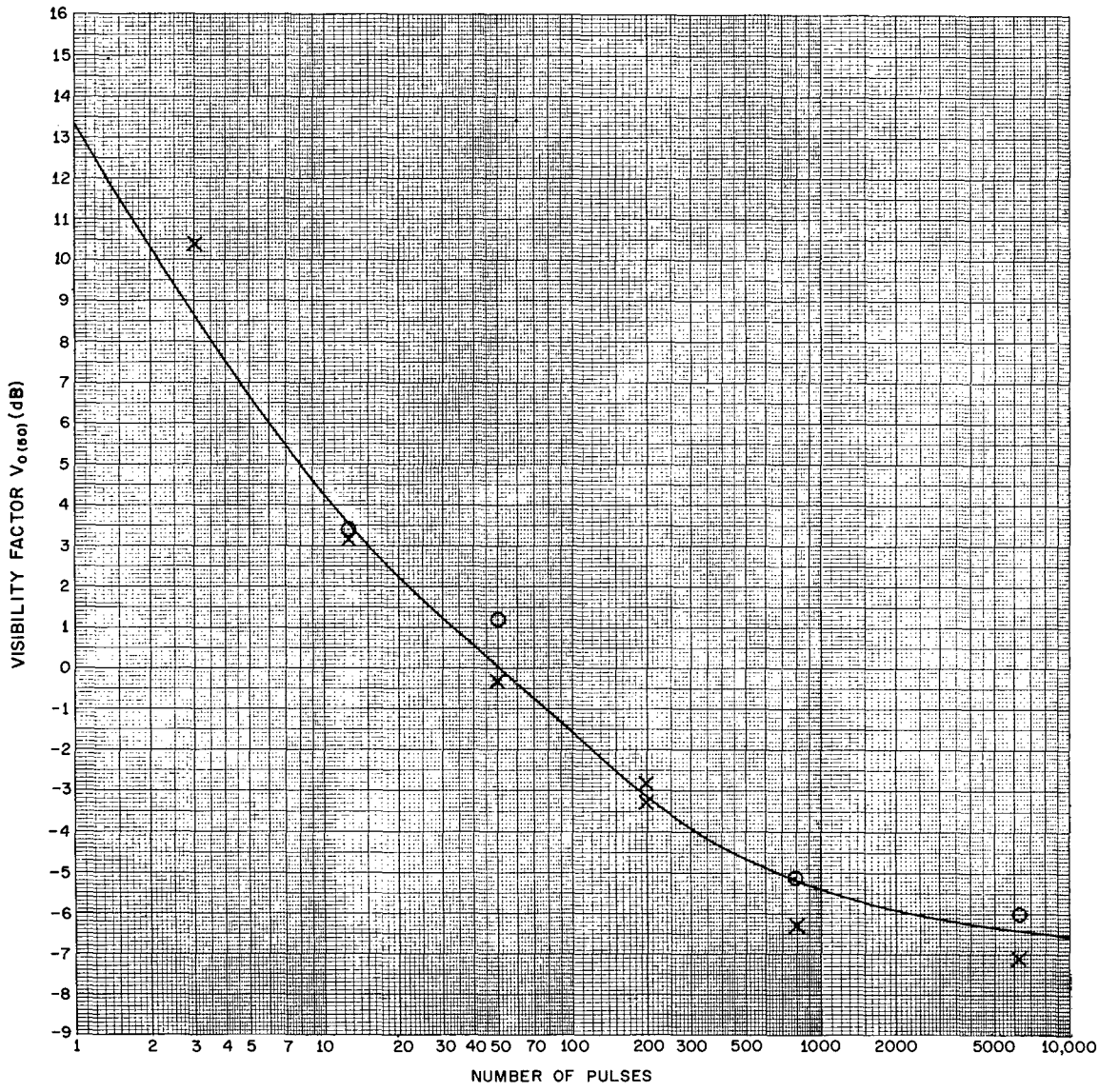

Fig. 9 - Visibility factor as a function of pulses in a half-power beamwidth interval on a PPI display (visual detection by human observer), replotted from experimental results at the MIT Radiation Laboratory during World War II, modified to apply for 0.5 probability of detection. (Note: This figure also appears in an appendix at the end of the report.)

5. SYSTEM NOISE TEMPERATURE

The concept of a noise temperature is derived from Nyquist's theorem (28), which states that if a resistive circuit element is at temperature T (degrees Kelvin), there will be generated in it a thermal noise voltage given by

$$V_n = \sqrt{4kTRB} \ , \tag{31}$$

where k is Boltzmann's constant (1.38054×10^{-23} watt-sec/°K), R is the resistance (ohms), and B is the bandwidth (hertz) within which the voltage is measured (that is, the passband of the voltmeter). The absence of the frequency in this expression implies that the spectrum is uniform — that the noise is white, and extends to infinitely high frequency, implying infinite energy. But, as this implies, Eq. (31) is an approximation, and a more exact expression, which does have frequency dependence, must be used at extremely high frequencies and extremely low temperatures. The noise spectrum becomes significantly nonwhite if the ratio f/T exceeds about 10^8, where f is the frequency in hertz and T is the Kelvin temperature of the resistor. The probability distribution of thermal noise voltage is gaussian.

V_n as thus defined is the open-circuit voltage at the resistor terminals. If an external load is connected, the available noise power (16) that can be delivered to it is

$$P_n = kTB \ , \tag{32}$$

which does not depend on the value of R.

The concepts of available power, available gain, and its reciprocal, available loss, are used in all noise temperature and noise factor measurements. These concepts are explained fully in Refs. 16 and 29. Briefly, available power at an output port is that which would be delivered to a load that matches, in the complex conjugate sense, the impedance of the source. Available gain of a two-port transducer or cascade of transducers is the ratio of the available power at the output port to that available from the source connected to the input port, with the stipulation that the available output power is measured with the actual input source connected but not necessarily impedance-matched. Available loss is the reciprocal of available gain.

The usual noise that exists in a radar receiving system is partly of thermal origin and partly from other noise-generating processes, but these processes produce noise which, within the radio frequency spectrum, has the same spectral and probabilistic nature. Therefore it can all be lumped together and regarded as thermal noise. This is done, and the available power level is described by assigning to the noise a semifictitious noise temperature

$$T_n = P_n / kB_n \ . \tag{33}$$

This is of course simply an inversion of Eq. (32). The temperature thus defined is semifictitious because of the nonthermal origin of some of the noise. When this temperature represents the available noise power output of the entire receiving system, it is commonly called the system noise temperature (or operating noise temperature) (16); it is then used to calculate the system noise power and signal-to-noise ratio, as may be seen from Eqs. (3) through (5).

A receiving system may be represented as a cascade of transducers, beginning with a source (the antenna) and ending with a load (such as a cathode-ray-tube display or automatic decision device). However, in discussion of system noise temperature, only

those parts of the receiver that precede the detector (demodulator) are of significance, for the noise level at that point determines the signal-to-noise ratio for signal-detection-calculation purposes.

Noise may arise at any and all points in this cascade, so that the noise level changes from point to point. The important quantity is the output noise power P_{no}. For purposes of signal-noise calculation, however, it is convenient to refer this output noise to the system input terminals, by defining the system noise temperature T_s so that it satisfies the relation

$$kT_s B_n = P_{no}/G_o \ , \tag{34}$$

where G_o is the overall-system available power gain (16), and B_n is the noise bandwidth of the system (Eq. (16)).

Each component of the receiving-system cascade can be regarded as having its own effective input noise temperature T_e (16) representing its available output noise power referred to its own input terminals. Then, for an N-component cascade,

$$T_s = T_a + \sum_{i=1}^{N} T_{e(i)}/G_i \ , \tag{35}$$

where T_a is the antenna noise temperature, representing the available noise power at the antenna terminals (18), and G_i is the available gain of the system between its input terminals and the input terminals of the ith cascaded component. (Note that by this definition $G_1 = 1$ always.)

This formula will here be applied to a two-component cascade representing a typical receiving system (Fig. 10). The first component is the transmission line that connects the antenna to the receiver input terminals, and the second component is the predetection portion of the receiver itself. (As mentioned above, for purposes of signal-noise analysis subsequent portions of the receiver are not considered.) (If desired, a many-component receiving system could be further broken down, with a preamplifier and possibly other units considered as separate elements of the cascade.)

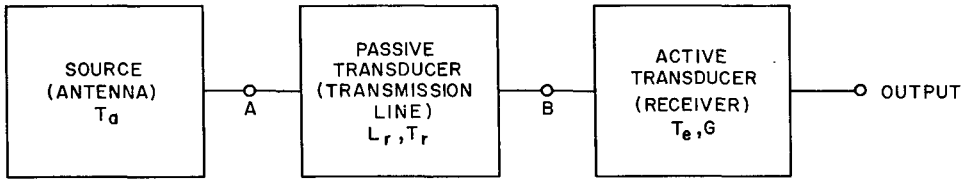

Fig. 10 - Cascade receiving system used as basis of system noise temperature calculation

For this system, if the transmission-line noise temperature is represented by T_r and its loss factor is $L_r (= 1/G_2)$, and if the receiver effective input noise temperature is T_e, Eq. (35) becomes

$$T_s = T_a + T_r + L_r T_e \ . \tag{36}$$

It now remains to discuss evaluation of T_a, T_r, L_r, and T_e.

Antenna Noise Temperature

The noise temperature of the antenna expresses the noise power density available (power per unit bandwidth) at the antenna terminals, in accordance with Eq. (33) (the ratio P_n/B_n is the noise power density if this ratio is evaluated at a particular frequency for the limiting case of $B_n \to 0$). The antenna noise temperature depends in a somewhat complicated way on the noise temperatures of various radiating sources within the receiving antenna pattern, including its side lobes and back lobes. (The concept of noise temperature of a radiating source of noise is based on Planck's law, or the Rayleigh-Jeans approximation to it, to which Nyquist's theorem for thermal noise in a resistor is analogous.)

Fortunately, however, the antenna noise temperature is not basically dependent on the antenna gain and beamwidth, in an overall-average sense. If a high-gain antenna is pointed at a very-high-temperature point source, such as a radio star, its noise temperature will be higher than that of a low-gain antenna pointed at the same source. But the noise temperatures of the two antennas with upward-pointed beams, averaged over all possible directions of the sky, will be approximately the same, if their side-lobe and back-lobe levels are equivalent. (This assumes that both antennas are of at least moderate directivity, as most radar antennas are.) Therefore, it is possible to calculate the noise temperature of a typical antenna (one assumed to have typical side-lobe and back-lobe levels), which will apply in this overall-average sense. This temperature is, however, a function of frequency (that is, antenna noise is not truly white, although within any typical receiver passband it is virtually white.) In the microwave region, it is also a function of the antenna beam elevation angle, because in this region most of the sky noise is the result of atmospheric radiation, which is greater at low angles where the antenna beam sees a thicker slice of the lossy atmosphere than it does at higher angles.

Curves of antenna temperature for a lossless antenna are shown in Fig. 11, calculated for the following conditions judged to be typical (29): (a) average galactic noise (which actually varies greatly with beam direction, but not in a manner expressible in geocentric coordinates); (b) sun noise temperature 10 times the quiet level, with the sun viewed in a side lobe of unity gain; (c) a cool temperate-zone atmosphere; and (4) a uniform 2.7°K cosmic-blackbody-radiation contribution, independent of frequency and elevation angle.

The curves of Fig. 11 apply to a lossless antenna that has no side lobes directed toward a warm earth or to a lossless antenna above a perfectly reflecting earth. In most practical cases a ground-noise-temperature component must be added; but then also the sky noise component, given by Fig. 11, must be reduced somewhat because part of the total antenna pattern is not directed at the sky. The reduction factor is $1 - T_g/T_{tg}$, where T_g is the ground noise temperature contribution to the total antenna temperature and T_{tg} is the effective thermal temperature of the ground. If α is the fraction of the antenna power pattern subtended by the earth, then $T_g = \alpha T_{tg}$. If the earth is perfectly absorptive (a blackbody), its effective noise temperature may be assumed to be approximately 290°K. A suggested conventional value for T_g is 36°K, which would result if a 290°K earth were viewed over a π-steradian solid angle by side and back lobes averaging 0.5 gain (-3 dB). These side lobes are typical of a good radar antenna but not one of the ultra-low-noise variety.

Moreover, some practical antennas have appreciable ohmic loss, expressed by the loss factor L_a (Section 3). An additional thermal noise contribution of amount $T_{ta}(1-1/L_a)$ then results, where T_{ta} is the thermal temperature of the lossy material of the antenna. However, the noise from external sources is then also reduced by the factor $1/L_a$. The total correction to the temperature values given by Fig. 11 to account for both ground noise contribution and antenna loss is given by

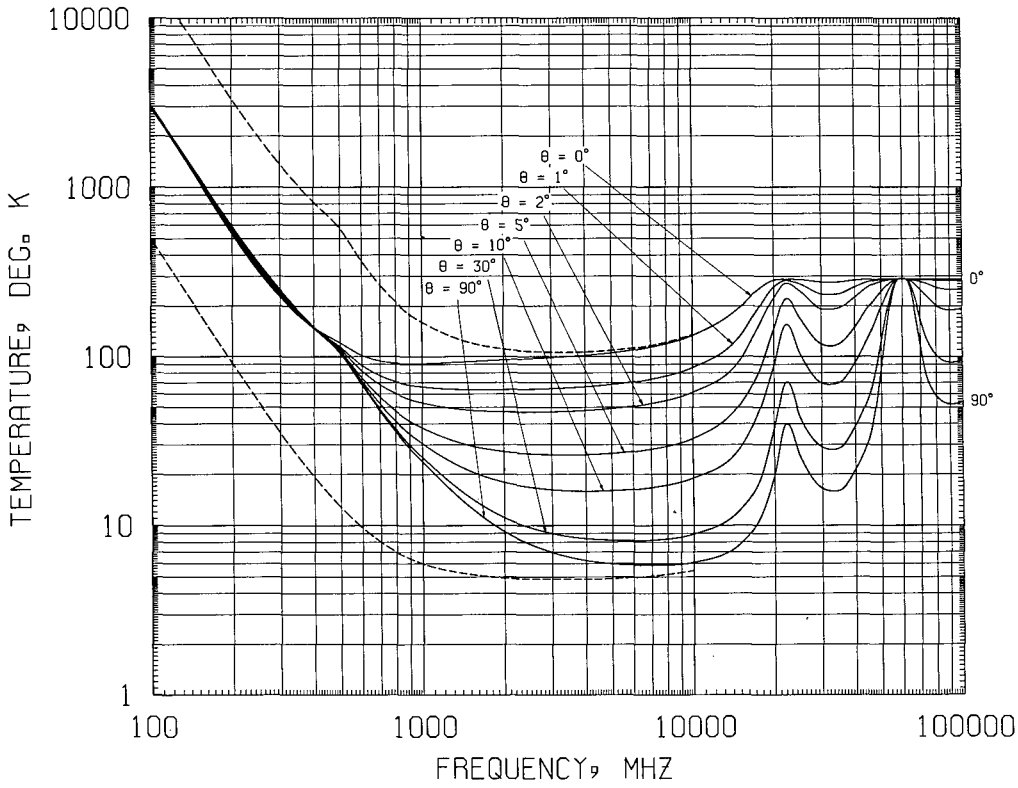

Fig. 11 - Noise temperature of an idealized antenna (lossless, no earth-directed side lobes) at the earth's surface as a function of frequency for a number of beam elevation angles. The solid curves are for the geometric-mean galactic temperature, sun noise 10 times the quiet level, the sun in a unity-gain side lobe, a cool temperate-zone troposphere, 3°K cosmic blackbody radiation, and zero ground noise. The upper dashed curve is for maximum galactic noise (center of galaxy, narrow-beam antenna), sun noise 100 times the quiet level, zero elevation angle, and other factors the same as for the solid curves. The lower dashed curve is for minimum galactic noise, zero sun noise, and a 90-degree elevation angle. The slight bump in the curves at about 500 MHz is due to the sun noise characteristic. The curves for low elevation angles lie below those for high angles at frequencies below 400 MHz because of the reduction of galactic noise by atmospheric absorption. The maxima at 22.2 GHz and 60 GHz are due to water-vapor and oxygen absorption resonances. (Note: This figure also appears in a larger size in an appendix at the end of the report.)

$$T_a = [T'_a(1 - T_g/T_{tg}) + T_g]/L_a + T_{ta}(1 - 1/L_a) , \tag{37}$$

where T'_a is the temperature given by Fig. 11. For $T_g = 36°K$ and $T_{tg} = T_{ta} = 290°K$, Eq. (37) becomes

$$T_a = (0.876\ T'_a - 254)/L_a + 290 , \tag{37a}$$

and if $L_a = 1$ (lossless antenna), it further simplifies to

$$T_a = 0.876\ T'_a + 36 . \tag{37b}$$

Transmission-Line Noise Temperature

Dicke (30) has shown that if a passive transducer of noise bandwidth B_n connected in a cascade system is at a thermal temperature T_t degrees Kelvin and if its loss factor is L, the thermal noise power available at its output terminals due to the thermal noise generated in it is

$$P_{no} = kT_t B_n (1 - 1/L) . \tag{38}$$

From Eqs. (33) and (34) the effective input noise temperature of a passive transducer is

$$T_i = P_{no} L/kB_n . \tag{39}$$

From Eqs. (38) and (39), the formula for the receiving-transmission-line effective input noise temperature is

$$T_r = T_{tr} (L_r - 1) , \tag{40}$$

where T_{tr} is the transmission-line thermal temperature. A suggested conventional value for T_{tr} is 290°K. The receiving-transmission-line loss factor L_r is defined in terms of a CW signal received at the nominal radar frequency by the antenna. It is the ratio of the signal power available at the antenna terminals to that available at the receiver input terminals (points A and B in Fig. 10).

Receiver Noise Temperature

The effective input noise temperature of the receiver T_e may sometimes be given directly by the manufacturer or designer. In other cases the noise factor F_n may be given. The relationship between the noise factor and the effective input noise temperature of the receiver, or of any transducer, is given (16) by

$$T_e = T_0 (F_n - 1) , \tag{41}$$

where T_0 is by convention 290°K. In this formula F_n is a power ratio (often given in decibels).

This formula is applicable to a *single-response* receiver (one for which a single RF input frequency corresponds to only one output or IF frequency and vice versa). Methods of computing noise temperatures when a double- or multiple-response receiver is used (e.g., a superheterodyne receiver without preselection) are described in Refs. 16 and 29. Single-response receivers are ordinarily used in radar systems.

It is worth mentioning a point that has been well emphasized in the literature but is nevertheless easily forgotten. A receiver noise temperature or noise factor rating applies only when a particular terminating impedance is connected at the receiver input. If this impedance changes, the receiver noise temperature changes. Therefore in principle when a noise temperature rating is quoted for a receiver, the source impedance (impedance "seen" by the receiver from its input terminals) should be specified, especially since the optimum (lowest) noise temperature does not necessarily occur when impedances are matched. However, when a receiver noise temperature is quoted without this impedance specification, it is presumable that the optimum source impedance is implied.

6. PATTERN-PROPAGATION FACTOR

The factors F_t and F_r in the range equations account for the facts that the target may not be in the antenna-pattern maximum and that the wave propagation between antennas and target may not be free-space propagation. Thus F_t and F_r contain antenna pattern factors and also account for reflection-interference (multipath) effects, diffraction and shadowing, absorption losses, and abnormal refraction effects. (The normal refraction, which is slight, does not affect detection range significantly when the target is above the radar horizon, but it does affect the range-height-angle relationship in plotting coverage diagrams.)

In most cases, the effects of absorption are more conveniently taken into account by including an absorption-loss factor in the system-loss-factor product L. Therefore, absorption propagation losses are not considered under this heading, although under some conditions absorption loss should be included in the evaluation of the pattern-propagation factors rather than being expressed as part of the system loss factor.

The pattern-propagation factor F is the ratio, at a point in space, of the field strength E that is actually present to that which would have been present, E_0, if free-space propagation had occurred and the point were in the antenna-pattern maximum. (This definition is actually for F_t but applies to F_r as well through the principle of reciprocity.) Symbolically,

$$F(R, \phi, \theta) = E(R, \phi, \theta)/E_0(R) \quad , \tag{42}$$

where R, ϕ, and θ are the range, azimuth, and elevation coordinates of the point in space. Thus F has the dimensions of a voltage ratio, and so in the range equation where power ratios (such as G_t and G_r) occur to the first power, the pattern-propagation factors occur as F_t^2 and F_r^2.

The discussion that follows will be in terms of an unsubscripted quantity F, which may be taken to be either F_t or F_r. Also, of course, for a monostatic radar that uses the same antenna for both transmitting and receiving, $F_t = F_r = F$. (However, not all monostatic radars use the same antenna for transmitting and receiving.)

At the usual radar frequencies (VHF and higher), a radar antenna can ordinarily see only targets that are above the horizon. (Diffraction, which results in some field strength below the horizon, is ordinarily too weak an effect to be useful for radar detection, and anomalous refraction effects, which sometimes create very strong fields below the normal horizon, are unreliable in most parts of the world.) Consequently, below the horizon, ordinarily $F = 0$ as a result of shadowing by the spherical earth. Exceptions occur for radar using frequencies below VHF, at which ionospheric reflection takes place, or at which a vertically polarized surface wave will propagate beyond the horizon. Radar employing these modes of propagation will detect targets below the normal line of sight. Range prediction for radar employing ionospheric reflection for beyond-the-horizon detection has been discussed by Ross and Schwartzman (31).

The primary usefulness of the pattern-propagation factor is in calculating the effect of multipath interference that occurs when the radar antenna overlooks a surface that produces specular reflection. If the vertical-plane pattern of the antenna is broad, so that some of the radiation can reach a target by way of a reflected path in addition to that which goes by a direct path, the two waves will in general arrive at the target with a phase difference as well as an amplitude difference. The field at the target is then the vector-phasor sum of these two waves. If absorption is ignored and the target is in the antenna pattern maximum, the direct-path-wave field strength E_d can be used for E_0 in Eq. (42). If the target is not in the pattern maximum, this field strength must be multiplied by the antenna pattern factor $f(\theta)$, which describes the antenna vertical-plane

field-strength pattern, normalized to unity at the beam maximum, as a function of the vertical-plane angle θ. Numerically, $f(\theta) \leq 1$.

The three following classes of reflection-interference problems require successively more elaborate procedures for their solution:

1. One terminal of the propagation path is low, and the reflection point is close enough to this terminal so that the earth's surface may be considered a plane reflector (flat-earth case).

2. The distance from the lower terminal of the path to the reflection point is appreciable, so that the earth's curvature is significant (spherical-earth case), but yet the grazing angle is great enough so that the path-length difference of the direct and reflected rays is an appreciable fraction of a half wavelength, or larger.

3. The target is nearly on the radio horizon, so that the postulation of the separate existence of direct and reflected rays becomes questionable and ray optics is no longer applicable.

In cases 1 and 2 the target is said to be in the interference region. A target below the horizon would be in the diffraction region. In case 3 the target is said to be in the intermediate region. The theoretical solution of this problem is difficult, but an approximate result can be obtained by straightforward calculation (14).

The sea surface is in general a fairly good specular reflector. (Surface roughness does not fully destroy the specularity of reflection, though it reduces it.) Under special conditions, land surfaces can also act as specular reflectors (1). The methods that will be described are quite general and can be applied to any reflecting surface. Special attention will be given to the reflection characteristics of the sea, because it is a reflecting surface often encountered in practical radar applications.

To solve any reflection-interference problem, it is necessary to know the reflection coefficient of the surface. In general

$$\Gamma = \rho \, e^{-j\phi} , \tag{43}$$

where Γ is the complex reflection coefficient of magnitude ρ and phase angle ϕ (the angle by which the phase of the reflected wave lags that of the incident wave).

The general formula for F when reflection-interference occurs is

$$F = |f(\theta_1) + \rho D \, f(\theta_2) \, e^{-j\alpha}| \tag{44}$$

where θ_1 is a vertical-plane angle that defines the direction of the direct-path ray and θ_2 similarly defines the direction of the reflected ray at the antenna (Fig. 12). The pattern factor $f(\theta)$ is, in transmitting terms, the ratio of the radiated electric field intensity in the direction θ to that in the maximum-intensity direction. An analogous definition applies for the receiving antenna. Equation (44) applies for either a flat or curved earth. In the flat-earth case, the divergence factor D is equal to 1. Its evaluation in the general case will be discussed under the heading Spherical-Earth Reflection.

The angle α is the phase difference, at the target, of the direct and reflected waves. It is the sum of the reflection-coefficient phase angle ϕ and a phase difference β that results from the path-length difference δ of the direct and reflected rays. This path-length phase difference is given by

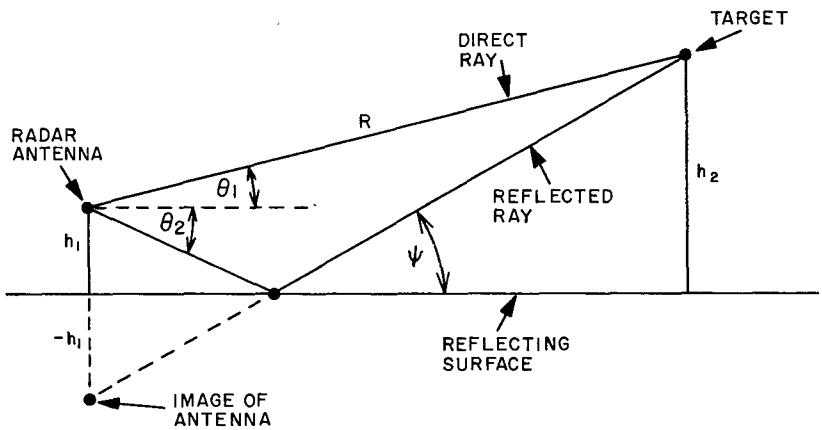

Fig. 12 - Geometry of reflection from a plane earth

$$\beta = 2\pi\delta/\lambda \text{ radians} \tag{45}$$

where λ is the wavelength.

Flat-Earth Reflection

The geometry of flat-earth reflection is shown in Fig. 12. For simplicity it is assumed that $\theta = 0$ in the horizontal direction. It can be shown that if the target is at a distance R that is much greater than the antenna height h_1, which is typically true for earth-based or ship-based radars, and if the target is above the horizontal plane, that is, at a positive elevation angle, the angles θ_1 and θ_2 can be considered equal. The equation for F then becomes

$$F = f(\theta_1) \left|\sqrt{1 + \rho^2 + 2\rho \cos(\phi + 2\pi\delta/\lambda)}\right| . \tag{46}$$

The reflection coefficient of the surface depends on its roughness, the grazing angle ψ (angle between the ray and the surface at the reflection point), the complex dielectric constant of the material below the surface, and the polarization (14, Ch. 5). The roughness affects only ρ, in such a manner that

$$\rho = r\rho_0 , \tag{47}$$

where $r\ (= \rho/\rho_0)$ may be called the roughness factor and ρ_0 is the reflection coefficient of a smooth surface. Curves for ρ_0 and ϕ for the sea, taken from Kerr (14), are given in Figs. 13a, 13b, and 13c. A curve for the horizontal-polarization value of ϕ is not given, because it is almost constant and equal to 180 degrees; it is exactly 180 degrees at $\psi = 0$, and increases linearly to a maximum value that is less than 184 degrees at $\psi = 90$ degrees, for frequencies in the range 100 to 10,000 MHz.

Note that ϕ is also 180 degrees for vertical polarization at $\psi = 0$, and that $\rho_0 = 1$ for both polarizations at this grazing angle. The result is that near $\psi = 0$ (grazing incidence), since $\delta \approx 0$ the reflected ray very nearly cancels the direct ray, resulting in $F = 0$ (no field strength) with either polarization. This result is modified in the curved-earth case by the divergence factor D, but only slightly. This cancellation effect is the

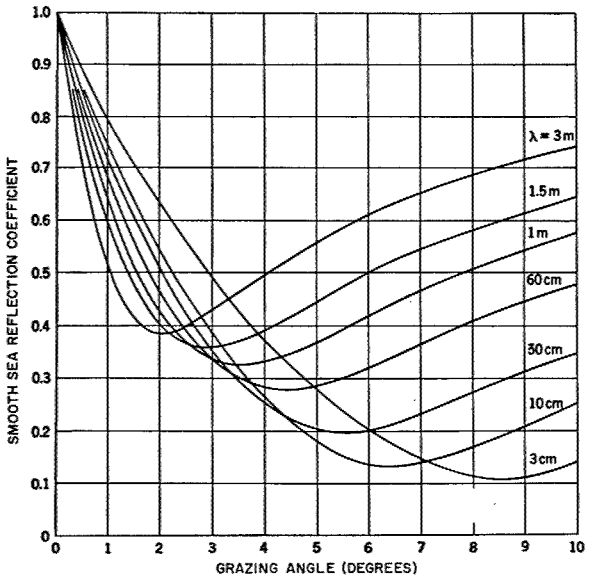

Fig. 13a - Magnitude of the reflection coefficient for a smooth sea and vertical polarization at a number of wavelengths (from Ref. 14, Fig. 5.4). (Note: This figure also appears in a larger size in an appendix at the end of the report.)

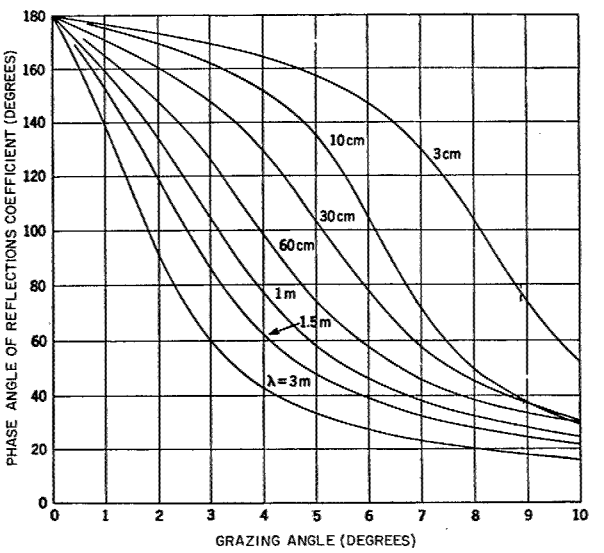

Fig. 13b - Phase angle of the reflection coefficient for a smooth sea and vertical polarization at a number of wavelengths (from Ref. 14, Fig. 5.5). (Note: This figure also appears in a larger size in an appendix at the end of the report.)

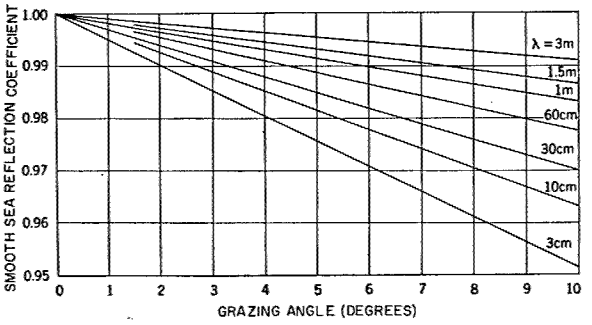

Fig. 13c - Magnitude of the reflection coefficient for a smooth sea and horizontal polarization for a number of wavelengths (from Ref. 14, Fig. 5.6). (Note: This figure also appears in a larger size in an appendix at the end of the report.)

reason for poor radar detection capability at very small grazing angles (low-altitude targets), although at sufficiently high frequencies the cancellation effect rapidly disappears as ψ is increased, and radar detection improves rapidly for targets that are only a small distance (h_2 in Fig. 12) above the surface. In fact, at some small value of ψ for typical radar antenna heights and frequencies the cancellation changes to a reinforcement (when $\delta = \lambda/2$), and, if $\rho = 1$, $F = 2$. The radar detection range is then doubled compared to its free-space value. That is, $R_{max} = FR_0$, where R_0 is the maximum range calculated for free space ($F = 1$). This relation indicates the great importance of the pattern-propagation factor when reflection interference occurs.

If F is calculated and plotted as a function of θ from Eq. (46), the result is a pattern of lobes (maxima and minima) corresponding to the values of ψ for which $\phi + 2\pi\delta/\lambda$ is either an even multiple (maxima) or an odd multiple (minima) of π. If $\rho = 1$ and $f(\theta) = 1$ (a smooth perfectly reflecting flat surface and an isotropic antenna), then $F = 0$ in the minima, which are therefore nulls, and in the maxima $F = 2$. This result is approximated at low elevation angles for smooth-sea reflection and horizontal polarization. For vertical polarization the result is modified in detail but not in the general nature of the lobe structure. The antenna pattern factor $f(\theta)$ also modifies the isotropic-pattern result. A typical sea-reflection lobe structure calculated for the flat-earth assumptions with horizontal polarization is shown in Fig. 14.

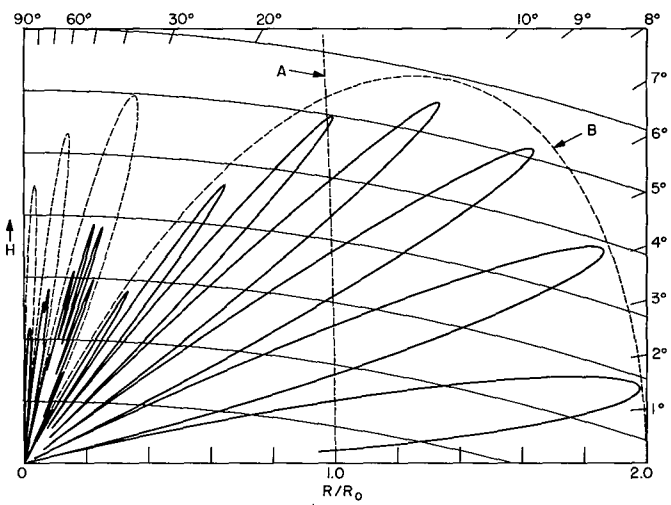

Fig. 14 - A typical reflection-interference lobe pattern, calculated for 100 MHz, an antenna height of 100 feet, a vertical-plane $(\sin x)/x$ antenna pattern of 20-degree half-power beamwidth, the beam maximum on the horizon, and horizontal polarization. Reflection from a sea of 2.1-foot-standard-deviation wave height (approximately 6 feet from crest to trough) was assumed, using Eq. (56) to be introduced in the text. The range scale is relative to assumed free-space maximum range R_0 of 150 naut mi. Height H units are 0.2 times the range units. Dashed line A is the detection range contour that would apply for free-space propagation with an isotropic vertical antenna pattern and the same gain as the $(\sin x)/x$ pattern maximum. Dashed contours B are loci of lobe maxima that would exist if the reflection coefficient of the surface were -1 at all angles, with divergence $D = 1$, a $(\sin x)/x$ antenna pattern, and a 20-degree half-power beamwidth.

If the assumption is made that the target is at a distance much greater than the antenna height, F can be regarded as a function of θ alone, independent of the target range and height. When this assumption can be made, the following simple formula for δ can be used, as may be deduced by a geometric analysis of Fig. 12 with the assumption that $\theta_1 \approx \theta_2$:

$$\delta = 2h_1 \sin \theta_1 \tag{48}$$

If also $\phi = 180$ degrees, as is approximately true for sea reflection with horizontal polarization at all target elevation angles and for vertical polarization at very low angles, Eq. (46) becomes

$$F = f(\theta_1)\left|\sqrt{1 + \rho^2 - 2\rho \cos\left(\frac{4\pi h_1 \sin \theta_1}{\lambda}\right)}\right| . \tag{49}$$

If in addition $\rho = 1$ (smooth surface or very small grazing angle), the following simple formula is obtained:

$$F = 2f(\theta_1)\left|\sin\left(\frac{2\pi h_1 \sin \theta_1}{\lambda}\right)\right| . \tag{50}$$

Equation (50) can also be written in the form

$$F = 2f(\theta_1)\,|\sin\,(0.366\, h_{ft} f_{MHz} \sin \theta_1)|\ , \tag{51}$$

in which h is in feet, f is in megahertz, and the argument of the outer sine function is in degrees. For $\phi = 180$ degrees the maxima and minima of F occur at angles

$$\theta_{min} = \sin^{-1}[(n-1)\lambda/2h] = \sin^{-1}[492\,(n-1)/(f_{MHz}h_{ft})] \tag{52}$$

and

$$\theta_{max} = \sin^{-1}[(2n-1)\lambda/4h] = \sin^{-1}[246\,(2n-1)/(f_{MHz}h_{ft})], \tag{53}$$

in which $n = 1, 2, 3, \ldots, N$. N is the number of complete lobes in the pattern and is the integer nearest to and smaller than $(2h/\lambda) + 1/2$. (If this number is not an exact integer, a partial lobe will exist at $\theta_1 = 90$ degrees (straight up) if the antenna pattern permits radiation in the vertical directions.)

These flat-earth formulas are reasonably valid, from the viewpoint of calculating δ using Eq. (48), if h_1 is less than about 1000 feet and if the following inequality is satisfied:

$$\tan \theta_1 > \sqrt{h_1} \times 10^{-3}\ , \tag{54}$$

where h_1 is in feet. This formula is derived by requiring that the reflection point on the actual curved earth shall be below the plane tangent to the earth's surface at the antenna by less than 1% of h_1, assuming standard refraction. This inequality also insures that the tilt of the earth's surface at the reflection point, relative to the tangent plane at the antenna, will be negligible compared to θ_1. Also, the divergence factor will be approximately equal to unity if Eq. (54) is satisfied and if h_1 is less than about 1000 feet (as deduced from Kerr (14, p. 137, Fig. 2.25)). If h_1 is greater than 1000 feet, in general D is

significantly less than unity even when Eq. (54) is satisfied. A graphical method for determining D in that case will be given in the discussion of the spherical-earth calculation of F.

Another flat-earth approximation for δ that is sometimes useful is given in terms of the two heights h_1 and h_2 and their horizontal separation G (the ground range):

$$\delta \approx \frac{2h_1h_2}{G}, \tag{55}$$

which holds if $G^2 >> (h_1 + h_2)^2$, without requiring that $\theta_1 \approx \theta_2$.

Rough-Surface Reflection Coefficient

There is an extensive literature on the reflection of electromagnetic waves from rough surfaces (32-36), but the problem of predicting the specular reflection coefficient of a rough surface has not been fully solved. Ament (34) gives* the following formula for a randomly rough surface with a gaussian height distribution:

$$r = \rho/\rho_0 = \exp\left[-2\left(\frac{2\pi H \sin\psi}{\lambda}\right)^2\right], \tag{56}$$

in which H is the standard deviation of the height distribution, ψ is the grazing angle (Fig. 12), and λ is the wavelength. This formula is not claimed to take all elements of the problem into account, but it does give fair agreement with rough-sea reflection experiments reported by Beard, Katz, and Spetner (35). Specifically, it does not take into account shadowing and autocorrelation interval — the rapidity with which the surface height varies as a function of horizontal distance. Also, of course, the sea surface is not truly gaussian. The experimental results give larger values of r than predicted by Eq. (56) for values of $H(\sin\psi)/\lambda$ greater than about 0.1. A plot of this equation in terms of the parameter $Hf \sin\psi$ is given in Fig. 15 for H in feet and f in megahertz. In using this curve it is important to remember that H is the standard deviation of the surface, which is roughly 35% of the crest-to-trough wave height for sinusoidal waves. The dashed curve approximately represents the experimental data in the region of large $Hf \sin\psi$.

When a surface is rough, there is in addition to the specular reflection a diffuse or scattered reflection component which fluctuates as the sea moves. Its behavior in this respect is similar to that of the backscattered signal that causes the well-known phenomenon of sea clutter. The forward-scattered signal is not usually considered in calculations of F, but it does combine with the direct wave and with the specularly reflected wave as a third component of the total field at the target, and it will cause F to fluctuate (32,35,36). Therefore, even though the target cross section is nonfluctuating, the received signal will then fluctuate. If the target cross section is fluctuating, the fluctuation of F will cause additional fluctuation of the received echo signal.

*Ament derives this result but states that it was originally derived by Pekeris and, independently, by MacFarlane during World War II.

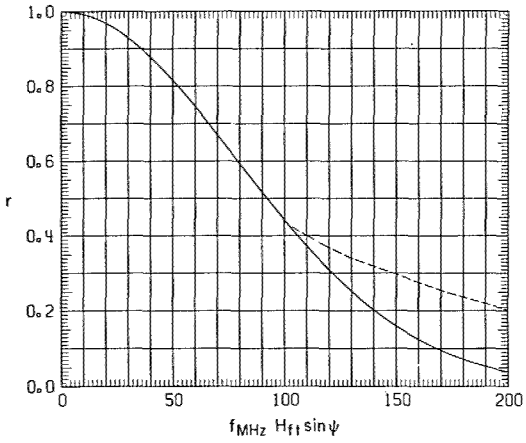

Fig. 15 - Ratio of the rough-sea to the smooth-sea reflection coefficient r as a function of the parameter $f_{MHz} H_{ft} \sin\psi$ (f = frequency, H = standard deviation of the wave height distribution, and ψ = grazing angle). The solid curve was computed from Eq. (56). The dashed curve represents experimental results of Beard, Katz, and Spetner (35). (Note: This figure also appears in a larger size in an appendix at the end of the report.)

Spherical-Earth Reflection

When the condition of Eq. (54) is not met, the equation for the ray path difference δ cannot be based on the flat-earth assumption. The geometry of curved-earth reflection is shown in Fig. 16. To find δ when the earth's curvature is significant requires solution of a cubic equation. However, a method has been devised that simplifies the computation when certain conditions, which will be specified, are met. This method makes use of a pair of parameters S and T and three graphs (14). These parameters are defined by the equations

$$S = \frac{G}{1.23\left(\sqrt{h_1} + \sqrt{h_2}\right)} \tag{57}$$

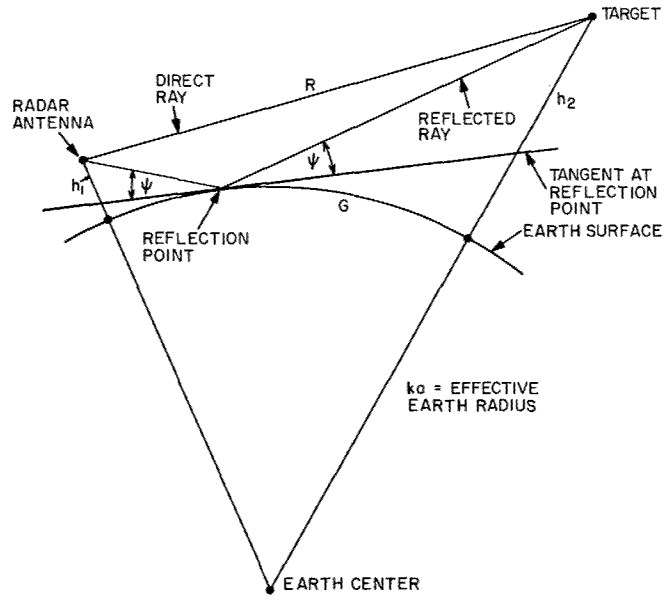

Fig. 16 - Geometry of reflection from a spherical earth

and

$$T = \sqrt{h_1/h_2} \quad \text{or} \quad \sqrt{h_2/h_1} \ , \tag{58}$$

where (Fig. 16) G is the ground range in nautical miles, h_1 is the antenna height in feet, and h_2 is the target height in feet. In Eq. (58) the right-hand side is chosen to make $T \leqq 1$.

The three graphs give correction factors, as functions of these parameters, that are applied to the flat-earth formulas when earth's curvature is significant. Figure 17a gives a correction factor J which is applied to Eq. (55) as follows:

$$\delta = \left(\frac{2h_1h_2}{G}\right) J(S,T) \ . \tag{59}$$

Figure 17b gives a correction factor K which is used to find the grazing angle ψ from the formula

$$\tan \psi = \left(\frac{h_1 + h_2}{G}\right) K(S,T) \ . \tag{60}$$

This value of ψ is used to find ρ_0 from Fig. 13a or 13c and to find ϕ from Fig. 13b if the polarization is vertical. (For horizontal polarization, $\phi \approx 180$ degrees.) It is also used for determining r from Fig. 15 or Eq. (56).

The remaining quantity needed for computing F from Eq. (44) is the divergence factor D. This is given directly as $D(S,T)$ by Fig. 17c.

Equation (44) can be rewritten in a form, analogous to Eq. (46), that is convenient for these curved-earth calculations as follows:

$$F = f(\theta_1) \left|\sqrt{1 + x^2 + 2x \cos(\phi + 2\pi\delta/\lambda)}\right| , \tag{61}$$

where

$$x = \frac{r\rho_0 D f(\theta_2)}{f(\theta_1)} \ . \tag{62}$$

The parameter x may be thought of as a generalized reflection coefficient.

Equations (57), (59), and (60) are given in terms of the ground range G. However, the curved-earth calculations will ordinarily be used only at very small target-elevation angles, and then the radar range R and the ground range G can be equated with negligible error. In fact, certain approximations made in developing Eqs. (57) through (60) require that they be used only at small elevation angles. But, as Eq. (54) shows, the flat-earth formulas can be used at the higher target elevation angles with negligible error, if the antenna height h_1 is not too great. The flat-earth formulas can also be applied if h_1 is large and h_2 is sufficiently small; that is, h_2 can be substituted for h_1 in Eq. (54) and θ is then interpreted as the elevation angle of the radar as viewed from the target, assuming $h_1 > h_2$.

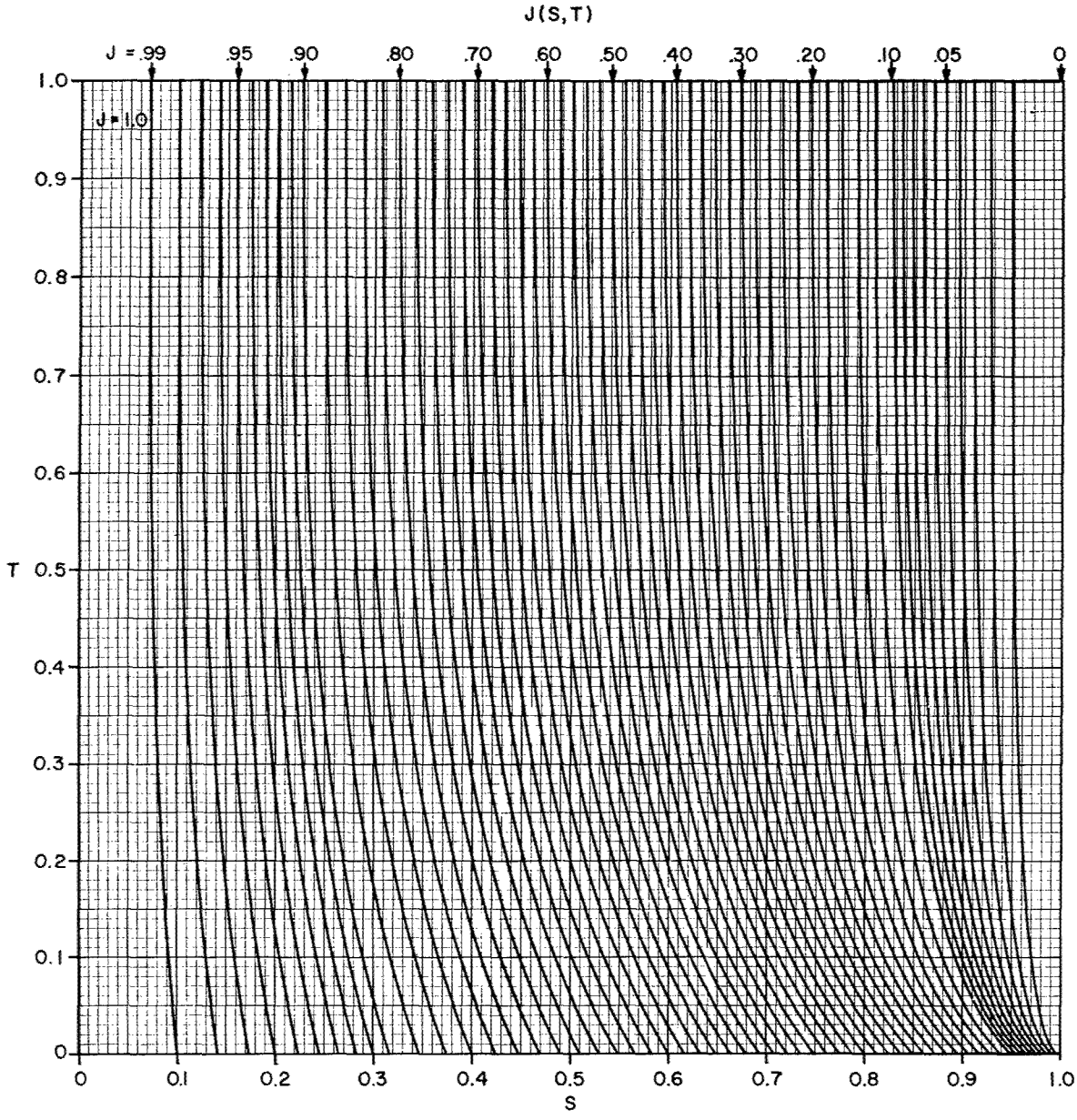

Fig. 17a - Correction factor J used in curved-earth pattern-propagation factor calculation, plotted as a function of parameters S and T. (Note: This figure also appears in an appendix at the end of the report.)

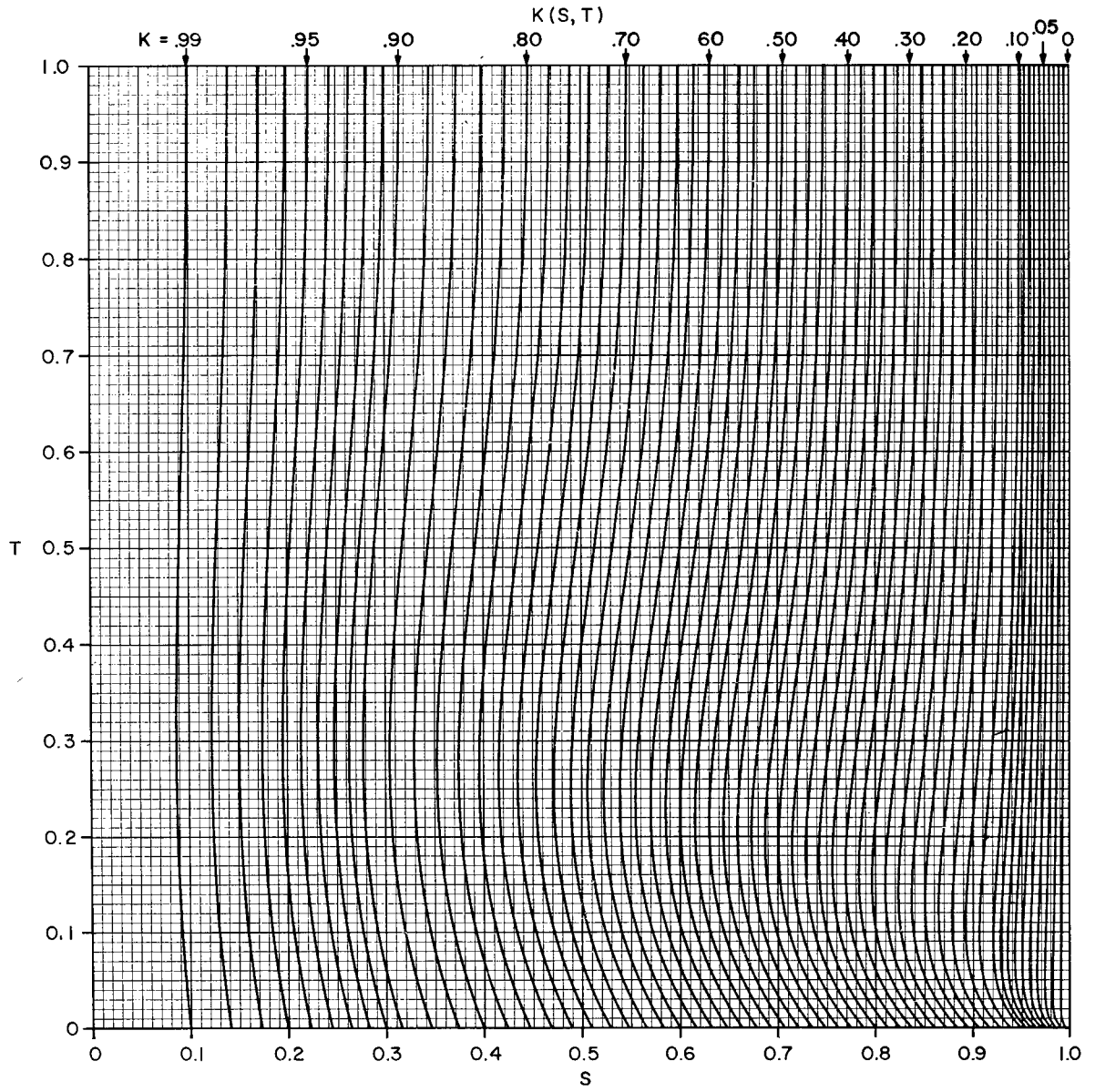

Fig. 17b - Correction factor K used in curved-earth pattern-propagation factor calculation, plotted as a function of parameters S and T. (Note: This figure also appears in a larger size in an appendix at the end of the report.)

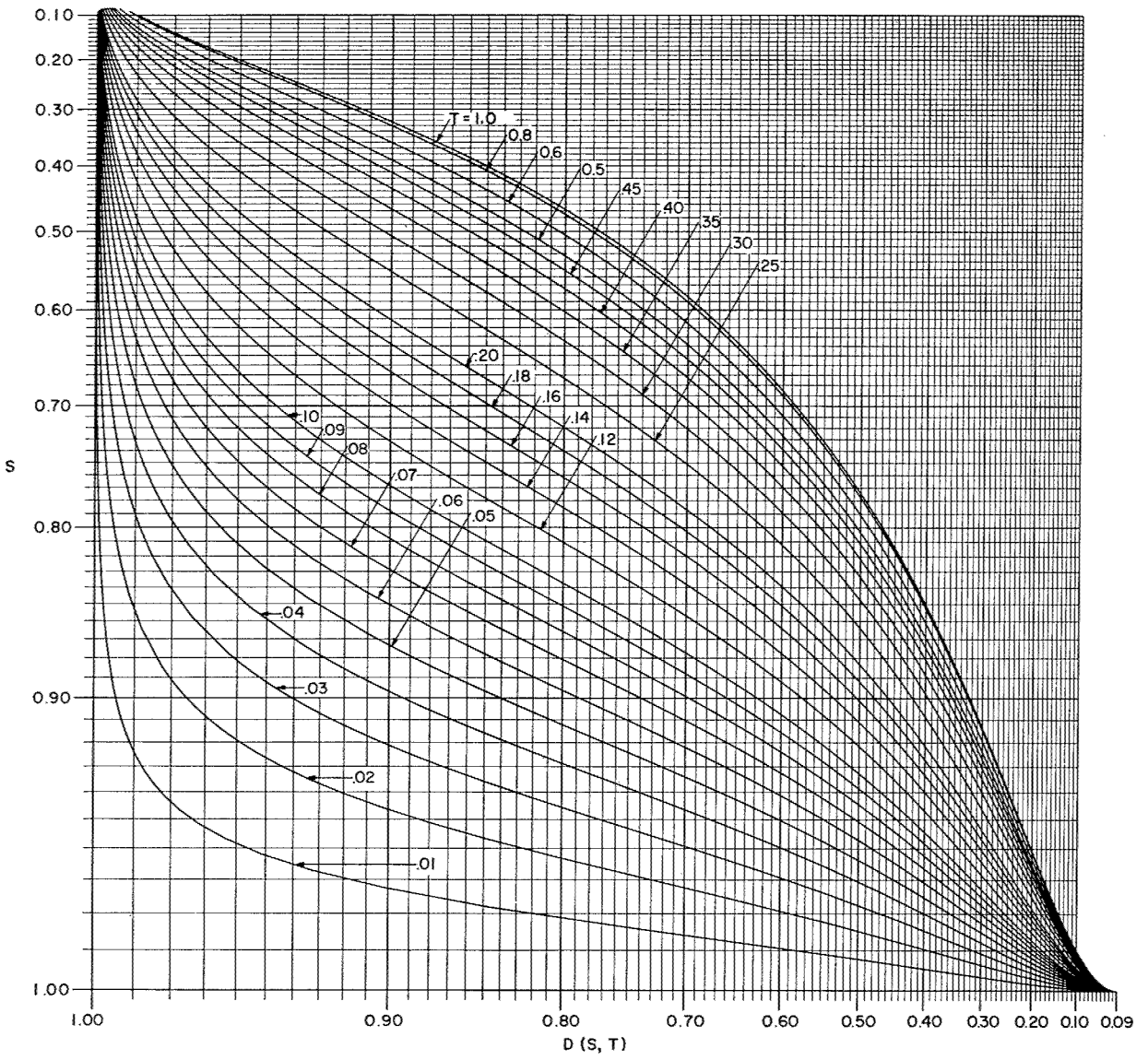

Fig. 17c - Divergence factor D plotted as a function of parameters S and T.
(Note: This figure also appears in an appendix at the end of the report.)

The only situation requiring curved-earth calculation of F for which the assumptions inherent in the above equations are not satisfied is that in which h_1 and h_2 are both large. This situation would exist, for example, with airborne radar detecting air targets. If there is appreciable sea or ground reflection in that case, a more rigorous analysis must be made.

The procedure that has been described allows a plot to be made of F as a function of range for a constant target height. This does not give a direct solution for the radar maximum range, because the value of F to be used in the range equation depends on R_{max}. One has in effect a transcendental equation. A graphical solution is readily obtained, however, as illustrated by Fig. 18. This is a plot of F as a function of range (interpreting G as equivalent to the radar range R) in rectangular coordinates with F as ordinate and R as abscissa. A straight line is drawn representing the equation $F = R/R_0$, where R_0, the free-space maximum range, is calculated from the range equation with $F_t = F_r = 1$. The greatest range at which the plot of $F(R)$ intersects this straight line is the radar maximum range for the specified target size and height. The intersections at lesser ranges demarcate the interference fade zones.

The Intermediate Region

When the target range is such that it is close to the radio horizon, then, as has been mentioned, ray-optical methods ("interference" concepts) become invalid. Diffraction effects become significant. An exact diffraction solution at or near the horizon is, however, quite complicated. Kerr (14) suggests the following method of "bold interpolation." First, two or more values of F are computed, for the given value h_2, that are well inside the interference region. Suggested points are those for which $\delta = \lambda$ and $\delta = \lambda/4$, with $\phi = 180$ degrees. Then, several points are calculated for values of range well into

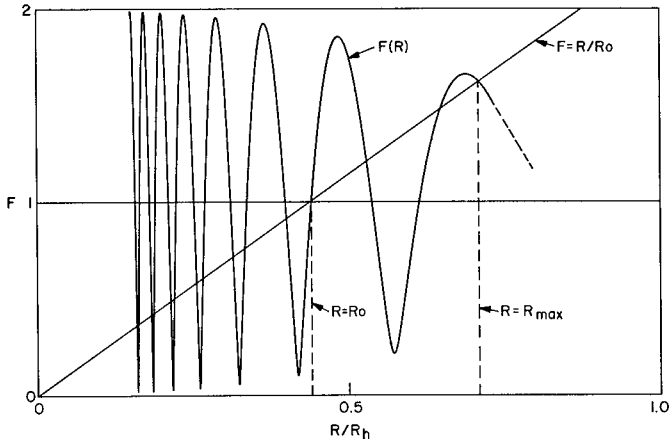

Fig. 18 - Graphical solution for the maximum range (labeled R_{max}), for a target at a constant altitude above a curved earth. The calculated F pattern is for 2800 MHz, antenna height 100 feet, target height 500 feet, reflection coefficient -1, and an isotropic vertical-plane antenna pattern. The range scale R/R_h is the ratio of the range to the total horizon distance, equivalent to the parameter S, Eq. (57). The upward-sloping straight line corresponds to $F = 1$ at $R = R_0$, the calculated free-space detection range.

the diffraction region (below the radio horizon). This calculation is relatively straightforward. The intermediate-region solution is then found by interpolating between these points.

The diffraction-field solution is in the form of an infinite series of terms, called modes. At and near the horizon, many terms must be summed to obtain an accurate solution; the terms of the series are decreasing very slowly. Well below the horizon, however, the first term represents the field to a very good approximation. This is called a one-mode solution. The first mode can be represented as the product of three factors. The first factor, V, is called the attenuation function, and the other two, U_1 and U_2, are called height-gain functions. V is a function of the range G, and U_1 and U_2 are functions of height. (Actually U_1 and U_2 are the same function U evaluated for the heights h_1 and h_2.) Figures 19a and 19b are graphs for evaluating V and U. They are applicable, subject to certain restrictions that are ordinarily met (14, pp. 109ff.), for either horizontal or vertical wave polarization at frequencies above about 100 MHz.

In the use of these graphs the range and height must be expressed in so-called natural units. The natural unit of range is (14, p. 97, Eq. (358))

$$L = k_1/f^{1/3} , \tag{63}$$

and the natural unit of height is (14, p. 96, Eq. (351))

$$H = k_2/f^{2/3} , \tag{64}$$

where $\log_{10} k_1 = 2.011591$ and $\log_{10} k_2 = 3.844342$ when f is the frequency in megahertz, L is in nautical miles, and H is in feet. The range in natural units is $X = G/L$, and the heights in natural units are $Z_1 = h_1/H$ and $Z_2 = h_2/H$. The graphs give V and U in decibels. (The numerical factor is 20 because F is a voltage ratio.) In these terms,

$$F = \text{antilog}\left\{\frac{1}{20}\left[V(X)_{dB} + U(Z_1)_{dB} + U(Z_2)_{dB}\right]\right\} . \tag{65}$$

Kerr (14, pp. 133-136) illustrates this procedure by a sample calculation, including determination of the maximum range by a slightly different graphical method from the one described in connection with Fig. 18.

Refraction and Coverage Diagrams

The ultimate goal of pattern-propagation-factor calculations is usually a plot of the radar maximum range as a function of either the target elevation angle θ_1 or the target height h_2. For distant targets, F can be computed as a function of θ_1, for targets that satisfy Eq. (54) by using the flat-earth formulas. However, even when Eq. (54) is satisfied, the target height h_2 cannot be calculated from the elevation angle θ_1 and the range R by means of the flat-earth formula $h_2 = R \sin \theta_1$. The earth's curvature must be taken into account in this calculation. Moreover, it is also necessary to take into account the slight downward bending (refraction) of rays in the atmosphere.

This refractive effect is approximately accounted for, for heights that are not too great, by the "effective earth's radius" method of Schelleng, Burrows, and Ferrell (37). The refractive index is assumed to decrease linearly with height; that is $dn/dh = C$, where C is a negative constant. The curvature of the rays is then such that, if plotted in a geometry where the earth has a radius k times greater than its true radius, they will

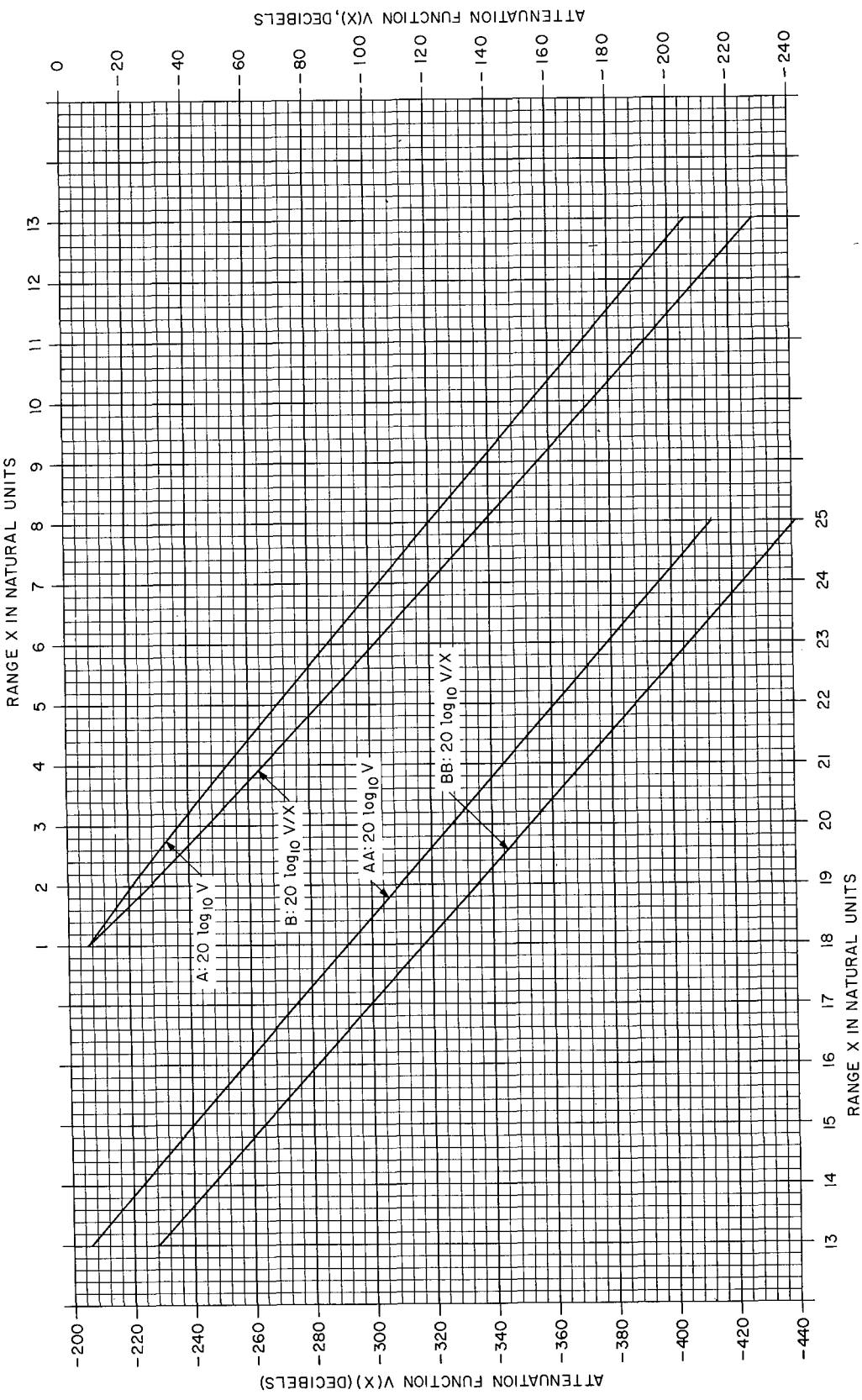

Fig. 19a – Attenuation function V used in intermediate-region pattern-propagation factor calculation. For curves AA and BB use left and bottom scales; for A and B, use top and right scales. (Note: This figure also appears in an appendix at the end of the report.)

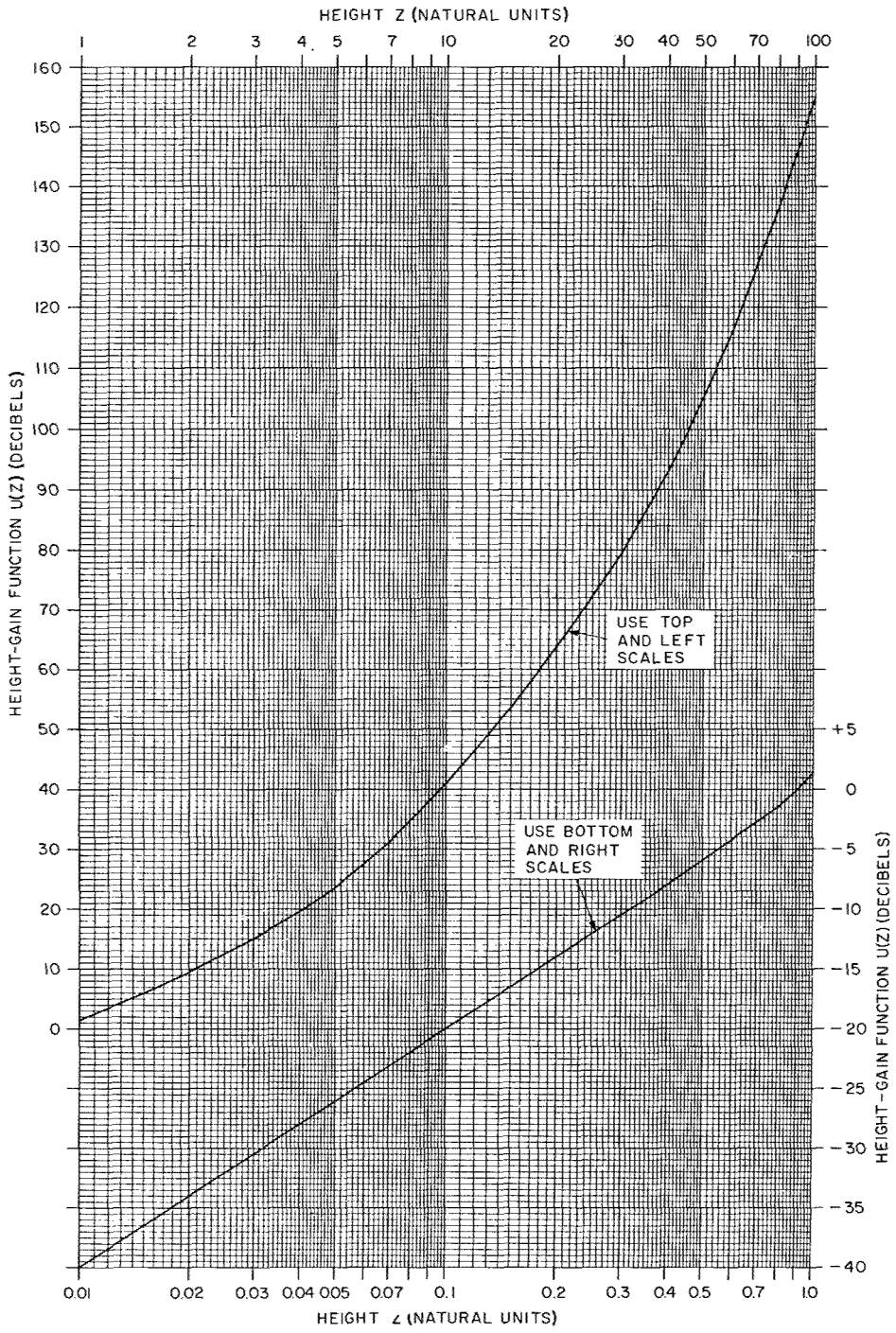

Fig. 19b - Height-gain function U used in intermediate-region pattern-propagation factor calculation (adapted from Ref. 14, Fig. 2.20). (Note: This figure also appears in an appendix at the end of the report.)

appear as straight lines. A standard (conventional) value for k is 4/3. The range-height-angle relationship for these assumptions, for radar ranges very much smaller than the earth's radius a is

$$h_2 = \frac{R^2 \cos^2 \theta_1}{2ka} + R \sin \theta_1 + h_1 . \tag{66}$$

If the heights are expressed in feet and the range is in nautical miles, with $k = 4/3$ and $a = 3440$ naut mi, this relationship becomes

$$h_2 = 0.6624\, R^2 \cos^2 \theta_1 + 6076\, R \sin \theta_1 + h_1 . \tag{67}$$

A range-height-angle chart can be constructed on the basis of Eq. (66), in which the rays are straight lines and (if the range and height scales are in the same units) the constant-range lines are circles with the origin as center. (If the range and height scales are not the same, the constant-range lines will be ellipses.) The constant-height contours on this chart will curve downward, with a curvature that is equal to that of the fictitious earth of radius $a_e = k(a + h_1)$. Plots of radar range as a function of elevation angle can be made on such charts; such plots are called coverage diagrams. When reflection interference occurs, these diagrams will exhibit the lobe structure that has been described.

The curved-earth and intermediate-region calculation procedures that have been described are all based on the assumption that the refraction can be described by the effective-earth-radius method. Since these procedures are meant to be used mainly for low-altitude-target problems, this assumption is not seriously in error. The ray height computed by this method is fairly accurate for heights up to about 10,000 feet (3 km).

Above 10,000 feet, however, the error gradually increases, and it is serious at heights of about 30,000 feet or more for ray paths that have a low initial elevation angle. A more realistic refractive index model that has been proposed and extensively studied is the exponential model (38-40),

$$n(h) = 1 + (N_s \times 10^{-6})\, e^{-\gamma h} , \tag{68}$$

in which N_s is the surface refractivity and γ is a decay constant. Unfortunately, this model does not result in simple formulas for the range-height-angle relationship; a numerical integration is required to trace a ray path (41,42). However, machine-computed results can be used to plot a range-height-angle chart for this model, on which the ray-path lines are straight; this result is accomplished by suitably distorting the contours of constant height (42). Two such charts are shown in Figs. 20a and 20b, based on the values $N_s = 313$ and $\gamma = 0.04385$ with h in thousands of feet. This is the "CRPL Exponential Reference Atmosphere for $N_s = 313$" (40).

A chart of this type is very useful for plotting radar coverage diagrams. For example, if the maximum range contours obtained from flat-earth calculations, as a function of elevation angle, are plotted on such a chart, the plot will give correct target heights for the plotted points. Conversely, results calculated on the basis of target height, plotted on this chart, will show the correct elevation angles. If the calculations were made on the basis of the effective-earth's-curvature method, it would of course be more appropriate to plot them on a chart based on that model, but for low-altitude targets the discrepancies will not be serious.

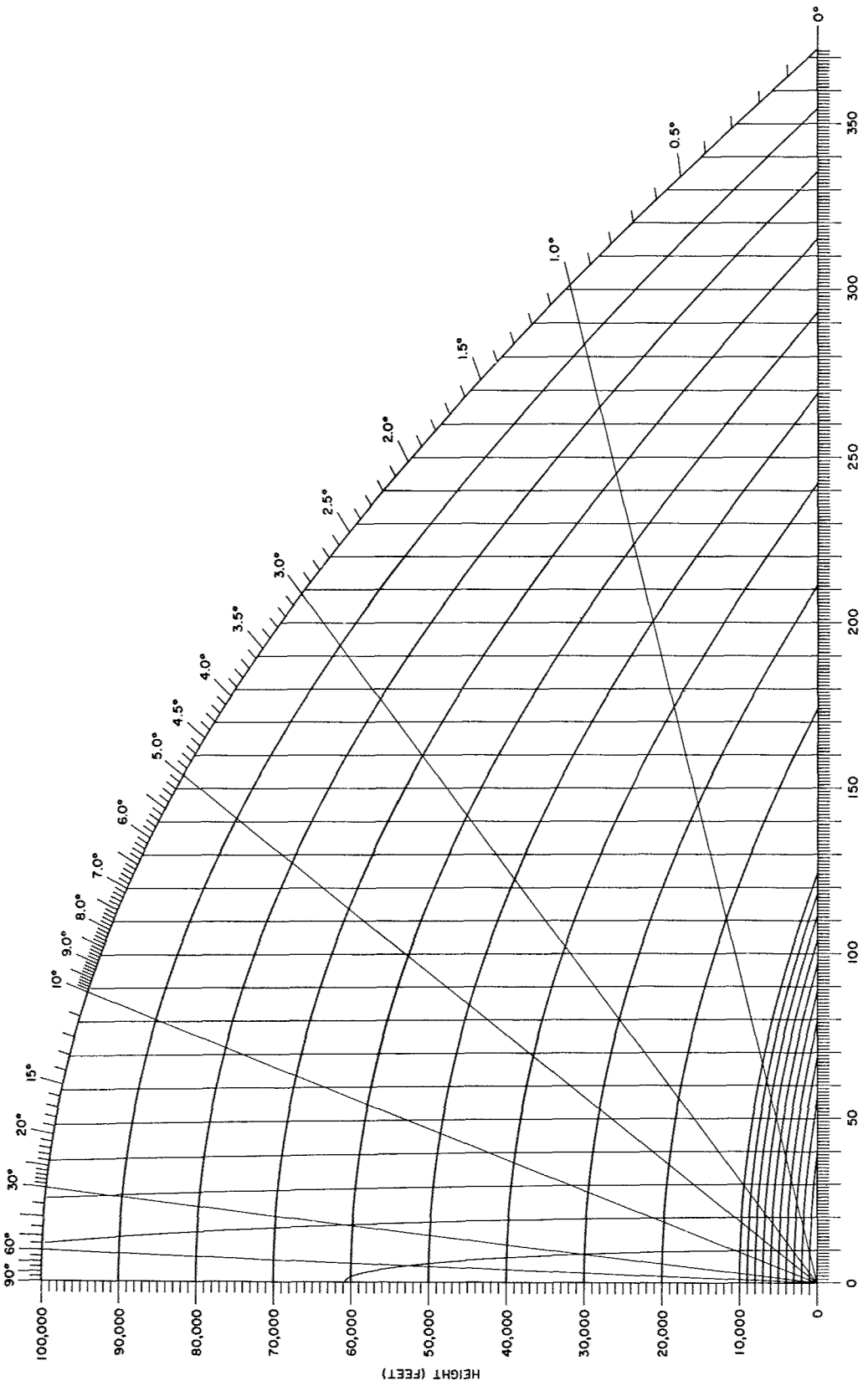

Fig. 20a - Radar range-height-angle chart for targets in the troposphere with refracted rays represented as straight lines, calculated for the CRPL Exponential Reference Atmosphere with $N_s = 313$ and plotted with linear range and height scales and a nonlinear angle scale (from Ref. 42). (Note: This figure also appears in an appendix at the end of the report.)

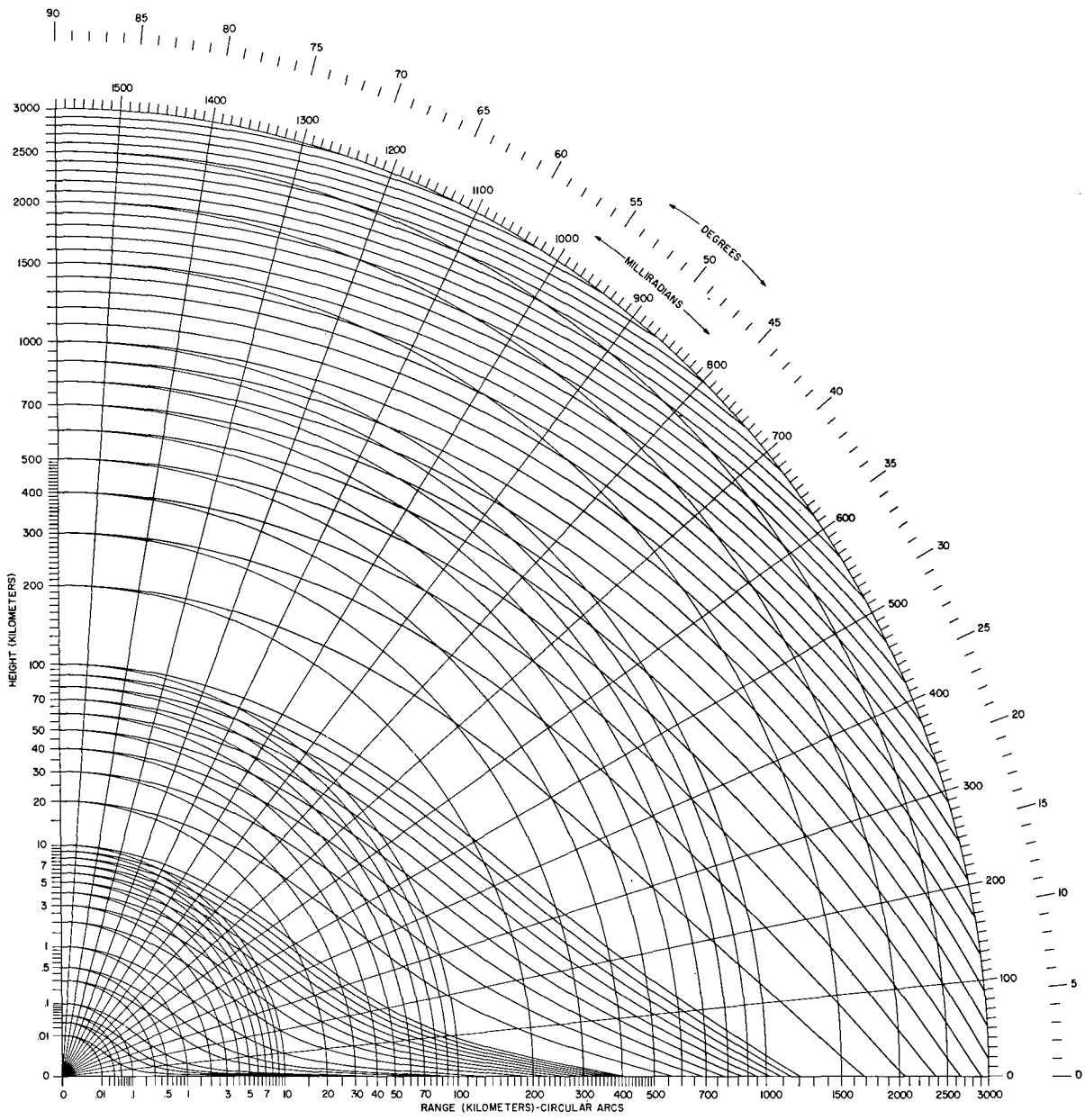

Fig. 20b - Radar range-height-angle chart for targets to 3000 km altitude with refracted rays represented as straight lines, calculated for the CRPL Exponential Reference Atmosphere with N_s = 313 and plotted with nonlinear range and height scales and a linear angle scale (from Ref. 42). Chart is not valid above 100 km for frequencies at which ionospheric refraction occurs. (Note: This figure also appears in an appendix at the end of the report.)

Refraction by the ionosphere occurs for targets at great heights (e.g., space objects), at frequencies below 1000 MHz. (At higher frequencies ionospheric refraction is negligible.) Since this refraction is frequency-dependent, undergoes diurnal and longer-period time variations, and is also under some conditions a complicated function of the direction of the ray in relation to the earth's magnetic field, no general chart can be made to represent the radar range-height-angle relationship in and above the ionosphere. Typical results are given by Millman (43), as will be discussed in Part 2.

7. LOSS FACTORS

Loss is defined as the reciprocal of gain. The loss factor for a twoport (four-terminal) transducer is the ratio of the power input to the power output. If the power is defined as the available power (Section 5), the resultant loss factor is called the available loss (reciprocal of available gain). The available-loss concept must be used in calculations of noise temperature.

The general system loss factor L of the radar range equations represents the product of all individual loss factors that may occur in connection with the various radar range factors. The transmitting loss factor L_t has been mentioned in Section 3; it is the ratio of the transmitter power output to the power actually delivered to the antenna terminals. It represents the losses in the transmission line, duplexer, and any other components inserted between the transmitter and the antenna.

The receiving-transmission-line loss factor L_r does *not* appear as a component of the general system loss factor, nor does the antenna loss factor L_a. These losses are fully accounted for by the definitions of G_t, G_r, and T_s. Both of these loss factors enter into the calculation of T_s. L_a is defined in Section 3, and L_r is defined in Section 5.

In addition to L_t, two losses that are often present are the antenna-pattern loss factor L_p (this applies to scanning radars only), and the propagation absorption loss factor L_α. These two factors will be discussed in some detail, and briefer discussions will be given on several other loss factors that sometimes occur. If these occasional loss factors are lumped together as L_x, the system loss factor in terms of the losses that have been mentioned is

$$L = L_t L_p L_\alpha L_x . \tag{69}$$

Loss factors are often expressed as decibel values, which are appropriate for direct entry into range equations in decibel-logarithmic form, such as Eq. (13). In this case, of course, the product on the right-hand side of Eq. (69) is replaced by a summation.

Antenna Pattern Loss

Search radars may detect targets by searchlighting (pointing the antenna in a fixed direction that is of special interest) or by scanning (moving the beam through an angular sector in a regular and repetitive fashion). In the searchlighting case, if the target happens to be in a direction other than that of the beam maximum, correction for this fact is made by means of the pattern-propagation factor F (Section 6). In the scanning case the target is in different parts of the beam for successive pulses, if the beam position changes by a constant or nearly constant amount in each pulse period. Therefore the received train of pulses, as the beam traverses the target, is modulated by the two-way pattern of the antenna; that is, if the receiving and transmitting pattern factors (defined in Section 6) are $f_t(\phi)$ and $f_r(\phi)$, where ϕ is the angular coordinate in the plane of the scanning motion of the beam axis, the received power will vary as

$$P_r(\phi) \propto f_t^2(\phi)\ f_r^2(\phi)\ . \tag{70}$$

This effect cannot properly be taken into account by assigning values to f_t and f_r. If during the scan the target is angularly displaced from the beam maximum in the direction *orthogonal* to the scan direction, this fact *can* be accounted for by f_t and f_r, but the effect described by Eq. (70) is customarily accounted for by means of a loss factor L_p.

For the assumption that there exists an optimum angular gate width,* such that pulses modulated by the antenna pattern are accepted by the gate only within this angle centered on the beam maximum, the computed pattern loss for a typical beam shape is L_p = 1.6 dB (44). This result assumes that the accepted pulses are postdetection-integrated with equal weighting. The result applies strictly only if the assumed gate is actually implemented, but it may be assumed to apply at least approximately for human observers of visual displays, by postulating that the eye-brain combination somehow looks at an optimum arc width on the PPI display, a not unreasonable supposition.

An important factor in arriving at this loss figure is the convention employed for assigning a number of pulses integrated M to the determination of the detectable signal-to-noise ratio (S/N or V, Section 4). The convention is to use the number of pulses received between the half-power beamwidth points. The pattern loss factor then accounts for the facts that (a) the number of pulses actually integrated within the limits of the optimum-width angle gate is not M and (b) the actual pulses are not all of beam-maximum amplitude, as assumed by the detectable-signal curves for M pulses integrated.

Pencil-beam radars sometimes scan simultaneously in two angular directions — for example, in elevation and azimuth. The elevation scan is typically a sawtooth motion (in the sense that a graph of angle versus time has a sawtooth appearance), not necessarily linear, while the azimuth scan is usually a uniform rotation, although it can also be a sawtooth scan. The rates are usually adjusted so that the angular motion in one direction is at most a beamwidth during one complete scan in the other direction; this insures no holes in the coverage. For such a bidirectional scan the problem of analyzing the loss is more complicated and probably depends on the particular scanning pattern employed.

Equation (30) has been given for calculating the number of pulses received between half-power beamwidth points for an azimuth scanning radar. This equation actually applies only for targets that are at low elevation angles and for a beam axis directed at or near the horizon. If, for some reason, a narrow (pencil) beam of azimuthal width ϕ is scanned in azimuth only but with its axis directed upward at an elevation angle θ_e, the appropriate formula is

$$M = \frac{\phi\ \overline{\text{prf}}}{6\ \overline{\text{rpm}}\ \cos\theta_e}\ , \tag{71}$$

provided that $\phi/\cos\theta_e$, the effective azimuth beamwidth, is less than 360 degrees. (At values of θ_e for which $\phi/\cos\theta_e$ is greater than 360 degrees, the number of pulses computed from this formula will obviously be meaningless. Practically, it is suggested that it be applied only for elevation angles such that $\phi/\cos\theta_e$ is less than about 90 degrees.) This formula is necessary because of the peculiarities of spherical geometry.

The formula for the number of pulses within the half-power beamwidth for an azimuth-and-elevation-scanning radar (which can be applied with minor modification to a radar scanning simultaneously in any two orthogonal angular directions) is

*This optimum varies from 0.84 times the half-power beamwidth, for small signal-to-noise ratios, to 1.2 times, when the signal-to-noise ratio is large (44).

$$M = \frac{\phi\ \theta\ \overline{\text{prf}}}{6\ \omega_v\ t_v\ \overline{\text{rpm}}\ \cos\ \theta_e}\ , \tag{72}$$

where ϕ and θ are the azimuth (horizontal-plane) and elevation (vertical-plane) beamwidths in degrees, $\overline{\text{prf}}$ is the radar pulse repetition frequency in hertz, ω_v is the vertical scanning speed in degrees per second, t_v is the vertical-scan period in seconds (including dead time if any), and $\overline{\text{rpm}}$ is the azimuth rotation speed in revolutions per minute. This formula should also be restricted to elevation angles for which $\phi/\cos\ \theta_e$ is less than about 90 degrees. M is not only a function of the target elevation angle explicitly but also implicitly in that ω_v may be a function of θ_e.

Radars using phase- or frequency-scanning arrays may employ step scanning, in which the beam remains stationary while pulses are transmitted in one direction, then moves to a new position (usually one or more beamwidths away) and remains there while another set of pulses is transmitted. The pulses transmitted in each position are all of equal amplitude, so that there is no pattern loss in the sense of the preceding discussion. However, there may be a pattern loss in the pattern-propagation-factor sense, since a target may sometimes be exactly in the direction of one of the beam positions, and sometimes not. Thus, some kind of a statistical average loss can be computed.

Marcum (3) considered the pattern-loss problem in his machine-computation study of signal detectability. The details of his analysis and assumptions are not given in his report, but he states that the loss is "in the neighborhood of 1.5 dB." Hall and Barton (45) have extended the analysis to more general cases, calculating the loss in relation to the ideal utilization of the total signal energy within the entire beam pattern.

Atmospheric Absorption Loss

Attenuation of radar signals by absorption in the troposphere was at one time thought to be unimportant below about 10 GHz. However, calculations made subsequently indicate that significant absorption can occur for propagation through long tropospheric paths, e.g., through the entire troposphere at low elevation angles at frequencies of only a few hundred megahertz. The calculations were made independently and with somewhat different models of the atmosphere by Bean and Abbott (46), Hogg (47), and Blake (48); the general agreement of their results is good. The calculated two-way (radar) loss at 1000 MHz (Fig. 21) for a ray leaving an earth-based antenna at zero-degree elevation angle and traversing the entire troposphere is 3 dB, which is not inconsiderable. (The outgoing ray may be considered to have left the troposphere when it reaches a height of about 60,000 feet, corresponding to a range of about 300 naut mi for zero initial elevation angle, as seen in Fig. 22a.) At 300 MHz the corresponding loss is 1.2 dB, still appreciable. At 100 MHz, however, it is only 0.2 dB, and tropospheric absorption therefore may be considered negligible below this frequency. Detailed calculation was not made in the near vicinity of the oxygen-molecule resonances, at about 60 GHz; approximate behavior of the absorption in this region is indicated in Fig. 21 by the dashed lines. Detailed calculations for this region have been made by Meeks and Lilley (49).

Figure 21, and the comparable results of other calculations (46,47), cannot be used for radar targets that are within the troposphere. For such targets, the curves of Fig. 22 are provided. In order to use them in a range calculation, the range must first be calculated assuming no absorption but with the pattern-propagation factor included. Then, from the appropriate curve (elevation angle and frequency), the absorption loss L_α corresponding to the calculated range is read. The calculated range is then reduced by a factor $L_\alpha^{-1/4}$, or by antilog $[-(1/40)L_{\alpha(\text{dB})}]$. If this range reduction is considerable, it may then be necessary to find a second value $L_{\alpha(2)}$ corresponding to the corrected

range, and then to *increase* the second range figure by the factor $(L_{\alpha(1)}/L_{\alpha(2)})^{+1/4}$. In principle this iteration process would be repeated indefinitely to obtain a result infinitesimally different from the correct result; but in practice the first correction gives a good enough result, except at frequencies well above 10 GHz where the absorption loss is severe. The iteration process is greatly facilitated by the use of Table 2, which will be introduced in the last section of this report.

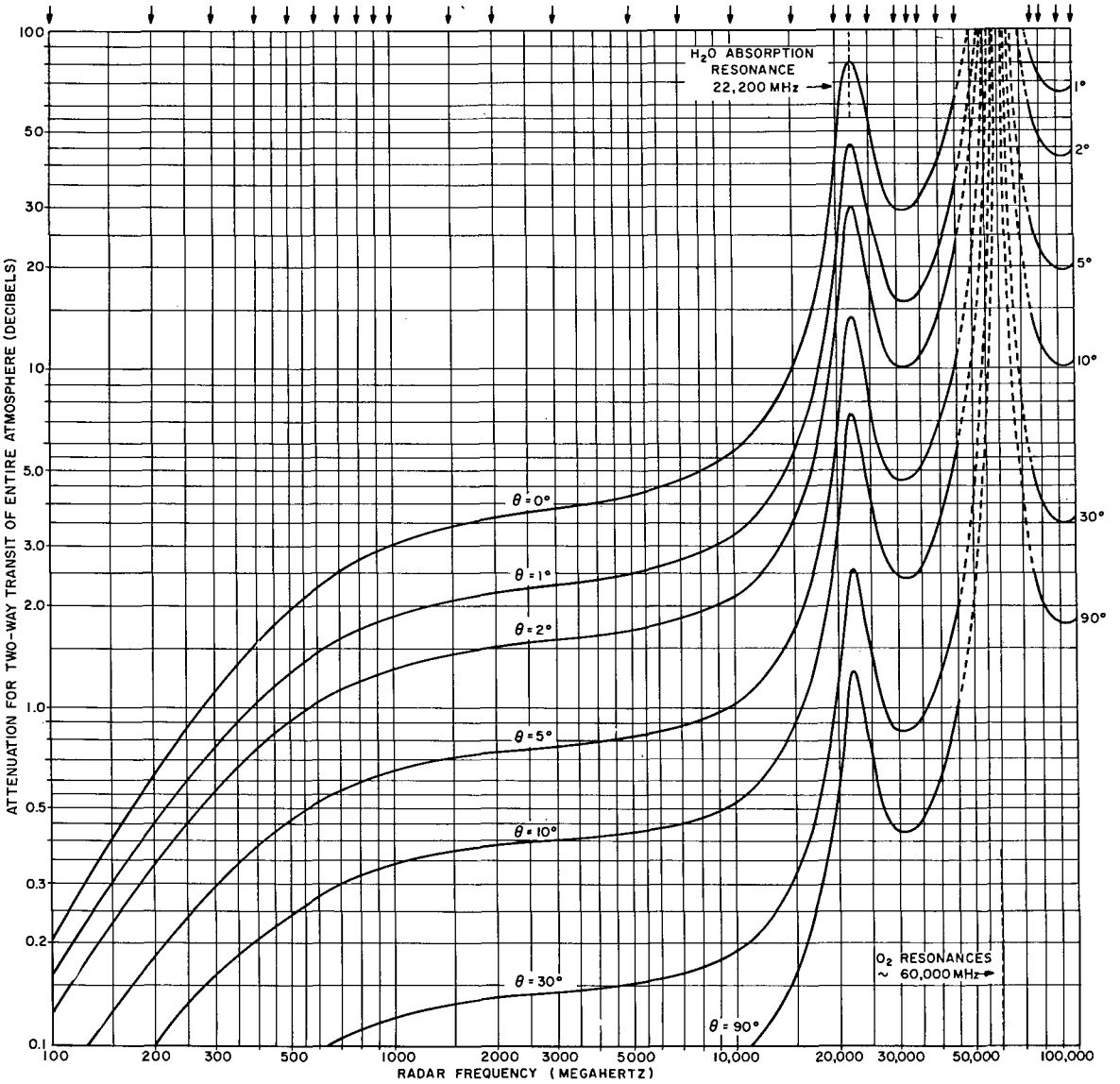

Fig. 21 - Absorption loss for two-way transit of the entire troposphere, at various elevation angles, calculated using Van Vleck theory for oxygen and water vapor absorption. The ray paths were computed for the CRPL Exponential Reference Atmosphere with $N_s = 313$. The pressure-temperature profile is based on the ICAO Standard Atmosphere. The surface water-vapor content was assumed to be 7.5 grams per cubic meter. An approximation was employed between 45 GHz and 75 GHz (oxygen resonance region). Arrows at top denote frequencies for which absorption was computed. (Note: This figure also appears in an appendix at the end of the report.)

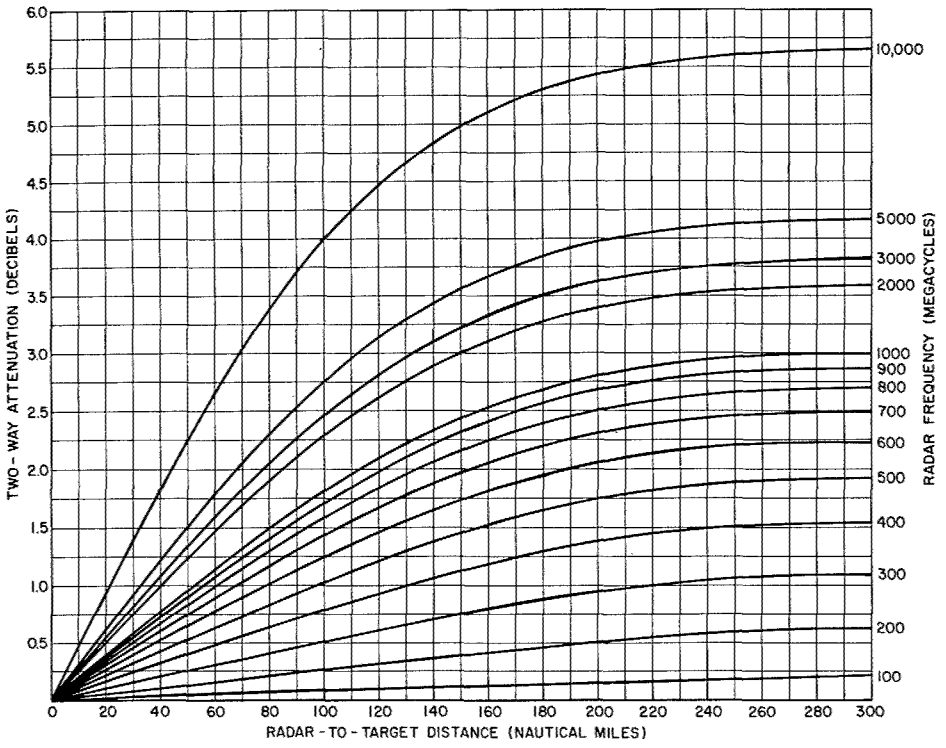

Fig. 22a - Absorption loss for two-way (radar) propagation with the target in the troposphere, plotted as a function of radar range for various frequencies and a zero elevation angle. The calculations were made on the same basis as given in the title for Fig. 21. (Note: This figure also appears in an appendix at the end of the report.)

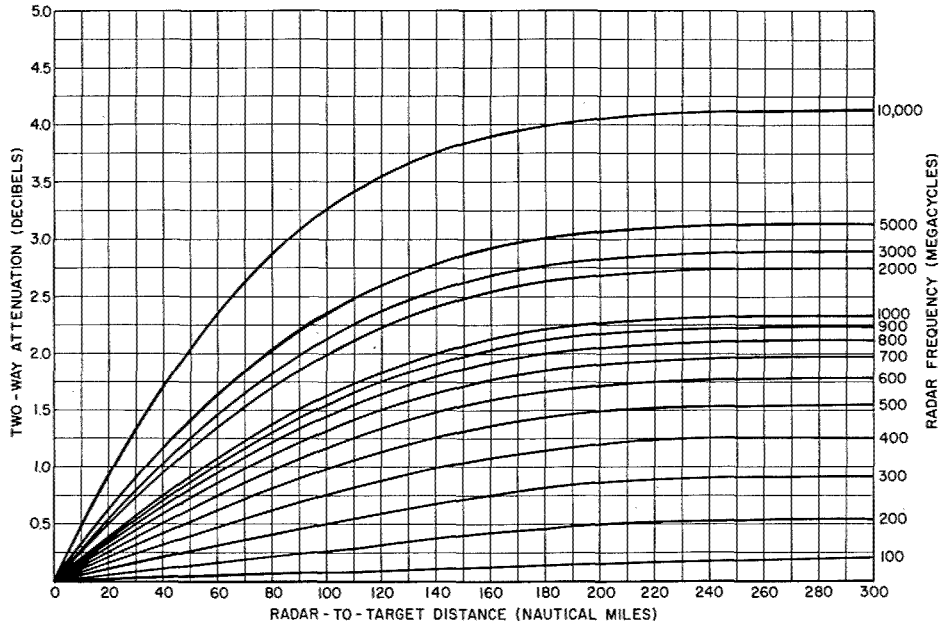

Fig. 22b - Absorption loss for two-way (radar) propagation with the target in the troposphere, plotted as a function of radar range for various frequencies and an 0.5-degree elevation angle. (Note: This figure also appears in an appendix at the end of the report.)

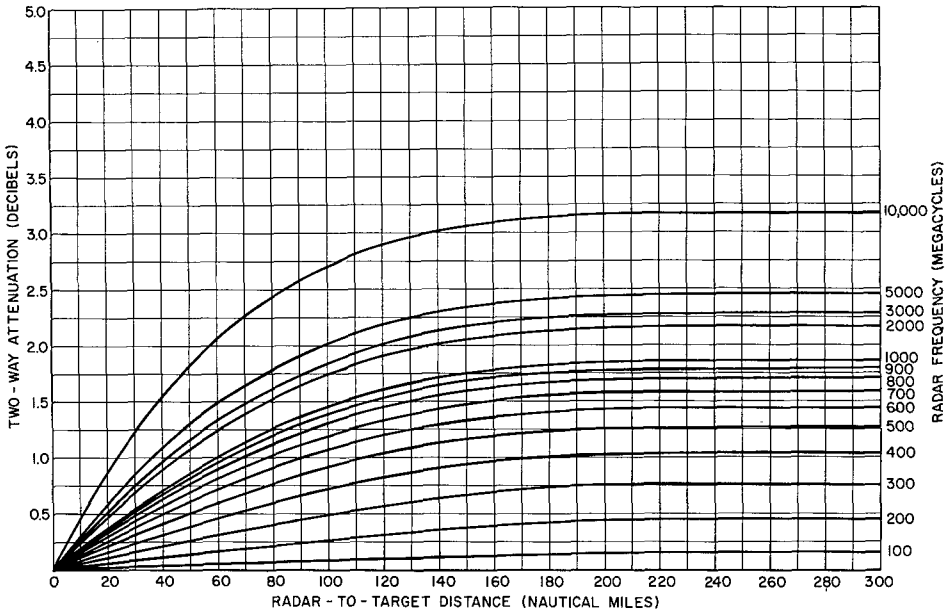

Fig. 22c - Absorption loss for two-way (radar) propagation with the target in the troposphere, plotted as a function of radar range for various frequencies and a 1.0-degree elevation angle. (Note: This figure also appears in an appendix at the end of the report.)

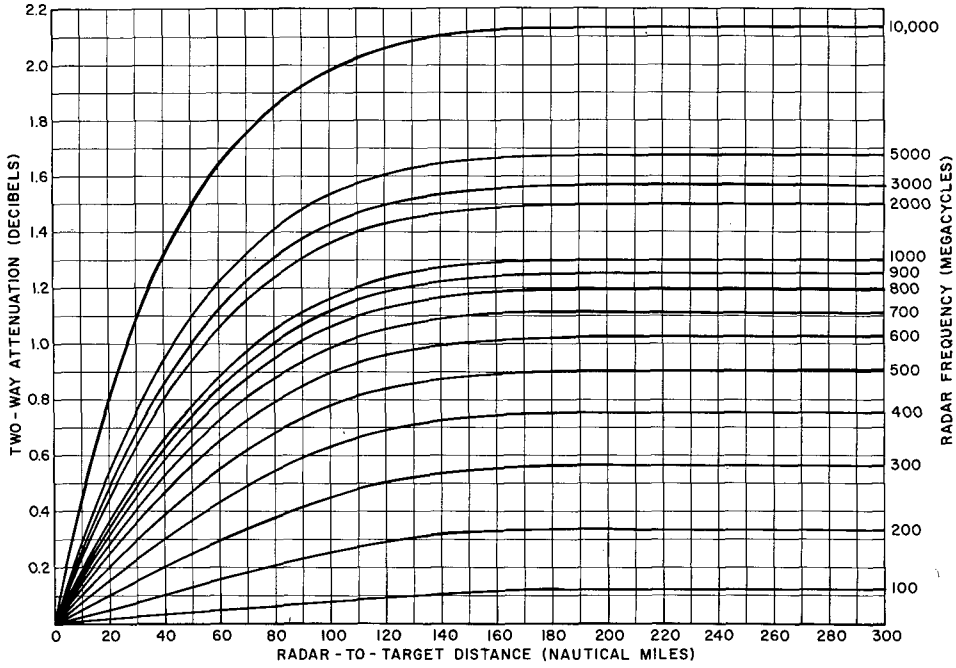

Fig. 22d - Absorption loss for two-way (radar) propagation with the target in the troposphere, plotted as a function of radar range for various frequencies and a 2.0-degree elevation angle. (Note: This figure also appears in an appendix at the end of the report.)

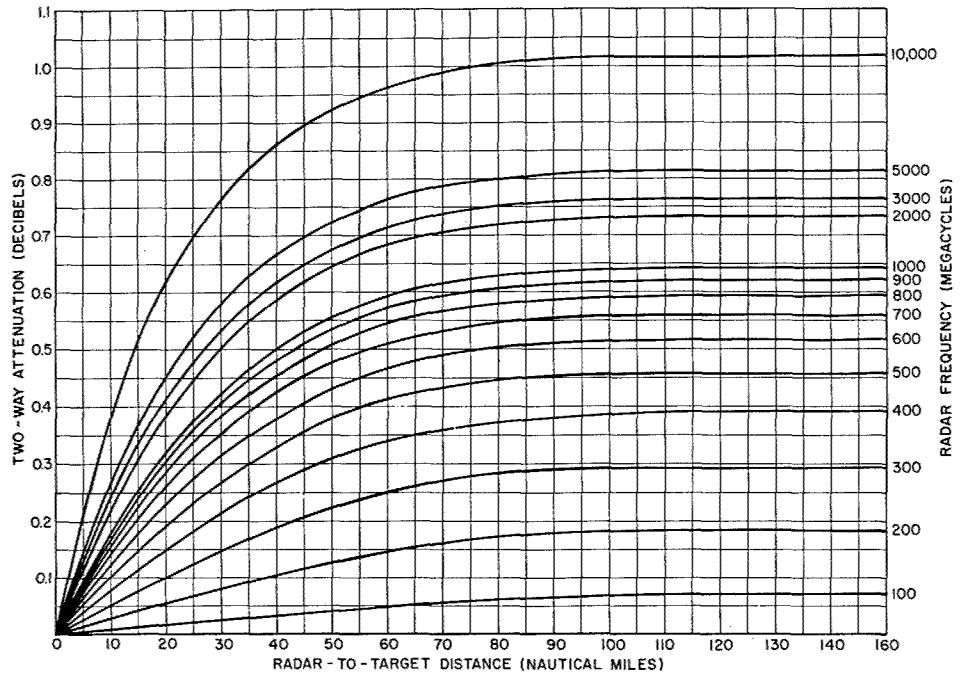

Fig. 22e - Absorption loss for two-way (radar) propagation with the target in the troposphere, plotted as a function of radar range for various frequencies and a 5.0-degree elevation angle. (Note: This figure also appears in an appendix at the end of the report.)

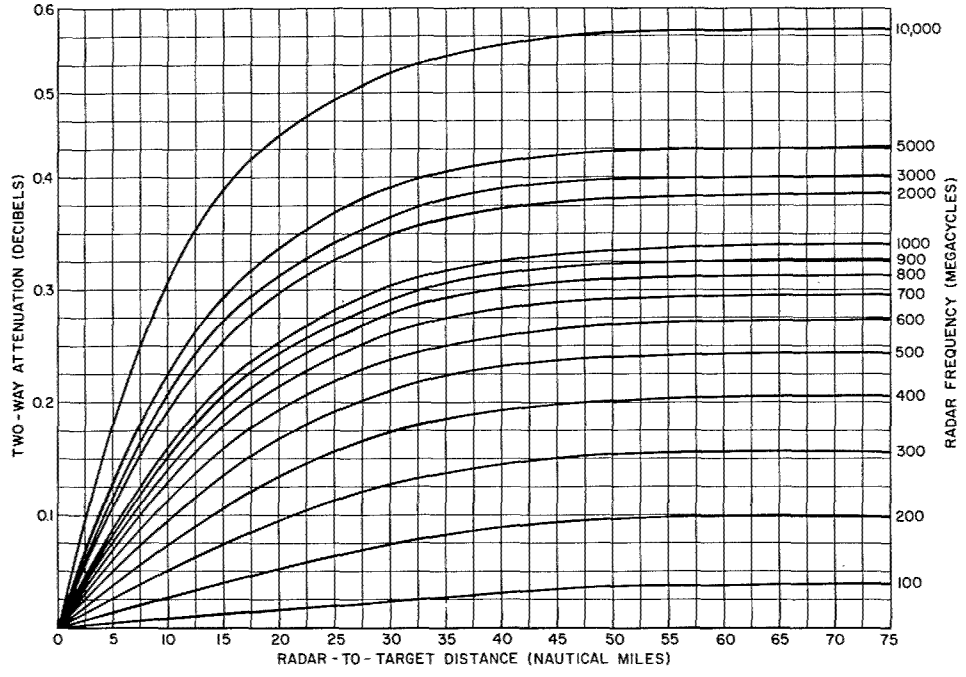

Fig. 22f - Absorption loss for two-way (radar) propagation with the target in the troposphere, plotted as a function of radar range for various frequencies and a 10.0-degree elevation angle. (Note: This figure also appears in an appendix at the end of the report.)

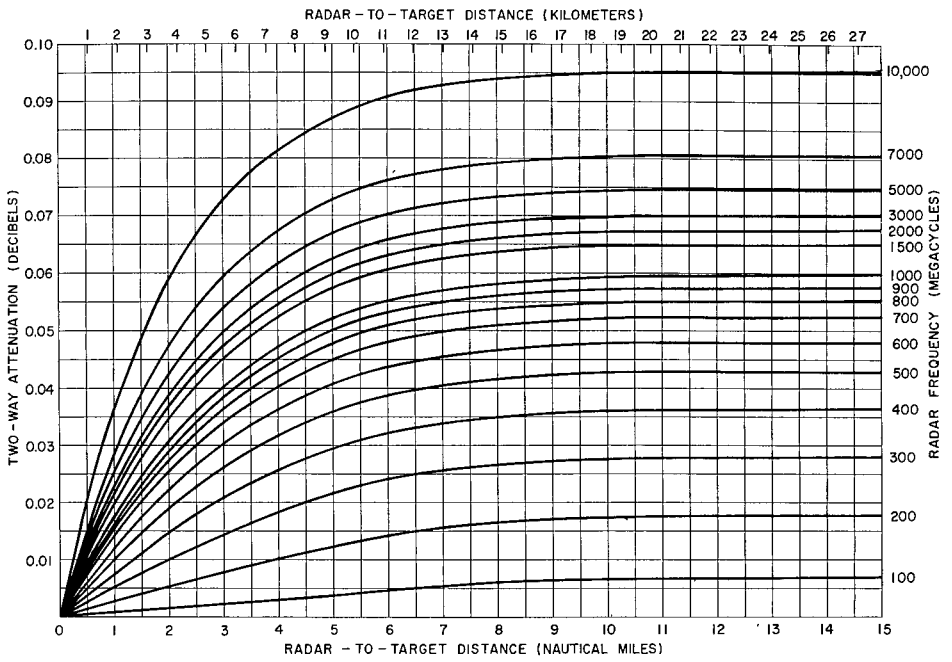

Fig. 22g - Absorption loss for two-way (radar) propagation with the target in the troposphere, plotted as a function of radar range for various frequencies and a 90.0-degree elevation angle. (Note: This figure also appears in an appendix at the end of the report.)

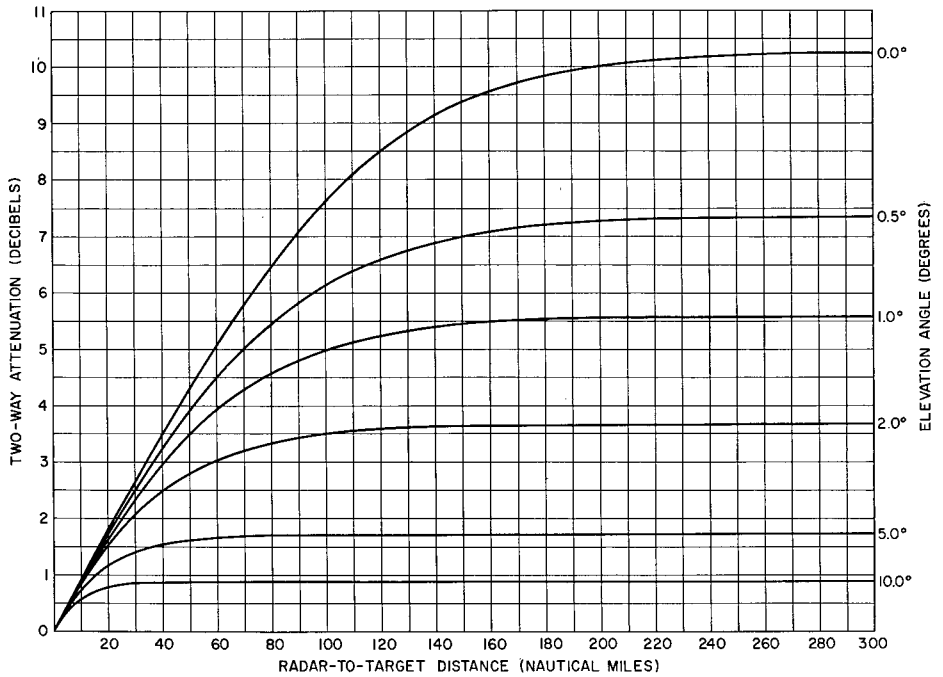

Fig. 22h - Absorption loss for two-way (radar) propagation, targets in troposphere, as a function of radar range, for various ray elevation angles, frequency 15 GHz. (Note: This figure also appears in an appendix at the end of the report.)

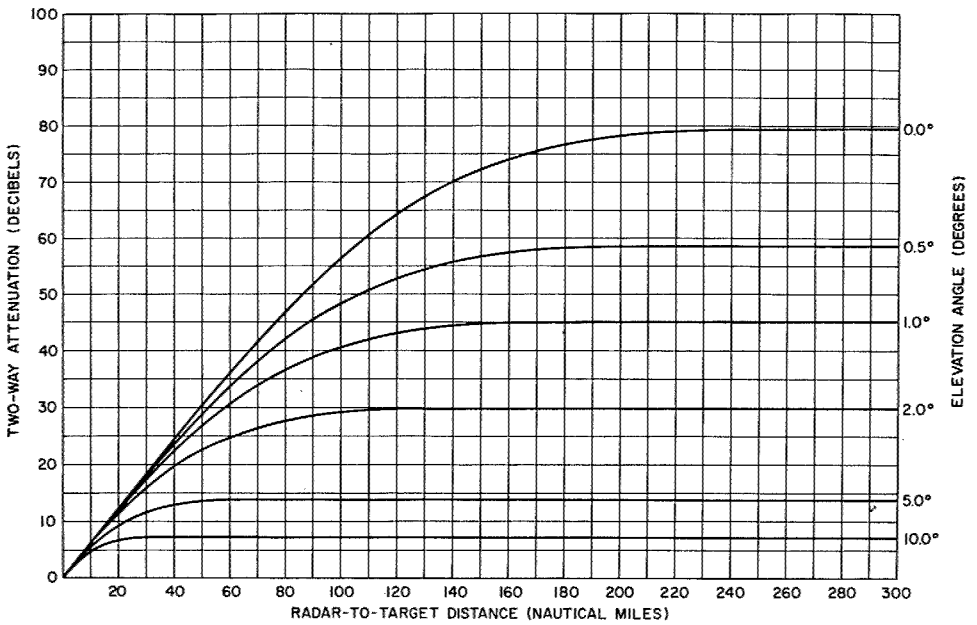

Fig. 22i - Absorption loss for two-way (radar) propagation, targets in troposphere, as a function of radar range, for various ray elevation angles, frequency 22.2 GHz (water-vapor resonance frequency). (Note: This figure also appears in an appendix at the end of the report.)

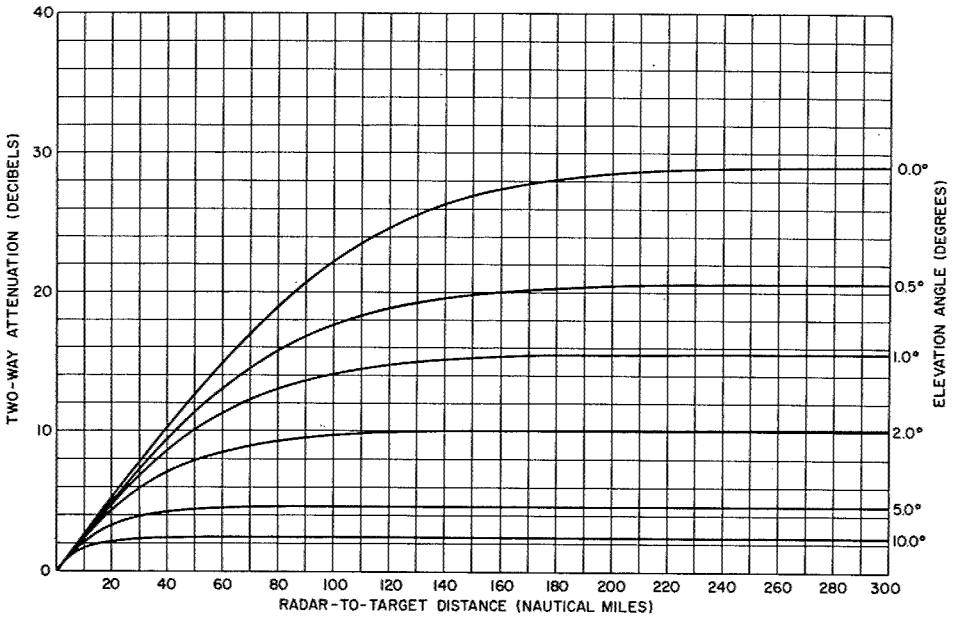

Fig. 22j - Absorption loss for two-way (radar) propagation, targets in troposphere, as a function of radar range, for various ray elevation angles, frequency 32.5 GHz. (Note: This figure also appears in an appendix at the end of the report.)

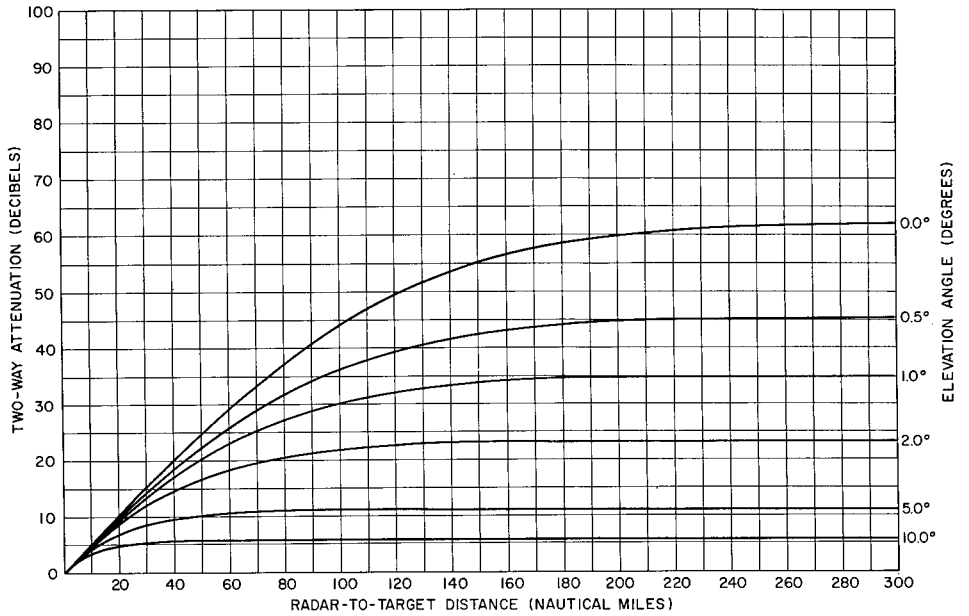

Fig. 22k - Absorption loss for two-way (radar) propagation, targets in troposphere, as a function of radar range, for various ray elevation angles, frequency 45 GHz. (Note: This figure also appears in an appendix at the end of the report.)

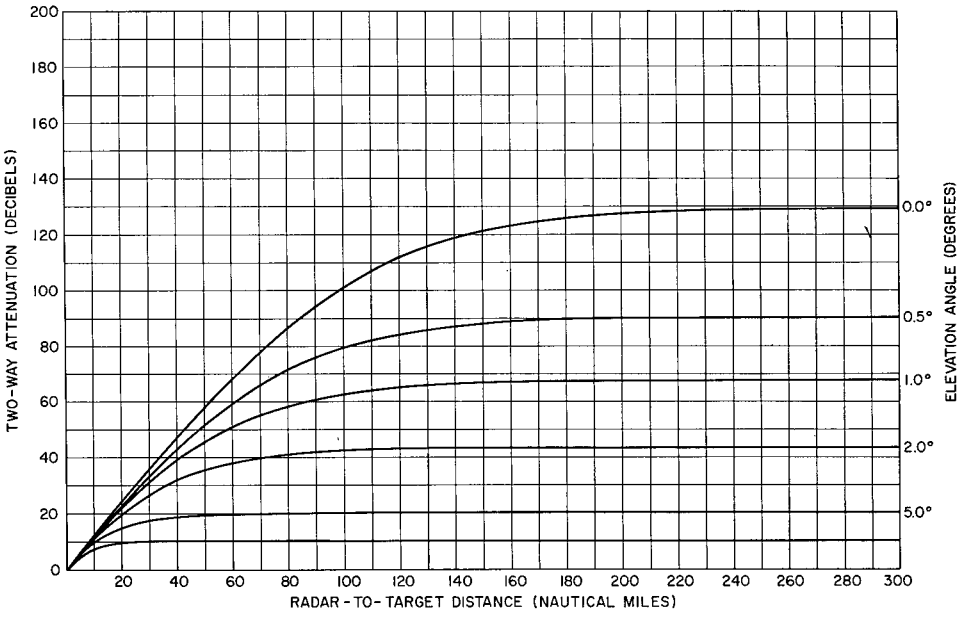

Fig. 22l - Absorption loss for two-way (radar) propagation, targets in troposphere, as a function of radar range, for various ray elevation angles, frequency 100 GHz. (Note: This figure also appears in an appendix at the end of the report.)

These absorption loss curves were calculated for ray paths refracted in accordance with the CRPL Exponential Reference Atmosphere refraction model for $N_s = 313$ (Eq. (68)), and for the pressure and temperature values of the U.S. extension to the ICAO standard atmosphere (50). The absorption is due to collision-broadened resonances of the oxygen and water-vapor molecules, and the calculations were made using the equations given by Van Vleck (51). A water-vapor model assuming a density of 7.5 grams per cubic meter at zero altitude, decreasing exponentially with height, was used. At frequencies above 3 GHz the water-vapor contribution to the total absorption becomes appreciable, and in the vicinity of the 22.2-GHz water-vapor absorption resonance it predominates. In this region, variable atmospheric water-vapor conditions will result in considerable deviation from the absorption values given by these curves. The possible range of water-vapor density is from about 2 to 20 grams per cubic meter. The 7.5-g/m^3 value is a conventional one. The water-vapor decibel component of the total absorption is directly proportional to the water-vapor density. The decibel values for oxygen and water-vapor absorption are directly additive.

Above 10 GHz, absorption loss is serious in regions of rainfall. Rain is of such variable intensity both in time and space that it is difficult to take it into account in range calculation. It would be helpful, for the purpose of a standard calculation of radar range during rain conditions if conventional models of a standard light rain, standard moderate rain, and standard heavy rain existed, but no such models exist to the author's knowledge. For this purpose it would be necessary to specify not only the rainfall rates but also the spatial extent both horizontally and vertically of a typical rainstorm.*

If a rainstorm is idealized by considering that the rainfall rate is uniform within a bounded region and zero outside the region, the radar range can be calculated fairly simply. If the rain occupies only a part of the path from radar to target, with its range extent along the path designated R_α, and if the average one-way rain attenuation in the rainfall region is α decibels per unit distance, then it suffices to include in the range equation a loss factor given in decibels by the product $2\alpha R_\alpha$. The range thus calculated must of course be greater than R_α, otherwise an incorrect assumption has been made.

However, if the rain occupies the entire space between the radar and the target, a graphical solution is necessary. The procedure required is illustrated by Fig. 23. The range R_0 is the radar maximum range as calculated in the absence of rainfall. (This is not necessarily the free-space range, which R_0 sometimes designates.) The straight line represents the rainfall attenuation in decibels, which has the value $2\alpha R_0$ at $R/R_0 = 1$. The nonlinear curve represents the decibel value of the ratio P_r/P_{r0}, where in the absence of rain P_{r0} is the received echo power at range R_0 and P_r is the received echo power at range R for the same value of target cross section σ and constant values of all other range-equation factors. This ratio, expressed in decibels, is given by

$$(P_r/P_{r0})_{\mathrm{dB}} = 40 \log_{10} (R_0 F/R) \ . \tag{73}$$

The curve shown in Fig. 23 is for $F = 1$. When F is not equal to 1 everywhere, it is in general a function of the range R, so that a more complicated curve results. Similarly, if α cannot be considered a constant, the rain attenuation cannot be represented by the straight line $\mathrm{dB} = 2\alpha R$. Instead, it would be a curve defined by

$$\mathrm{dB} = 2 \int_0^R \alpha(r)\, dr \ .$$

Ionospheric absorption is not included in Fig. 21. It is ordinarily negligible above a few hundred megahertz. Millman (43) has computed this loss for typical ionospheric

*Tentative models are proposed in Part 2 (NRL Report 7010).

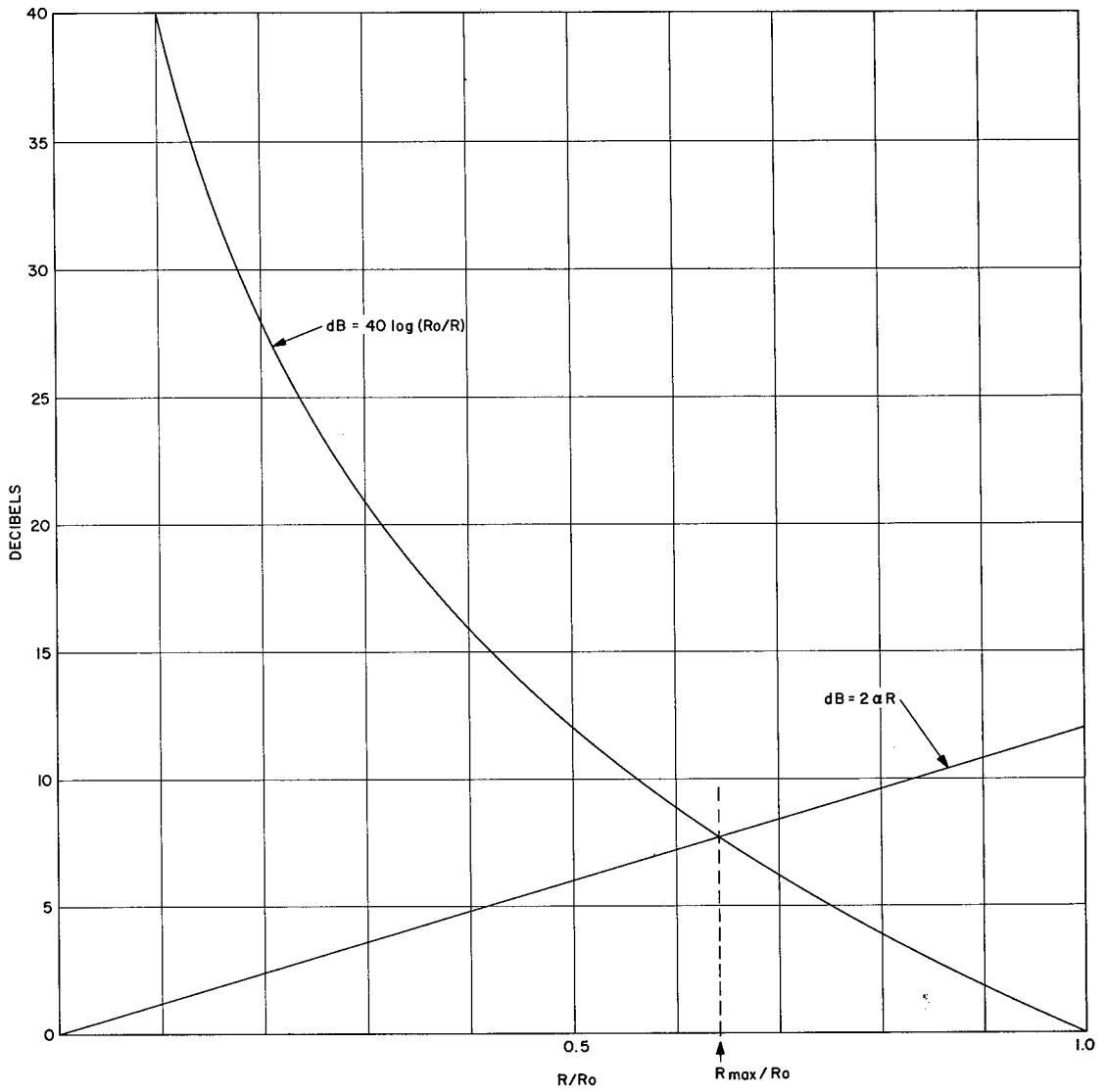

Fig. 23 - Graphical solution for the maximum range in an absorbing propagation medium such as rain

conditions. At frequencies in the VHF region and above, the decibel loss is inversely proportional to the square of the frequency, so that it can be estimated for any sufficiently high frequency f if the constant A is known in the formula

$$L_{I(\mathrm{dB})} = A/f^2 \ . \tag{74}$$

If f is expressed in megahertz, the value of A for rays that leave the earth's surface at low elevation angles is about 1.8×10^4 for daytime conditions and 5.4×10^2 for nighttime conditions. For high angles, $A \approx 4\times10^3$ daytime and 2×10^2 nighttime. $L_{I(\mathrm{dB})}$ is the two-way (radar) loss for transionospheric propagation.

Collapsing Loss

A loss occurs when a radar that is obtaining n-coordinate information displays it on an $(n-m)$-coordinate display, where $n > m$ and m is a positive integer. Then m coordinates are said to be collapsed. The loss occurs because signals in a portion of the collapsed dimension have to compete not only with the noise corresponding to that portion, but with the noise corresponding to the entire collapsed dimension. For example, if an azimuth-and-elevation scanning radar has its output displayed on a PPI scope, which shows only azimuth and range, the elevation coordinate is collapsed. A target at a given elevation angle then has to compete with noise from other elevation positions of the beam as well as with that occurring while the beam is actually pointed at the target. This loss could be eliminated by gating the receiver output in elevation, so as to display only the beam position of the target; but, the ability to detect targets at other elevation angles would then be lost, unless additional displays were provided (one for each elevation beam position).

Marcum (3) has defined a collapsing ratio ρ_c for this type of situation:

$$\rho_c = \frac{p+q}{q} \ , \tag{75}$$

where $p+q$ is the total number of "resolution cells" in the collapsed dimension and q is the number that contain signals and noise (p is the number that contain noise only). The collapsing loss L_c ranges in value from ρ_c^0 to ρ_c^1. The references given for specific cases should be consulted when applicable. When specific data or theory are not available, the typical value $\rho_c^{1/2}$ may be assumed.

In the case of the elevation-scanning radar with a PPI display, if the total vertical angular section scanned is θ_s and the vertical-plane beamwidth of the antenna is θ_v, then

$$\rho_c = \frac{\theta_s}{\theta_v} \ . \tag{76}$$

Similarly, if the range dimension of a cathode-ray-tube display is compressed by using too low a writing speed, a form of collapsing occurs for which

$$\rho_c = \frac{d+s\tau}{s\tau} \ , \tag{77}$$

where d is the cathode-ray-tube spot size (mm), s is the sweep speed (mm/sec), and τ is the pulse length (sec). Another form of collapsing effectively occurs if the video

bandwidth B_v of the receiver is too narrow in relation to the predetection (IF) bandwidth B_{IF}. The collapsing ratio as given by Marcum is*

$$\rho_c = \frac{B_{IF} + B_v}{B_v} . \tag{78}$$

A form of collapsing occurs when the video outputs of $p + q$ receivers are mixed (are applied to a single display) and only q of them contain the signal. Assuming that all have equal and statistically independent noise output and that the signal levels in the q channels are all equal, Eq. (75) applies.

These are representative applications of the concept of a collapsing ratio; numerous others may occur in special situations. Marcum (3) gives curves for collapsing loss as a function of the collapsing ratio. This matter is also discussed by Hall (11), Lawson and Uhlenbeck (15), and Payne-Scott (53). Their results and conclusions are not in complete agreement with one another or with those of Marcum, but there is an approximate general agreement. In some cases the apparent disagreement may be based on the method of presenting the results; for example, Lawson and Uhlenbeck (15) give results of a sweep-speed experiment (15, Fig. 9.1) in which the detectable signal is shown as a function of the sweep speed, and the curve shows a minimum when the speed has a particular value, increasing for faster speeds as well as for slower. However, the spot size d is not considered as a parameter of the experiment. It is entirely possible that d increased as s increased (because as the speed of the sweep increased, the intensity was probably turned up to maintain brightness, and this would cause some increase of the spot size), so that if the detectable signal had been plotted as a function of the collapsing ratio, Eq. (77), instead of as a function of s alone, the curve would have become monotonic decreasing and with steeper slope, in better agreement with Marcum (3) and Payne-Scott (53).

Miscellaneous Losses

It is difficult to list all of the possible losses that may occur in special situations, but a few that are known to occur at times will be mentioned. A *polarization loss* can occur if for some reason the received signal polarization does not agree with the polarization for which the receiving antenna is designed. This can happen when the target is beyond the ionosphere and the polarization is rotated by the ionospheric Faraday effect, which occurs at frequencies below about 1000 MHz. If the receiving and transmitting antennas are both linearly polarized, the polarization of the received signal may be rotated by some angle γ with respect to the antenna polarization. The applicable power loss factor in this case is $\sec^2 \gamma$. (This loss can be avoided by using circular polarization or by adjusting the receiving antenna polarization.)

A *pulse-length loss* can occur when an array antenna with a certain type of feed system is used (e.g., the "serpentine feed" used in frequency-scanned arrays), such that a finite time elapses between the arrival of the leading edge of the rf pulse waveform at the first element of the array and its arrival at the last element. Since the beam is not fully formed until the latter event occurs, a portion of the pulse length is lost (actually, some radiation occurs during the "fill time" of the array, but at much reduced antenna gain). If the pulse length is τ and the fill time is t_f, the loss factor may be as great as

*However, logic indicates that if $B_v \geq B_{IF}$, then $\rho_c = 1$. Moreover, experiments indicate that $\rho_c \approx 1$ if $B_v \geq B_{IF}/2$. Marcum's formula therefore seems to give too-large values of ρ_c for this case. Barton (52, p. 129) substitutes $2B_v$ for B_v in Marcum's formula, but this does not fully eliminate the difficulty.

$\tau/(\tau - 2t_f)$, if $2t_f < \tau$. The factor 2 occurs because the pulse length loss occurs on both transmission and reception. The actual loss is probably somewhat less than this formula indicates, because some useful signal may be radiated and received before the array is completely filled, and also while it is emptying.

A *squint loss* occurs when a phase- or frequency-scanning array scans off the broadside direction, due to the loss of effective aperture size. If the gains G_t and G_r are interpreted as those applicable to the broadside direction, then a squint loss factor should be included in the system loss for targets off the broadside direction. The loss factor, to a first approximation, is $\sec^2 \psi$, where ψ is the angle between the target direction and the broadside direction of the array. Element pattern effects may increase this loss at large squint angles.

Integration Loss and Operator Loss

The concept of *integration loss* is encountered in the literature of radar range calculation (3,11). In this approach the quantity V_0 (or some similar factor) is evaluated on the assumption that coherent integration of the M pulses has occurred. Then a loss factor is applied, accounting for the difference in value of V_0 for coherent and noncoherent integration of the M pulses.

This approach is not used here. The values of V_0 given by Figs. 5 through 9 are those for noncoherent integration, which is the form of integration ordinarily employed. For special cases in which coherent integration is possible, the method of calculating V_0 has been described (Section 4). The integration-loss approach requires an additional factor and an additional step in the calculation and conveys the implication that integration is a process that results in loss. Integration is of course a gainful process, and the term "integration loss" really means "the loss incurred by integrating noncoherently instead of coherently." "Noncoherent-integration loss" would be more appropriate but more cumbersome.

The concept of *operator loss* is also sometimes employed, to describe the increase in V_0 required by a typical operator compared to an ideal operator. However, again the approach here has been to express V_0 directly, in Figs. 8 and 9, as the value applicable to an actual human operator. The operator loss tends in practice to become an arbitrary factor to account for observed discrepancies between computed and observed radar performance, and while in some cases it may be a valid explanation, it may in other cases tend to be misused. In any case it is too vague a concept to employ in a range calculation aimed at evaluating the merit of a particular radar design or for other engineering purposes.

System-Degradation Loss

A loss factor is sometimes included in range calculations to account for the degradation of radar performance that sometimes occurs "in the field," as a result of inadequate or inexpert maintenance and adjustment or of deterioration due to aging of components. The evaluation of this loss factor, like that of operator loss, is somewhat arbitrary. Even though it may be based on statistical studies, the applicability of statistics for the past performance of one type of radar to the future performance of a different type is questionable. Its use tends to vitiate the effect of whatever care has been taken to make the range prediction as accurate as possible. As an alternate to the system degradation loss, each system parameter in the range equation should be assigned a realistic value, one that represents the performance of a reasonably well maintained and adjusted unit in the field and not a laboratory peak value. The range thus calculated is

that of which the radar is inherently capable, and is the one that should be quoted as a measure of its merit and that should be used as a yardstick for performance evaluation. The effect of some arbitrary amount of field degradation of performance can then be expressed by calculating the range reduction factor that would result, and apply it to the undegraded range prediction. By this procedure the different significance of the two predicted-range figures can be emphasized.

8. JAMMING AND CLUTTER

Jamming

The basic problem in radar detection, which was considered in Sections 4 and 5, is the discernment of signals in a background of noise of the thermal type, which originates both in the receiving system and in the external environment as the result of natural phenomena. In the practical application of radar, the noise that competes with signals may originate in other ways. For military radars, deliberate radiation of jamming signals may introduce additional noise into the receiving system. When the jamming signals are either CW or have various forms of periodic modulation, much can be done to discriminate against them. But if the jammer uses noise modulation, so that the jamming signal essentially just adds to the already-present thermal noise, its effect is exactly the same as would be an increase in the system noise temperature due to the factors discussed in Section 5. Therefore the effect of this type of jamming is completely predictable.

This statement assumes, however, that means are provided to avoid saturation of the receiver, which can occur if a large signal is applied. The same assumption is in fact tacitly made in all of the discussion of detecting signals in a background of noise or clutter.

Range Equations for Noise Jamming

If the radar target is carrying a jammer (self-screening), a maximum detection range equation can be obtained by a modification of Eq. (12). If the jamming noise power density is assumed to be much larger than the receiver noise in the absence of jamming, the equation is derived by replacing the noise power density kT_s in Eq. (12)* by the received-jamming-signal power density $\mathcal{P}_{rj}$, watts per hertz, which is given by

$$\mathcal{P}_{rj} = \frac{\mathcal{P}_{tj} G_j G_r \lambda^2 F_j^2}{(4\pi R_j)^2} , \tag{79}$$

where $\mathcal{P}_{tj}$ is the spectral power density at the jammer antenna terminals in watts per hertz, G_j is the jammer antenna power gain *in the radar direction*, G_r is defined in the paragraph containing Eq. (15), λ is the radar wavelength, F_j is the pattern-propagation factor for the jammer-to-radar path (which includes the pattern factor of the radar receiving antenna in the jammer direction), and R_j is the jammer-to-radar range. For the self-screening case, $F_j = F_r$ and $R_j = R_{max}$, where F_r and R_{max} are defined as for Eq. (12). When Eq. (79) is substituted for kT_s in Eq. (12), F_j and F_r cancel, λ and f cancel each other (after converting from λ to f) and G_r cancels. The resulting equation, using the system of units of Eq. (12) and expressing $\mathcal{P}_{tj}$ in watts per megahertz, is

*The factor k is Boltzmann's constant, which does not appear explicitly in Eq. (12) because it has been incorporated in the numerical factor 129.2.

$$R_{max} = \cancel{4.187} \; 4.817 \times 10^{-3} \, F_t \left[\frac{P_{t\,(kW)} \tau_{\mu sec} G_t \sigma_{(sq\ m)}}{\mathcal{P}_{tj\,(W/MHz)} G_j V_0 C_B L} \right]^{1/2} . \tag{80}$$

However, the loss factor L_α, which is a component of L (Eq. (69)), must now be defined as the *one-way* absorption loss (half of the decibel values given by Figs. 21 and 22), and L_p is less than the two-way value (roughly half) to account for the fact that the jamming power as well as the received echo is reduced when the jammer is not in the receiving-antenna pattern maximum, during scanning. The half-power exponent on the right-hand side results from equating R_j and R_{max}.

Another equation can be derived for the case in which the jammer is at a fixed location with respect to the radar (standoff jamming), rather than moving with the target. In this case R_j and R_{max} are not the same (in general), and F_j is not in general equal to F_r. (The pattern factor of the radar receiving antenna, included in F_j in Eq. (79), may represent the fact that the jammer can be in a side lobe rather than in the main beam.) The resulting equation therefore retains the exponent 1/4 and contains more factors than does Eq. (80):

$$R_{max} = 6.940 \times 10^{-2} \left[\frac{P_{t\,(kW)} \tau_{\mu sec} G_t \sigma_{(sq\ m)} F_t^2 F_r^2 R_j^2}{\mathcal{P}_{tj\,(W/MHz)} G_j F_j^2 V_0 C_B L} \right]^{1/4} . \tag{81}$$

It is evident that if, in these equations, the product $\mathcal{P}_{tj} G_j$ is made very small, or if in Eq. (81) R_j is very large or F_j very small, large values of R_{max} can result. If the value of R_{max} obtained from these equations is larger than or even comparable to the value that would be calculated from Eq. (12), it is a false result and is so because the assumption that $\mathcal{P}_{rj}$ is much greater than kT_s has been violated.

If the maximum range calculated from Eq. (80) or (81) is less than half that calculated from Eq. (12), it may be considered a valid result. If it is more than twice the range given by Eq. (12), then the jamming signal can be considered negligible compared to kT_s and Eq. (12) applies. (These results mean that the ratio of $\mathcal{P}_{rj}$ to kT_s is greater than 16 or less than 1/16.) If the range calculated from these jamming equations lies between these values, it is not an accurate result and more complicated equations must be used if high accuracy is needed. The correct equations are obtained by replacing kT_s of Eq. (12) by $kT_s + \mathcal{P}_{rj}$, where the second term is given by Eq. (79). For a fixed-position jammer (standoff jamming) the required calculation is straightforward, though more complicated; but for a jammer carried by the target (self screening) a quadratic equation in R_{max}^2 results and therefore the solution is still more complicated, though not fundamentally difficult.

Clutter

In the discussion of signal detectability given in Section 4, it was assumed that only one echo signal is present within the range and angle sector being considered. If a few other targets are present within the total coverage volume of the radar, little or no harm is done. But if there are so many targets that they "run together" on the cathode-ray-tube screen or other type of display, or if they overlap in time when time-gated automatic detection devices are employed, detection of a desired signal will be seriously affected. A profusion of echoes sufficient to produce this effect is called *clutter* or clutter echoes. Such echoes can be produced by the surface of the sea or land, by weather, and at times even by birds or insects. A standard military radar countermeasure is the deliberate

creation of an airborne cloud of lightweight reflecting objects (typically strips of aluminum foil called chaff) to produce clutter echoes in a region of space.

Targets in Clutter

Clutter echoes from a rough sea, from chaff, from rain, and from some types of terrain have many characteristics in common with receiver noise, in that they are randomly fluctuating in amplitude and phase, and in many cases they even have a probability density function like that of thermal noise. However, they differ in one important respect — their fluctuation rate is much slower, which means that their frequency spectrum is narrower.

When the clutter level is much higher than the receiver noise level, the detection problem is in terms of the signal-to-clutter ratio rather than signal-to-noise ratio. It has many properties in common with the problem of detecting a signal in thermal noise. But, because of the slower fluctuation rate, integration of pulses is relatively ineffective; the clutter is usually correlated for time separations which may be of the order of pulse periods. Also, some clutter may be spiky in character, which means that its statistics are different from those of the receiver noise. But the basic problem of detection is the same: the signal power must on the average be great enough to produce a probability of detection substantially greater than the false-alarm probability.

The maximum range of detection, therefore, is analyzed by considering how the target echo and the clutter echoes vary with the range, so as to determine at what range the necessary target-to-clutter-signal ratio is reached. In the absence of specific information on the clutter statistics, a reasonable assumption to make for the required signal-to-clutter ratio is that, for given detection probability and false-alarm probability, it corresponds to the required signal-to-noise ratio for single-pulse detection (no integration). This value can be determined from Figs. 4 through 7 with $M = 1$. For a steady signal, 0.5 probability of detection, and 10^{-10} false-alarm probability, it is about 13.5 dB.

The signal-to-clutter ratio S/C is given by the ratio of the effective radar cross sections of the target and the clutter, σ_t and σ_c, if both target and clutter are subject to the same propagation factors. However, the propagation factors may be different, because of the reflection-interference effect discussed in Section 6. The criterion of detectability of the target therefore becomes

$$S/C = \frac{\sigma_t F^4}{\sigma_c F_c^4} , \tag{82}$$

where it is assumed for simplicity that the pattern-propagation factor for the target is $F = F_t = F_r$, and (with a similar assumption) F_c is the pattern-propagation factor for the clutter. When the clutter is from a surface, however, the propagation factor is included in the evaluation of σ_c, so that F_c becomes f_c, the antenna pattern factor applicable to the illuminated clutter area at the range being considered.

When the clutter is from a rough surface, σ_c is the product of the cross section per unit area σ^0 and the area of the surface A illuminated by the radar. For a radar of horizontal beamwidth ϕ radians* and pulse length τ seconds viewing the surface at a grazing angle ψ, this area is, for small values of ψ,

*As mentioned in Section 3, a special definition of beamwidth is required here (14, pp. 483-484). A similar modification of the pulse-length definition is also required.

$$A = R\phi \frac{c\tau}{2} \sec \psi \ , \tag{83}$$

where R is the radar range to the surface and c is the radar wave propagation velocity (3×10^8 m/sec). Consequently Eq. (82) can be rewritten as a range equation. However, this allows a solution for the range only if the quantities σ^0, F, and ψ are all range independent. Generally σ^0 is not range independent; it is a function of ψ, and ψ is in turn a monotonic-decreasing function of the range. The variation of σ^0 with range can in general be quite nonlinear and frequency dependent, as well as dependent on such factors as the type of surface and the wave polarization. Therefore, in general no simple range equation which takes these dependences into account can be written.

However, if data on the variation of σ^0 with range (or equivalently with grazing angle) are available, a graphical solution for the range can be obtained by plotting the right-hand side of Eq. (82) as a function of range, using Eq. (83) and the relation $\sigma_c = \sigma^0 A$. A point at which this quantity equals the minimum-detectable signal-to-clutter ratio $(S/C)_{min}$ is a boundary between the regions of detection and no detection. Because of the peculiarities of the behavior of σ^0 and A with range, it can happen, especially with airborne radar, that a target will be detectable within a certain range interval, not detectable beyond this range because of insufficient signal-to-noise ratio, not detectable within an interval at closer range because of insufficient signal-to-clutter ratio, and then finally detectable at still closer ranges where the illuminated clutter area declines to a small value or the pattern factor f_c becomes small while F remains close to unity or larger.

If the clutter is from scatterers distributed within a volume (rain or chaff) rather than over a surface, the principle of range calculation is the same except that now $\sigma_c = \eta V$, where η is a cross section per unit volume and V is the instantaneously illuminated volume, given by

$$V = \Omega R^2 c\tau/2 \ , \tag{84}$$

where Ω is the solid angle of the radar beam. In the volume-clutter case, however, F_c of Eq. (82) is not taken into account in evaluation of η. In some circumstances, F_c will vary within the region illuminated, and then an effective value must be determined. If η, F, and F_c are independent of range, a direct solution for detection range can be obtained by combining Eqs. (82) and (84):

$$R_{max} = \left[\frac{\sigma_t F^4}{\eta \Omega (c\tau/2) F_c^4 (S/C)_{min}} \right]^{1/2} . \tag{85}$$

The detection of signals from moving targets in clutter can be enhanced by suitable signal processing. The methods of accomplishing this improvement are called doppler filtering and MTI (moving-target indication). The signal-to-clutter ratio calculated by the methods just described should then be modified to reflect the improvement produced by this signal processing, with the proviso that the range depends on this ratio only so long as the clutter-to-noise ratio is considerably greater than unity.

9. BLIP/SCAN RATIO AND CUMULATIVE PROBABILITY

The concepts of blip/scan ratio and cumulative probability of detection were developed by the Operational Evaluation Group of the Office of the Chief of Naval Operations during the latter part of World War II and in the early postwar years. It had been noted that with scanning radars the echo (blip) strength fluctuated from scan to scan, and when

the target was near maximum range, the echo would appear on some scans and be absent on others. The fraction of scans on which a blip was observed, averaged over a small range interval, was named the blip/scan (B/S) ratio. It is apparent that this quantity is a function of target range and corresponds to the probability of detection when the observer's integration time (t_i, Eq. (29)) is less than the scan period of the radar.

The concept of cumulative probability of detection was developed to express the operational effectiveness of scanning radars against approaching targets. It answers the question, "What is the probability that an approaching target (e.g., aircraft) will have been detected by the time it reaches a given range?" Evidently this question requires a knowledge of the target speed and the radar scan rate as well as the variation of the blip/scan ratio as a function of range.

Range-Dependence of the Blip/Scan Ratio

The variability of blip strength, and of the presence or absence of a blip on a particular scan, would in principle be observed even for a target of steady cross section (e.g., a sphere) because of the combining of the signal with the noise in the detector. If this were the only factor operating, the range dependence of blip/scan ratio would be readily calculated, and moreover, the ratio would go from very small (near zero) to very large (near unity) values of blip/scan ratio fairly steeply as a function of range.

This behavior is radically modified, however, for targets whose cross sections fluctuate, as do those of typical aircraft. It is then observed that the variation of blip/scan ratio with range is much more gradual. When the combined effect of the receiver noise and the cross-section fluctuation is considered, the calculation of blip/scan ratio as a function of range is fairly complicated. But if the signal fluctuation is large compared to the noise fluctuation, a very good approximate calculation of the blip/scan ratio can be made simply, by assuming that there is a threshold value of the cross section σ_t that is detectable. The blip/scan ratio is then

$$\psi(R) = \int_{\sigma_t(R)}^{\infty} p(\sigma)\, d\sigma \ , \tag{86}$$

in which

$$\sigma_t(R) = \sigma_{50} \left(\frac{R}{F R_{50}} \right)^4 \ , \tag{87}$$

where F is the pattern-propagation factor (in general a function of the range R), σ_{50} is the median value of the radar cross section, and R_{50} is the free-space range for an 0.5 probability of detection on a steady-signal basis. (That is, R_{50} is the range calculated from Eq. (12) with $\sigma = \sigma_{50}$, $V_0 = V_{0(50)}$, and $F_t = F_r = 1$.) It then follows that if $p(\sigma)$ is of the Rayleigh-target form,*

$$p(\sigma) = \left(\frac{\ell n 2}{\sigma_{50}} \right) 2^{-\sigma/\sigma_{50}} \ . \tag{88}$$

*See also Eq. (24), which is equivalent. The form of Eq. (88) is more convenient here, since it has σ_{50} rather than $\bar{\sigma}$ as the normalizing parameter.

The blip/scan ratio is then given by

$$\psi(R) = 2^{-(R/FR_{50})^4} . \tag{89}$$

The more rigorous approach of considering the combined effects of the noise fluctuations and the target cross-section fluctuations has been taken by Mallett and Brennan (54), assuming free-space propagation.

When $F = 1$ (free-space propagation), the curve for ψ is a monotonic decreasing function of the range. When F is a function of target elevation angle, however, the range dependence of F must be obtained by assuming a specific target altitude, and a much more complicated $\psi(R)$ function results. Moreover, Eqs. (87) and (89) assume that such factors as L_α and T_s do not vary appreciably as the target (presumably at a fixed altitude) changes range; hence these are essentially for the lower radar frequencies (VHF or UHF).

Another consideration at higher frequencies is the fineness of the reflection-interference lobe structure. A high-speed aircraft may fly through an appreciable portion of a lobe during the scan period of a radar. F is no longer a slowly varying function of time and range, in relation to the usual radar scan rates. The statistical nature of ψ no longer permits F to be considered as a quasi-stationary parameter; rather, it becomes part of the statistics, contributing fluctuation due to the random part of the lobe structure in which the target is observed from scan to scan. This fine-lobe-structure case has been analyzed by Alderson, for the Rayleigh target, neglecting the fluctuation contribution of the receiver noise. (Alderson's analysis will be summarized in Part 2.) Alderson also has analyzed the effect of roll and pitch of the radar platform (ship) for an unstabilized antenna, with the same simplifying assumptions and the further assumption that the roll and pitch periods are not integrally or nearly integrally related to the scan period.

Cumulative Probability and Operator Factor

In principle, if the probability of detecting the target on a single scan at range R_i is P_i, assuming that the target fluctuation is independently random from scan to scan, the cumulative probability $P_c(R)$ that the approaching target will be detected at least once by the time it reaches range R is

$$P_c(R) = 1 - \prod_{i=1}^{n} (1 - P_i) , \tag{90}$$

where the scans occurring prior to the target reaching range R are numbered $1,2,3,\ldots n$. A more detailed formula is given by Mallett and Brennan (54).

The assumption that the fluctuation is independently random from scan to scan may not be justified in all cases, so caution must be used in applying this formula. Moreover, evaluation of the P_i's may be very difficult. If they are known as a tabulation of values from experimental data, calculation of $P_c(R)$ from this formula will require excessive labor unless a digital computer is employed. However, for certain assumptions concerning the form of P_i as a function of range, the product term of Eq. (90) can be represented as an integral.

There are many questions concerning the validity of assumptions necessary for computing cumulative probability. However, under some circumstances the necessary

assumptions may be realized, and calculations of cumulative probability may then be of value.

The probability of detection on the ith scan, at range R_i, would be $\psi(R_i)$ ideally. Generally, however, analysts have postulated that the human operator suffers from fatigue, boredom, etc., so that P_i is somewhat less than ψ_i, the latter being taken as the ideal or theoretical value that would apply with an alert or alerted observer (operator). An operator factor p_0 has been defined to express this relationship:

$$P_i = p_0 \psi_i \ . \tag{91}$$

The operator factor is defined as the probability that the operator will see the echo assuming that it appears (is detectable). In practice, however, p_0 has tended to be used as a curve-fitting parameter to account for all differences between theory and experiment. Thus its status as an engineering quantity based on extensive experimental data is dubious. Moreover, it was originally assumed that p_0 was a constant for a given experiment or a given operator and environment. Later it was realized that operator factor would certainly be a function of the signal strength, and hence of ψ itself, and possibly of other factors. Although some analysis and experiments have been performed to explore this more sophisticated viewpoint, the role of the operator factor in radar range theory remains in a somewhat nebulous and unsatisfactory state.

It has also been proposed that an operator recognizes the presence of a target only if it is observed on two or more scans in succession. The probability of successful outcome for this sequence of events is $p_0 \psi^k$, where k is the number of successive observations required. The assumption is made that p_0 applies only on the first scan of the sequence, the operator thereafter being assumed alert and attentive ($p_0 = 1$). (It is also assumed that the k scans all occur within a small range interval, so that ψ remains constant.)

10. ACCURACY OF RADAR RANGE PREDICTIONS

Calculations of radar maximum ranges were notoriously unreliable in the early days of radar, for a number of reasons. Numerous losses that occur were not recognized. Propagation effects were often ignored (free-space propagation was assumed). The sky noise temperature was often incorrectly assumed to be 290 or 300 degrees Kelvin (the input-termination temperature adopted as standard for receiver noise factor measurement). The probabilistic aspect of radar detection and the role of integration were not always properly taken into account.

In this report, methods of handling these factors correctly have been given, and if the factors in the equations are correctly determined, the predicted range will be correct, in the probabilistic sense. But since the maximum range is a probabilistic variable, a precise agreement between prediction and the results of limited experiment cannot be expected.

Moreover, the factors in the range equation are never known with absolute accuracy (although some of them may be known quite accurately). A quantity sometimes subject to inaccuracy is the radar-target cross section σ. Another factor that is not always known accurately is the pattern-propagation factor F. Because of the strong dependence of the range on the factor F compared to most of the other factors, this error is more significant than comparable errors in some of the other factors. It may arise especially through incorrect estimation of the magnitude of the earth- or sea-surface reflection coefficient ρ. In some cases superrefractive effects may also cause unexpectedly large or small values of F. At microwave frequencies, excessive atmospheric moisture, or

precipitation, may cause absorption losses much higher than those predicted for the normal atmosphere. Also, numerous unrecognized losses may occur within the radar system.

A measured antenna gain figure should be used in radar range calculation whenever possible; however, accurate gain measurement is sometimes fairly difficult to accomplish. The system noise temperature contains two components that may be subject to appreciable error: the sky noise varies greatly over the celestial sphere, and the receiver noise temperature is not always accurately known. In view of all these possible sources of error it is of some interest to consider the relative effects of errors in the individual range-equation factors upon the total calculated-range error.

The effect of definite increments of the independent variables is well known. For example, the range is proportional to the fourth root of the transmitter power and of several other quantities in the equation. Hence a change in one of these quantities by the factor x changes the range by the factor $x^{1/4}$. However, the range is directly proportional to the pattern-propagation factor F and inversely proportional to the square root of the frequency f (except that, as stated in Section, this inverse square-root dependence on f is only the explicit part of the dependence and assumes that all other factors in the equation are constant as the frequency changes or that their variation with frequency is taken into account separately).

In considering the effect of sky-noise variations on the accuracy of the range calculation, it is to be noted that the inverse fourth-root dependence is on the system noise temperature, of which the sky noise is an additive component. Therefore, the sensitivity of the range to the value of the sky noise temperature will depend partly upon the relative magnitudes of the sky noise temperature and the other components of system noise temperature; of course similar statements are true of the other temperature components, such as the receiver noise temperature.

The foregoing discussion has been concerned with the relationship between exactly known variations in the individual range-equation factors and the corresponding range variations. It is also of interest to consider the range-calculation error that results when it may be assumed that each range-equation factor is subject to an error that can be estimated statistically but is not known exactly — that is, the error can be specified or estimated in terms of a standard deviation. It is further assumed that the errors of the various quantities are statistically independent. Generally this assumption will be approximately correct even though there may be some interdependence as discussed in relation to the radar frequency.

The following equation, based on Eq. (12), has been derived* for this relationship, where the symbol $\mathcal{E}$ denotes the fractional standard error, or deviation, of the quantity that follows in parentheses; for example $\mathcal{E}(P_t)$ is the ratio of the standard deviation of the transmitter power to its nominal or assumed value:

$$\mathcal{E}(R_{max}) = \left\{ \frac{1}{4} \left[\mathcal{E}^2(F_t) + \mathcal{E}^2(F_r) + \mathcal{E}^2(f) \right] + \frac{1}{16} \left[\mathcal{E}^2(P_t) \right.\right.$$

$$+ \mathcal{E}^2(\tau) + \mathcal{E}^2(G_t) + \mathcal{E}^2(G_r) + \mathcal{E}^2(\sigma) + \mathcal{E}^2(T_s)$$

$$\left.\left. + \mathcal{E}^2(V_0) + \mathcal{E}^2(C_B) + \mathcal{E}^2(L) \right] \right\}^{1/2} . \qquad (92)$$

*The derivation was made by John Wood of NRL and will be given in Part 2.

In practice, radar engineers usually estimate the uncertainty of the assigned values of the range equation quantities which have the dimensions of power, or power ratio, as decibel values. Such estimates usually do not have the statistical precision implied by the standard-deviation definition of $\mathcal{E}$ in Eq. (92). For purposes of approximate calculation, however, decibel errors thus estimated, designated E_{dB}, may be converted to values of $\mathcal{E}$ by the formula

$$\mathcal{E} = (\text{antilog } |0.1\, E_{dB}|) - 1 \ . \tag{93}$$

This formula implies that the decibel error value E_{dB} is actually 10 times the logarithm of the ratio of the sum of the assigned value and the standard deviation to the assigned value of the range-equation factor.

Equation (92) gives the range error (standard deviation) in terms of the symbols of Eq. (12). A similar error equation in terms of the symbols of Eq. (11) may be obtained by substituting the terms of this equation that are comparable to those of Eq. (12) into Eq. (92). That is, B and S/N of Eq. (11) substitute for τ and V_0, and C_B drops out.

11. A SYSTEMATIC PROCEDURE FOR RANGE PREDICTION

The work sheet that follows has proven to be helpful in making the computations necessary for radar range prediction. It is based on the decibel-logarithmic range equation (Eq. (13)) and is basically self-explanatory. The work sheet insures against omitting any of the factors in the range equation, and it simplifies the computation. Figures 24 and 25, or Tables 1 and 2, simplify some of the calculations required.

When many calculations of range for different values of the variables are required, programming of the range equation for a digital computer may be preferable, but when a few calculations or intermittent calculations are required, this form is useful, and it provides a more accurate method than the mechanical radar range calculators that are often used, although they in turn are useful for rough quick calculations.

12. ACKNOWLEDGMENTS

The author's study of the subject of this report has been carried out over a period of many years, and has been helped by discussions with many people both at the Naval Research Laboratory and elsewhere. To list all of them here would be impractical, but especially valuable discussions with the following persons are gratefully acknowledged: R.C. Guthrie, I.H. Page, A.A. Varela, W.S. Alderson, R.J. Adams, S.K. Meads, W.S. Ament, S.F. George, and M.I. Skolnik, all now or formerly of the Naval Research Laboratory; W.M. Hall and D.K. Barton of the Raytheon Company; and L.E. Davies of Stanford Research Institute. It is also a pleasure to acknowledge the helpful encouragement received from many people, including those mentioned above, and especially from G.D. Greenwood, formerly of the agency then called Bureau of Ships, W.B. Renhult of MIT Lincoln Laboratory, LCDR W.T. Barron of STIC (Office of Naval Intelligence), and F.P. Theriot of the Naval Ship Engineering Center. Funding for the work has, at various times, come from the Bureau of Ships, STIC, and the Office of Naval Research.

PULSE-RADAR RANGE-CALCULATION WORK SHEET

Based on Eq. (13)

1. Compute the system input noise temperature T_s, following the outline in section A below.
2. Enter range factors known in other than decibel form in section B below, for reference.
3. Enter logarithmic and decibel values in section C below, positive values in the plus column and negative values in the minus column. For example, if $V_{0\,(dB)}$ as given by Figs. 4 through 9 is negative, then $-V_{0\,(dB)}$ is positive and goes in the plus column. For C_B, see Figs. 1 through 3. For definitions of the range factors, see Eq. (13).

Radar antenna height: h = ft. Target elevation angle: θ = °. (See Fig. 13.)

A. Computation of T_s:

$T_s = T_a + T_r + L_r T_e$

(a) Compute T_a.
For $T_{t\acute{g}} = T_{ta} = 290$ and $T_{\acute{g}} = 36$ use Eq. (37a).
Read T_a' from Fig. 11.

$L_{a(dB)}$: _____ L_a: _____

$T_a = (0.876\,T_a' - 254)/L_a + 290$

T_a = °K

(b) Compute T_r using Eq. (40).
For $T_{tr} = 290$ use Table 1.

$L_{r(dB)}$: _____ T_r = °K

(c) Compute T_e using Eq. (41) or using Table 1.

$F_{n(dB)}$: _____ T_e: _____ °K

L_r: _____ $L_r T_e$ = °K

Add. T_s = °K

B. Range Factors		C. Decibel Values	Plus (+)	Minus (-)
$P_{t\,(kW)}$		10 log $P_{t\,(kW)}$	.	.
$\tau_{\mu sec}$		10 log $\tau_{\mu sec}$	.	.
G_t		$G_{t\,(dB)}$	.	.
G_r		$G_{r\,(dB)}$	.	.
$\sigma_{(sq\ m)}$		10 log σ	.	.
f_{MHz}		−20 log f_{MHz}	.	.
T_s (°K)		−10 log T_s	.	.
V_0		$-V_{0\,(dB)}$	.	.
C_B		$-C_{B\,(dB)}$		.
L_t		$-L_{t\,(dB)}$		.
L_p		$-L_{p\,(dB)}$		.
L_x		$-L_{x\,(dB)}$		.
Range-equation constant (40 log 1.292)			4.45	
4. Obtain the column totals →			.	.
5. Enter the smaller total below the larger →			.	.
6. Subtract to obtain the net decibels (dB) →			+ .	- .

7. In Table 2 find the range ratio corresponding to this net decibel (dB) value, taking its sign (±) into account. Multiply this ratio by 100. This is R_0 → _____

8. Multiply R_0 by the pattern-propagation factor F = _____ (see Eqs. (42) through (65) and Figs. 12 through 19):

$R_0 \times F = R'$ → _____

9. On the appropriate curve of Figs. 21 and 22 determine the atmospheric-absorption loss factor, $L_{\alpha(dB)}$, corresponding to R'. This is $L_{\alpha(dB)(1)}$. → _____

10. Find the range factor δ_1 corresponding to $-L_{\alpha(dB)(1)}$ from the formula δ = antilog $(-L_{\alpha(dB)}/40)$ or by using Table 2. → _____

11. Multiply R' by δ_1. This is a first approximation of the range R_1. → _____

12. If R_1 differs appreciably from R', on the appropriate curve of Figs. 21 and 22, find the new value of $L_{\alpha(dB)}$ corresponding to R_1. This is $L_{\alpha(dB)(2)}$. → _____

13. Find the range-increase factor (Table 2) corresponding to the difference between $L_{\alpha(dB)(1)}$ and $L_{\alpha(dB)(2)}$. This is δ_2. → _____

14. Multiply R_1 by δ_2. This is the radar range in nautical miles, R. → _____

Note: If the difference between $L_{\alpha(dB)(1)}$ and $L_{\alpha(dB)(2)}$ is less than 0.1 dB, R_1 may be taken as the final range value, and steps 12 through 14 may be omitted. If $L_{\alpha(dB)(1)}$ is less than 0.1 dB, R' may be taken as the final range value, and steps 9 through 14 may be omitted. (For radar frequencies up to 10,000 megahertz, correction of the atmospheric attenuation beyond the $L_{\alpha(dB)(2)}$ value would amount to less than 0.1 dB.)

Table 1
Power Ratios and Noise Temperatures

Opposite the decibel value of the transmission-line available loss L_r, in the first column, find in the second column the corresponding power-ratio value of L_r. In the third column, find the corresponding value of transmission-line input noise temperature $T_{r(I)}$, assuming that the thermal temperature T_t is approximately equal to $T_o = 290°K$, according to the formula

$$T_{r(I)} = T_o (L_r - 1).$$

If in the actual case T_t has an appreciably different value, multiply these values of $T_{r(I)}$ by $T_t/290$.

Opposite the decibel value of receiver noise factor $\overline{NF}$ in the first column, find in the third column the corresponding value of receiver input noise temperature T_e, according to the formula

$$T_e = T_o (\overline{NF} - 1).$$

$\overline{NF}$ L_r decibels	$\overline{NF}$ L_r power ratios	T_e $T_{r(I)}$ ° Kelvin	$\overline{NF}$ L_r decibels	$\overline{NF}$ L_r power ratios	T_e $T_{r(I)}$ ° Kelvin	$\overline{NF}$ L_r decibels	$\overline{NF}$ L_r power ratios	T_e $T_{r(I)}$ ° Kelvin
0	1.0000	0.00	2.2	1.660	191	6.2	4.169	919
0.01	1.0023	0.67	2.3	1.698	202	6.3	4.266	947
0.02	1.0046	1.33	2.4	1.738	214	6.4	4.365	976
0.03	1.0069	2.00	2.5	1.778	226	6.5	4.467	1005
0.04	1.0093	2.70	2.6	1.820	238	6.6	4.571	1036
0.05	1.0116	3.36	2.7	1.862	250	6.7	4.677	1066
0.06	1.0139	4.03	2.8	1.905	262	6.8	4.786	1098
0.07	1.0162	4.70	2.9	1.950	276	6.9	4.898	1130
0.08	1.0186	5.39	3.0	1.995	289	7.0	5.012	1163
0.09	1.0209	6.06	3.1	2.042	302	7.1	5.129	1197
0.10	1.0233	6.76	3.2	2.089	316	7.2	5.248	1232
0.15	1.0351	10.2	3.3	2.138	330	7.3	5.370	1267
0.20	1.0471	13.7	3.4	2.188	345	7.4	5.495	1304
0.25	1.0593	17.2	3.5	2.239	359	7.5	5.623	1341
0.30	1.0715	20.7	3.6	2.291	374	7.6	5.754	1379
0.35	1.0839	24.3	3.7	2.344	390	7.7	5.888	1418
0.40	1.0965	28.0	3.8	2.399	406	7.8	6.026	1458
0.45	1.1092	31.7	3.9	2.455	422	7.9	6.166	1498
0.50	1.1220	35.4	4.0	2.512	438	8.0	6.310	1540
0.55	1.1350	39.2	4.1	2.570	455	8.1	6.457	1583
0.60	1.1482	43.0	4.2	2.630	473	8.2	6.607	1626
0.65	1.1614	46.8	4.3	2.692	491	8.3	6.761	1671
0.70	1.1749	50.7	4.4	2.754	509	8.4	6.918	1716
0.75	1.1885	54.7	4.5	2.818	527	8.5	7.079	1763
0.80	1.2023	58.7	4.6	2.884	546	8.6	7.244	1811
0.85	1.2162	62.7	4.7	2.951	566	8.7	7.413	1860
0.90	1.2303	66.8	4.8	3.020	586	8.8	7.586	1910
0.95	1.2445	70.9	4.9	3.090	606	8.9	7.762	1961
1.00	1.2589	75.1	5.0	3.162	627	9.0	7.943	2013
1.1	1.288	83.5	5.1	3.236	648	9.1	8.128	2067
1.2	1.318	92.2	5.2	3.311	670	9.2	8.318	2122
1.3	1.349	101	5.3	3.388	693	9.3	8.511	2178
1.4	1.380	110	5.4	3.467	715	9.4	8.710	2236
1.5	1.413	120	5.5	3.548	739	9.5	8.913	2295
1.6	1.445	129	5.6	3.631	763	9.6	9.120	2355
1.7	1.479	139	5.7	3.715	787	9.7	9.333	2417
1.8	1.514	149	5.8	3.802	813	9.8	9.550	2480
1.9	1.549	159	5.9	3.890	838	9.9	9.772	2544
2.0	1.585	170	6.0	3.981	864	10.0	10.000	2610
2.1	1.622	180	6.1	4.074	891			

Temperature conversion relations: $T_{Kelvin} = 273.16 + T_{centigrade} = 255.38 + (5/9)\, T_{Fahrenheit}$
290° Kelvin = 16.84° centigrade = 62.32° Fahrenheit

Table 2

Radar Range Factors for a System Power Change from 0 to 40 dB (In Steps of 0.1 db)

The table is intended for use with an equation of the type:

$$R = k\left[\frac{P_t G^2 \lambda^2 \sigma F^4}{P_r L}\right]^{1/4} = k P^{1/4}; \text{ i.e., } R \propto P^{1/4},$$

where R is the radar range and P may be regarded as an equivalent system power variable. The table is based on the relation:

$$R/R_0 = \text{antilog}\left[\frac{1}{40}(10 \log P/P_0)\right],$$

where R/R_0 is the range factor, and 10 log P/P_0 is the power change in decibels. P_t is transmitter power, G antenna gain, λ wavelength, σ target cross section, L loss factor, F pattern-propagation factor, and P_r received echo power.

Range factors for power changes greater than 40 dB can be obtained from the table by the following procedure: (1) subtract from the absolute value of the power change in dB the integral multiple of 40 which results in a positive remainder less than 40; (2) look up the range factor corresponding to the remainder; (3) shift the decimal point one place for each 40 dB subtracted; for range increase, shift to the right, for decrease shift to the left. For example, the range increase for a power change of 47.3 dB is 15.22, and for 87.3 it is 152.2, because for 7.3 dB it is 1.522. The decrease factor for 47.3 dB is 0.06569, and for 87.3 it is 0.006569, etc.

Power Change, Decibels ±	Range Increase Factor (Decimal Point)	Range Decrease Factor (Decimal Point)	± Decibels Power Change
0.0	1 0000	1 0 000	40.0
0.1	1 0058	9 943	39.9
0.2	1 0116	9 886	39.8
0.3	1 0174	9 829	39.7
0.4	1 0233	9 772	39.6
0.5	1 0292	9 716	39.5
0.6	1 0351	9 661	39.4
0.7	1 0411	9 605	39.3
0.8	1 0471	9 550	39.2
0.9	1 0532	9 495	39.1
1.0	1 0593	9 441	39.0
1.1	1 065	9 386	38.9
1.2	1 072	9 333	38.8
1.3	1 078	9 279	38.7
1.4	1 084	9 226	38.6
1.5	1 090	9 173	38.5
1.6	1 096	9 120	38.4
1.7	1 103	9 068	38.3
1.8	1 109	9 016	38.2
1.9	1 116	8 964	38.1
2.0	1 122	8 913	38.0
2.1	1 129	8 861	37.9
2.2	1 135	8 810	37.8
2.3	1 142	8 760	37.7
2.4	1 148	8 710	37.6
2.5	1 155	8 660	37.5
2.6	1 161	8 610	37.4
2.7	1 168	8 561	37.3
2.8	1 175	8 511	37.2
2.9	1 182	8 463	37.1
3.0	1 189	8 414	37.0
3.1	1 195	8 366	36.9
3.2	1 202	8 318	36.8
3.3	1 209	8 270	36.7
3.4	1 216	8 222	36.6
3.5	1 223	8 175	36.5
3.6	1 230	8 128	36.4
3.7	1 237	8 082	36.3
3.8	1 245	8 035	36.2
3.9	1 252	7 989	36.1
4.0	1 259	7 943	36.0
4.1	1 266	7 898	35.9
4.2	1 274	7 852	35.8
4.3	1 281	7 807	35.7
4.4	1 288	7 763	35.6
4.5	1 296	7 718	35.5
4.6	1 303	7 674	35.4
4.7	1 311	7 630	35.3
4.8	1 318	7 586	35.2
4.9	1 326	7 542	35.1

Power Change, Decibels ±	Range Increase Factor (Decimal Point)	Range Decrease Factor (Decimal Point)	± Decibels Power Change
5.0	1 334	7 499	35.0
5.1	1 341	7 456	34.9
5.2	1 349	7 413	34.8
5.3	1 357	7 371	34.7
5.4	1 365	7 328	34.6
5.5	1 372	7 286	34.5
5.6	1 380	7 244	34.4
5.7	1 388	7 203	34.3
5.8	1 396	7 162	34.2
5.9	1 404	7 120	34.1
6.0	1 413	7 080	34.0
6.1	1 421	7 039	33.9
6.2	1 429	6 998	33.8
6.3	1 437	6 958	33.7
6.4	1 445	6 918	33.6
6.5	1 454	6 879	33.5
6.6	1 462	6 839	33.4
6.7	1 471	6 800	33.3
6.8	1 479	6 761	33.2
6.9	1 488	6 722	33.1
7.0	1 496	6 683	33.0
7.1	1 505	6 645	32.9
7.2	1 514	6 607	32.8
7.3	1 522	6 569	32.7
7.4	1 531	6 531	32.6
7.5	1 540	6 494	32.5
7.6	1 549	6 457	32.4
7.7	1 558	6 420	32.3
7.8	1 567	6 383	32.2
7.9	1 576	6 346	32.1
8.0	1 585	6 310	32.0
8.1	1 594	6 273	31.9
8.2	1 603	6 237	31.8
8.3	1 612	6 202	31.7
8.4	1 622	6 166	31.6
8.5	1 631	6 131	31.5
8.6	1 641	6 095	31.4
8.7	1 650	6 061	31.3
8.8	1 660	6 026	31.2
8.9	1 669	5 991	31.1
9.0	1 679	5 957	31.0
9.1	1 689	5 923	30.9
9.2	1 698	5 888	30.8
9.3	1 708	5 855	30.7
9.4	1 718	5 821	30.6
9.5	1 728	5 788	30.5
9.6	1 738	5 754	30.4
9.7	1 748	5 721	30.3
9.8	1 758	5 689	30.2
9.9	1 768	5 656	30.1

Power Change, Decibels ±	Range Increase Factor (Decimal Point)	Range Decrease Factor (Decimal Point)	± Decibels Power Change
10.0	1 778	5 623	30.0
10.1	1 789	5 591	29.9
10.2	1 799	5 559	29.8
10.3	1 809	5 527	29.7
10.4	1 819	5 495	29.6
10.5	1 830	5 464	29.5
10.6	1 841	5 433	29.4
10.7	1 851	5 401	29.3
10.8	1 862	5 370	29.2
10.9	1 873	5 340	29.1
11.0	1 884	5 309	29.0
11.1	1 895	5 278	28.9
11.2	1 905	5 248	28.8
11.3	1 916	5 218	28.7
11.4	1 928	5 188	28.6
11.5	1 939	5 158	28.5
11.6	1 950	5 129	28.4
11.7	1 961	5 099	28.3
11.8	1 972	5 070	28.2
11.9	1 984	5 041	28.1
12.0	1 995	5 012	28.0
12.1	2 007	4 983	27.9
12.2	2 018	4 954	27.8
12.3	2 030	4 926	27.7
12.4	2 042	4 898	27.6
12.5	2 054	4 870	27.5
12.6	2 065	4 842	27.4
12.7	2 077	4 814	27.3
12.8	2 089	4 786	27.2
12.9	2 101	4 759	27.1
13.0	2 113	4 732	27.0
13.1	2 126	4 704	26.9
13.2	2 138	4 677	26.8
13.3	2 150	4 650	26.7
13.4	2 163	4 624	26.6
13.5	2 175	4 597	26.5
13.6	2 188	4 571	26.4
13.7	2 200	4 545	26.3
13.8	2 213	4 519	26.2
13.9	2 226	4 493	26.1
14.0	2 239	4 467	26.0
14.1	2 252	4 441	25.9
14.2	2 265	4 416	25.8
14.3	2 278	4 390	25.7
14.4	2 291	4 365	25.6
14.5	2 304	4 340	25.5
14.6	2 317	4 315	25.4
14.7	2 331	4 290	25.3
14.8	2 344	4 266	25.2
14.9	2 358	4 241	25.1

Power Change, Decibels ±	Range Increase Factor (Decimal Point)	Range Decrease Factor (Decimal Point)	± Decibels Power Change
15.0	2 371	4 217	25.0
15.1	2 385	4 193	24.9
15.2	2 399	4 169	24.8
15.3	2 413	4 145	24.7
15.4	2 427	4 121	24.6
15.5	2 441	4 097	24.5
15.6	2 455	4 074	24.4
15.7	2 469	4 050	24.3
15.8	2 483	4 027	24.2
15.9	2 497	4 004	24.1
16.0	2 512	3 981	24.0
16.1	2 526	3 958	23.9
16.2	2 541	3 936	23.8
16.3	2 556	3 913	23.7
16.4	2 570	3 890	23.6
16.5	2 585	3 868	23.5
16.6	2 600	3 846	23.4
16.7	2 615	3 824	23.3
16.8	2 630	3 802	23.2
16.9	2 645	3 780	23.1
17.0	2 661	3 758	23.0
17.1	2 676	3 737	22.9
17.2	2 692	3 715	22.8
17.3	2 707	3 694	22.7
17.4	2 723	3 673	22.6
17.5	2 738	3 652	22.5
17.6	2 754	3 631	22.4
17.7	2 770	3 610	22.3
17.8	2 786	3 589	22.2
17.9	2 802	3 569	22.1
18.0	2 818	3 548	22.0
18.1	2 835	3 528	21.9
18.2	2 851	3 508	21.8
18.3	2 867	3 487	21.7
18.4	2 884	3 467	21.6
18.5	2 901	3 447	21.5
18.6	2 917	3 428	21.4
18.7	2 934	3 408	21.3
18.8	2 951	3 388	21.2
18.9	2 968	3 369	21.1
19.0	2 985	3 350	21.0
19.1	3 003	3 330	20.9
19.2	3 020	3 311	20.8
19.3	3 037	3 292	20.7
19.4	3 055	3 273	20.6
19.5	3 073	3 255	20.5
19.6	3 090	3 236	20.4
19.7	3 108	3 217	20.3
19.8	3 126	3 199	20.2
19.9	3 144	3 181	20.1
20.0	3 162	3 162	20.0

Decimal Point Range Decrease Factor	Decimal Point Range Increase Factor	± Decibels Power Change
1 000	1 000	0.0
9 943	1 0058	0.1
9 886	1 0116	0.2
9 829	1 0174	0.3
9 772	1 0233	0.4
9 716	1 0292	0.5
9 661	1 0351	0.6
9 605	1 0411	0.7
9 550	1 0471	0.8
9 495	1 0532	0.9
9 441	1 0593	1.0
9 386	1 065	1.1
9 333	1 072	1.2
9 279	1 078	1.3
9 226	1 084	1.4
9 173	1 090	1.5
9 120	1 096	1.6
9 068	1 103	1.7
9 016	1 109	1.8
8 964	1 116	1.9
8 913	1 122	2.0
8 861	1 129	2.1
8 810	1 135	2.2
8 760	1 142	2.3
8 710	1 148	2.4
8 660	1 155	2.5
8 610	1 161	2.6
8 561	1 168	2.7
8 511	1 175	2.8
8 463	1 182	2.9
8 414	1 189	3.0
8 366	1 195	3.1
8 318	1 202	3.2
8 270	1 209	3.3
8 222	1 216	3.4
8 175	1 223	3.5
8 128	1 230	3.6
8 082	1 237	3.7
8 035	1 245	3.8
7 989	1 252	3.9
7 943	1 259	4.0
7 898	1 266	4.1
7 852	1 274	4.2
7 807	1 281	4.3
7 763	1 288	4.4
7 718	1 296	4.5
7 674	1 303	4.6
7 630	1 311	4.7
7 586	1 318	4.8
7 542	1 326	4.9

Decimal Point Range Decrease Factor	Decimal Point Range Increase Factor	± Decibels Power Change
7 499	1 334	5.0
7 456	1 341	5.1
7 413	1 349	5.2
7 371	1 357	5.3
7 328	1 365	5.4
7 286	1 372	5.5
7 244	1 380	5.6
7 203	1 388	5.7
7 162	1 396	5.8
7 120	1 404	5.9
7 080	1 413	6.0
7 039	1 421	6.1
6 998	1 429	6.2
6 958	1 437	6.3
6 918	1 445	6.4
6 879	1 454	6.5
6 839	1 462	6.6
6 800	1 471	6.7
6 761	1 479	6.8
6 722	1 488	6.9
6 683	1 496	7.0
6 645	1 505	7.1
6 607	1 514	7.2
6 569	1 522	7.3
6 531	1 531	7.4
6 494	1 540	7.5
6 457	1 549	7.6
6 420	1 558	7.7
6 383	1 567	7.8
6 346	1 576	7.9
6 310	1 585	8.0
6 273	1 594	8.1
6 237	1 603	8.2
6 202	1 612	8.3
6 166	1 622	8.4
6 131	1 631	8.5
6 095	1 641	8.6
6 061	1 650	8.7
6 026	1 660	8.8
5 991	1 669	8.9
5 957	1 679	9.0
5 923	1 689	9.1
5 888	1 698	9.2
5 855	1 708	9.3
5 821	1 718	9.4
5 788	1 728	9.5
5 754	1 738	9.6
5 721	1 748	9.7
5 689	1 758	9.8
5 656	1 768	9.9

Decimal Point Range Decrease Factor	Decimal Point Range Increase Factor	± Decibels Power Change
5 623	1 778	10.0
5 591	1 789	10.1
5 559	1 799	10.2
5 527	1 809	10.3
5 495	1 819	10.4
5 464	1 830	10.5
5 433	1 841	10.6
5 401	1 851	10.7
5 370	1 862	10.8
5 340	1 873	10.9
5 309	1 884	11.0
5 278	1 895	11.1
5 248	1 905	11.2
5 218	1 916	11.3
5 188	1 928	11.4
5 158	1 939	11.5
5 129	1 950	11.6
5 099	1 961	11.7
5 070	1 972	11.8
5 041	1 984	11.9
5 012	1 995	12.0
4 983	2 007	12.1
4 954	2 018	12.2
4 926	2 030	12.3
4 898	2 042	12.4
4 870	2 054	12.5
4 842	2 065	12.6
4 814	2 077	12.7
4 786	2 089	12.8
4 759	2 101	12.9
4 732	2 113	13.0
4 704	2 126	13.1
4 677	2 138	13.2
4 650	2 150	13.3
4 624	2 163	13.4
4 597	2 175	13.5
4 571	2 188	13.6
4 545	2 200	13.7
4 519	2 213	13.8
4 493	2 226	13.9
4 467	2 239	14.0
4 441	2 252	14.1
4 416	2 265	14.2
4 390	2 278	14.3
4 365	2 291	14.4
4 340	2 304	14.5
4 315	2 317	14.6
4 290	2 331	14.7
4 266	2 344	14.8
4 241	2 358	14.9

Decimal Point Range Decrease Factor	Decimal Point Range Increase Factor	± Decibels Power Change
4 217	2 371	15.0
4 193	2 385	15.1
4 169	2 399	15.2
4 145	2 413	15.3
4 121	2 427	15.4
4 097	2 441	15.5
4 074	2 455	15.6
4 050	2 469	15.7
4 027	2 483	15.8
4 004	2 497	15.9
3 981	2 512	16.0
3 958	2 526	16.1
3 936	2 541	16.2
3 913	2 556	16.3
3 890	2 570	16.4
3 868	2 585	16.5
3 846	2 600	16.6
3 824	2 615	16.7
3 802	2 630	16.8
3 780	2 645	16.9
3 758	2 661	17.0
3 737	2 676	17.1
3 715	2 692	17.2
3 694	2 707	17.3
3 673	2 723	17.4
3 652	2 738	17.5
3 631	2 754	17.6
3 610	2 770	17.7
3 589	2 786	17.8
3 569	2 802	17.9
3 548	2 818	18.0
3 528	2 835	18.1
3 508	2 851	18.2
3 487	2 867	18.3
3 467	2 884	18.4
3 447	2 901	18.5
3 428	2 917	18.6
3 408	2 934	18.7
3 388	2 951	18.8
3 369	2 968	18.9
3 350	2 985	19.0
3 330	3 003	19.1
3 311	3 020	19.2
3 292	3 037	19.3
3 273	3 055	19.4
3 255	3 073	19.5
3 236	3 090	19.6
3 217	3 108	19.7
3 199	3 126	19.8
3 181	3 144	19.9
3 162	3 162	20.0

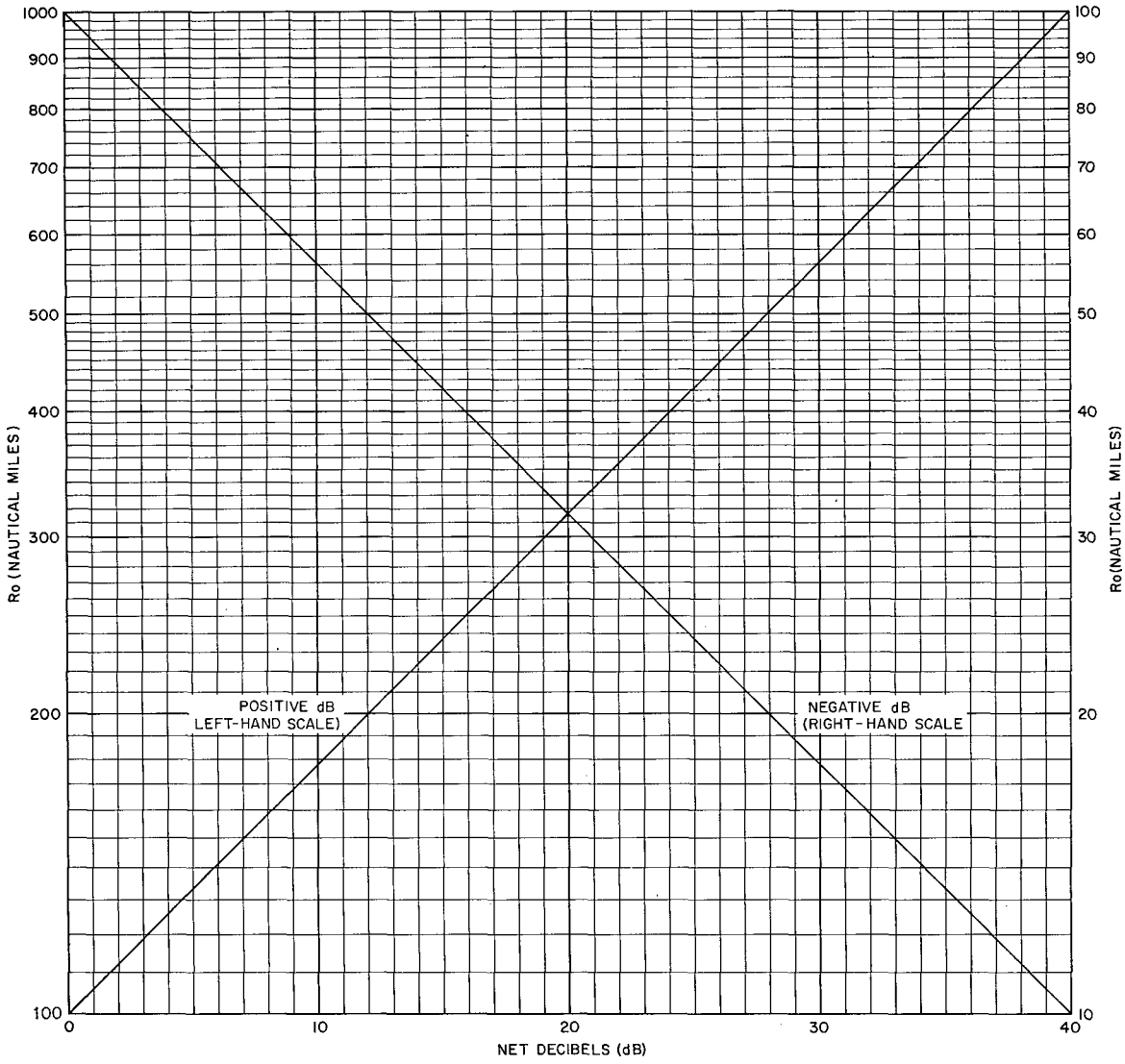

Fig. 24 - Free-space radar range R_0, nautical miles, as a function of the net decibel factor (dB) from the range-calculation work sheet, plotted from $R_0 = 100$ antilog (dB/40). For $|dB| > 40$, subtract an integral number M times 40 from $|dB|$ to make the remainder lie in the range 0 to 40 dB; then multiply the left range scale by 10^M and the right range scale by 10^{-M}, and read range corresponding to remainder. (Note: This figure also appears in an appendix at the end of the report.)

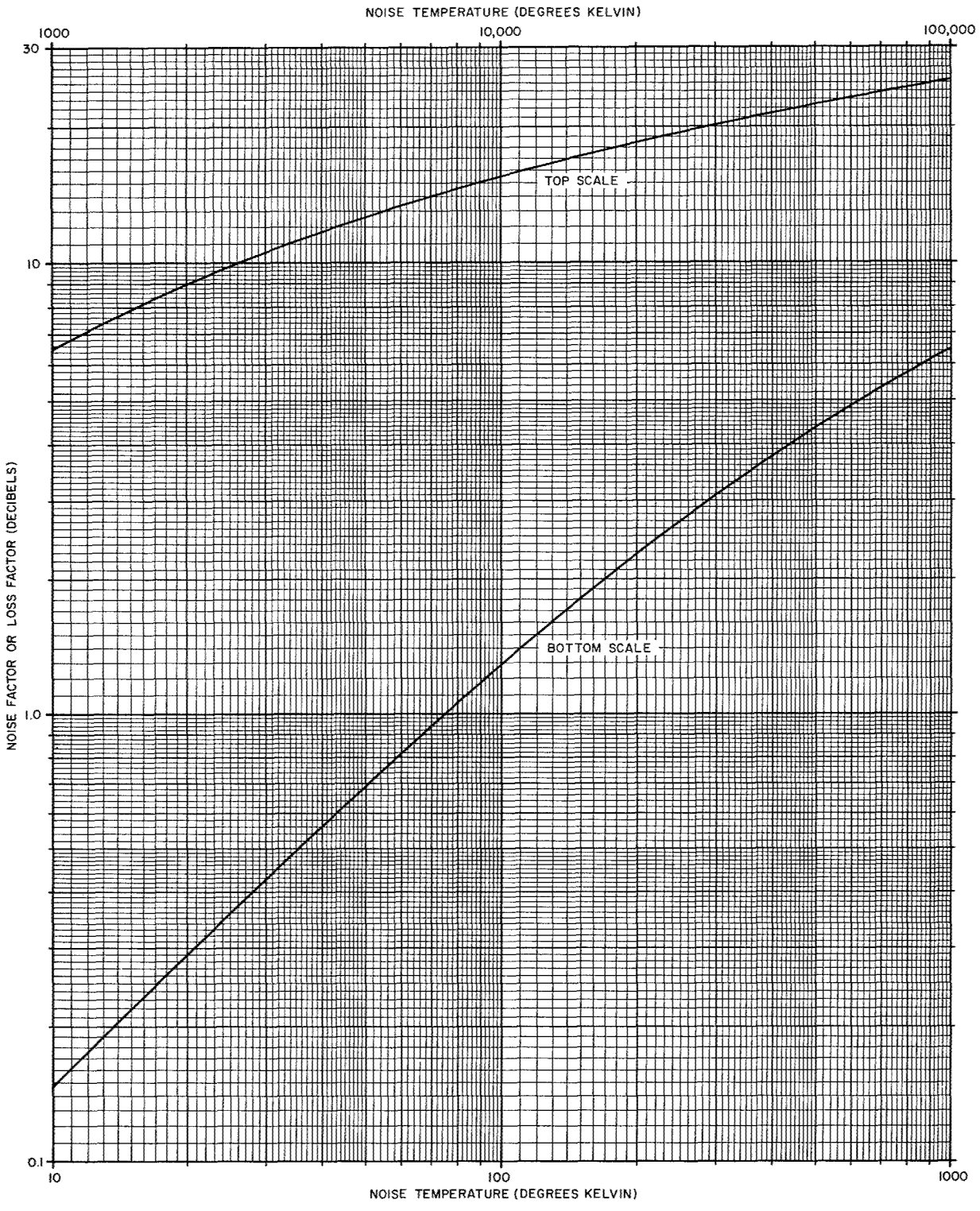

Fig. 25 - Effective receiver input noise temperature T_e or transmission-line input noise temperature T_r as a function of receiver noise factor F_n or transmission-line loss factor L_r. (Note: This figure also appears in an appendix at the end of the report.)

REFERENCES

1. Norton, K.A., and Omberg, A.C., "The Maximum Range of a Radar Set," Proc. IRE 35(No. 1):4-24 (Jan. 1947); originally issued as Report ORG-P-9-1, Operational Research Group, Office of Chief Signal Officer, U.S. Army, Feb. 1943

2. North, D.O., "An Analysis of the Factors Which Determine Signal/Noise Discrimination in Pulsed-Carrier Systems," Proc. IEEE 51(No. 7):1016-1027 (July 1963); originally issued as RCA Laboratories Report PTR-6C, June 1943

3. Marcum, J.I., "A Statistical Theory of Target Detection by Pulsed Radar, and Mathematical Appendix," Trans. IRE IT-6(No. 2):59-267 (Apr. 1960); originally issued as Rand Corporation Research Memoranda RM-754, Dec. 1947, and RM-753, July 1948

4. Robertson, G.H., "Operating Characteristics for a Linear Detector of CW Signals in Narrow-Band Gaussian Noise," Bell System Tech. J. 46(No. 4):755-774 (Apr. 1967)

5. Swerling, P., "Probability of Detection for Fluctuating Targets," IRE Trans. IT-6 (No. 2):269-308 (Apr. 1960); originally issued as Rand Corporation Research Memorandum RM-1217, Mar. 1954

6. Fehlner, L.F., "Marcum and Swerling's Data on Target Detection by a Pulsed Radar," Johns Hopkins University Applied Physics Laboratory Report TG-451, July 1962, and Supplement, TG-451A, Sept. 1964

7. Kaplan, E.L., "Signal-Detection Studies with Applications," Bell System Tech. J. 34 (No. 2):403-437 (Mar. 1955); also issued as BTL Monograph 2394

8. Schwartz, M., "Effects of Signal Fluctuation on the Detection of Pulsed Signals in Noise," Trans. IRE IT-2(No. 2):66-71 (June 1956)

9. Heidbreder, G.R., and Mitchell, R.L., "Detection Probabilities for Log-Normally Distributed Signals," IEEE Trans. AES-3(No. 1):5-13 (Jan. 1967)

10. Bates, R.H.T., "Statistics of Fluctuating Target Detection," IEEE Trans. AES-2 (No. 1):137-138 (Jan. 1966); also, "Discussion," IEEE Trans. AES-2 (No. 9):621-622 (Sept. 1966)

11. Hall, W.M., "Prediction of Pulse Radar Performance," Proc. IRE 44(No. 2):224-231 (Feb. 1956)

12. Blake, L.V., "Recent Advancements in Basic Radar Range Calculation Technique," IRE Trans. MIL-5(No. 2):154-164 (Apr. 1961)

13. Blake, L.V., "A Guide to Basic Pulse-Radar Maximum-Range Calculation, Part 1 - Equations, Definitions, and Aids to Calculation," NRL Report 5868, Dec. 1962

14. Kerr, D.E., editor, "Propagation of Short Radio Waves," Vol. 13 of MIT Radiation Laboratory Series, McGraw-Hill, New York, 1951

15. Lawson, J.L., and Uhlenbeck, G.E., editors, "Threshold Signals," Vol. 24 of MIT Radiation Laboratory Series, McGraw-Hill, New York, 1950

16. IEEE Standards 57IRE 7.S2, 59IRE 20.S1, 62IRE 7.S2, and accompanying tutorial papers, available from IEEE Headquarters, New York; also published in Proc. IEEE (IRE 45(No. 7):983-1010 (July 1957); 48(No. 1):60-68 (Jan. 1960); and 51(No. 3):434-442 (Mar. 1963)

17. North, D.O., "The Absolute Sensitivity of Radio Receivers," RCA Review 6(No. 3): 332-343 (Jan. 1942)

18. Haeff, A.V., "Minimum Detectable Radar Signal and Its Dependence upon Parameters of Radar Systems," Proc. IRE 34(No. 11):857-861 (Nov. 1946); originally issued as an NRL Report (No. RA-3A-208A) in 1943

19. IEEE Standard 149, IEEE Test Procedure for Antennas, Jan. 1965, available from IEEE Headquarters, New York; also published in IEEE Trans. AP-13(No. 3):437-466 (May 1965)

20. Jasik, H., editor, "Antenna Engineering Handbook," pp. 2-13, McGraw-Hill, New York, 1961

21. Bennett, W.R., "Response of a Linear Rectifier to Signal and Noise," J. Acoust. Soc. Amer. 15(No. 3):164-172 (Jan. 1944); also, Bell System Tech. J. 23(No. 1):97 (Jan. 1944)

22. Rice, S.O., "Mathematical Analysis of Random Noise," Bell System Tech. J. 23(No. 4): 282-332 (July 1944) and 24(No. 1):46-156 (Jan. 1945) (see especially Eq. 4.2-3 in vol. 23, p. 119)

23. Woodward, P.M., "Probability and Information Theory, with Applications to Radar," McGraw-Hill, New York, 1953; second edition, Pergamon, New York, 1964

24. Davenport, W.B., and Root, W.L., "An Introduction to the Theory of Random Signals and Noise," McGraw-Hill, New York, 1958

25. Berkowitz, R.S., editor, "Modern Radar," Wiley, New York, 1965

26. Swerling, P., "Detection of Radar Echoes in Noise Revisited," IEEE Trans. IT-12 (No. 3):348-361 (July 1966)

27. Bussgang, J.J., Nesbeda, P., and Safran, H., "A Unified Analysis of Range Performance of CW, Pulse, and Pulse Doppler Radar," Proc. IRE 47(No. 10):1753-1762 (Oct. 1959)

28. Nyquist, H., "Thermal Agitation of Electric Charge in Conductors," Phys. Rev. 32: 110-113 (July 1928)

29. Blake, L.V., "Antenna and Receiving-System Noise-Temperature Calculation," Proc. IEEE (Correspondence) 49(No. 10):1568-1569 (Oct. 1961) (this correspondence summarizes NRL Report 5668, same title, Sept. 1961)

30. Dicke, R.H., et al., "Atmospheric Absorption Measurements with a Microwave Radiometer," Phys. Rev. 70:340 (1946)

31. Ross, G.F., and Schwartzman, L., "Prediction of Coverage for Trans-Horizon HF Radar Systems," IRE Trans. MIL-5(No. 2):164-172 (Apr. 1961)

32. Beckmann, P., and Spizzichino, A., "The Scattering of Electromagnetic Waves from Rough Surfaces," Pergamon, New York, 1963

33. Burrows, C.R., chairman, and Attwood, S.S., editor, "Radio Wave Propagation; Consolidated Summary Technical Report of the Committee on Propagation of the National Defense Research Committee," Academic Press, New York, 1949

34. Ament, W.S., "Toward a Theory of Reflection by a Rough Surface," Proc. IRE 41 (No. 1):142-146 (Jan. 1953)

35. Beard, C.I., Katz, I., and Spetner, L.M., "Phenomenological Vector Model of Microwave Reflection from the Ocean," IRE Trans. AP-4(No. 2):162-167 (Apr. 1956); and Beard, C.I., "Coherent and Incoherent Scattering of Microwaves from the Ocean," IRE Trans. AP-9(No. 5):470-483 (Sept. 1961)

36. Blake, L.V., "Reflection of Radio Waves from a Rough Sea," Proc. IRE 38(No. 3): 301-304 (Mar. 1950)

37. Schelleng, J.C., Burrows, C.R., and Ferrell, E.B., "Ultra-Short-Wave Propagation," Proc. IRE 21(No. 3):427-463 (Mar. 1933)

38. Bauer, J.R., Mason, W.C., and Wilson, F.A., "Radio Refraction in a Cool Exponential Atmosphere," MIT Lincoln Laboratory Report 186, Aug. 1958

39. Bean, B.R., and Thayer, G.D., "Models of the Atmospheric Radio Refractive Index," Proc. IRE 47(No. 5):740-755 (May 1959); also "CRPL Exponential Reference Atmosphere," National Bureau of Standards Monograph 4, U.S. Government Printing Office, Washington, D.C., Oct. 1959

40. Bean, B.R., and Dutton, E.J., "Radio Meteorology," National Bureau of Standards Monograph 92, U.S. Government Printing Office, Washington, D.C., 1966

41. Blake, L.V., "Ray Height Computation for a Continuous Nonlinear Atmospheric Refractive-Index Profile," Radio Science 3(new series)(No. 1):85-92 (Jan. 1968)

42. Blake, L.V., "Radio Ray (Radar) Range-Height-Angle Charts," NRL Report 6650, Jan. 22, 1968; and Microwave J. 11(No. 10):49-53 (Oct. 1968)

43. Millman, G.H., "Atmospheric Effects on VHF and UHF Propagation," Proc. IRE 46 (No. 8):1492-1501 (Aug. 1958)

44. Blake, L.V., "The Effective Number of Pulses per Beamwidth for a Scanning Radar," Proc. IRE 41(No. 6):770-774 (June 1953); and "Addendum," Proc. IRE 41(No. 12): 1785 (Dec. 1953)

45. Hall, W.M., and Barton, D.K., "Antenna Pattern Loss Factor for Scanning Radars," Proc. IEEE (Correspondence) 53(No. 9):1257-1258 (Sept. 1965)

46. Bean, B.R., and Abbott, R., "Oxygen and Water Vapor Absorption of Radio Waves in the Atmosphere," Geofisica Pura E Applicata (Milano) 37:127-144 (1957)

47. Hogg, D.C., "Effective Antenna Temperatures Due to Oxygen and Water Vapor in the Atmosphere," J. Appl. Phys. 30:1417-1419 (Sept. 1959)

48. Blake, L.V., "Tropospheric Absorption Loss and Noise Temperature in the Frequency Range 100-10,000 Mc," Trans. IRE AP-10(No. 1):101-102 (Jan. 1962) (summarizes NRL Report 5601, "Curves of Atmospheric-Absorption Loss for Use in Radar Range Calculation," Mar. 1961; originally presented at URSI-IRE meeting at Washington, D.C., May 6, 1959)

49. Meeks, M.L., and Lilley, A.E., "The Microwave Spectrum of Oxygen in the Earth's Atmosphere," J. Geophys. Res. 68(No. 6):1683-1703 (Mar. 15, 1963)

50. Minzner, R.A., Ripley, W.S., and Condron, T.P., "U.S. Extension to the ICAO Standard Atmosphere," U.S. Dept. of Commerce Weather Bureau and USAF ARDC Cambridge Research Center, Geophysics Research Directorate, U.S. Government Printing Office, Washington, D.C., 1958

51. Van Vleck, J.H., "The Absorption of Microwaves by Oxygen," and "The Absorption of Microwaves by Uncondensed Water Vapor," Phys. Rev. 71(No. 7):413-424, 425-433 (Apr. 1, 1947)

52. Barton, D.K., "Radar Systems Analysis," Prentice-Hall, Englewood Cliffs, N.J., 1964

53. Payne-Scott, R., "The Visibility of Small Echoes on Radar PPI Displays," Proc. IRE 36(No. 2):180-196, Feb. 1948

54. Mallett, J.D., and Brennan, L.E., "Cumulative Probability of Detection for Targets Approaching a Uniformly Scanning Search Radar," Proc. IRE 51(No. 4):596-601 (Apr. 1963)

Appendix

The following figures from the text of the report are collected here for ready reference in connection with the range-calculation work sheet. At the end of this appendix is a copy of the work sheet on a page with perforation for easy removal. This sheet may be used as a master for making copies of the form.

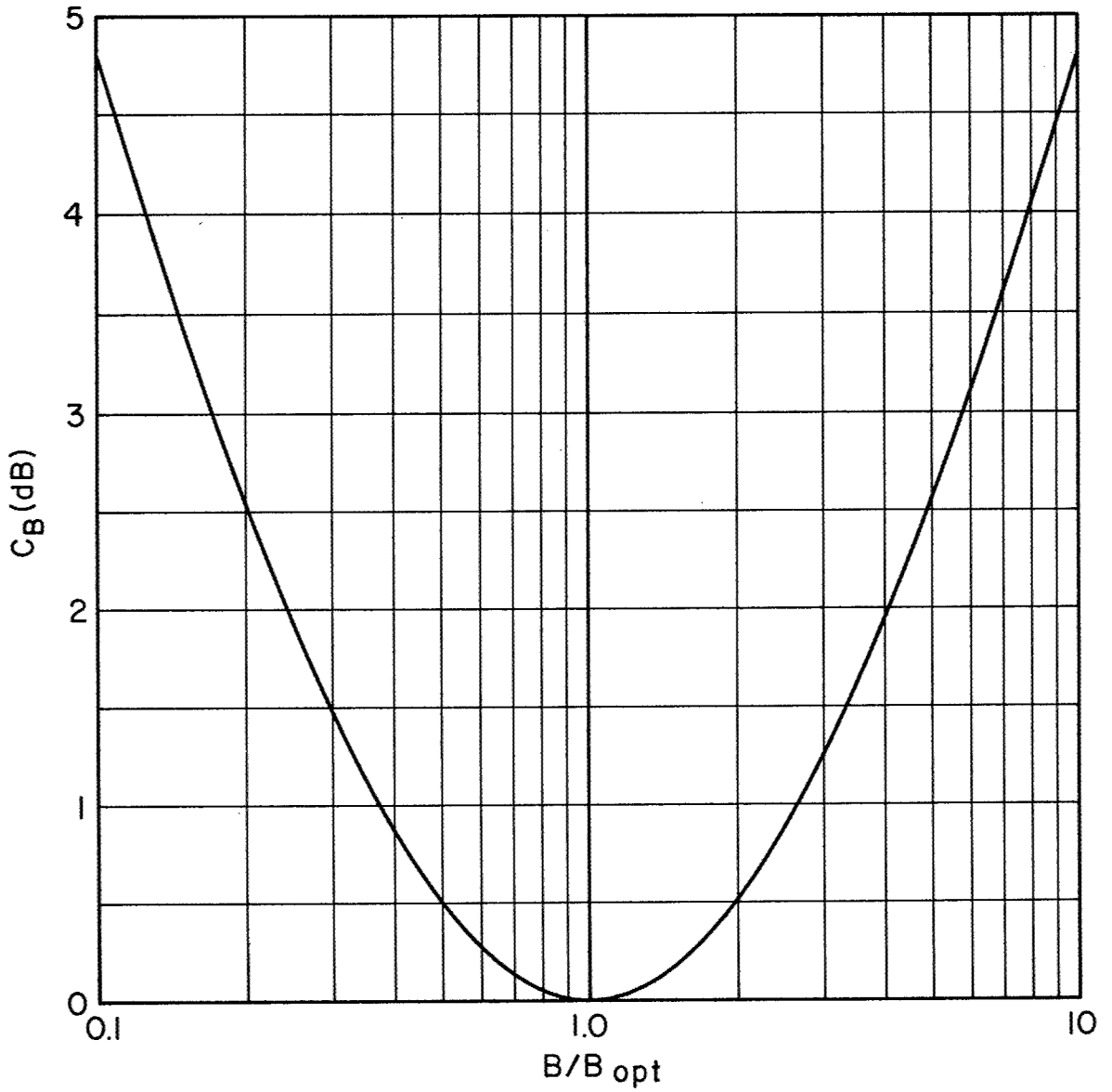

Fig. 1 - Bandwidth correction factor C_B plotted as a function of the ratio of bandwidth B to optimum bandwidth B_{opt} using Haeff's (20) empirical formula (Eq. (17))

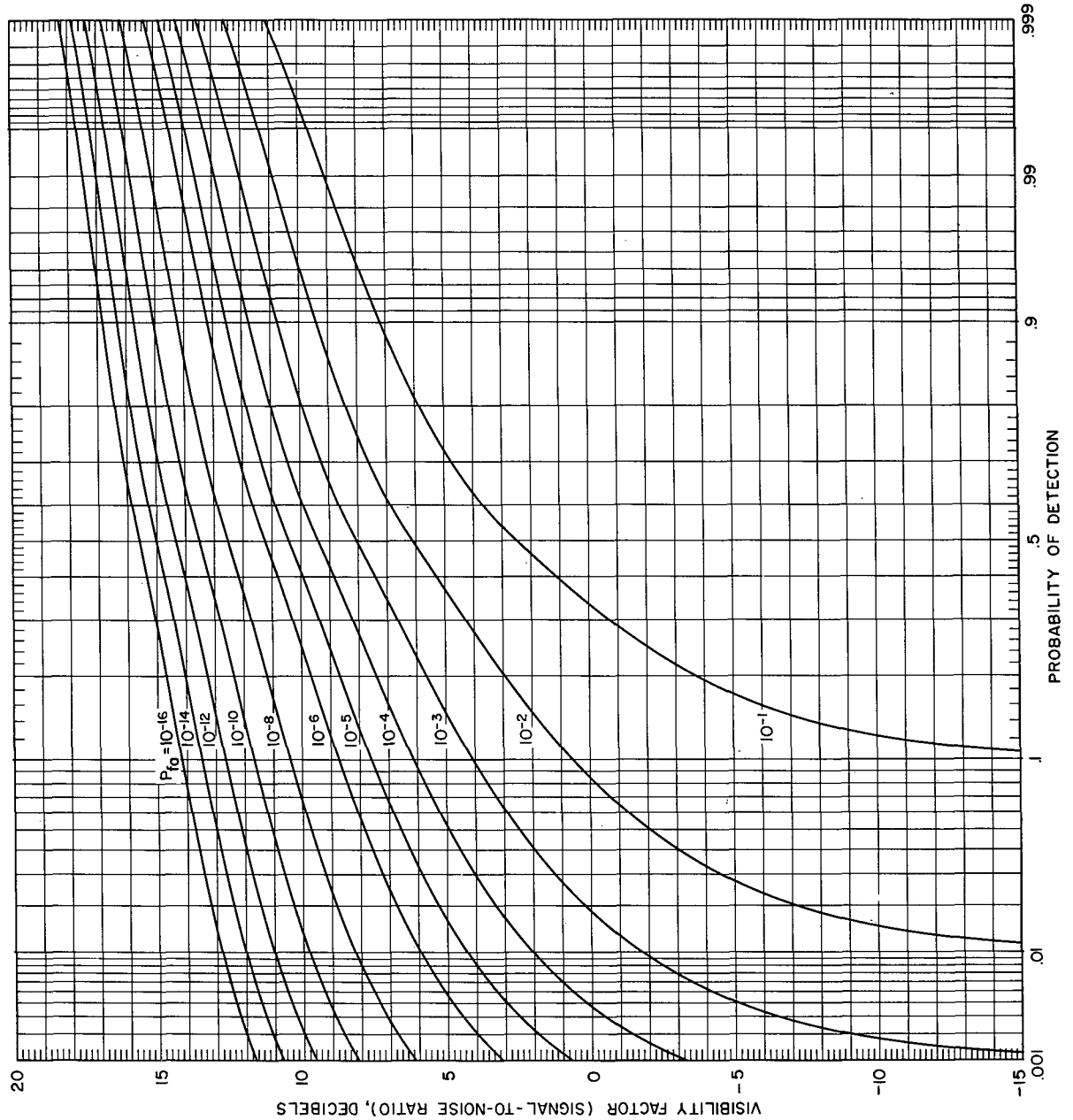

Fig. 4 - Required signal-to-noise (visibility factor) at the input terminals of a linear-rectifier detector as a function of probability of detection for a single pulse, with the false-alarm probability (P_{fa}) as a parameter, calculated for a nonfluctuating signal

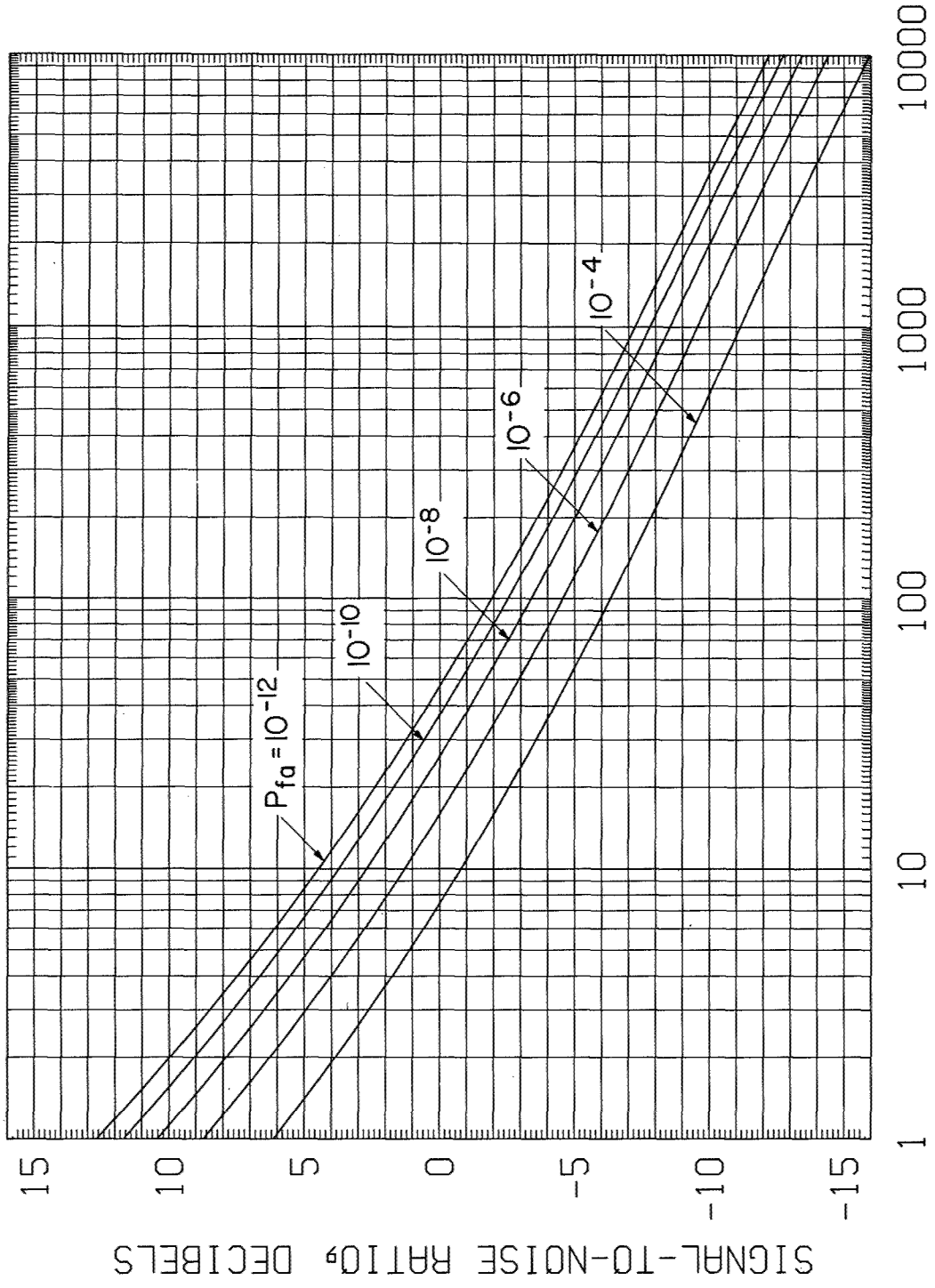

Fig. 5a - Required signal-to-noise ratio (visibility factor) for a linear detector as a function of number of pulses integrated, for 0.1 probability of detection, calculated for a nonfluctuating signal for five values of false-alarm probability (P_{fa})

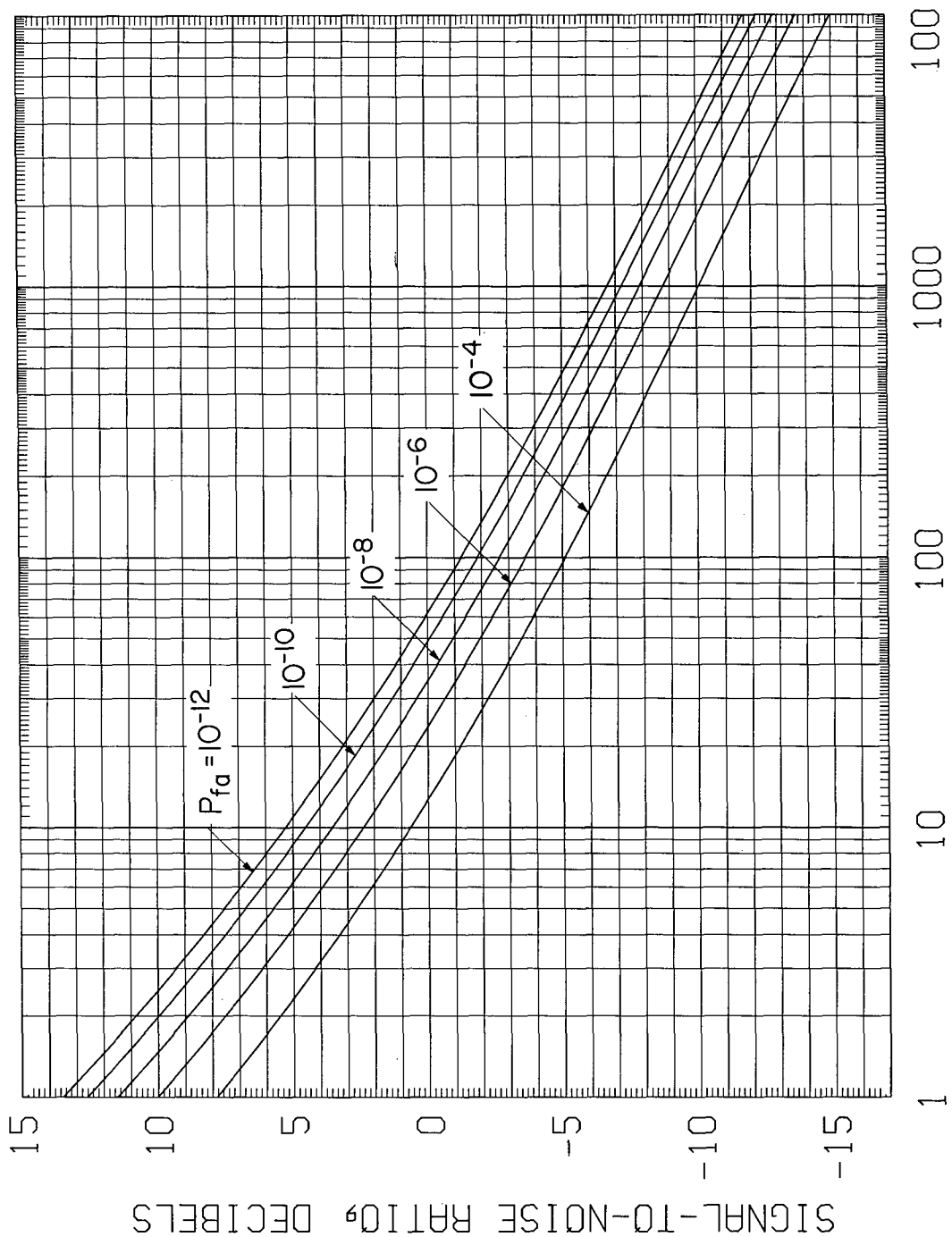

Fig. 5b – Required signal-to-noise ratio (visibility factor) for a linear detector as a function of number of pulses integrated, for 0.25 probability of detection, calculated for a nonfluctuating signal for five values of false-alarm probability (P_{fa})

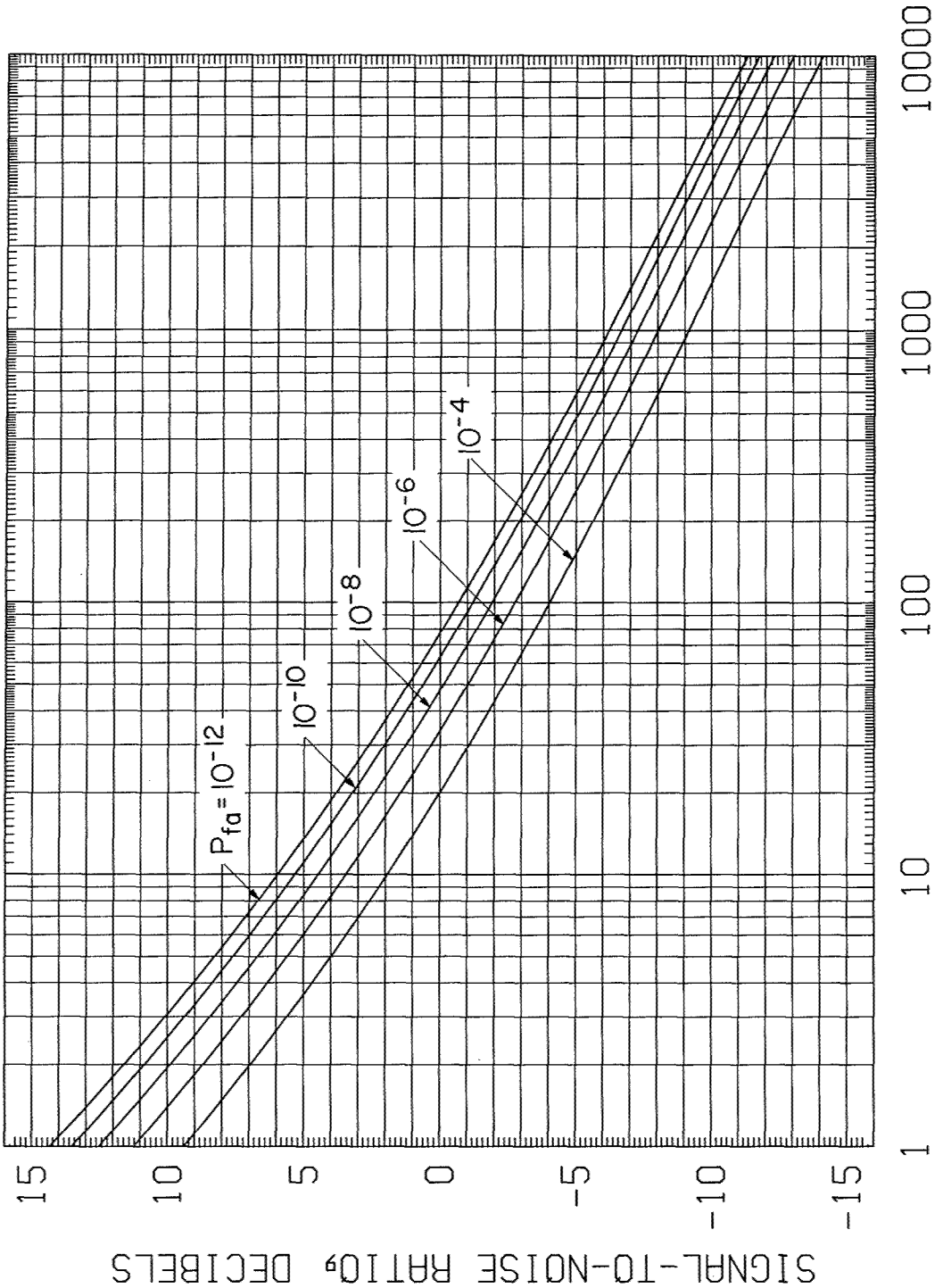

Fig. 5c - Required signal-to-noise ratio (visibility factor) for a linear detector as a function of number of pulses integrated, for 0.5 probability of detection, calculated for a nonfluctuating signal for five values of false-alarm probability (P_{fa})

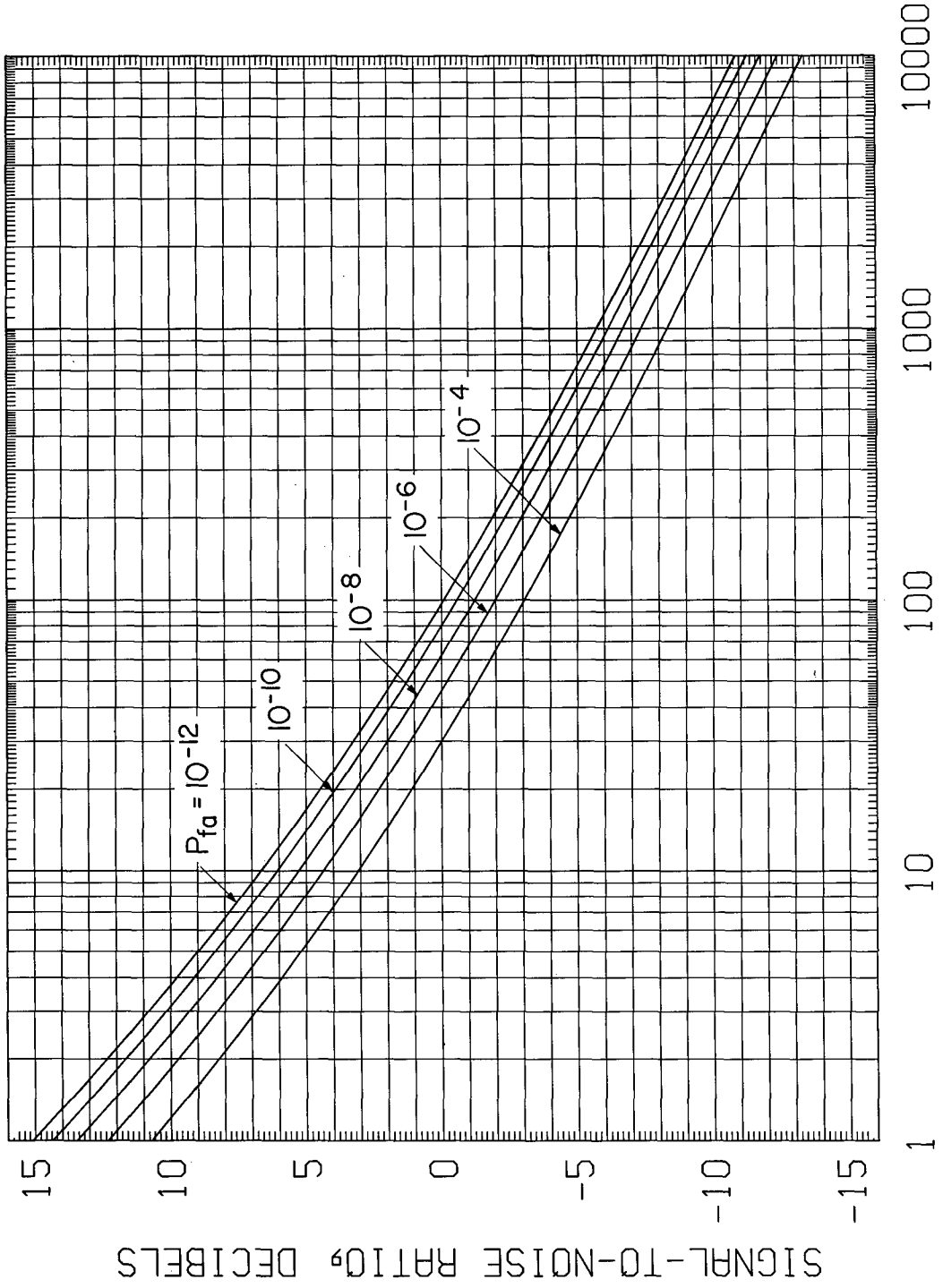

Fig. 5d - Required signal-to-noise ratio (visibility factor) for a linear detector as a function of number of pulses integrated, for 0.75 probability of detection, calculated for a nonfluctuating signal for five values of false-alarm probability (P_{fa})

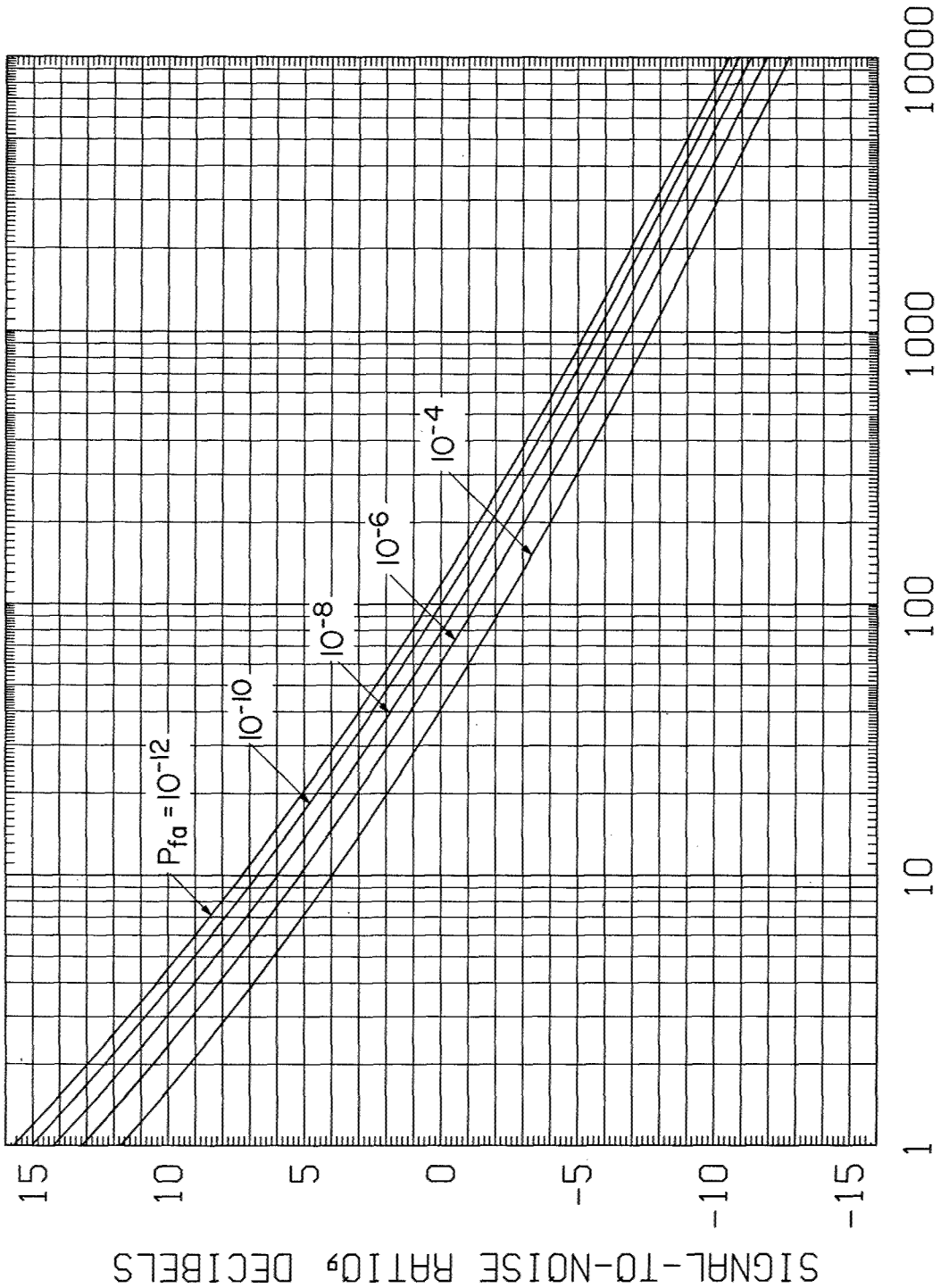

Fig. 5e - Required signal-to-noise ratio (visibility factor) for a linear detector as a function of number of pulses integrated, for 0.90 probability of detection, calculated for a nonfluctuating signal for five values of false-alarm probability (P_{fa})

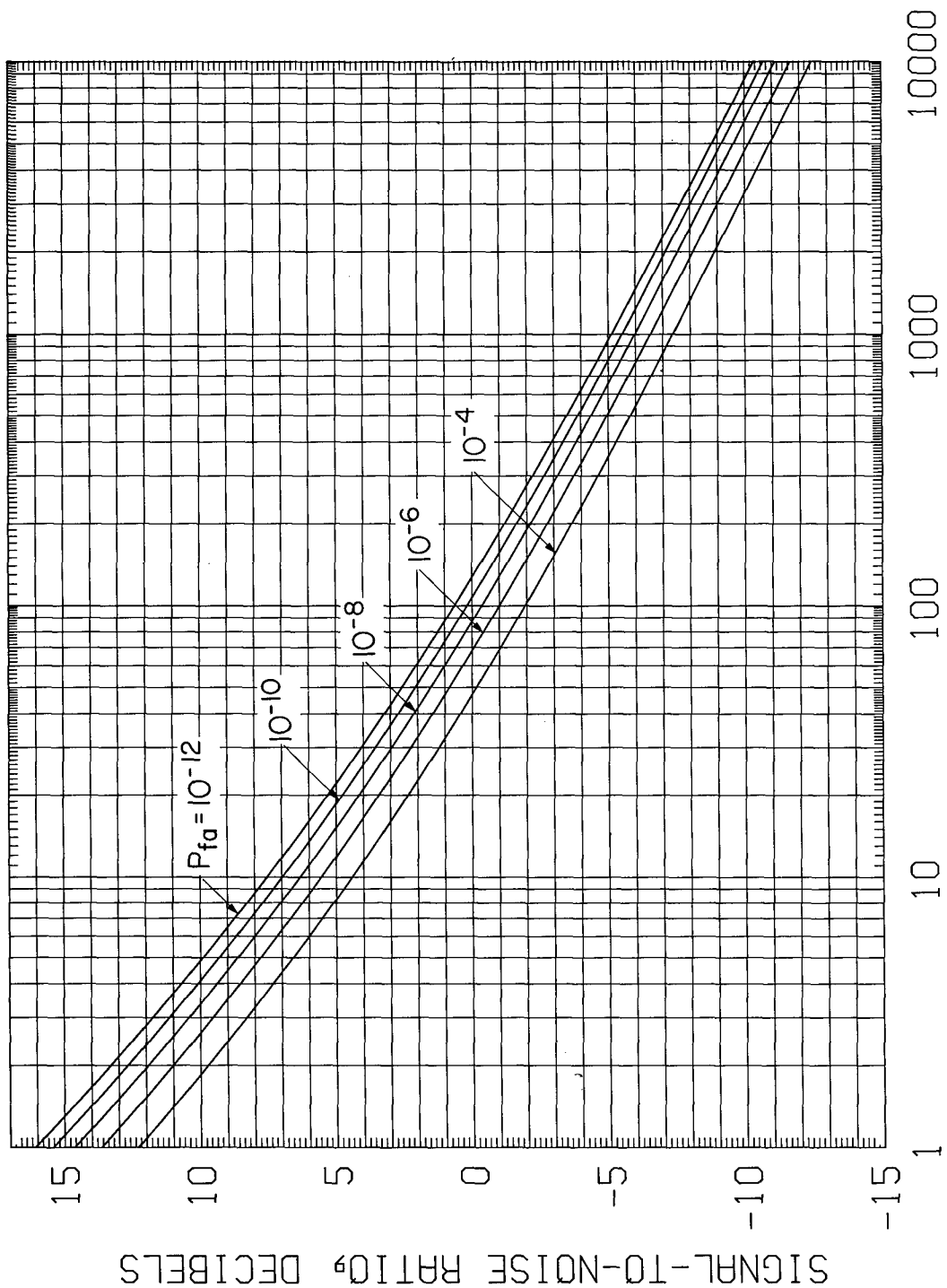

Fig. 5f – Required signal-to-noise ratio (visibility factor) for a linear detector as a function of number of pulses integrated, for 0.95 probability of detection, calculated for a nonfluctuating signal for five values of false-alarm probability (P_{fa})

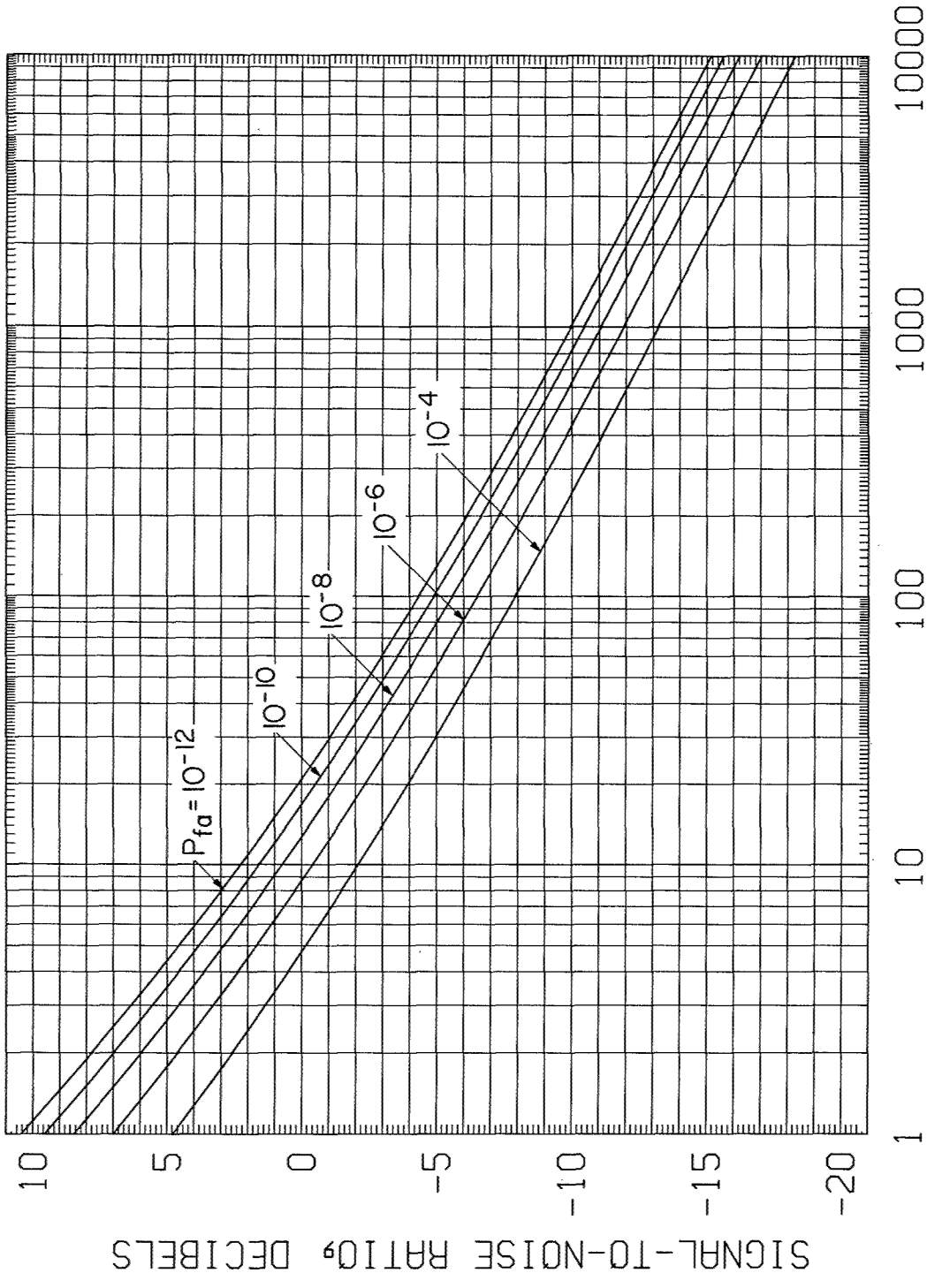

Fig. 6a - Required signal-to-noise ratio (visibility factor) for a square-law detector as a function of number of pulses integrated, for 0.1 probability of detection, calculated for Swerling Case 1 fluctuation for five values of false-alarm probability

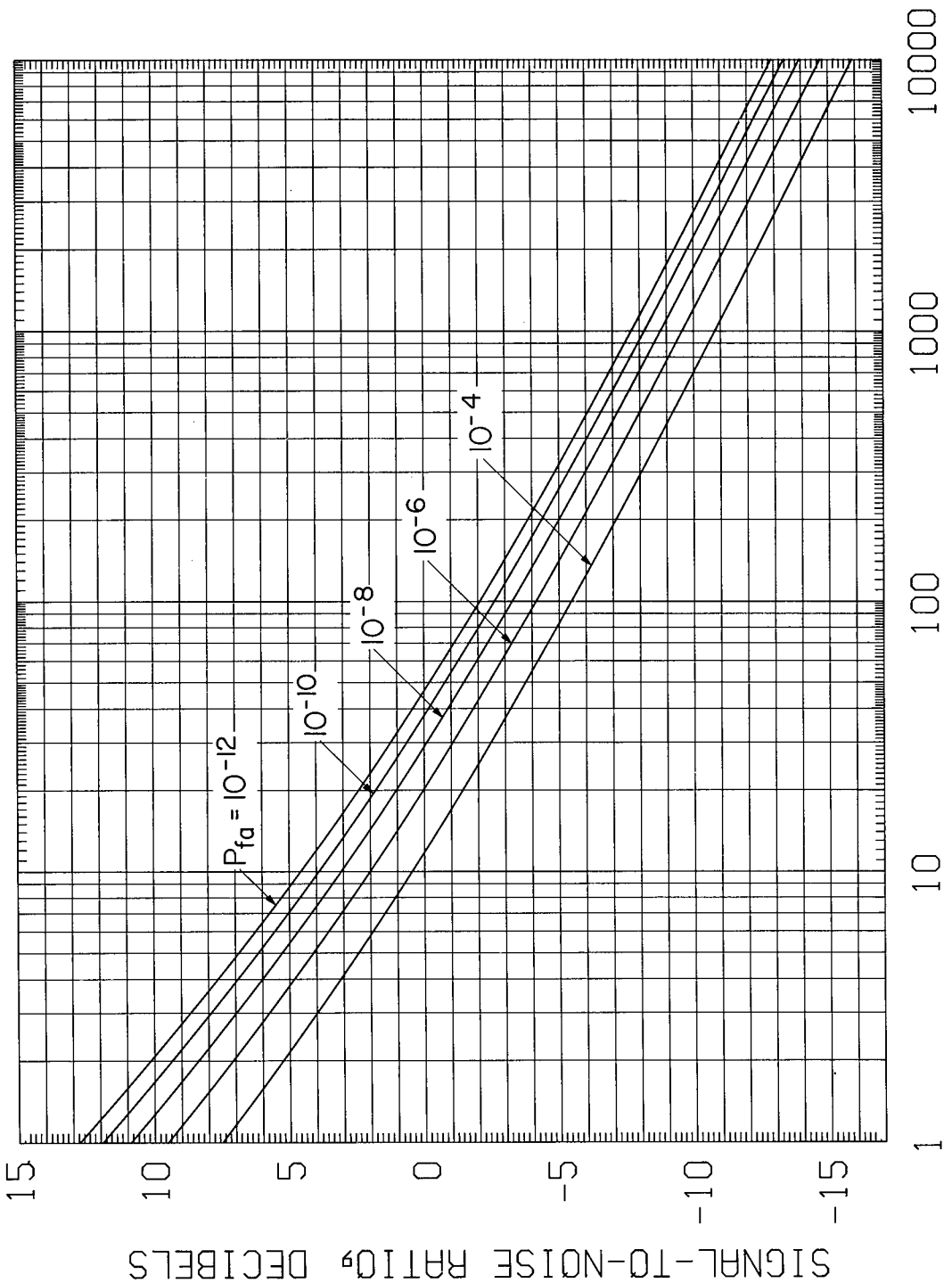

Fig. 6b - Required signal-to-noise ratio (visibility factor) for a square-law detector as a function of number of pulses integrated, for 0.25 probability of detection, calculated for Swerling Case 1 fluctuation for five values of false-alarm probability

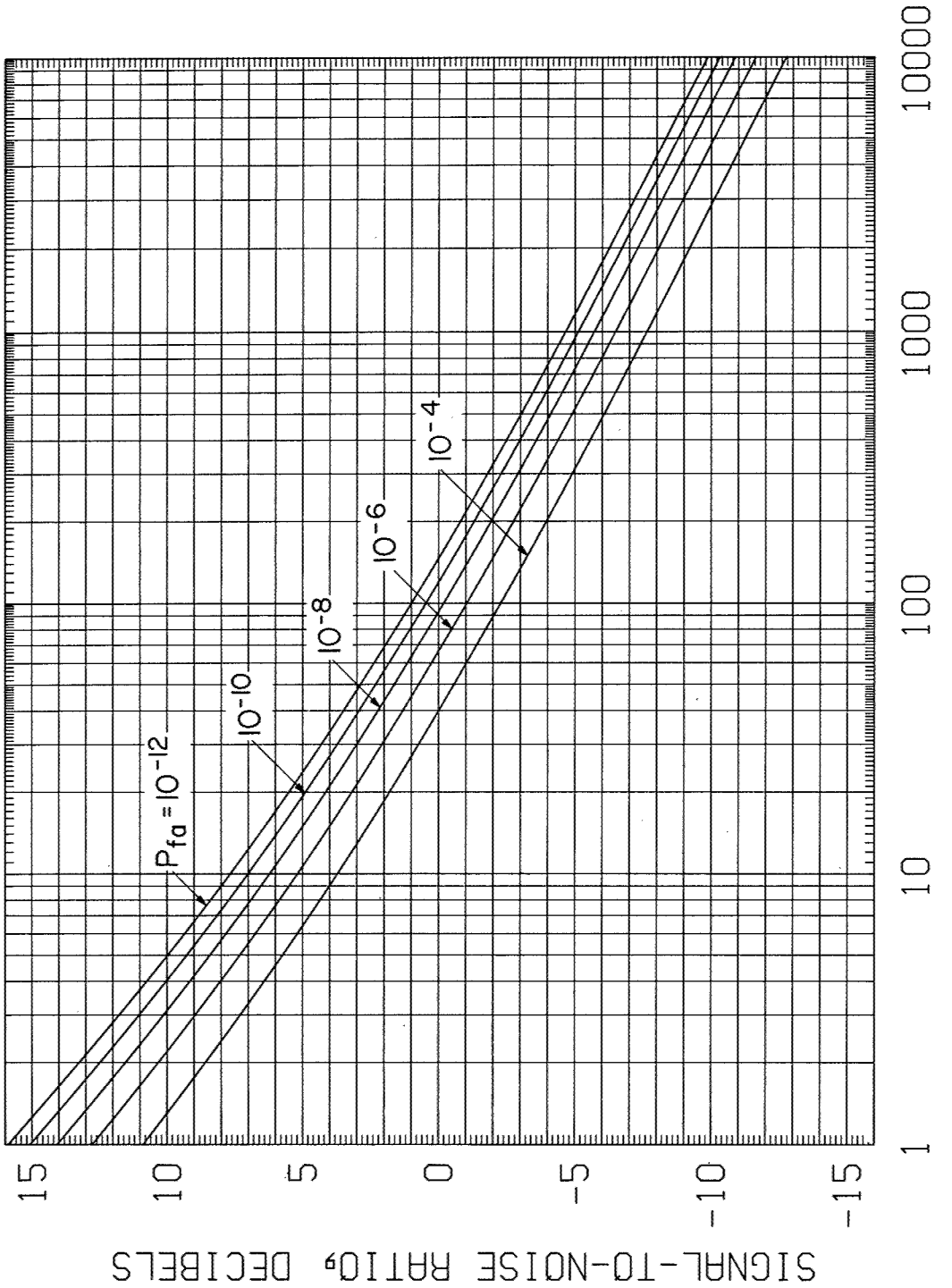

Fig. 6c - Required signal-to-noise ratio (visibility factor) for a square-law detector as a function of number of pulses integrated, for 0.50 probability of detection, calculated for Swerling Case 1 fluctuation for five values of false-alarm probability

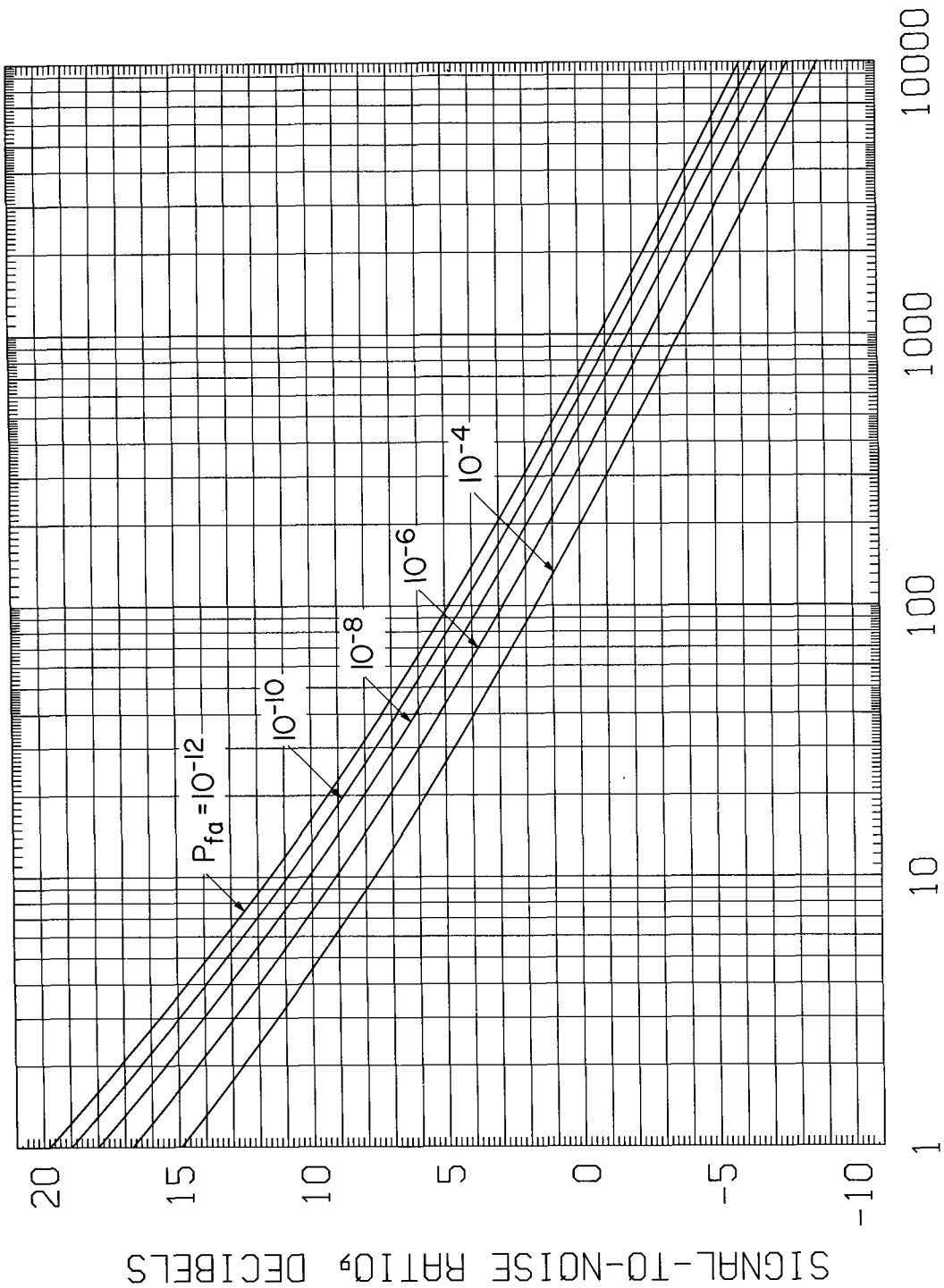

Fig. 6d – Required signal-to-noise ratio (visibility factor) for a square-law detector as a function of number of pulses integrated, for 0.75 probability of detection, calculated for Swerling Case 1 fluctuation for five values of false-alarm probability

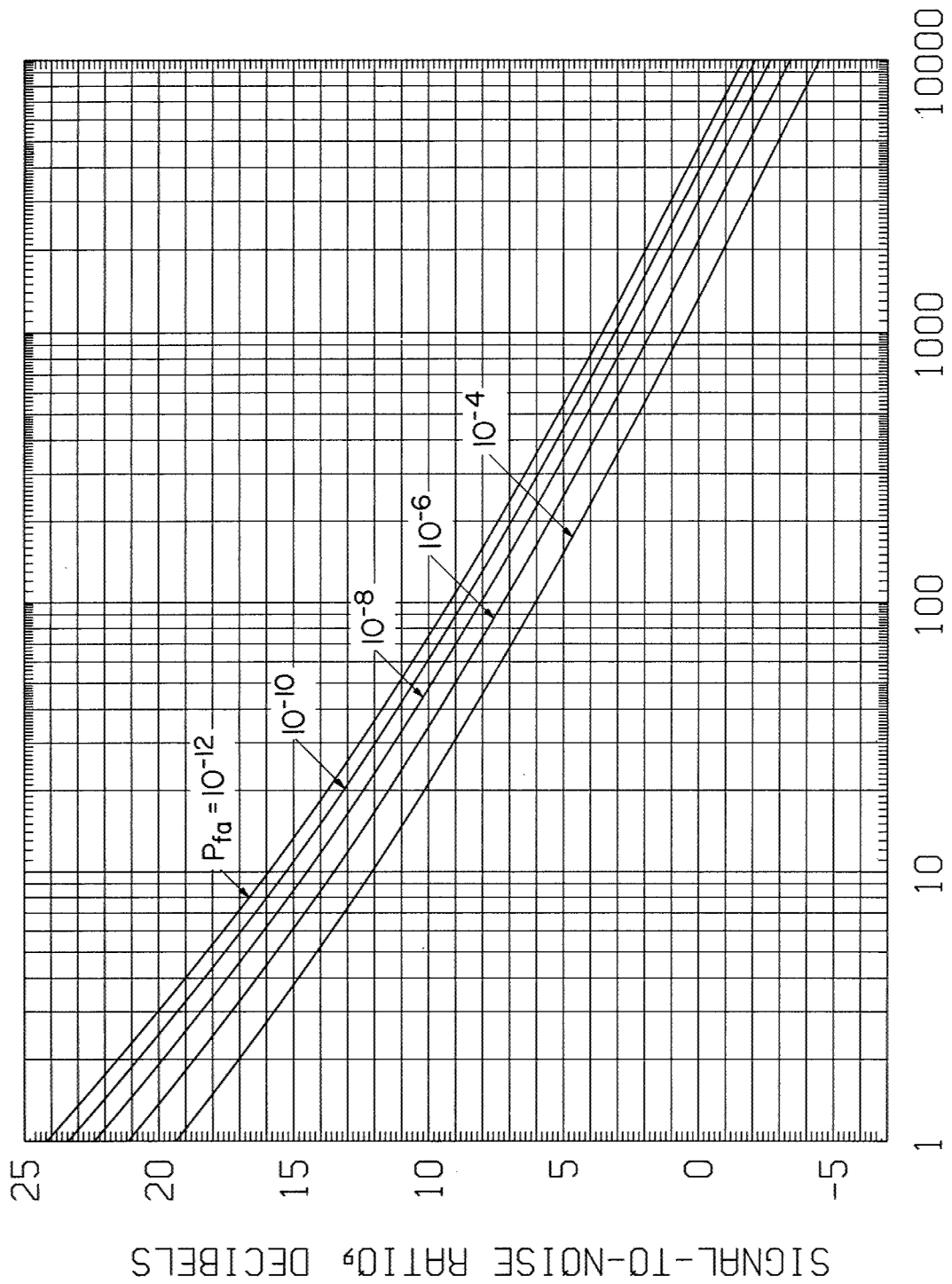

Fig. 6e - Required signal-to-noise ratio (visibility factor) for a square-law detector as a function of number of pulses integrated, for 0.90 probability of detection, calculated for Swerling Case 1 fluctuation for five values of false-alarm probability

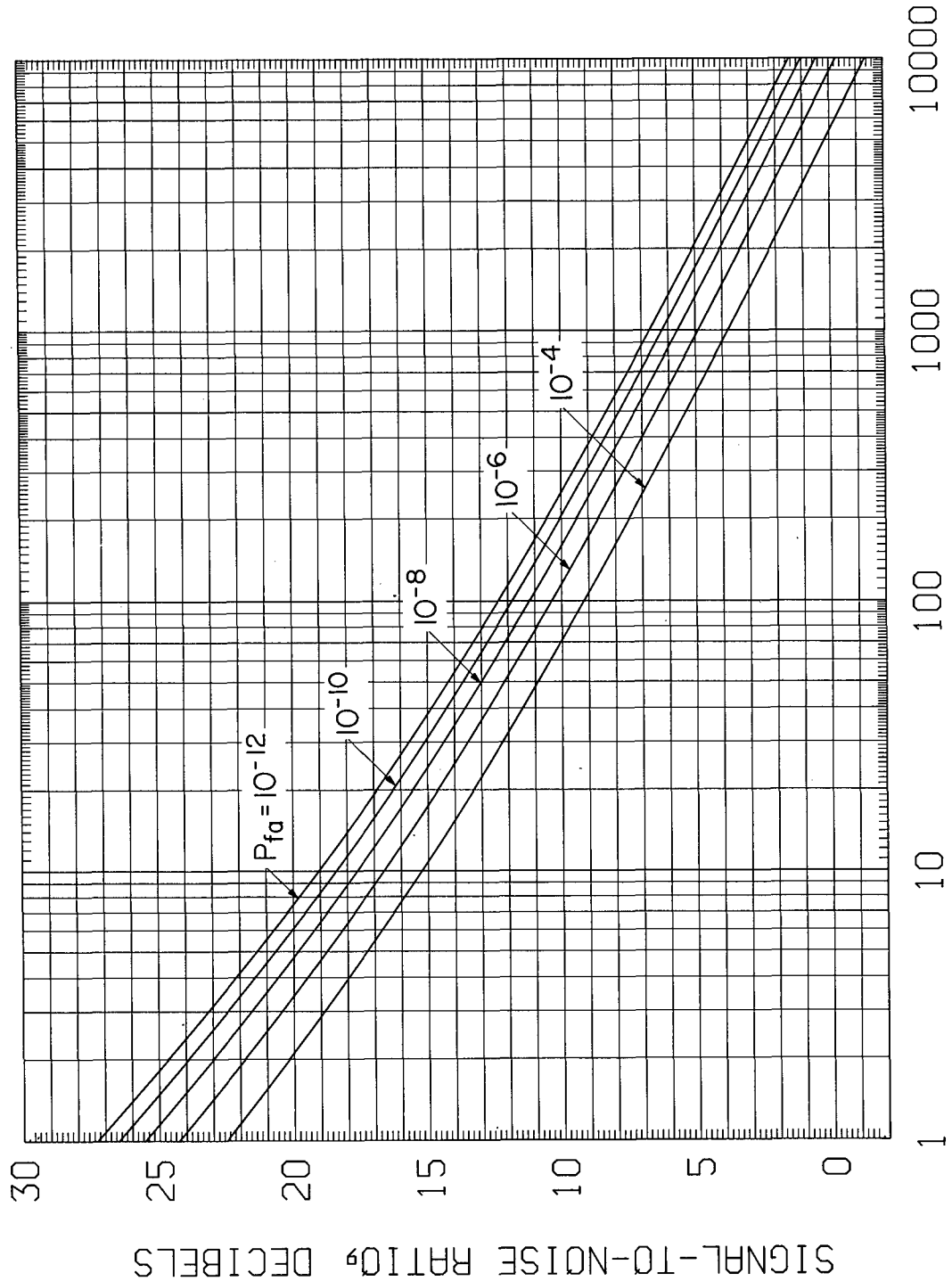

Fig. 6f - Required signal-to-noise ratio (visibility factor) for a square-law detector as a function of number of pulses integrated, for 0.95 probability of detection, calculated for Swerling Case 1 fluctuation for five values of false-alarm probability

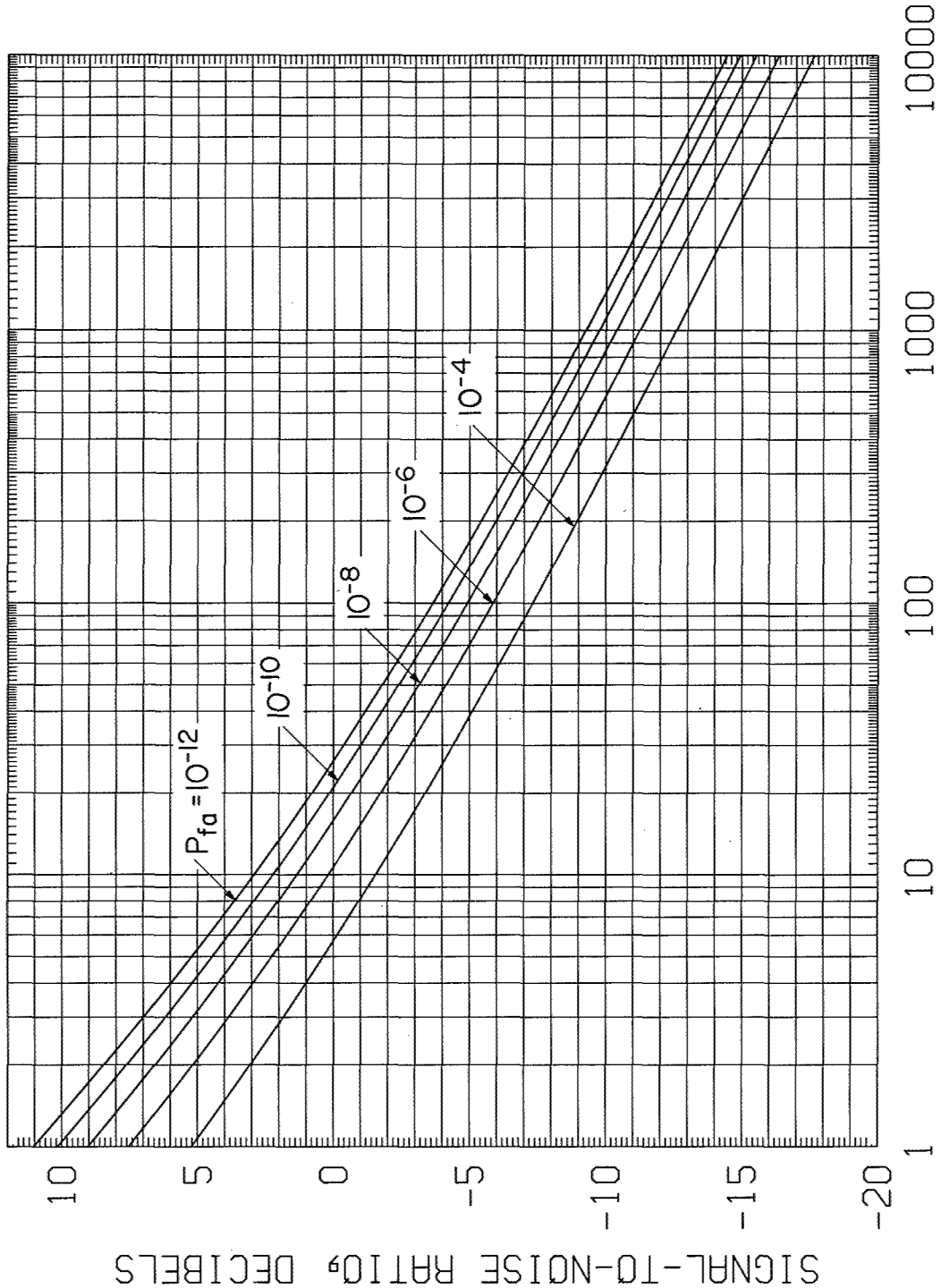

Fig. 7a - Required signal-to-noise ratio (visibility factor) for a square-law detector as a function of number of pulses integrated, for 0.10 probability of detection, calculated for Swerling Case 3 fluctuation for five values of false-alarm probability

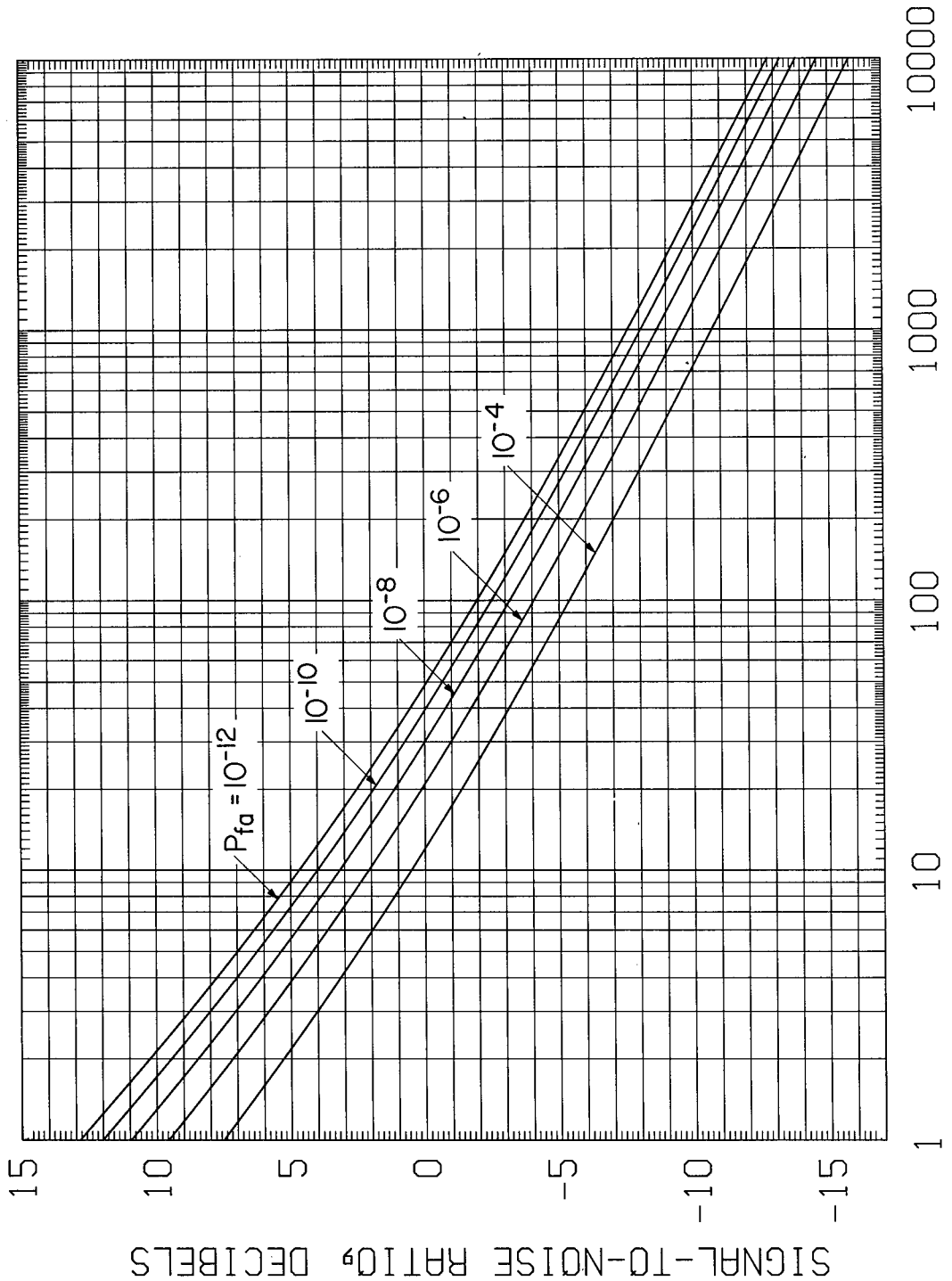

Fig. 7b - Required signal-to-noise ratio (visibility factor) for a square-law detector as a function of number of pulses integrated, for 0.25 probability of detection, calculated for Swerling Case 3 fluctuation for five values of false-alarm probability

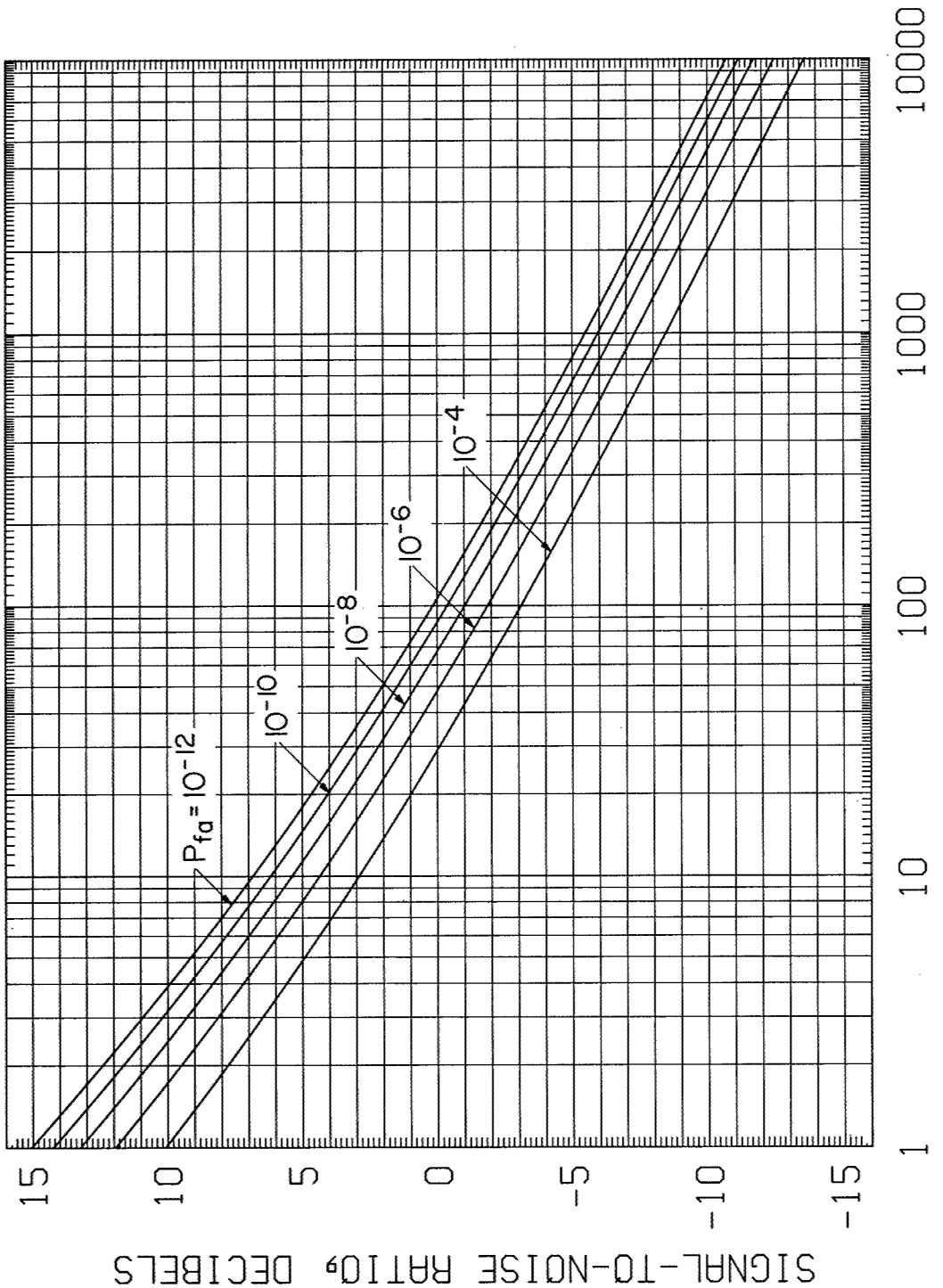

Fig. 7c - Required signal-to-noise ratio (visibility factor) for a square-law detector as a function of number of pulses integrated, for 0.50 probability of detection, calculated for Swerling Case 3 fluctuation for five values of false-alarm probability

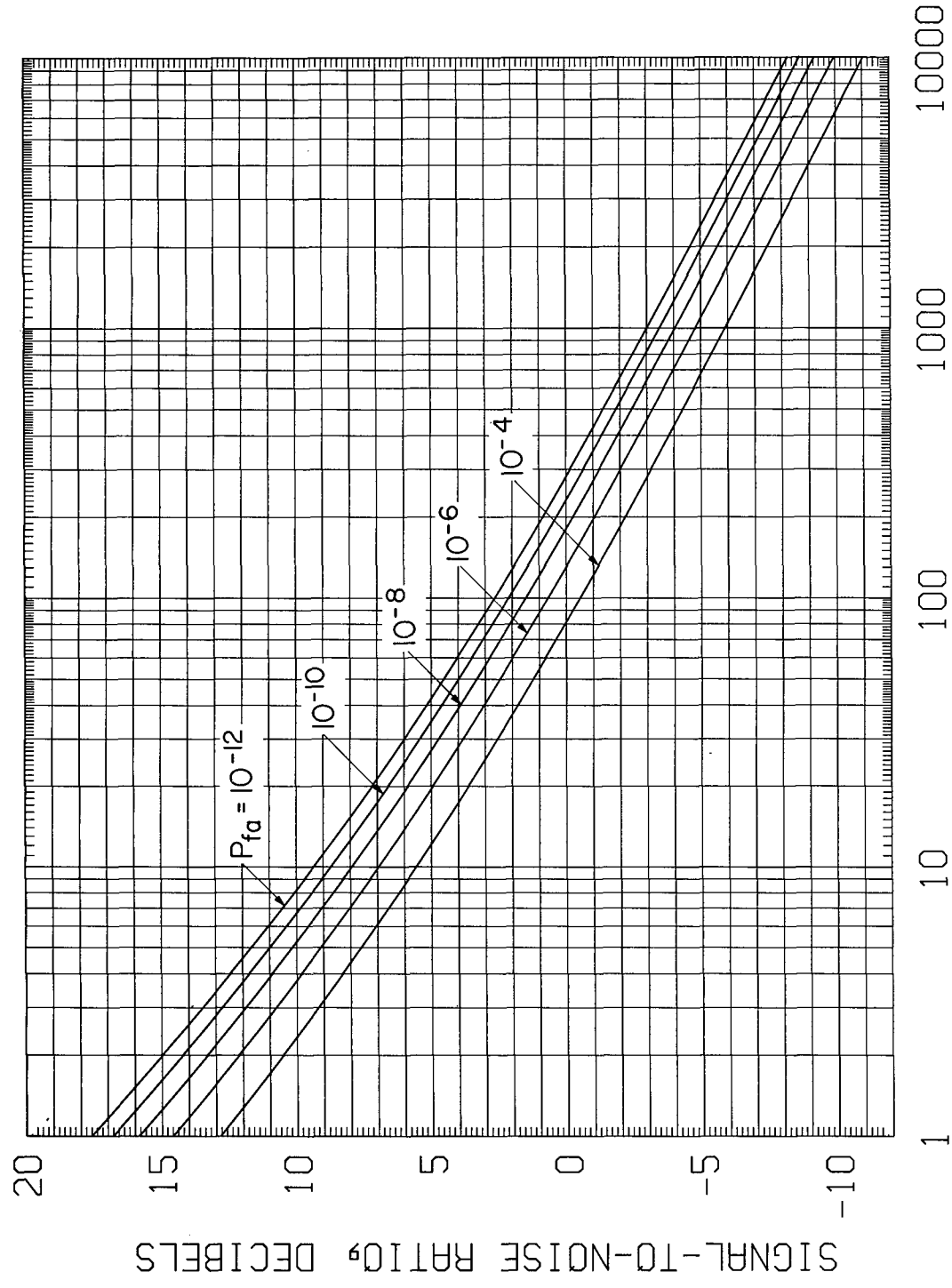

Fig. 7d - Required signal-to-noise ratio (visibility factor) for a square-law detector as a function of number of pulses integrated, for 0.75 probability of detection, calculated for Swerling Case 3 fluctuation for five values of false-alarm probability

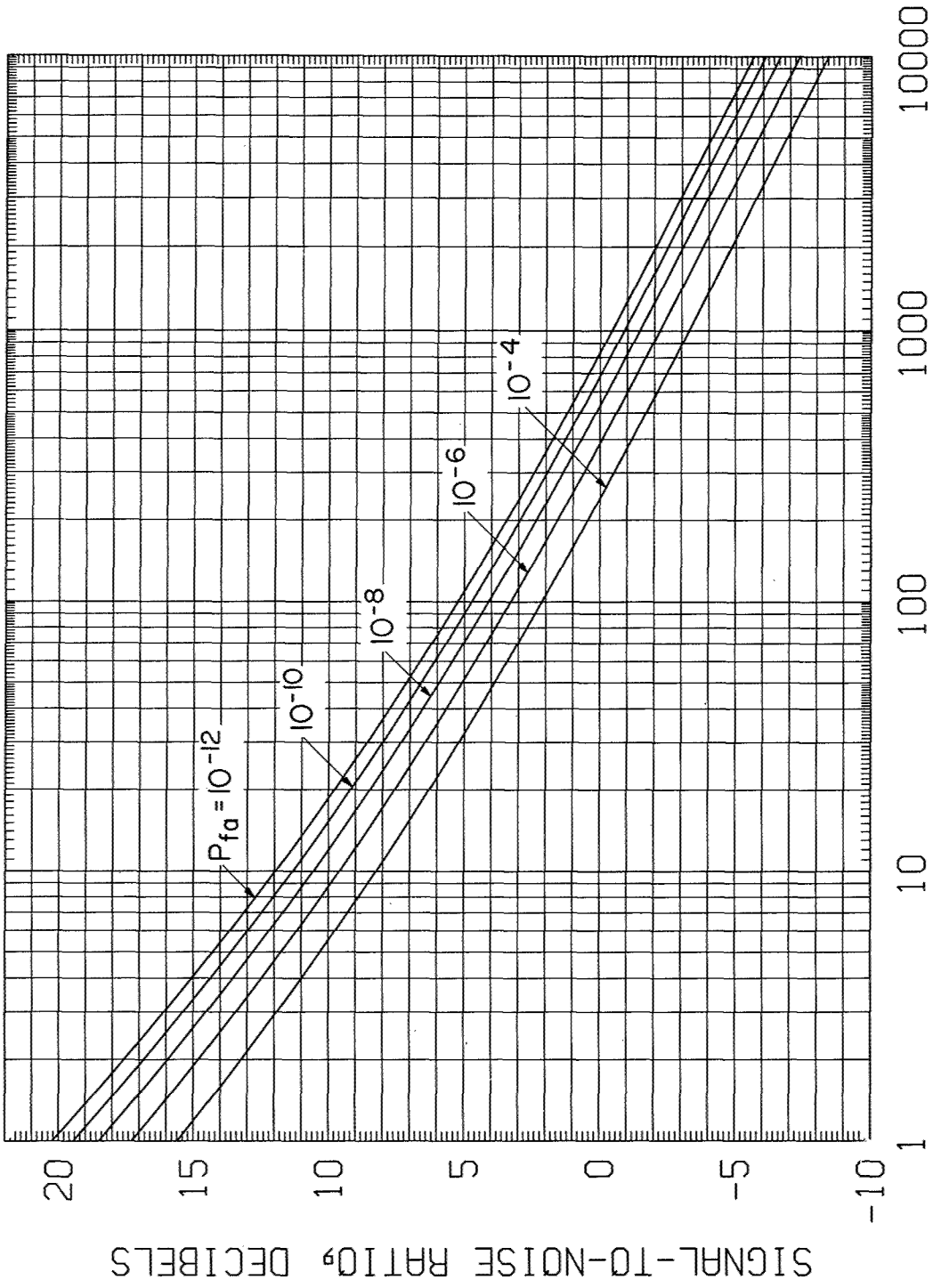

Fig. 7e - Required signal-to-noise ratio (visibility factor) for a square-law detector as a function of number of pulses integrated, for 0.90 probability of detection, calculated for Swerling Case 3 fluctuation for five values of false-alarm probability

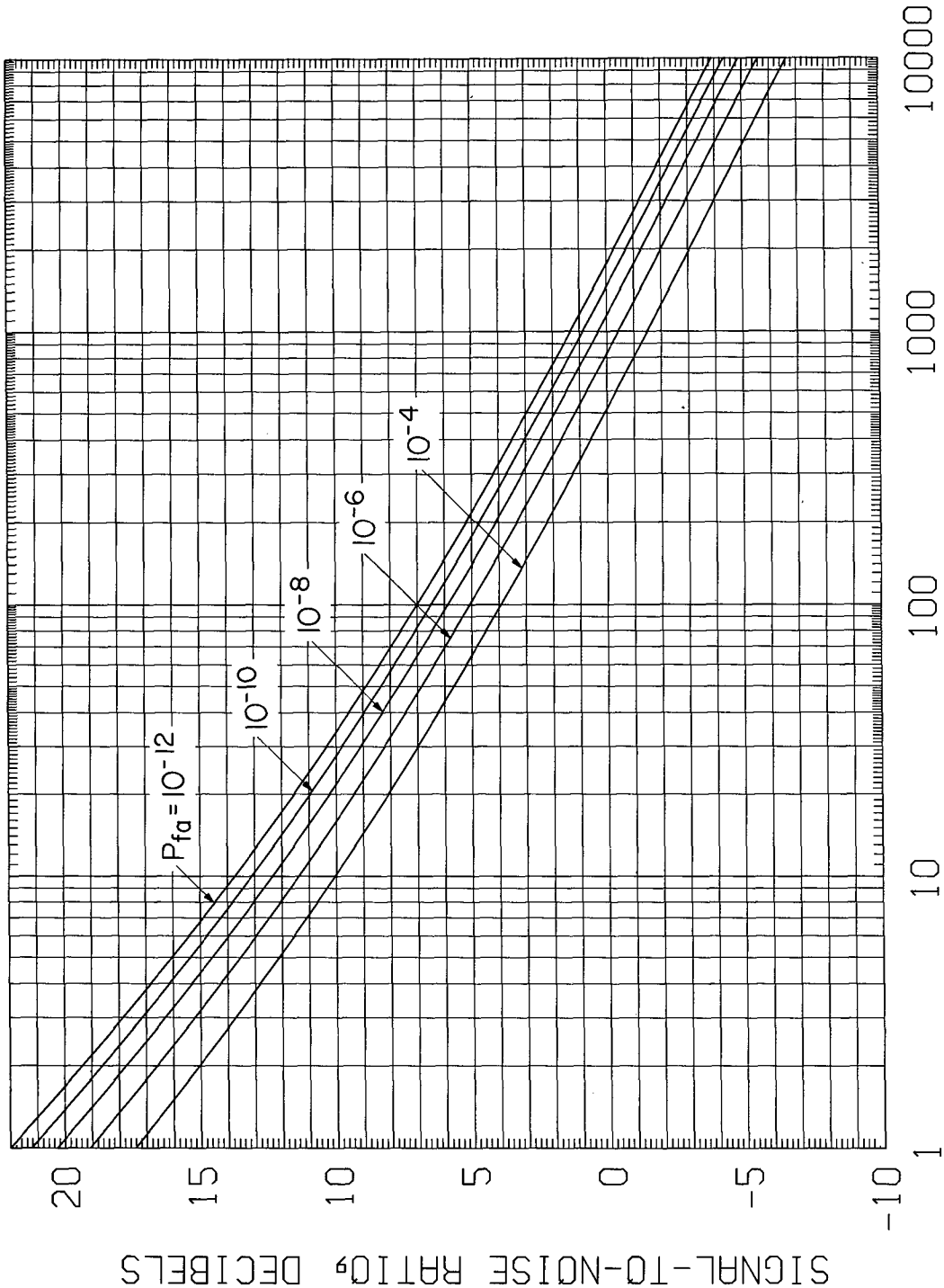

Fig. 7f - Required signal-to-noise ratio (visibility factor) for a square-law detector as a function of number of pulses integrated, for 0.95 probability of detection, calculated for Swerling Case 3 fluctuation for five values of false-alarm probability

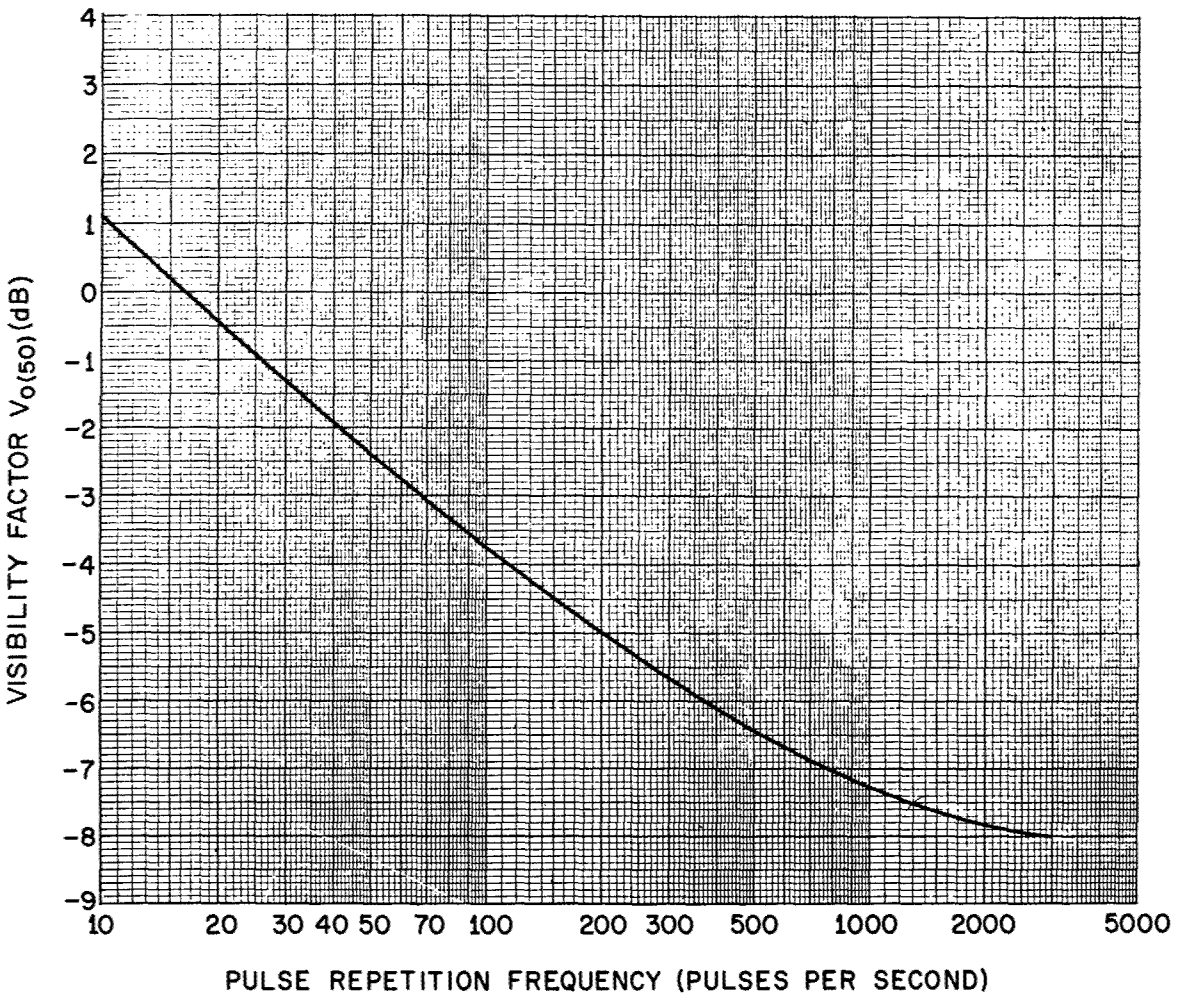

Fig. 8 - Visibility factor as a function of pulse repetition frequency for A-scope visual detection of signals by a human observer (from Ref. 15, Fig. 8.23) replotted to apply for 0.5 probability of detection (in accordance with Fig. 8.2 of Ref. 15), based on World War II experiments conducted at the MIT Radiation Laboratory

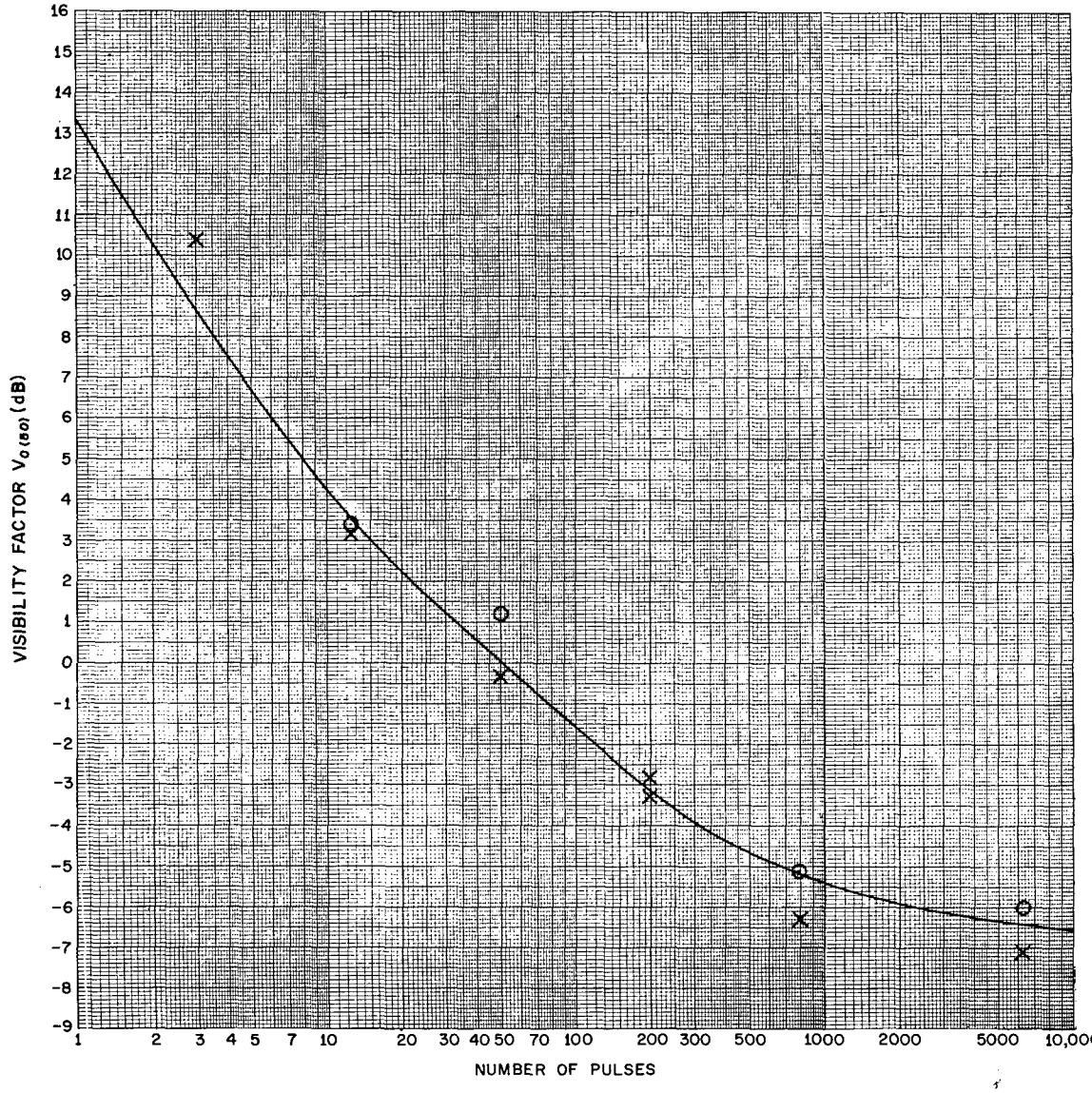

Fig. 9 - Visibility factor as a function of pulses in a half-power beamwidth interval on a PPI display (visual detection by human observer), replotted from experimental results at the MIT Radiation Laboratory during World War II, modified to apply for 0.5 probability of detection

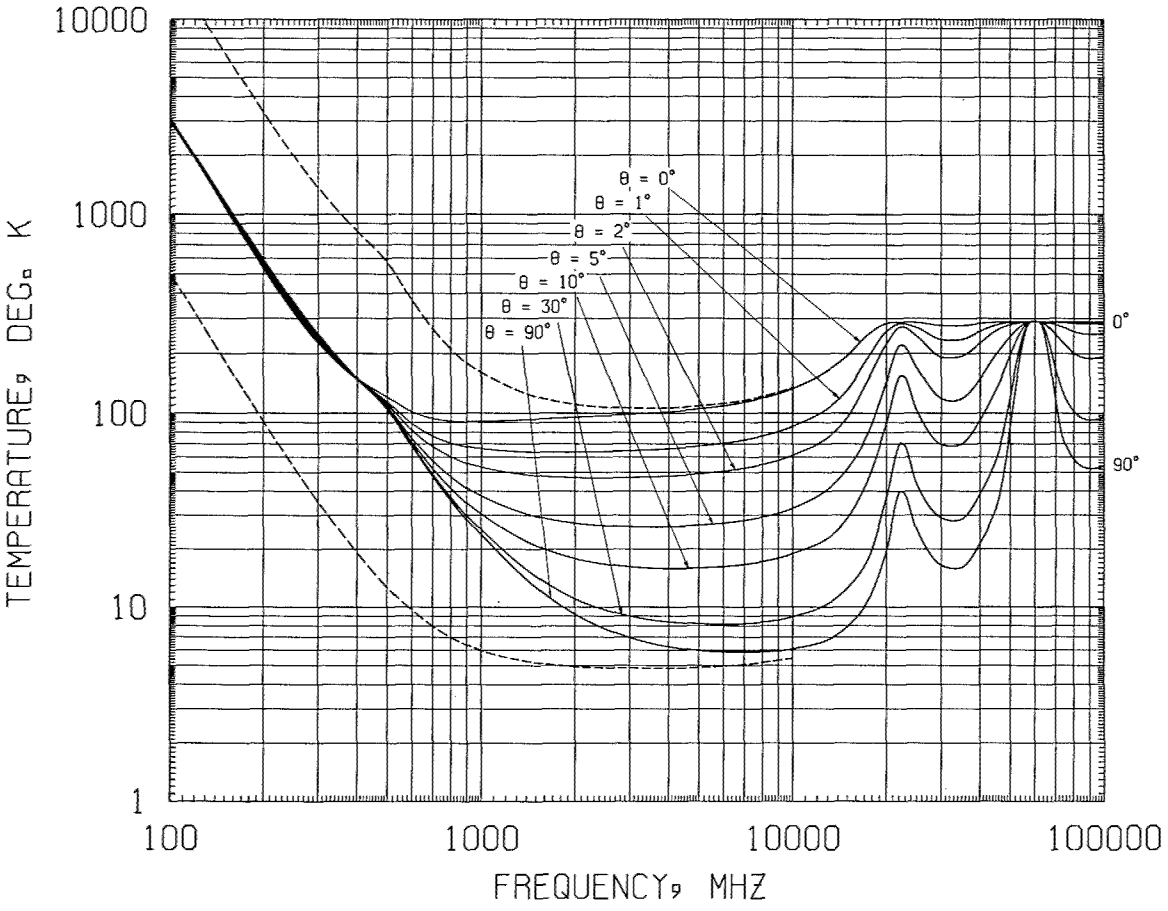

Fig. 11 - Noise temperature of an idealized antenna (lossless, no earth-directed side lobes) at the earth's surface as a function of frequency for a number of beam elevation angles. The solid curves are for the geometric-mean galactic temperature, sun noise 10 times the quiet level, the sun in a unity-gain side lobe, a cool temperate-zone troposphere, 3°K cosmic blackbody radiation, and zero ground noise. The upper dashed curve is for maximum galactic noise (center of galaxy, narrow-beam antenna), sun noise 100 times the quiet level, zero elevation angle, and other factors the same as for the solid curves. The lower dashed curve is for minimum galactic noise, zero sun noise, and a 90-degree elevation angle. The slight bump in the curves at about 500 MHz is due to the sun noise characteristic. The curves for low elevation angles lie below those for high angles at frequencies below 400 MHz because of the reduction of galactic noise by atmospheric absorption. The maxima at 22.2 GHz and 60 GHz are due to water-vapor and oxygen absorption resonances.

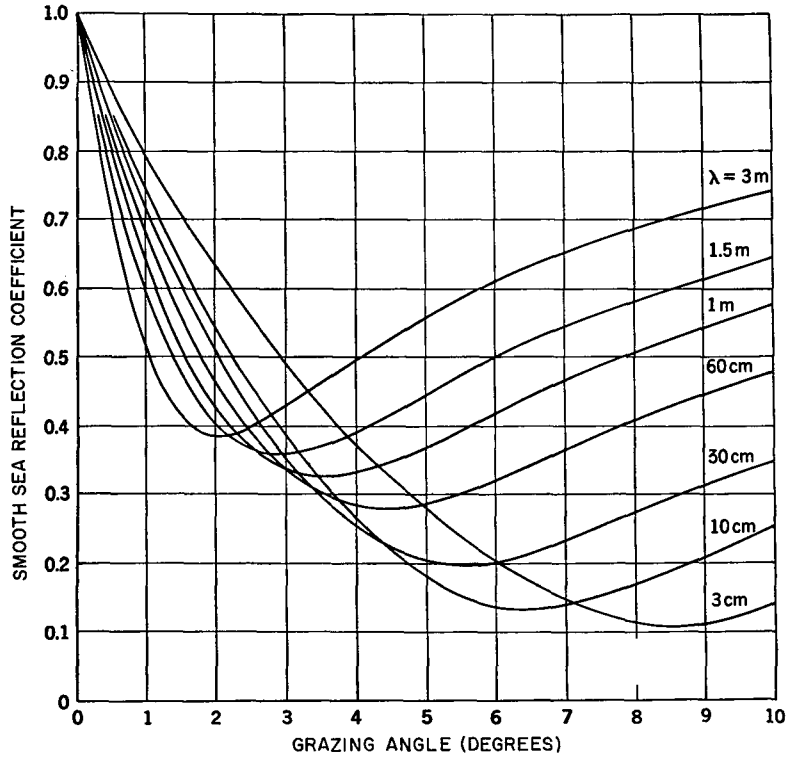

Fig. 13a - Magnitude of the reflection coefficient for a smooth sea and vertical polarization at a number of wavelengths (from Ref. 14, Fig. 5.4)

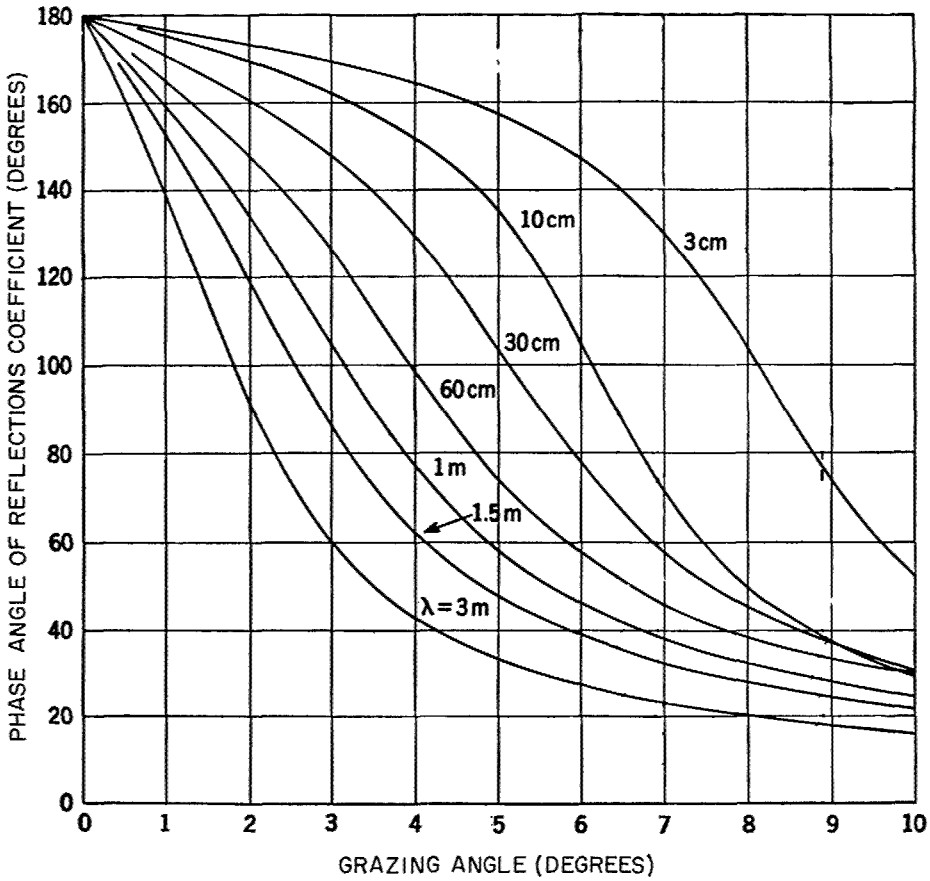

Fig. 13b - Phase angle of the reflection coefficient for a smooth sea and vertical polarization at a number of wavelengths (from Ref. 14, Fig. 5.5)

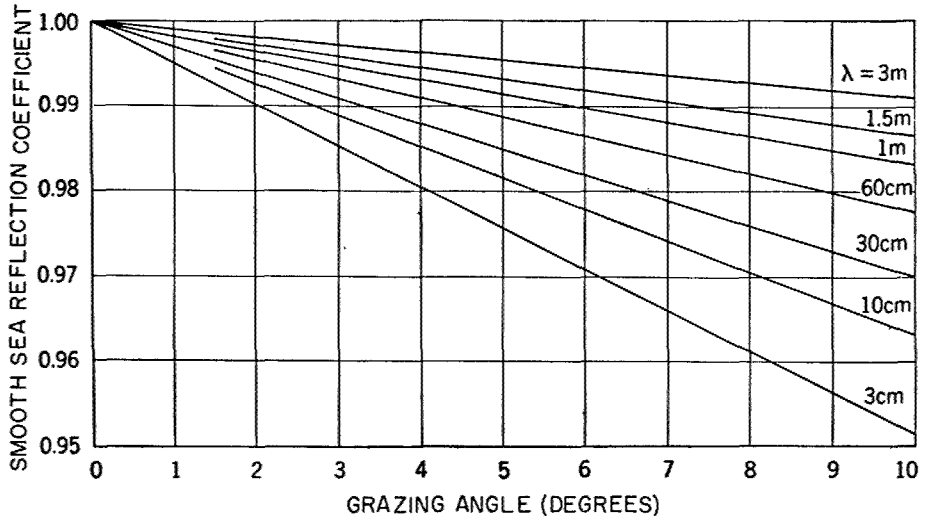

Fig. 13c - Magnitude of the reflection coefficient for a smooth sea and horizontal polarization for a number of wavelengths (from Ref. 14, Fig. 5.6)

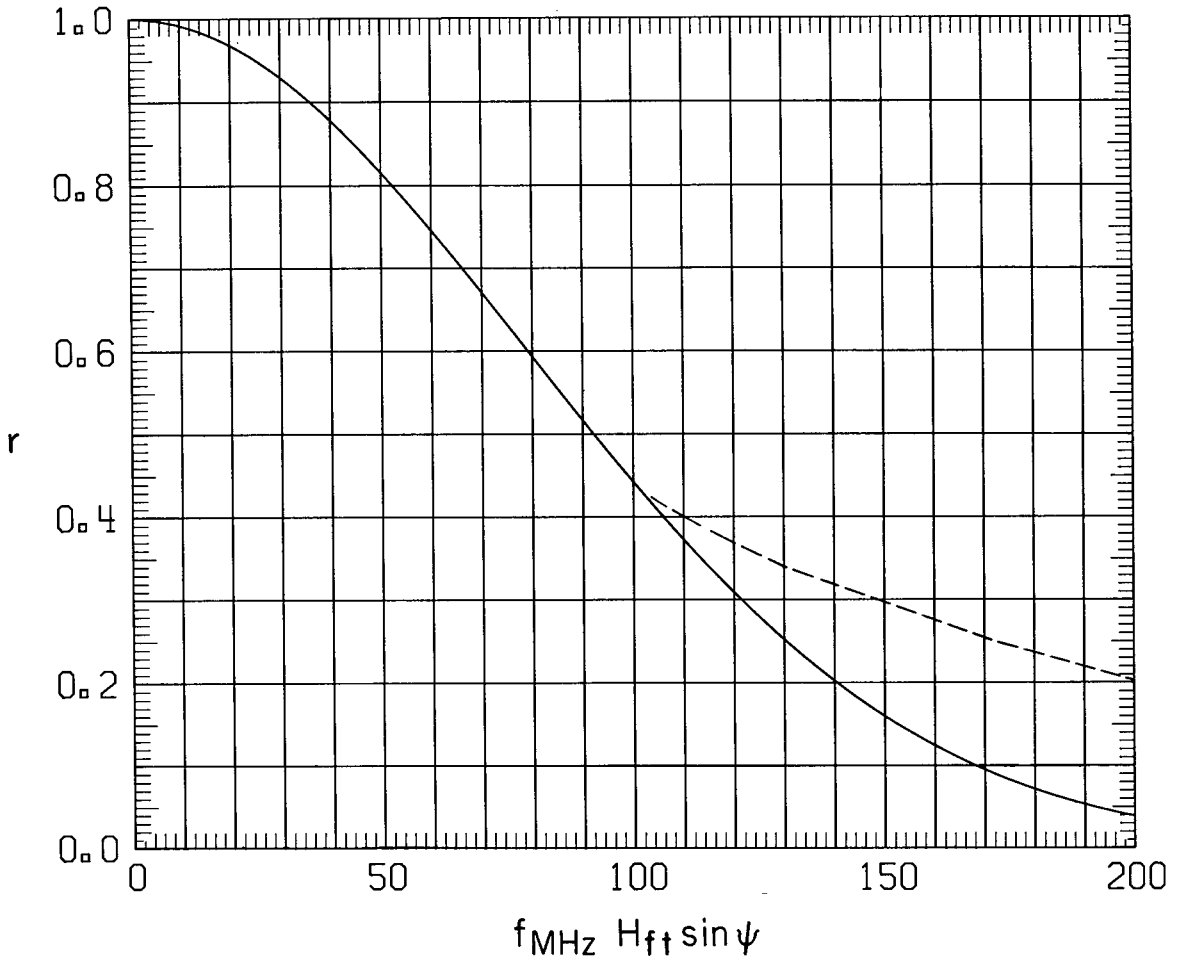

Fig. 15 - Ratio of the rough-sea to the smooth-sea reflection coefficient r as a function of the parameter $f_{MHz}H_{ft} \sin \psi$ (f = frequency, H = standard deviation of the wave height distribution, and ψ = grazing angle). The solid curve was computed from Eq. (56). The dashed curve represents experimental results of Beard, Katz, and Spetner (35).

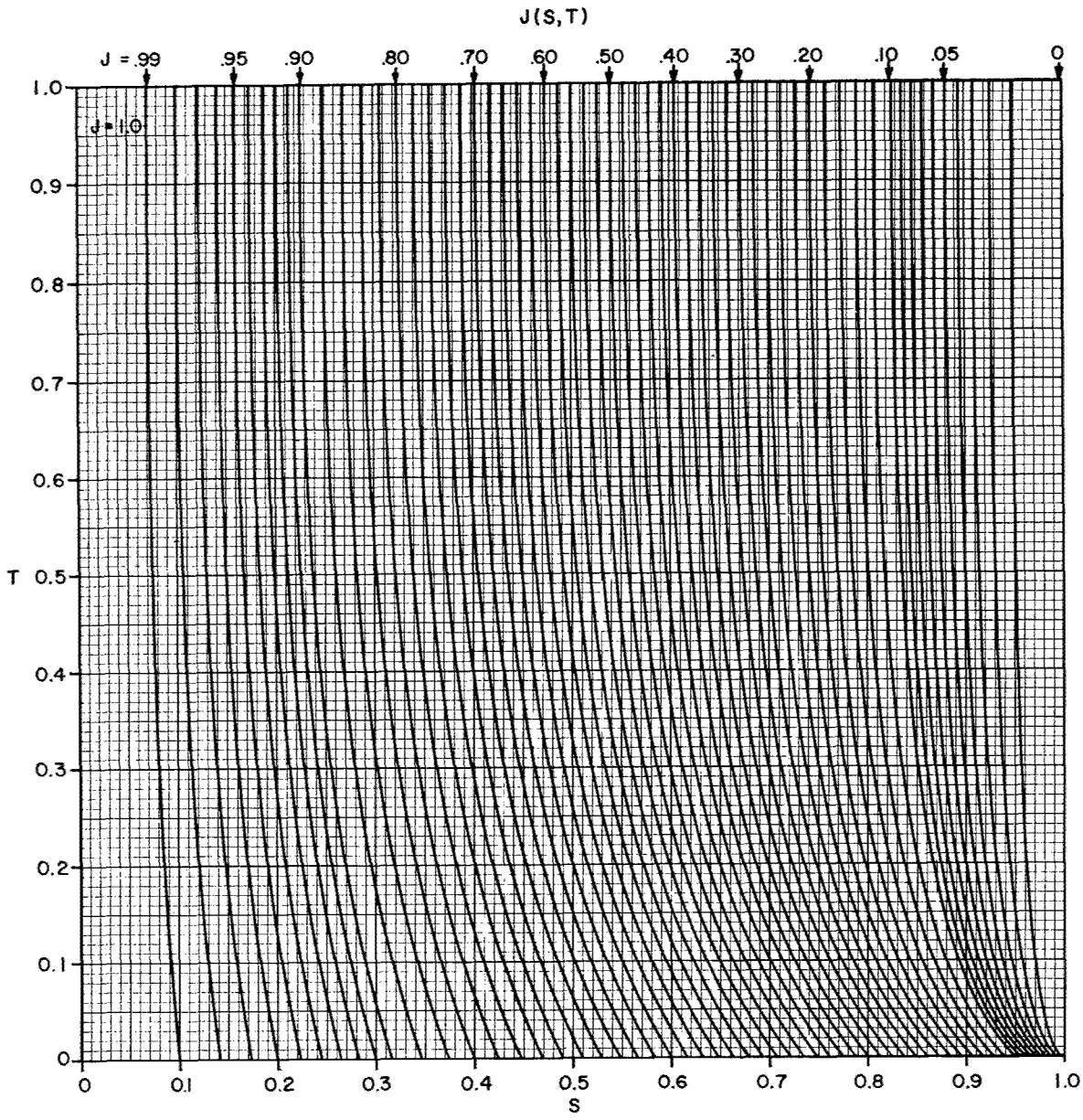

Fig. 17a - Correction factor J used in curved-earth pattern-propagation factor calculation, plotted as a function of parameters S and T

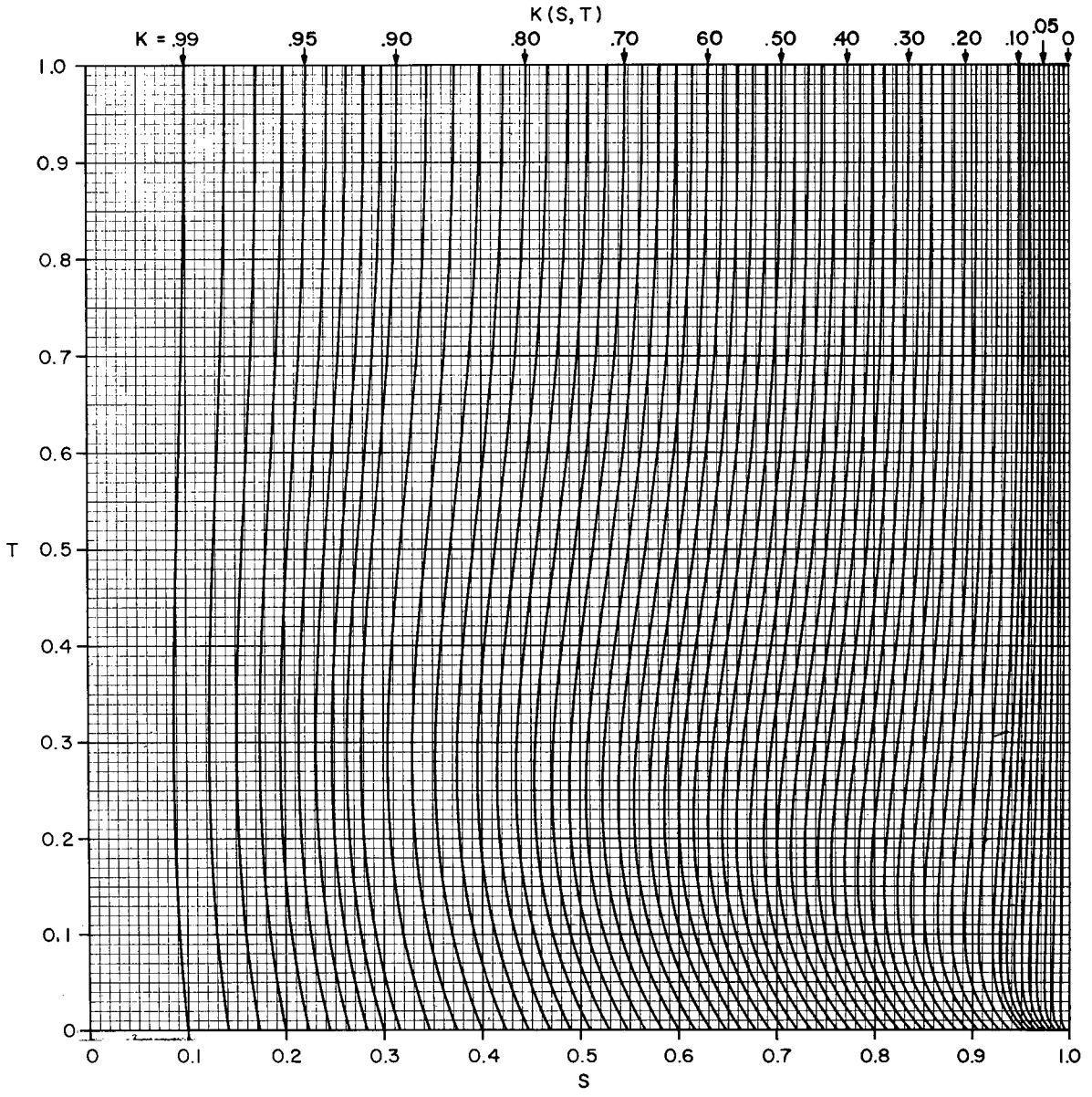

Fig. 17b - Correction factor K used in curved-earth pattern-propagation factor calculation, plotted as a function of parameters S and T

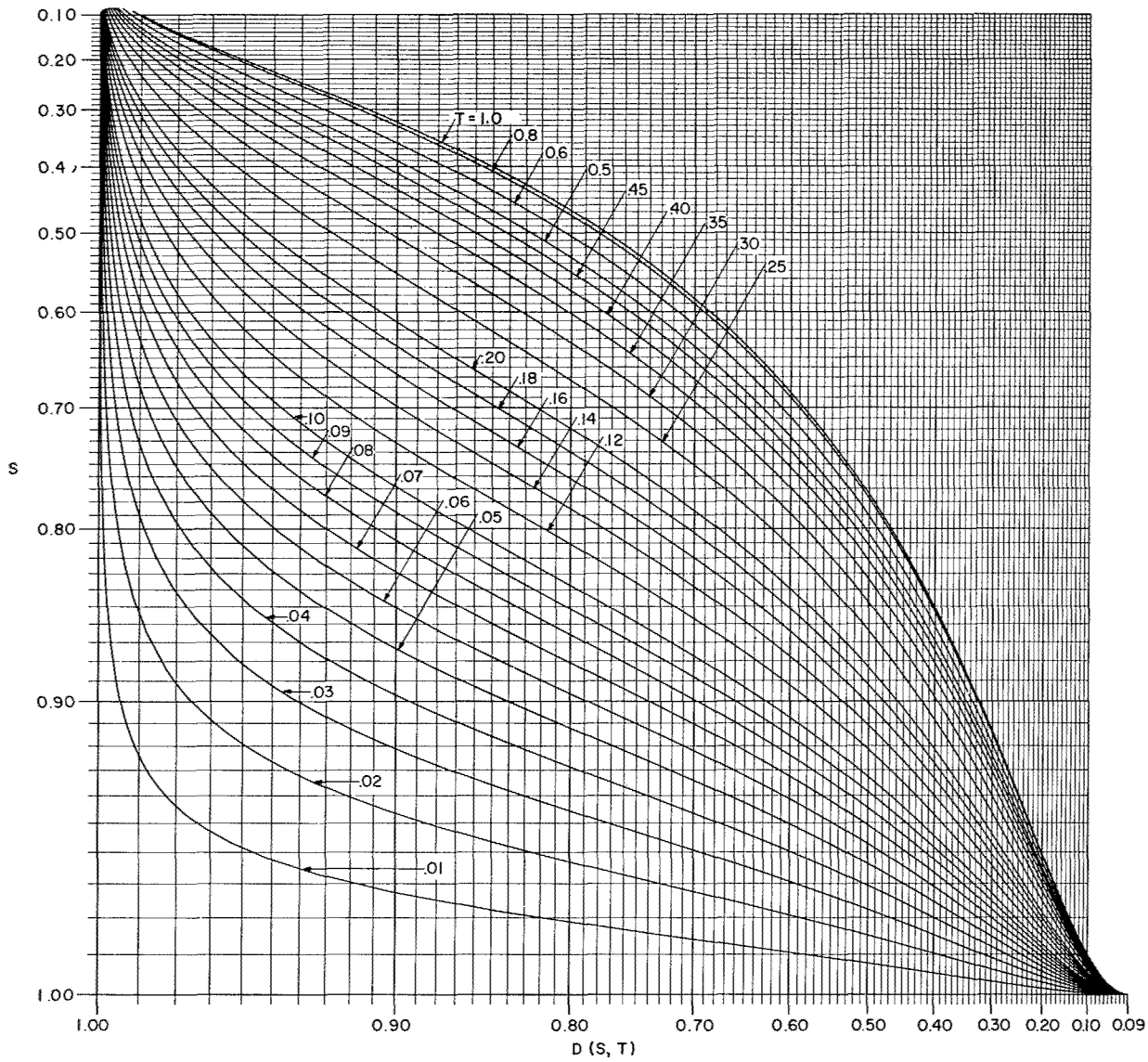

Fig. 17c - Divergence factor D plotted as a function of parameters S and T

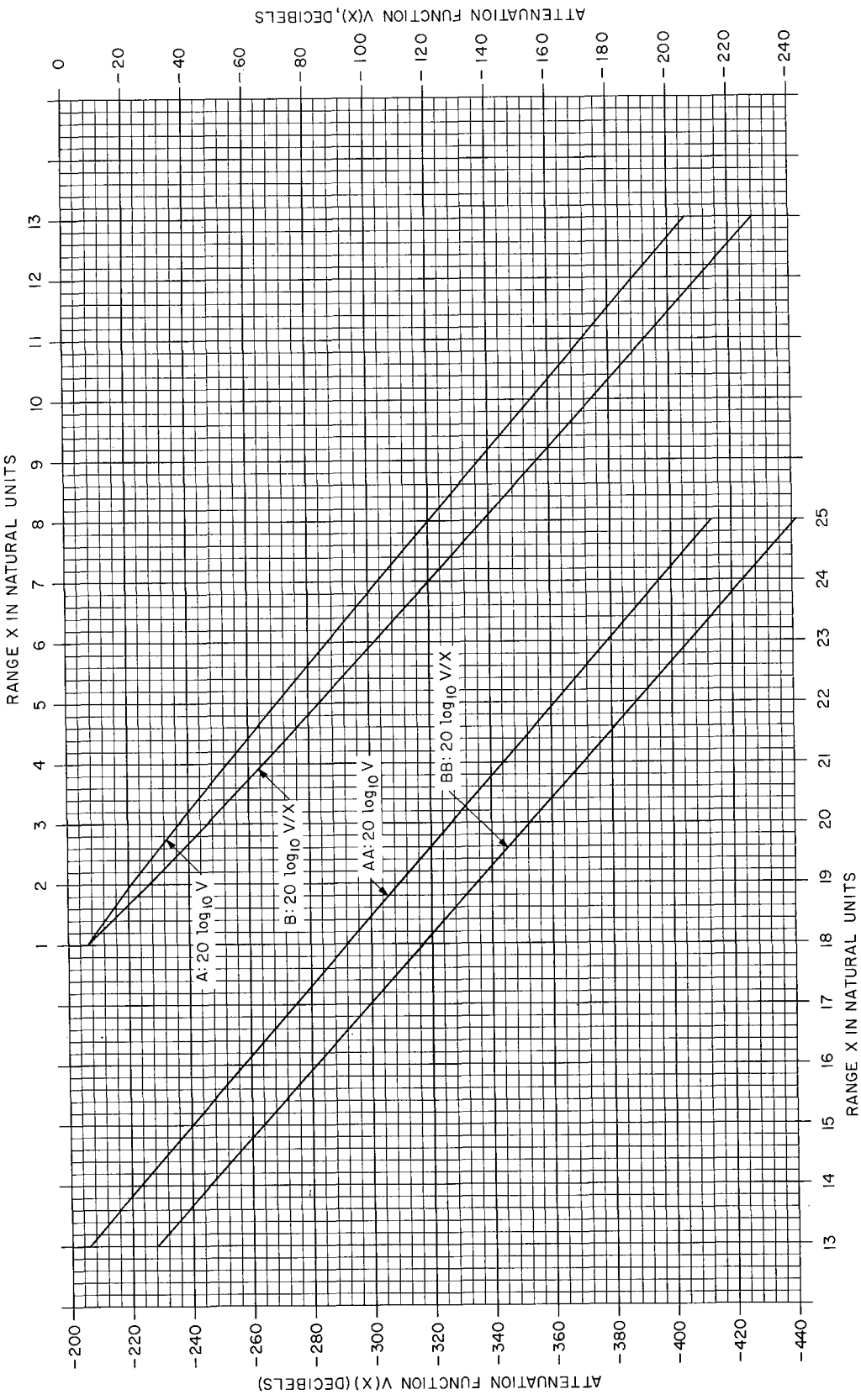

Fig. 19a – Attenuation function v used in intermediate-region pattern-propagation factor calculation. For curves A and B, use left and bottom scales; for AA and BB, use top and right scales.

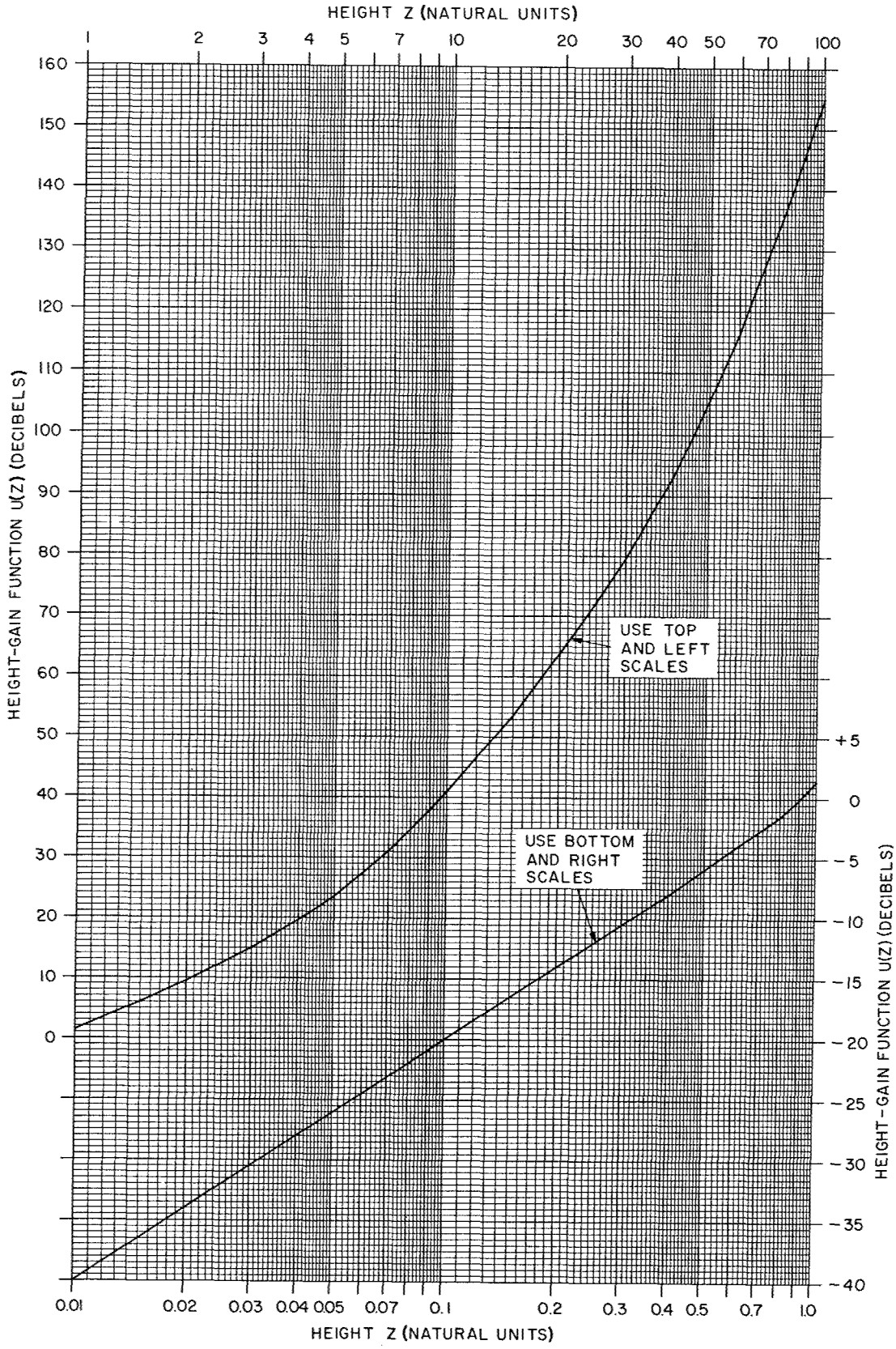

Fig. 19b - Height-gain function U used in intermediate-region pattern-propagation factor calculation (adapted from Ref. 14, Fig. 2.20)

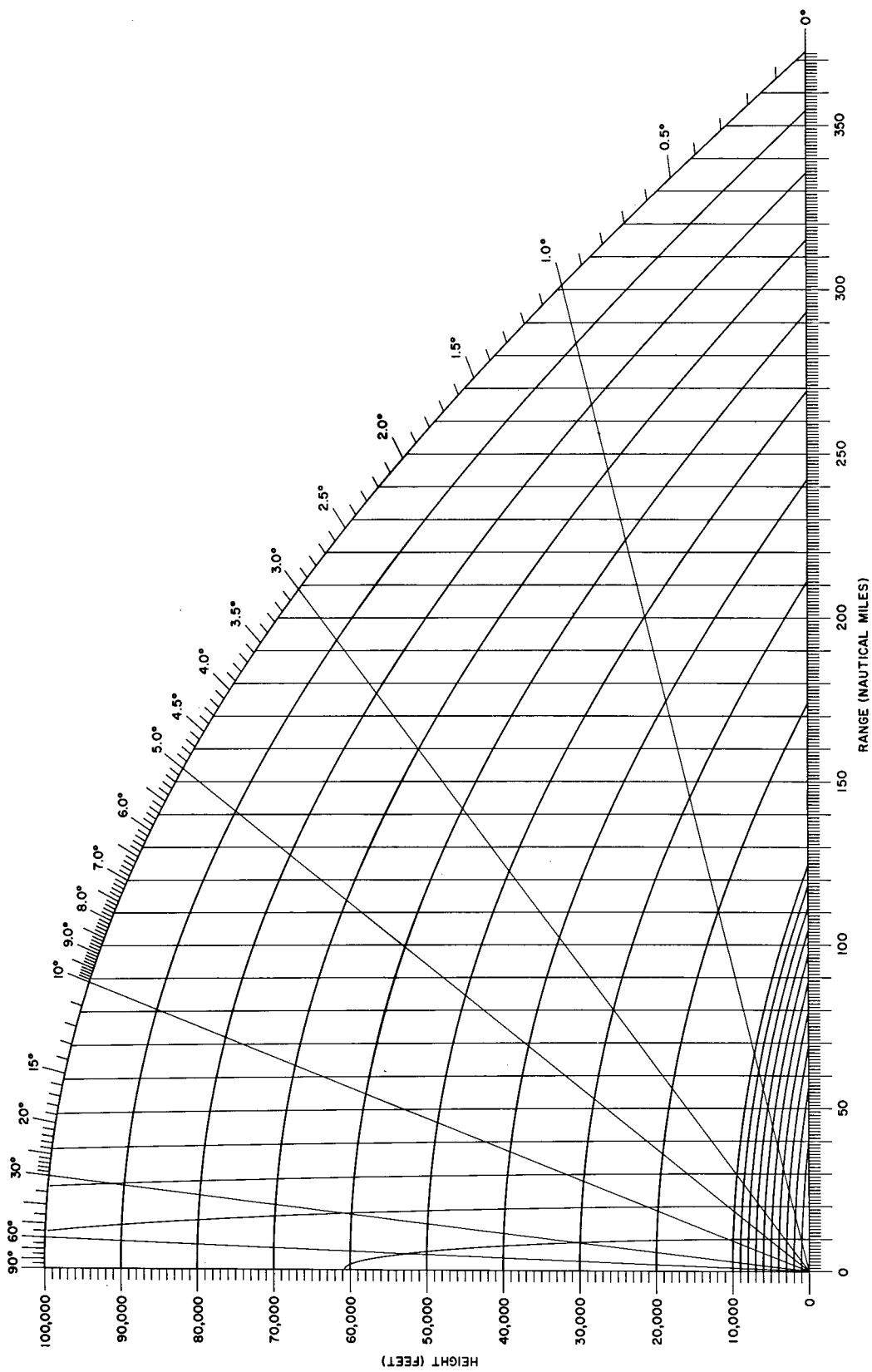

Fig. 20a – Radar range-height-angle chart for targets in the troposphere with refracted rays represented as straight lines, calculated for the CRPL Exponential Reference Atmosphere with N_s = 313 and plotted with linear range and height scales and a nonlinear angle scale (from Ref. 42)

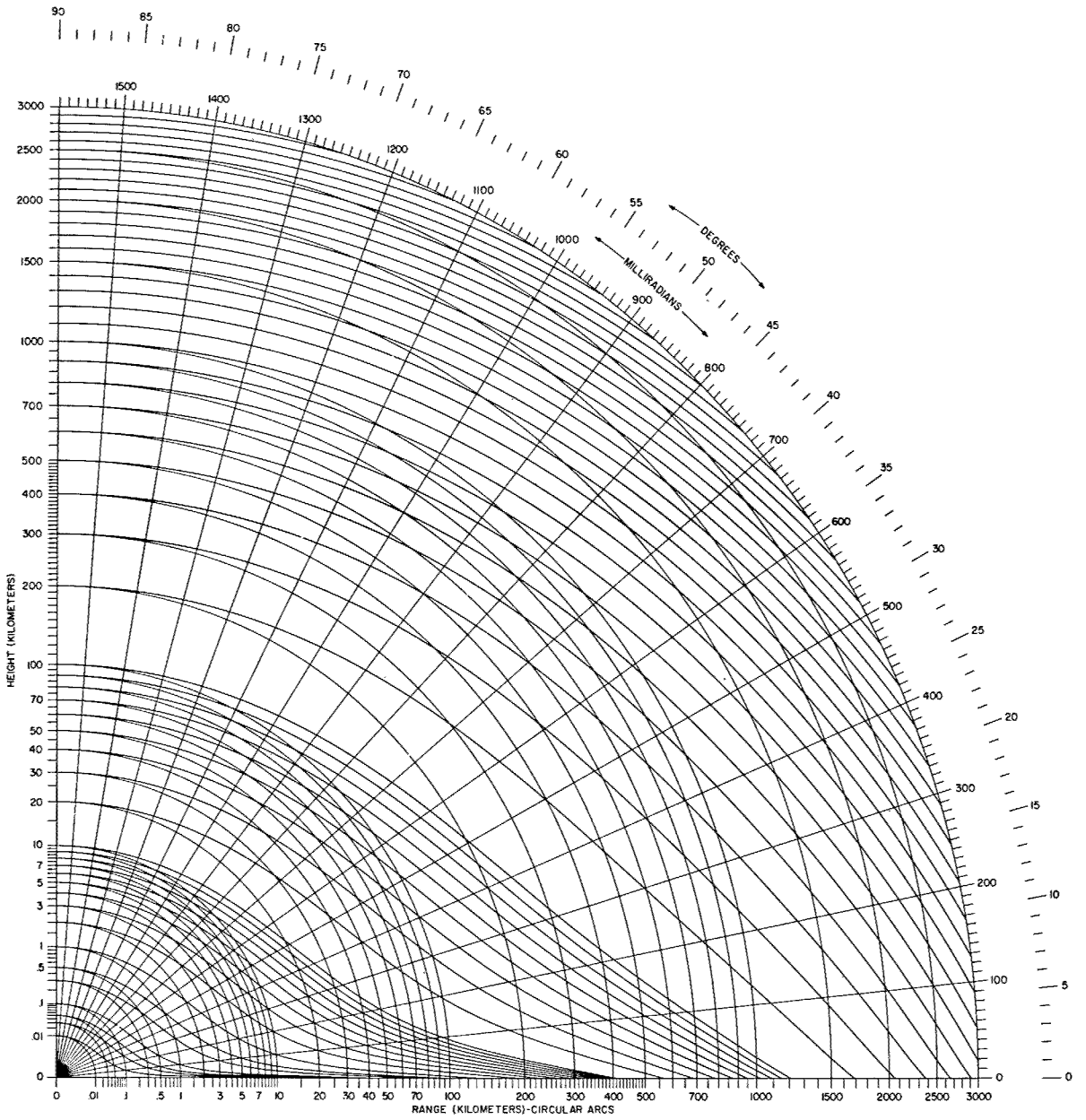

Fig. 20b - Radar range-height-angle chart for targets to 3000 km altitude with refracted rays represented as straight lines, calculated for the CRPL Exponential Reference Atmosphere with N_s = 313 and plotted with nonlinear range and height scales and a linear angle scale (from Ref. 42). Chart is not valid above 100 km for frequencies at which ionospheric refraction occurs.

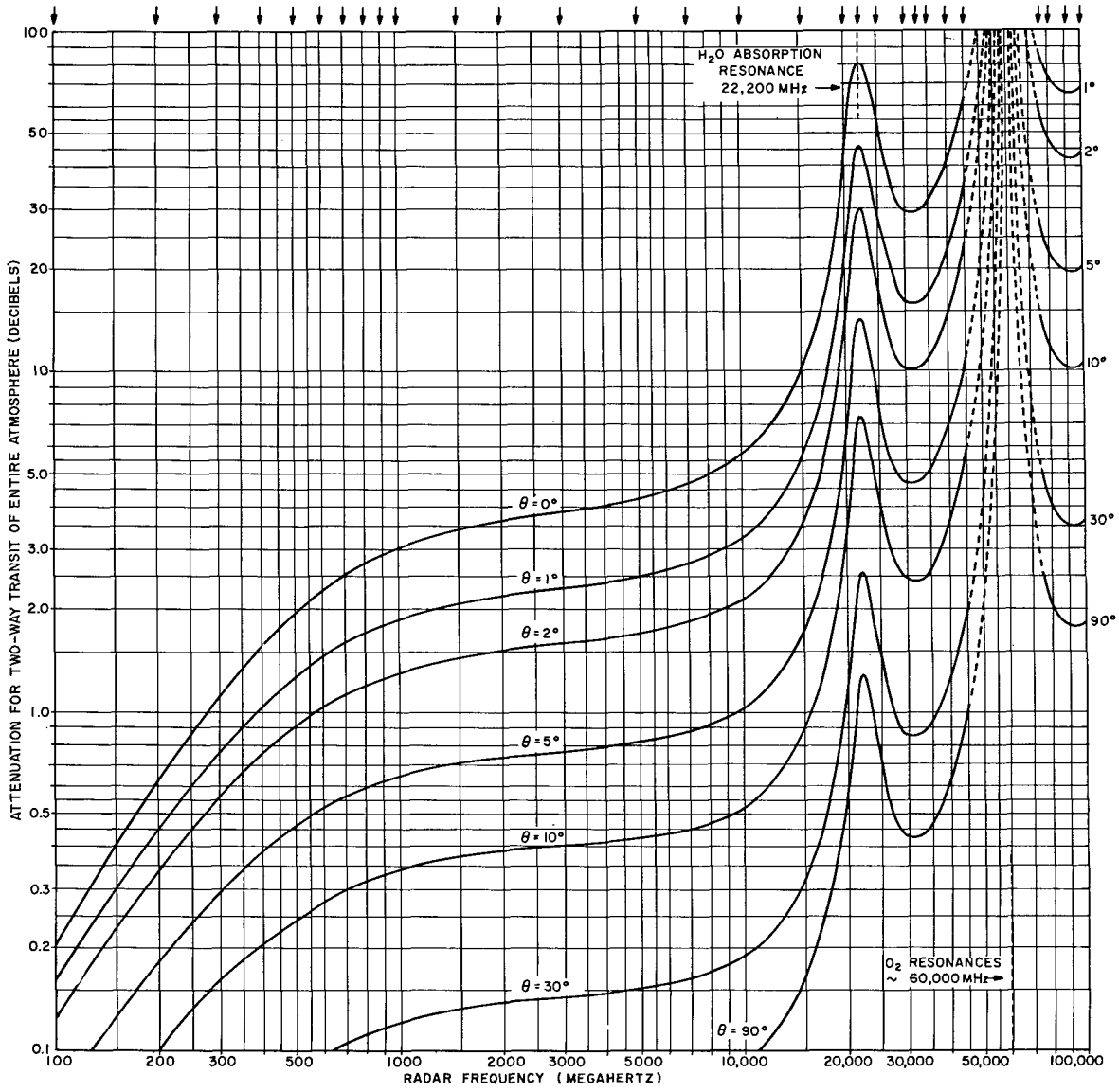

Fig. 21 - Absorption loss for two-way transit of the entire troposphere, at various elevation angles, calculated using Van Vleck theory for oxygen and water vapor absorption. The ray paths were computed for the CRPL Exponential Reference Atmosphere with N_s = 313. The pressure-temperature profile is based on the ICAO Standard Atmosphere. The surface water-vapor content was assumed to be 7.5 grams per cubic meter. An approximation was employed between 45 GHz and 75 GHz (oxygen resonance region). Arrows at top denote frequencies for which absorption was computed.

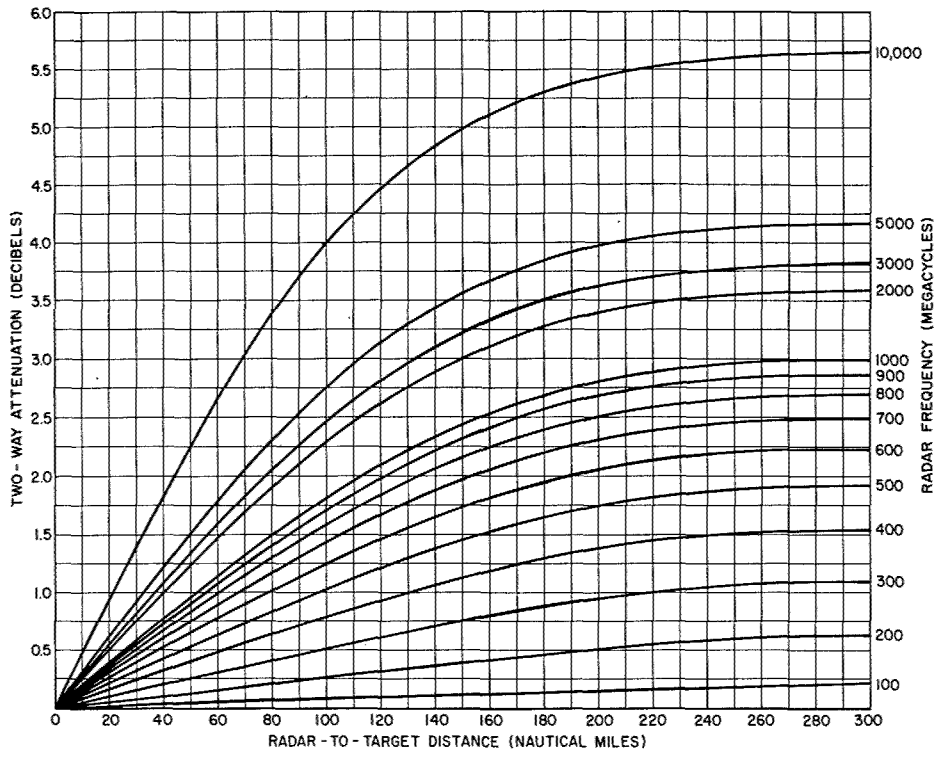

Fig. 22a - Absorption loss for two-way (radar) propagation with the target in the troposphere, plotted as a function of radar range for various frequencies and a zero elevation angle. The calculations were made on the same basis as given in the title for Fig. 21

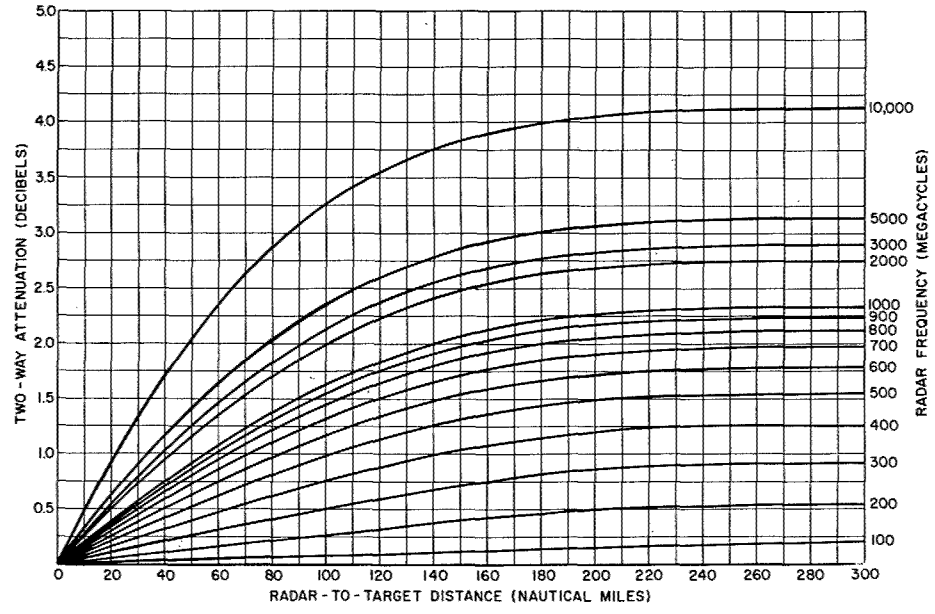

Fig. 22b - Absorption loss for two-way (radar) propagation with the target in the troposphere, plotted as a function of radar range for various frequencies and an 0.5-degree elevation angle

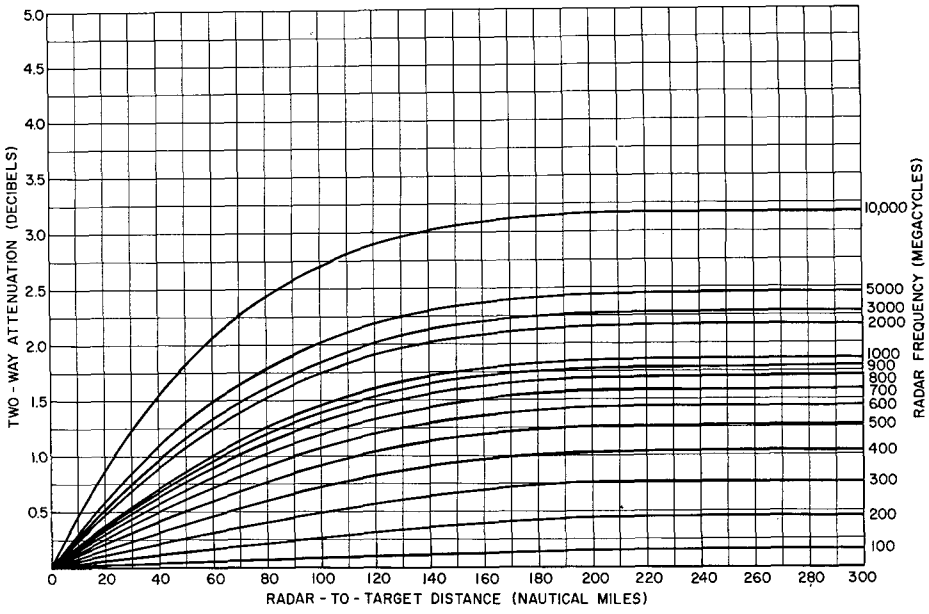

Fig. 22c - Absorption loss for two-way (radar) propagation with the target in the troposphere, plotted as a function of radar range for various frequencies and a 1.0-degree elevation angle

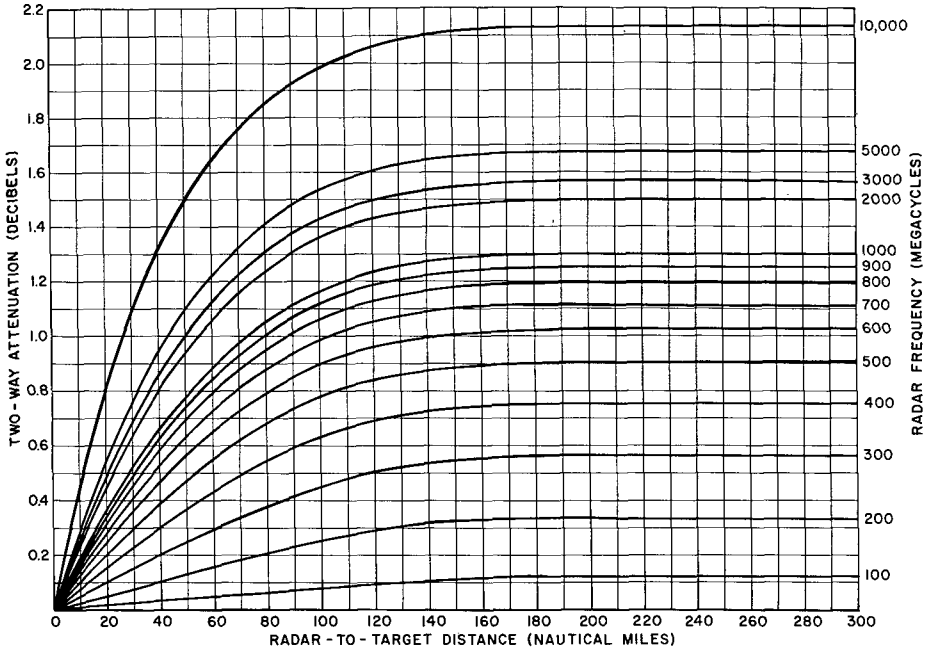

Fig. 22d - Absorption loss for two-way (radar) propagation with the target in the troposphere, plotted as a function of radar range for various frequencies and a 2.0-degree elevation angle

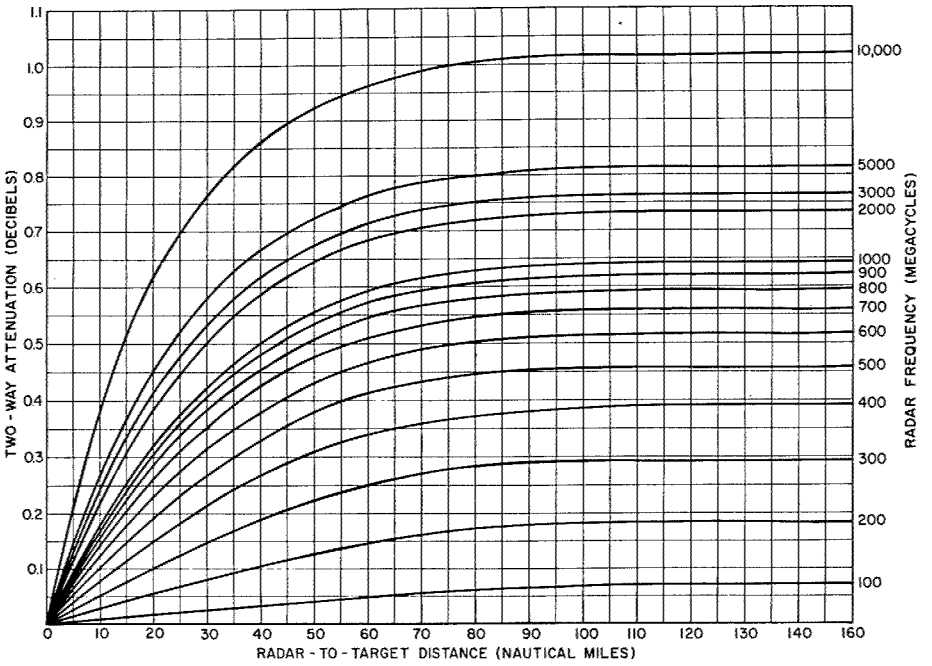

Fig. 22e - Absorption loss for two-way (radar) propagation with the target in the troposphere, plotted as a function of radar range for various frequencies and a 5.0-degree elevation angle

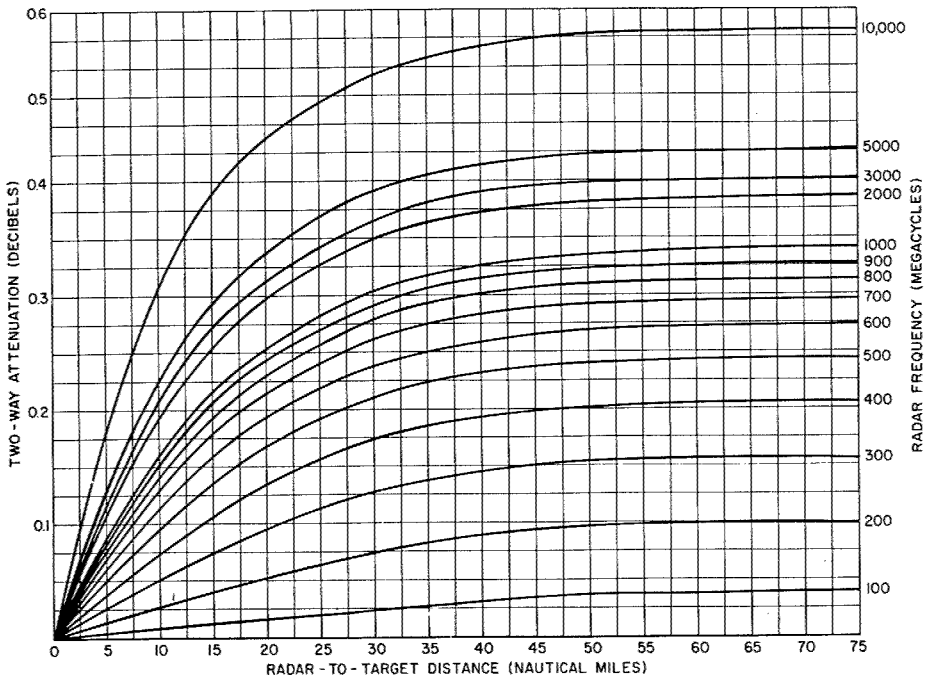

Fig. 22f - Absorption loss for two-way (radar) propagation with the target in the troposphere, plotted as a function of radar range for various frequencies and a 10.0-degree elevation angle

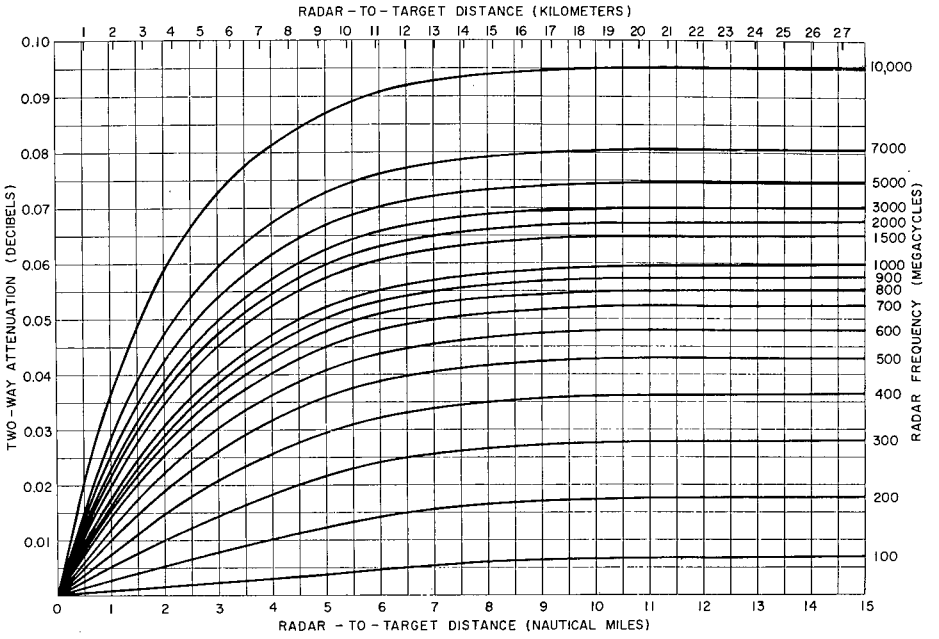

Fig. 22g - Absorption loss for two-way (radar) propagation with the target in the troposphere, plotted as a function of radar range for various frequencies and a 90.0-degree elevation angle

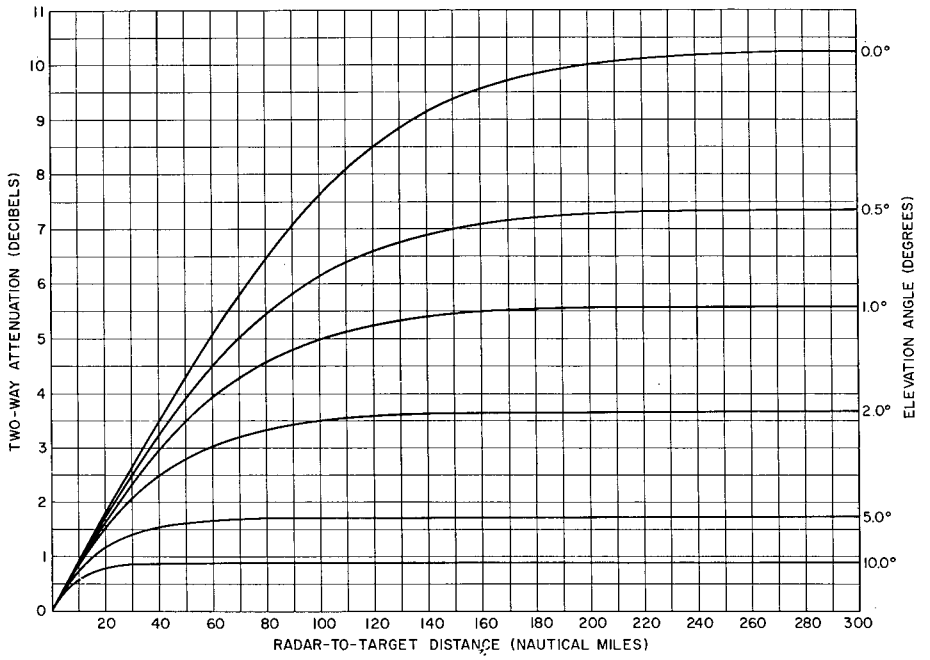

Fig. 22h - Absorption loss for two-way (radar) propagation, targets in troposphere, as a function of radar range, for various ray elevation angles, frequency 15 GHz

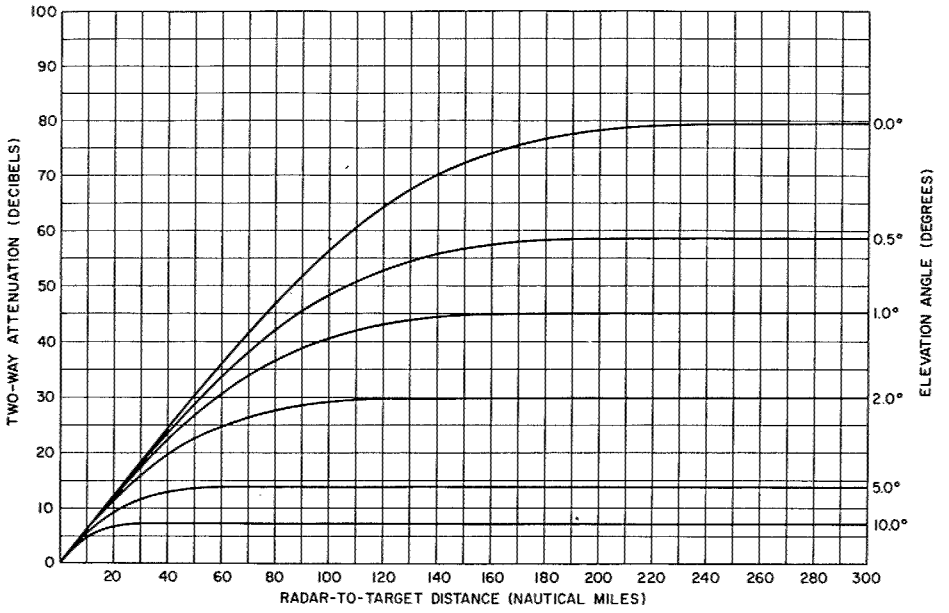

Fig. 22i - Absorption loss for two-way (radar) propagation, targets in troposphere, as a function of radar range, for various ray elevation angles, frequency 22.2 GHz (water-vapor resonance frequency)

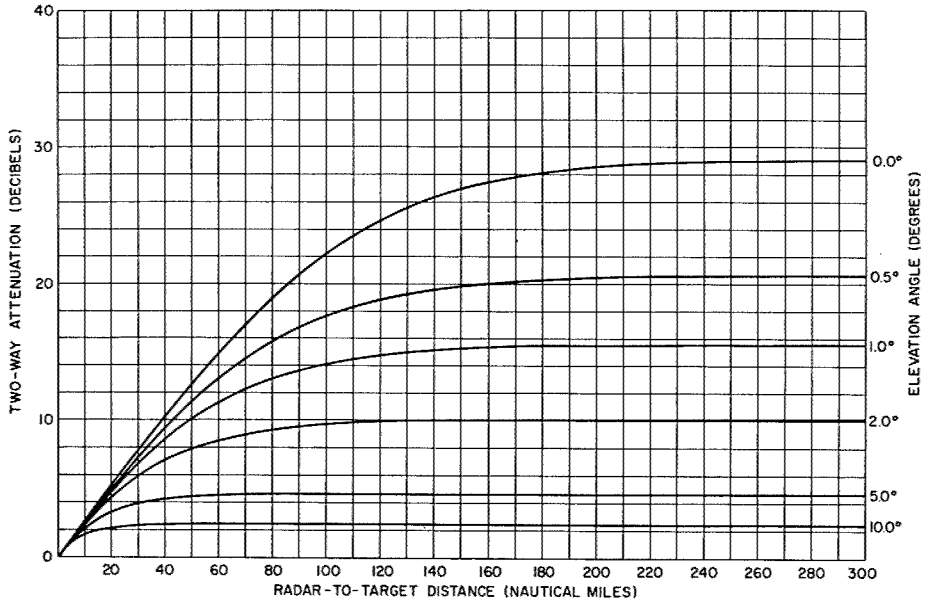

Fig. 22j - Absorption loss for two-way (radar) propagation, targets in troposphere, as a function of radar range, for various ray elevation angles, frequency 32.5 GHz

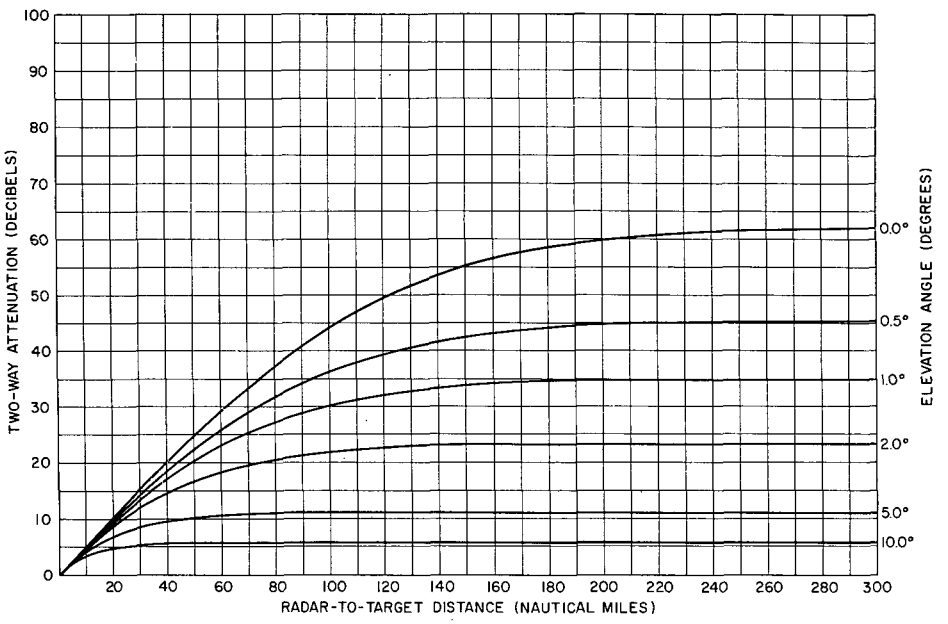

Fig. 22k - Absorption loss for two-way (radar) propagation, targets in troposphere, as a function of radar range, for various ray elevation angles, frequency 45 GHz

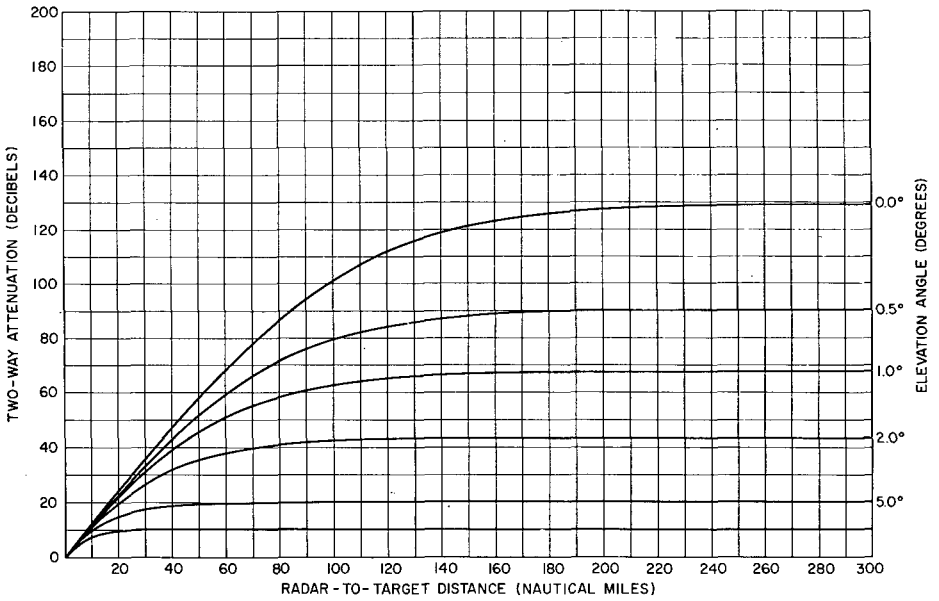

Fig. 22l - Absorption loss for two-way (radar) propagation, targets in troposphere, as a function of radar range, for various ray elevation angles, frequency 100 GHz

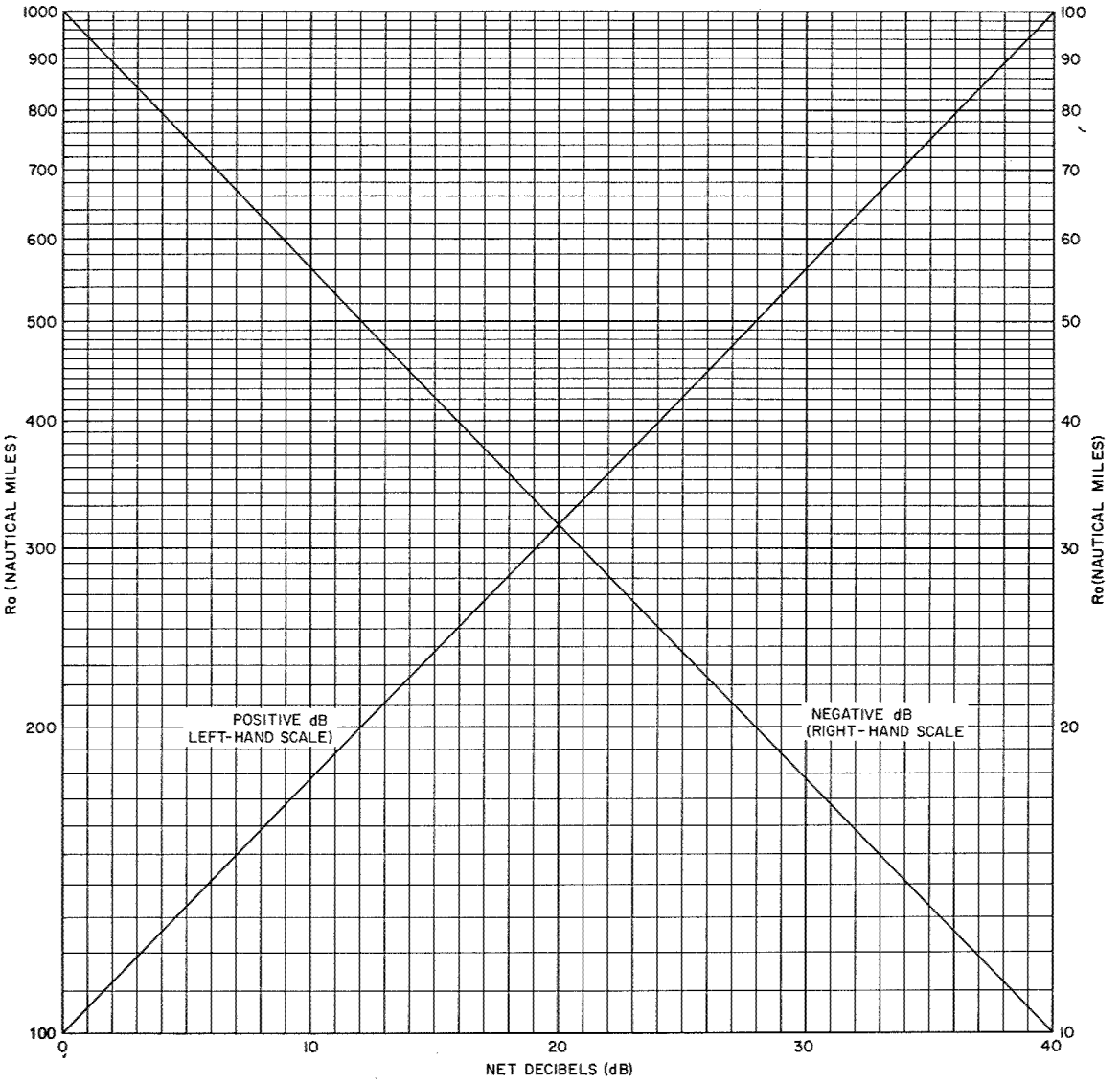

Fig. 24 - Free-space radar range R_0, nautical miles, as a function of the net decibel factor (dB) from the range-calculation work sheet, plotted from $R_0 = 100$ antilog (dB/40). For $|dB| > 40$, subtract an integral number M times 40 from $|dB|$ to make the remainder lie in the range 0 to 40 dB; then multiply the left range scale by 10^M and the right range scale by 10^{-M}, and read range corresponding to remainder.

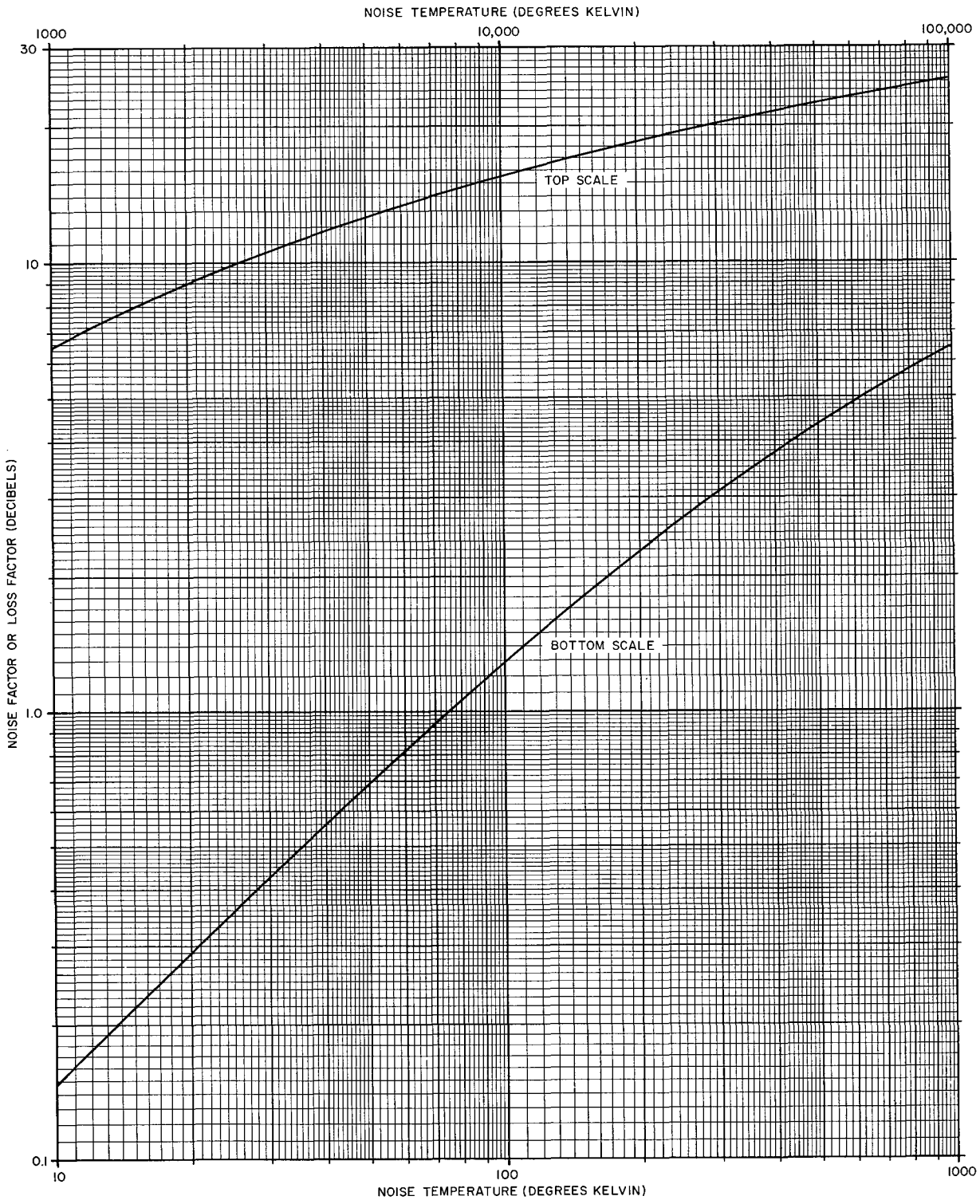

Fig. 25 - Effective receiver input noise temperature T_e or transmission-line input noise temperature T_r as a function of receiver noise factor F_n or transmission-line loss factor

INDEX

Absorption, 4, 51, 80
  atmospheric, 3, 72, 80
  loss, 72, 80, 92
Accuracy of range prediction, 91
  range, 11
Antenna beamwidth, 12, 13
  directivity, 12
  gain, 4, 12, 92
  loss factor, 12
  noise temperature, 5, 12, 47, 48
  pattern, 12
  pattern factor, 51
  pattern loss, 70
A-scope display, 42
Aspect angle, target, 13
Atmospheric absorption, 3, 72
Attenuation function, 64
Autocorrelation interval, 57
Automatic detection, 8
  radar, 9
Available gain, 46
  loss, 46, 70
  power, 46, 70
Average power, 7, 11

Bandwidth, 10, 14
  correction factor, 6, 9, 14
  half-power, 14
  noise, 5, 14, 20, 50
  predetection, 83
  receiver, 6
  video, 82
Beamwidth, 13, 87
  antenna, 12, 13
  half-power, 12, 14, 71
Beyond-the-horizon detection, 51
Bidirectional scan, 71
Birds, 86
Bistatic radar, 9
Blip/scan ratio, 88, 89
Boltzmann's constant, 5, 46, 85

Cascade system, 8
Chaff, 87
Clutter, 13, 86
Coded-pulse waveform, 7
Coherent integration, 11, 84
Collapsing loss, 82
  ratio, 82, 83
Contrast, luminous, 43
Conventions, 1, 71
Cosmic blackbody radiation, 48
Coverage diagrams, 3, 64
Cross section, bistatic, 9
  fluctuating, 8, 13
  median, 89
  monostatic, 9
  per unit area, 87
  per unit volume, 88
  target, 4, 8, 10, 12, 13
CRPL Exponential Reference Atmosphere, 67, 80
Cumulative probability of detection, 88, 90
CW radar, 11, 44

Decibel-logarithmic range equation, 10
Decision theory, 18
Delay-line integrator, 17
Detection, automatic, 8
Detector, 8
  laws, 3, 29
  linear, 3, 29
  square-law, 3, 29
Diffraction, 4, 51
  region, 52
Diffuse reflection, 57
Directivity, antenna, 12
Distributed target, 13
Divergence factor, 53, 59
Doppler filtering, 88
Duty factor, 11

Effective earth's radius, 64
  pulse power, 11
Error, range prediction, 2
Exponential atmosphere, 67, 80

False-alarm number, 3, 20
  probability, 3, 7, 8, 9, 18, 19, 28, 43
  time, 19
Fine lobe structure, 90
Flat-earth approximation, 57
Flat-earth reflection, 53

Fluctuating cross section, 8, 13, 28
signals, 3, 8, 14
Free-space propagation, 51
Frequency, 9, 10, 14

Gain, antenna, 4, 12, 92
available, 46
Galactic noise, 48
Generalized reflection coefficient, 59
Grazing angle, 53, 87
Ground noise, 48
range, 57

Half-power bandwidth, 14
beamwidth, 12, 71
Height-gain function, 64
Historical notes, 2
Horizon, radio, 52
Horizontal polarization, 53
Human observer, 42

ICAO standard atmosphere, 80
IF amplifier, 7
Insects, 86
Instantaneous power, 11
Integration, 3, 6, 12, 17
coherent, 11, 84
loss, 84
noncoherent, 84
postdetection, 3, 18, 44
predetection, 18, 29
time, 11, 43
video, 18, 44
Integrator, delay-line, 17
Interference, multipath, 3, 4, 51
Intermediate region, 52, 63
International nautical mile, 10
Ionospheric absorption, 80
reflection, 51
refraction, 70

Jamming, 85

Kilometers, 10

Linear detector, 29
rectifier, 19
Lobe pattern, 55
Log-normal distribution, 28
Loss, absorption, 92
antenna pattern, 70
available, 46, 70
Loss, absorption — Continued
collapsing, 82
factor, 6, 11, 12, 48, 51
factor, antenna, 12
factor, system, 70
integration, 84
operator, 84
polarization, 83
pulse length, 83
squint, 84
system-degradation, 84
Luminous contrast ratio, 43

Matched filter, 3, 7, 9, 15
load impedance, 12
Matching factors, 14
Maximum range equation, 4
Median cross section, 89
Monostatic radar, 9
Moon (distributed target), 13
Moving-target indication, 88
Multipath interference, 3, 4, 51

Natural units, 64
Nautical mile, international, 10
Noise bandwidth, 5, 14, 20, 50
cosmic blackbody, 48
factor, 50
factor, operating, 5
factor, system, 5
galactic, 48
ground, 48
jamming, 85
receiver, 50, 92
sky, 48, 92
spectral density, 6
sun, 48
temperature, 46
temperature, antenna, 5, 12, 47, 48
temperature, input, 5
temperature, operating, 5, 46
temperature, receiver, 47
temperature, system, 3, 5, 10, 46, 92
thermal, 7, 46
transmission line, 50
voltage, 7
Noncoherent integration, 84
Number of pulses, 18, 20, 71
Nyquist interval, 20
Nyquist's theorem, 46, 48

Operating noise factor, 5
noise temperature, 5, 46

Operator factor, 90, 91
loss, 84
Oxygen absorption, 80

Pattern, antenna, 12
factor, 12, 70
propagation factor, 4, 12, 51, 70, 87, 91
Pencil-beam radar, 71
Point target, 13
Polarization, 13, 53
horizontal, 53
loss, 83
vertical, 53
Postdetection integration, 3, 18, 44
Power, available, 46, 70
average, 7, 11
effective pulse, 7, 11
instantaneous, 11
pulse, 11
transmitter, 9, 10, 11
PPI display, 42
Practical units, 9
Predetection bandwidth, 83
filter, 7, 8
integration, 3, 18, 29
Probabilistic notation, 7
Probability of detection, 3, 7, 8, 9, 18, 43, 89
cumulative, 88, 90
false alarm, 3, 7, 8, 9, 18, 19, 28, 43
Propagation, free-space, 51
Pulse bursts,11
compression, 7
-doppler radar, 11, 44
energy, 6, 7, 11
length, 6, 9, 10, 11, 13, 87
-length loss, 83
period, 11
power, 7, 11
power, effective, 11
radar equation, 6
range, extent of, 13
repetition frequency, 7, 11, 42

Radar cross section, 13
Radiation efficiency, 12
Radio horizon, 52
Rain (distributed target), 13
attenuation, 80
Range accuracy, 11
-calculation error, 92
equation, decibel-logarithmic, 10, 93
extent of pulse, 13
Range accuracy — Continued
-height-angle chart, 67
resolution, 11
Rayleigh target, 28, 89, 90
Receiver bandwidth, 6
noise, 50, 92
noise temperature, 47
Reference temperature, standard, 5
Reflection coefficient, 52
coefficient, generalized, 59
interference, 51, 90
Refraction, 4, 51, 64
ionospheric, 70
Refractive index, 3, 64, 67, 80
Repetition frequency, pulse, 7, 11, 42
Resolution, range, 11
Roughness factor, 53, 57
Rough-surface reflection, 57

Scanning, 70
step, 72
Sea clutter, 57
surface, 52
Searchlighting, 70
Self screening, 85
Shadowing, 51, 57
Signal-to-clutter ratio, 87, 88
Signal-to-noise ratio, 5, 7, 8, 9, 17, 19, 28, 46, 71
Single-response receiver, 50
Sky noise, 48, 92
Specular reflection, 52, 57
Spherical-earth reflection, 58
Square-law detector, 29
Squint loss, 84
Stand-off jamming, 86
Statute mile, 10
Steady target, 8
Step scanning, 72
Sun noise, 48
Swerling cases, 28
System-degradation loss, 84
System loss factor, 70
noise factor, 5
noise temperature, 3, 5, 10, 46, 92

Target angular motion, 12
aspect angle, 13
cross section, 4, 8, 9, 10, 12, 13
distributed, 13
fluctuating, 8, 28
point, 13
steady, 8

Thermal noise, 7, 46
Threshold voltage, 8, 18
Transmission equation, 4, 11
Transmission-line noise, 50
Transmitter power, 9, 10, 11

Units, practical, 9, 10

Vertical polarization, 53
Video bandwidth, 82
  integration, 18, 44
Visibility factor, 6, 8
Visual detection, 42

Water-vapor absorption, 80
Wavelength, 9, 14
Weather, 86
Work-sheet form, 94

Security Classification

DOCUMENT CONTROL DATA - R & D

(Security classification of title, body of abstract and indexing annotation must be entered when the overall report is classified)

1. ORIGINATING ACTIVITY (Corporate author)	2a. REPORT SECURITY CLASSIFICATION
Naval Research Laboratory Washington, D.C. 20390	Unclassified
	2b. GROUP

3. REPORT TITLE

A GUIDE TO BASIC PULSE-RADAR MAXIMUM-RANGE CALCULATION
PART 1 — EQUATIONS, DEFINITIONS, AND AIDS TO CALCULATION

4. DESCRIPTIVE NOTES (Type of report and inclusive dates)
An interim report on a continuing NRL Problem.

5. AUTHOR(S) (First name, middle initial, last name)

Lamont V. Blake

6. REPORT DATE	7a. TOTAL NO. OF PAGES	7b. NO. OF REFS
December 23, 1969	157	54

8a. CONTRACT OR GRANT NO.	9a. ORIGINATOR'S REPORT NUMBER(S)
NRL Problem R02-55.101	
b. PROJECT NO.	NRL Report 6930
RF 05-151-402-4011	
c.	9b. OTHER REPORT NO(S) (Any other numbers that may be assigned this report)
d.	

10. DISTRIBUTION STATEMENT

This document has been approved for public release and sale; its distribution is unlimited.

11. SUPPLEMENTARY NOTES	12. SPONSORING MILITARY ACTIVITY
This is a second edition (revised) of a previously published report, NRL Report 5868, Dec. 1962 and Dec. 1963	Department of the Navy (Office of Naval Research), Washington, D.C. 20360

13. ABSTRACT

This report extensively revises NRL Report 5868 of the same title and introduces updated material on many of the topics and extended treatment of others. The basic equation for pulse-radar maximum-range calculation is presented in a form convenient for numerical computation. Charts, graphs, tables, and auxiliary equations are presented for evaluation of the various factors in the range equation. Included are graphs for the required signal-to-noise ratio as a function of probability of detection, false-alarm probability, and number of pulses integrated, for both nonfluctuating and fluctuating (Swerling Cases 1 and 3) echoes. Also treated are the effects of receiver bandwidth, antenna and receiver noise, sea-reflection interference, refraction and absorption by the atmosphere, and various system losses. Standard definitions of range-equation quantities are given. The effects of jamming and clutter echoes are treated briefly, as are also cumulative probability of detection and accuracy of radar range prediction. A systematic procedure for range calculation, employing a work sheet, is presented.

14. KEY WORDS	LINK A		LINK B		LINK C	
	ROLE	WT	ROLE	WT	ROLE	WT
Radar						
Pulse						
Range						
Detection						
Propagation						
Radio waves						
Probability of detection						
Signal detection						

PULSE-RADAR RANGE-CALCULATION WORK SHEET

Based on Eq. (13)

1. Compute the system input noise temperature T_s, following the outline in section A below.
2. Enter range factors known in other than decibel form in section B below, for reference.
3. Enter logarithmic and decibel values in section C below, positive values in the plus column and negative values in the minus column. For example, if $V_{0\,(dB)}$ as given by Figs. 4 through 9 is negative, then $-V_{0\,(dB)}$ is positive and goes in the plus column. For C_B, see Figs. 1 through 3. For definitions of the range factors, see Eq. (13).

Radar antenna height: h = ft. Target elevation angle: θ = °. (See Fig. 13.)

A. Computation of T_s:

$T_s = T_a + T_r + L_r T_e$

(a) Compute T_a.
For $T_{tg} = T_{ta} = 290$ and $T_g = 36$ use Eq. (37a).
Read T_a' from Fig. 11.

$L_{a\,(dB)}$:_____ L_a:_____

$T_a = (0.876\,T_a' - 254)/L_a + 290$

T_a = °K

(b) Compute T_r using Eq. (40).
For $T_{tr} = 290$ use Table 1.

$L_{r\,(dB)}$:____ T_r = °K

(c) Compute T_e using Eq. (41) or using Table 1.

$F_{n\,(dB)}$:_____ T_e:_____ °K

L_r:_____ $L_r T_e$ = °K

Add. T_s = °K

B. Range Factors		C. Decibel Values	Plus (+)	Minus (−)
$P_{t\,(kW)}$		$10 \log P_{t\,(kW)}$	.	.
$\tau_{\mu sec}$		$10 \log \tau_{\mu sec}$	.	.
G_t		$G_{t\,(dB)}$	.	.
G_r		$G_{r\,(dB)}$	.	.
$\sigma_{(sq\ m)}$		$10 \log \sigma$	.	.
f_{MHz}		$-20 \log f_{MHz}$	.	.
T_s (°K)		$-10 \log T_s$	.	.
V_0		$-V_{0\,(dB)}$	.	.
C_B		$-C_{B\,(dB)}$		.
L_t		$-L_{t\,(dB)}$		.
L_p		$-L_{p\,(dB)}$		.
L_x		$-L_{x\,(dB)}$		.
Range-equation constant (40 log 1.292)			4.45	
4. Obtain the column totals →			.	.
5. Enter the smaller total below the larger →			.	.
6. Subtract to obtain the net decibels (dB) →			+ .	− .

7. In Table 2 find the range ratio corresponding to this net decibel (dB) value, taking its sign (±) into account. Multiply this ratio by 100. This is R_0 →
8. Multiply R_0 by the pattern-propagation factor F = (see Eqs. (42) through (65) and Figs. 12 through 19):
   $R_0 \times F = R'$ →
9. On the appropriate curve of Figs. 21 and 22 determine the atmospheric-absorption loss factor, $L_{\alpha(dB)}$, corresponding to R'. This is $L_{\alpha(dB)(1)}$. →
10. Find the range factor δ_1 corresponding to $-L_{\alpha(dB)(1)}$ from the formula $\delta = \text{antilog}\,(-L_{\alpha(dB)}/40)$ or by using Table 2. →
11. Multiply R' by δ_1. This is a first approximation of the range R_1. →
12. If R_1 differs appreciably from R', on the appropriate curve of Figs. 21 and 22, find the new value of $L_{\alpha(dB)}$ corresponding to R_1. This is $L_{\alpha(dB)(2)}$. →
13. Find the range-increase factor (Table 2) corresponding to the difference between $L_{\alpha(dB)(1)}$ and $L_{\alpha(dB)(2)}$. This is δ_2. →
14. Multiply R_1 by δ_2. This is the radar range in nautical miles, R. →

Note: If the difference between $L_{\alpha(dB)(1)}$ and $L_{\alpha(dB)(2)}$ is less than 0.1 dB, R_1 may be taken as the final range value, and steps 12 through 14 may be omitted. If $L_{\alpha(dB)(1)}$ is less than 0.1 dB, R' may be taken as the final range value, and steps 9 through 14 may be omitted. (For radar frequencies up to 10,000 megahertz, correction of the atmospheric attenuation beyond the $L_{\alpha(dB)(2)}$ value would amount to less than 0.1 dB.)

GPO 885-394